Structural Engineering Report No. 82

CRACKING OF REINFORCED AND PRESTRESSED CONCRETE WALL SEGMENTS

by

J. G. MacGREGOR

S. H. RIZKALLA

S. H. SIMMONDS

March 1980

University of Alberta

Department of Civil Engineering

CRACKING OF REINFORCED AND PRESTRESSED CONCRETE WALL SEGMENTS

by

J.G. MacGregor
S.H. Rizkalla
S.H. Simmonds

A Technical Report to the
Atomic Energy Control Board
Nuclear Plant Licensing Directorate
P.O. Box 1046
Ottawa, Canada K1P 5S9

March, 1980

DISCLAIMER

ABSTRACT

Twelve prestressed concrete wall segments simulating portions of the walls of secondary containment vessels were loaded by uniaxial or biaxial tensile loads to obtain load-deformation and cracking behavior. During the tests the loads, strains and crack widths, were measured. This report briefly describes the test specimens, loading apparatus and test procedures. Following a review of crack width expressions in the literature, the crack data from this test series is analyzed. The analysis is based on crack width relationships proposed by Leonhardt and modified to reflect the observed cracking behavior of the wall segments. A procedure for estimating the number and widths of through-the-wall cracks in a containment structure is presented.

TABLE OF CONTENTS

Page

LIST OF TABLES

LIST OF FIGURES

Figure Number	Title	Page

NOTATION AND TERMINOLOGY

a_{cr}	cover measured radially from surface of bar to point on surface where crack width is measured.
A_b	area of one bar
A_c	area of concrete in cross-section
A	effective area of concrete around each bar, equal to the area of concrete concentric with one bar and bounded by the edges of the member or points half way between two bars.
A_s	cross-sectional area of reinforcing bars
c	minimum cover to surface of bar (measured perpendicular to surface)
d_b	diameter of bar
E_s	modulus of elasticity of steel
E_c	modulus of elasticity of concrete
$f_{t,max}$	maximum tensile stress in concrete between two cracks
f_t	tensile stress in concrete
f'_t	tensile strength of concrete
f_{s1}	stress in reinforcement prior to cracking
$f_{s1,cr}$	stress in reinforcement immediately prior to cracking
f_{s2}	stress in reinforcement at a crack
$f_{s2,cr}$	stress in reinforcement at a crack immediately after cracking
h_{cr}	height to which first flexural cracks extend
ℓ_o	unbonded length of bar at a crack
ℓ_t	transfer length
L	total length over which strain and crack width measurements were made

k_1, k_2 ..	empirical constants
N	number of through-the-wall cracks at a given load
N_{twc}	number of through-the-wall cracks at end of test
n	modular ratio = E_s/E_c, number of cracks
P	axial load
P_{cr}	cracking load
R	the distance from the neutral axis to the bottom of the beam divided by the distance from the neutral axis to the reinforcement
s	spacing of cracks
s_m	average crack spacing
t	bar spacing
w_m	average crack width
$\Delta f_{s,max}$	maximum reduction in steel stress between two cracks
ΔL_s	total elongation of steel between two cracks
ΔL_c	total elongation of concrete between two cracks
ε_{cm}	average strain in the concrete
ε_{cr}	strain just before cracking
ε_{cx}	concrete strain at point x
ε_m	average strain measured over a gage length which includes several cracks.
ε_{se}	strain in prestressing tendons after all losses
ε_{s2}	steel strain at a crack
ε_{sx}	steel strain at point x
ρ	reinforcement ratio, A_s/A_c
ρ_e	effective reinforcement ratio, A_b/A
μ	bond stress

Demec Strains - strain measurements made with a mechanical strain gage having a gage length of 2 or 5 in.

Face A - Side of specimen which was on top during casting and on south side during testing

Face B - Opposite side of specimen

1. INTRODUCTION

1.1 Introduction

Canadian nuclear power plants of the type constructed in Quebec and under construction in New Brunswick, Argentina and Korea have their nuclear reactors housed in circular prestressed concrete containment structures. Such a structure, shown schematically in Fig. 1.1 consists of a heavy concrete base, a cylindrical wall, a ring beam and a dome. Each of these elements contains a grid of conventional reinforcement and prestressing tendons.

In the event of a malfunction, pressurized gases or steam may be discharged. The function of the secondary containment vessel is to prevent such gases from escaping into the atmosphere. Near the top of the Canadian circular containment structures is a large water tank. If an overpressure ever were to develop, water would automatically be sprayed into the building to condense the steam, thus reducing the pressure. The design basis accident (DBA) pressure of 18.5 psi is the maximum pressure anticipated if a secondary steam line breaks and the water dousing system acts to condense the steam. The walls and dome of the containment structure are designed to have zero tension stress under 1.15 times the DBA pressure.

In the extremely unlikely event that a secondary steam line fails and the dousing system fails to act, the pressures may reach several times the DBA pressure. In such a case, the walls and dome will be stressed in biaxial tension due to the internal pressure. The research described in this report concerns the behavior of reinforced and prestressed concrete subjected to biaxial tensile forces large enough to crack the concrete. The overall experimental project consists of tests of concrete wall segments and a test of a model of a structure similar to a Canadian containment vessel. These tests have been carried out to study the behavior of such structures, and more important, to allow the calibration of analysis procedures developed in a companion project.

This report presents results of tests on wall segment specimens which represent a quarter-size model of an element cut from the wall of a nuclear containment building as shown in Figure 1.1. The element in the structure is initially subjected to a biaxial compression due to prestressing. At high internal pressure loads the compressive stresses change to tensile stresses as shown in this figure. The specimens in the test program are planar rather than curved since this adequately represents the biaxial loading state of the wall element.

1.2 Objective of Wall Segment Tests

The wall segment tests have two main purposes: first, to investigate the load-deflection and cracking behavior of biaxially loaded wall segments under high overloads; and second, to provide data for use in calibrating and extending the inelastic analyses under development in the analytical phase of this research project. In particular, the formation and propagation of cracks is being studied to develop techniques to estimate the number and width of cracks.

1.3 Scope of this Report

Reference 1 presents detailed information about the wall segment tests including specimen properties, testing procedures, instrumentation and data reduction. Reference 2 critically reviews the test results presented in Ref. 1 and compares them to the BOSOR5 analysis developed in the analytical phase of this project. The tensile strength of concrete in the walls of containment vessels is also discussed in Ref. 2. Air leakage data from the segment tests is presented and analyzed in Ref. 3.

This report analyzes the cracking behavior of the wall segments and presents methods to predict the crack spacings and widths in containment structures. Chapter 2 gives an overview of the wall segment tests. Published descriptions of cracking of reinforced concrete are summarized in Chapter 3. The cracking data from the wall segment tests is presented in Chapter 4 and analyzed in Chapter 5. A procedure for estimating crack widths in containment structures is presented in Chapter 6 and conclusions are stated in Chapter 7.

1.4 Acknowledgements

The research project "Study of Concrete Containment Structures under Overpressure Conditions" was sponsored by the Atomic Energy Control Board of Canada and was under the general supervision of Dr. W.D. Smythe and Dr. F. Campbell of AECB. The project was directed by J.G. MacGregor with assistance from D.W. Murray and S.H. Simmonds. Mr. Declan Whelan initially served as technical liaison between AECB and the project directors. Since the summer of 1977 Dr. G.J.K. Asmis has served in this capacity. The progress of the project has been reviewed from time to time by an Advisory Committee with representatives from the Atomic Energy Control Board, Atomic Energy of Canada Limited, Canatom

Limited, Hydro Quebec and Ontario Hydro. The project directors wish to thank the members of this committee for the help and guidance received during the work.

The testing was carried out at the I.F. Morrison Structural Engineering Laboratory at the University of Alberta, Edmonton, Canada. Dr. S. Rizkalla was in charge of the laboratory work.

2. AN OVERVIEW OF THE TEST PROGRAM, SPECIMENS AND TECHNIQUES

2.1 Major Variables in Test Program

A total of 14 reinforced and prestressed concrete wall segments representing 1/4 size models of portions of the wall of a nuclear containment structure are included in this test program. Twelve of these are discussed in this report. A typical specimen is 31.5 in. square by 10.5 in. thick, reinforced in two directions and prestressed in one or two directions as shown in Fig. 2.1 and 2.2. Photographs of a specimen prior to casting, after casting and after testing are given in Fig. 2.3 to 2.5. The main variables under consideration are listed in Table 2.1 and include:

(a) Ratio of forces in the two directions

An internal pressure loading stresses the walls with hoop stresses (σ_1 = horizontal stress on element in Fig. 1.1a) which are twice the longitudinal stresses (σ_2 = vertical stresses on element shown). In the prototype structure these are offset by prestressing forces which are larger in the hoop stress direction. The majority of the specimens represent this case.

In the dome, the membrane stresses due to internal pressure are equal in the two directions and near the crown the prestress is also equal in two directions. Near the edges of the dome the prestress can be different in the two directions due to the geometry of the net of prestressing tendons. Several specimens approximate this loading history.

For correlation with the analysis and for studies of scale effects, a series of uniaxial tests are also included in the test program.

(b) Variations in Cover and Bar Spacing

Major variables in any theory for calculation of crack widths include the concrete cover to the bars and the bar spacing. These two quantities were varied in Specimens 1, 2 and 8 and in Specimens 5 and 6 to examine their relative effects on the location of cracks and the number of cracks that penetrate through the wall segments.

(c) Combined Axial Tension and Moment

Near the ring beam and the base connection, the walls and dome of the prototype structure is loaded by both axial forces and moments. Two specimens (Nos. 12 and 13) were loaded with eccentrically applied tension forces to simulate this condition.

(d) Reinforced Concrete Segments

Two segments had only non-prestressed reinforcement. The prestressed segment 3 and the unprestressed segment 4 have similar reinforcing bars in the two directions and can be compared. Specimen 7 is also unprestressed and was included to study scale effects.

(e) Scale Effects

The basic test specimens were 1/4 of the thickness of the prototype wall with No. 3 (3/8 in.) reinforcing bars as the main reinforcement. Specimens 4 and 7 which were 1/4 and 3/8 times the actual wall thickness were tested to study the effect of the size of the specimen on crack widths. Both had only non-prestressed reinforcement.

The diameter and spacing of the bars in the 3/8 size specimen were both 150% of those in the 1/4 size specimen. As a result the reinforcement ratio was the same in both specimens.

(f) Lap Splices

The effect of biaxial tensions on the behavior of lap splices was studied in two specimens (Nos. 9 and 11). Only the non-prestressed reinforcement in the horizontal direction was spliced in these tests. In segment 9 all the horizontal bars were lap spliced. In segment 11 every second horizontal bar was lap spliced. In both cases the vertical bars were closer to the surface than the horizontal bars.

(g) Air Leakage

The leakage of pressurized air from a chamber on one side of the specimen chamber on the other side was measured in two specimens reported in a separate report (Nos. 10 and 14). This was done to study the relationship between crack width and air leakage through the cracks.

2.2 Test Specimens

As stated earlier, typical wall segment specimens are shown in Fig. 2.1 to 2.5. In general, the specimens consist of 31.5 in. square concrete blocks, 10.5 in. thick and have layers of deformed bars and prestressing tendons in each direction as shown in the drawings and photographs. The three tendons located at the mid-plane of the specimen represent the vertical tendons which are at the middle of the walls in the prototype. The four perpendicular tendons represent the circumferential tendons. In the prototype these are located near the outer quarter point of the wall thickness and, due to the curvature of the wall, they produce a uniform compressive hoop stress through the wall thickness. In the wall segment specimens, the center two of these tendons are placed adjacent to one face to simulate the actual cover and spacing of these tendons while the remaining two are adjacent to the other face to maintain a uniform state of prestress through the wall thickness.

The concrete had a nominal compressive strength of 4500 psi and the deformed bar reinforcing had yield strengths of 58.2, 54.5 and 52.9 ksi, respectively, for the #3, #4 and #6 bars. The prestressing tendons consisted of six or seven individual smooth 0.276 in diameter wires contained in a 1.26 in. or 1.62 in inside diameter flexible metal sheath, a little more than a quarter of the diameter of the sheaths used in the prototype. The prestressing wires had a yield strength (stress at 1% strain) of 236 ksi and an ultimate tensile strength of 264 ksi.

Further details of the specimens and material properties are given in Tables 2.1 to 2.3 and Reference 1.

2.3 Loading Apparatus

The loading apparatus employed a 1,400,000 lb capacity MTS testing machine to apply the "circumferential" load to the specimen and a specially designed load frame and four, 200 kips hydraulic rams to apply the "longitudinal" load to the specimen. In the tests the specimen is turned through 90 degrees so that the circumferential load (horizontal in the prototype) is applied vertically in the laboratory as shown in Fig. 1.1b. This is done to make use of the large capacity of the MTS machine to apply the larger of the two loads. Cross-sections through the loading frame are shown as Fig. 2.6 and 2.7.

The vertical test loads were controlled by the MTS electro-hydraulic loading rate controllers. The horizontal loads were applied by tension rams controlled by a manually operated console which used air pressure to apply pressure to the hydraulic fluid.

2.4 Instrumentation

Approximately 140 items were recorded at each load level in the first three tests, including loads, strains and crack widths. This was increased to about 160 items in subsequent tests. Briefly, the data obtained and measuring devices included:

Vertical load - Measured by differential pressure transducers in MTS testing machine.

Horizontal load - Measured by electric resistance strain gages mounted on clevises between hydraulic rams and end fittings.

Forces transferred to tendons - Measured by electric resistance strain gages mounted on pull rods between end fittings and specimens.

Forces transferred to reinforcement - Measured by electric resistance strain gages mounted on six reinforcing bars between the specimen and the end fittings on each end of the specimen.

Reinforcement strains - Measured by twelve electric resistance strain gages mounted on the reinforcing bars and tendons and by mechanical extensometers refered to as "Demec gages" measuring between points mounted on plugs welded to the reinforcing bars to give an average strain over a 5 inch gage line.

Concrete strains - Measured by Demec gage points attached to the surface of the concrete and, until first cracking, by two, 4 inch electric resistance strain gages on each face of the specimen.

Elongation - Measured by LVDT displacement transducers and extensometers bearing on the ends of the specimens.

Crack widths - Measured using a hand held microscope. Two vertical and two horizontal lines were marked on each face and all cracks crossing these lines were measured.

Slip of Tendons - Measured by dial gages mounted on end couplers.

Prestress - The initial prestress and losses prior to grouting were measured by electric resistance strain gage load cells between the bearing plates and end fittings of the tendons.

The electric resistance strain gates and MTS load values were read directly by the Nova computer in the laboratory data acquisition system. Other readings were read and recorded manually.

Further details on the instrumentation and data reduction are given in Reference 1.

2.5 Test Procedure

A typical test of a wall segment took roughly 6 days to set up, one day to run and one day to dismantle. The set up process included placing and aligning the specimen in the testing machine and load frame, attaching the instrumentation, connecting the tendon pull rods and reinforcing bars. During this process the specimen was loaded to roughly one-third the cracking load and unloaded a number of times with adjustments being made each time to the tendon pull rods until the force transferred to each tendon was approximately equal. Following this, angles welded to the reinforcing bars were bolted to the end-fittings to transmit load directly into the reinforcing bars.

Zero load readings were taken the day of the test. Testing took six to eight hours, each load level requiring about 30-40 minutes. The majority of this time was spent marking cracks and measuring their widths, reading dial gages, and taking the Demec strain readings.

The horizontal loads were manually controlled, care being taken to apply load at an even rate and to prevent horizontal displacement of the specimen due to uneven rates of loading at the two ends. The vertical loads were either manually controlled to be the correct multiple of the horizontal load currently on the specimen or were controlled by presetting the rate of loading adjustment on the machine.

The magnitude of the load was held constant during measurement intervals except at the last one or two intervals prior to the end of the test. At very high loads, the deformations continued to increase during the measurement intervals by an amount enough to disrupt the readings. When this occurred, the elongation of the specimen was held constant during the measurement intervals and the loads tended to drop off by up to 5 percent.

Testing was terminated when the maximum tendon forces reached 95 to 98 percent of the breaking strength of the tendons. This was done to avoid damage to the instrumentation on the tendon pull rods.

3. WIDTH AND SPACING OF CRACKS IN REINFORCED AND PRESTRESSED CONCRETE

3.1 Introduction

There are many research reports on crack widths in reinforced and prestressed concrete members. The results reported are, first of all, highly variable, and secondly, highly dependent on the type of specimen tested, the manner of loading, and the shape of the deformations on the reinforcing bars in the specimen. As a result, no universally accepted theory or equation for crack widths exists. The following paragraphs will review the manner in which cracks form in reinforced concrete. This review is based in part on papers by Leonhardt [4], Beeby [5] and Reis et al. [6]. This will be followed by a review of crack width equations in the literature. A final section will consider the similitude of crack widths. The test data from the wall segment tests will be presented in Chapter 4 and compared to the various theories in Chapter 5.

3.2 Formation of Cracks in Reinforced Concrete

Figure 3.1 shows an axially loaded prism with one axial reinforcing bar. The tensile strength of the concrete varies along the length of the bar as shown by the top line in Fig. 3.1(b). At points located some distance from the ends of the bar the concrete stress will be uniform at f_t as shown by the shaded area in Fig. 3.1(b). The steel stress will be nf_t where n is the modular ratio, E_s/E_c. The first crack will occur when the tensile stress f_t reaches the tensile strength of the concrete in the weakest part of the bar. At the location of the crack, the entire load is resisted by tensile stresses in the reinforcing bar. The stress distribution in the concrete will then be as shown in Fig. 3.1(c). Within the transfer length, ℓ_t, the concrete stress will be less than f_t.

Because the first crack occurred where the concrete was weakest, the load must be increased before another crack can form. This crack will form at the next point where the applied load stress, f_t, reaches the tensile strength, f_t'. This point will not be closer than ℓ_t to the first crack as shown in Fig. 3.1(c). Cracks will continue to form until the spacing between all cracks is less than or equal to $2\ell_t$. After this occurs the tensile stress between the cracks will not reach f_t'. In tests, the final crack pattern is reached at steel stresses between 20 and 45 ksi (strains of 0.0007 and 0.0015) [4,5,6].

As a result of this sequence of crack development, the final crack pattern will consist of cracks with spacing, s, in the range:

$$\ell_t \leq s \leq 2\ell_t \tag{3.1}$$

This extreme variability in crack spacings leads to an equally extreme variability in crack widths. Beeby [7] has suggested the average crack spacing is about $1.33\ell_t$.

Once the cracking has reached a stabilized state the average crack width, w_m, can be calculated as the product of the average crack spacing, s_m, multiplied by the average strain, ε_m, minus the average strain in the concrete at the level at which cracks are being measured, ε_{cm}. Thus:

$$w_m = s_m(\varepsilon_m - \varepsilon_{cm}) \tag{3.2}$$

Since the strain in the concrete will tend to be small, it is frequently ignored giving:

$$w_m = s_m \varepsilon_m \tag{3.3}$$

It should be noted, however, that during the period in which cracks are still forming, w_m increases more slowly than ε_m since s_m decreases as ε_m increases.

Immediately prior to cracking, the stress in the steel can be computed from the transformed area as:

$$f_{s1,cr} = \frac{P_{cr}}{A_s(1 + \frac{1}{\rho n})} \tag{3.4}$$

where the reinforcement ratio, ρ, is commonly 0.003 to 0.02 and the modular ratio, n, is 7 to 10. The subscript 1 refers to the uncracked state. Alternatively, this can be calculated as

$$f_{s1,cr} = E_s \varepsilon_{cr} \tag{3.5}$$

where ε_{cr} is the strain in the concrete immediately prior to cracking. Since concrete cracks at strains of 0.00015 to 0.00025, the stress in the steel immediately prior to cracking will be roughly 4500 to 7500 psi.

Once a crack has formed in a tension member, the entire load is carried by the reinforcement crossing the crack giving a stress at the crack of:

$$f_{s2} = P/A_s \tag{3.6a}$$

The subscript 2 refers to the cracked state. Immediately after cracking this stress is

$$f_{s2,cr} = P_{cr}/A_s \tag{3.6b}$$

where P_{cr} is the cracking load.

A comparison of Eq. 3.4 and 3.6b shows that the steel stress at a crack will increase suddenly and sharply when the crack forms as shown in Fig. 3.2 [4]. Thus, the steel stress after cracking is $(1+1/\rho n)$ times the stress before cracking. This jump in steel stress tends to destroy the bond between the steel and concrete adjacent to the crack. In the case of members reinforced with plain bars or prestressed with smooth wires, the bars will slip relative to the concrete. In the case of deformed bars the loss or weakening of the bond will occur due to internal cracks extending into the concrete from each deformation lug as shown in Fig. 3.3 [8]. Generally the relative slip is smaller in such a case than for smooth bars and hence the transfer length ℓ_t is smaller. In either case, however, the jump in steel stress increases as the steel percentage decreases and as a result, ℓ_t adjacent to a crack tends to increase as the steel percentage decreases.

The internal cracks shown in Fig. 3.3 increase in size throughout the loading history to accommodate the difference between the concrete and steel strains. One result of this internal cracking is that the width of the crack tends to increase as one moves radially from the surface of the bar to the surface of the concrete.

3.3 Spacing of Cracks

Equation 3.1 gave the crack spacing as from 1 to 2 times the bond transfer length, ℓ_t. Different investigators have expressed ℓ_t in different ways.

(a) Bond Slip Theories

In 1936 Saliger [9] assumed that the force, P, transferred by bond in a given length ℓ_t is:

$$P = k_1 \mu_{max}(\pi d_b)\ell_t \tag{3.7}$$

where the average bond stress is expressed as a constant k_1 times the maximum bond stress μ_{max}. The surface area over which this acts is the perimeter πd_b times the transfer length. The transfer length ℓ_t is the length required to raise the concrete stress to the tensile strength, f_t'. Thus:

$$P = A_c \quad f_t' \tag{3.8}$$

and

$$A_c f_t' = k_1 \mu_{max}(\pi d_b)\ell_t \tag{3.9}$$

Substituting the reinforcement ratio, $\rho = [(\pi d_b{}^2/4)/_A c]$, and replacing $1/4k_1$ with k_2 gives:

$$\ell_t = k_2 \frac{d_b}{\rho} \frac{f_t'}{\mu_{max}} \tag{3.10}$$

If it is assumed that μ_{max} is related to f_t' since bond failure involves splitting of the concrete:

$$\ell_t = k_3 d_b/\rho \tag{3.11}$$

As a result, Saliger and many subsequent investigators have expressed the crack spacing in terms of:

$$s_m = k_4 \, d_b/\rho \tag{3.12}$$

The constant is obtained experimentally.

This calculation assumes that plane sections remain plane in the concrete so that the tensile stress in the concrete can be calculated using Eq. 3.8. This implies relative slip of the concrete and steel and ignores the St. Venant effect where the loads are introduced.

(b) No Slip Theories

A very different theory of crack spacing was advanced by Base et al. [10] and by Broms [11]. This assumed no slip of the bars and assumed that when a reinforcing bar extending through a reinforced concrete prism is loaded as shown in Fig. 3.4, the stresses will spread out roughly within a 45 degree cone becoming uniform where this cone reaches the edges of the prism. In this theory ℓ_t is equal to the minimum cover, c, measured from the surface of the bar, and:

$$s = k_5 \, c \tag{3.13}$$

where k_5 ranges from 1 to 2 as given in Eq. 3.1.

(c) Localized Bond Slip Theories

The true behavior is somewhere between the extremes implied by Eq. 3.12 and 3.13. The loads do spread out essentially as assumed in Eq. 3.13 but there definitely is some movement of the bar relative to the concrete due to slip or internal cracking. For this reason, Ferry-Borges [12] expressed the crack spacing as the sum of Eq. 3.12 and

3.13 with the appropriate constants:

$$s_m = k_6 c_o + k_7 d_b/\rho \tag{3.14}$$

Welch and Janjua [13] assumed the crack spacing was the sum of the unbonded length adjacent to the crack due to internal cracking plus the transfer length, ℓ_t, which was taken equal to c. Allowing for variations in the spacing of the cracks they expressed the crack spacing as:

$$s_m = 1.5 c + 3 d_b \tag{3.15a}$$

for deformed bars and

$$s_m = 1.5 c + 5 d_b \tag{3.15b}$$

for plain bars. The second term in each expression is the assumed unbonded length which is smaller for deformed bars due to the mechanical anchorage provided by the deformation lugs as shown in Fig. 3.3.

Leonhardt [4] expressed the minimum crack spacing as:

$$s_{min} = 0.5 \ell_o + \ell_t \tag{3.16}$$

where ℓ_o is the length of "almost lost bond" which is assumed to extend equally each way from the crack as shown in Fig. 3.3. For deformed bars he estimated this to be

$$\ell_o = \frac{f_{s2,cr}}{6500} d_b \tag{3.17}$$

where $f_{s2,cr}$ is the stress in the steel at the crack immediately after cracking in psi. For normal steel ratios ℓ_o will be 2 to 4 d_b, the value increasing as ρ decreases.

Leonhardt [4] expressed ℓ_t using Eq. 3.14 with the constant k_7 dependent on the type of bars and the stress gradient in the region of the crack. For deformed bars in a region of pure tension:

$$\ell_t = 1.2\ c + 0.1\ d_b/\rho \tag{3.18}$$

Beeby [5,7] has observed that the crack pattern in a beam is the result of the interaction between two basic crack patterns. Near the reinforcement the spacing was given by an equation similar to Eq. 3.14. In beams, the first term of this equation predominated, and the mean spacing in the vicinity of the reinforcement approaches 1.33 c. At points at a considerable distance from the bar, the crack spacing in beams was found to be related to h_{cr}, the distance that flexural cracks initially extend into the beam. For tension members Beeby concludes that the first effect (Eq. 3.14) governs the crack pattern and the mean crack spacing is given by:

$$s_m = 1.33\ c + 0.08\ d_b/\rho \tag{3.19}$$

where ρ is A_s/A with A equal to the area of concrete concentric with the bar in question.

For cracks measured at points not directly over the bar Beeby suggests the crack width at a radial distance a_{cr} from the bar is a_{cr}/c times that directly over the bar (at a distance c from the bar).

(d) Effect of Transverse Reinforcement on Crack Spacing

A number of investigators have observed a strong correlation between the spacing of reinforcement parallel to the cracks and the spacing of the cracks themselves. Beeby [14] concluded that transverse bars such as stirrups in beams have some influence on crack spacing but that this influence is only effective where the stirrup spacing and the expected crack spacing are similar. Nawy [15] has shown a strong relationship between crack spacing and the spacing of perpendicular bars.

3.4 Width of Cracks

(a) Bond-Slip Models

In 1936 Saliger [9] and Thomas [16] presented what are generally referred to as "bond-slip" theories to predict crack widths. They assume that plane sections remain plane in the concrete and that relative slip of the concrete and steel can occur either due to actual slip or some internal cracking mechanism. At a crack in the member shown in Fig. 3.5 all the force is resisted by tensile stresses in the steel. Bond stresses transfer some of this stress to the concrete so that a portion of the force is resisted by tensile stresses in the concrete and a portion by stresses in the steel.

The total change in length from half way between two cracks to half way between the next two cracks is equal to the elongation of the steel, ΔL_s, in the same length:

$$\Delta L_s = \int_0^S \varepsilon_{sx}\, dx \tag{3.20}$$

where ε_{sx} = the steel strain at any point x

$= f_{sx}/E_s$

This change in length is partially accounted for by the crack width w and partially by the elongation of the concrete, ΔL_c:

$$\Delta L_c = \int_0^s \varepsilon_{cx}\, dx \tag{3.21}$$

where ε_{cx} = the concrete strain at any point

= f_{cx}/E_c

Thus: $$w = \Delta L_s - \Delta L_c \tag{3.22}$$

or $$w = \int_0^s (\varepsilon_{sx} - \varepsilon_{cx})dx \tag{3.23}$$

Equation 3.2 is a simplified version of Eq. 3.23. If, as shown in Fig. 3.5(b), the maximum reduction in the steel stress is referred to as $\Delta f_{s,max}$, equilibrium requires that:

$$\Delta f_{s,max}\, A_s = f_{t,max}\, A_c$$

or $$f_{t,max} = \Delta f_{s,max}\, \rho \tag{3.24}$$

where $f_{t,max}$ is the maximum tensile stress in the concrete and $\rho = A_s/A_c$. (Note that Fig. 3.5(b) and (c) are to different scales).

Using the terms illustrated in Fig. 3.5, Eq. 3.21 can be evaluated as:

$$\Delta L_c = \frac{f_{t,max}}{E_c} \cdot s \cdot C \tag{3.25}$$

where C is a constant relating the area of the concrete stress diagram in Fig. 3.5(c) to a rectangle of area $f_{t,max} \cdot s$. For the parabolic diagrams shown, C = 2/3, for a triangular diagram C = 1/2, etc. Similarly

$$\Delta L_s = \frac{f_{s2} \cdot s}{E_s} - \frac{\Delta f_{s,max} \cdot s \cdot C}{E_s} \tag{3.26}$$

and the crack width is:

$$w = \frac{f_{s2} \cdot s}{E_s} - \frac{\Delta f_{s,max} \cdot s \cdot C}{E_s} - \frac{\rho \Delta f_{s,max} \cdot s \cdot C \cdot n}{E_s} \tag{3.27}$$

or

$$w = \frac{s}{E_s} [f_{s2} - \Delta f_{s,max} C(1 + \rho n)] \tag{3.28}$$

The major unknowns here are s, $\Delta f_{s,max}$ and C. Reference 6 reviews a number of attempts to solve this expression.

(b) No Bond-Slip Model

Broms [11] expressed the crack width as:

$$w_m = s_m \varepsilon_m \tag{3.29}$$

where s_m was taken as $2(c+d_b/2)$ and ε_m was the average strain in the steel. Unfortunately, no method of computing ε_m was given.

(c) Localized Bond-Slip Theories

The crack width theories based on localized bond slip generally speaking use some form of Eq. 3.2, 3.22 or 3.23 (all of which are essentially the same) to compute the crack width. The various theories differ primarily in the way in which s_m and ε_m are defined.

Welch and Janjua [13] computed the average crack width using

$$w_m = s_m \varepsilon_m \tag{3.30}$$

where s_m is given by Eq. 3.15 and

$$\varepsilon_m = \frac{f_s - 3 \text{ ksi}}{E_s} \tag{3.31}$$

The term 3 ksi is approximately equal to $nf_t'/2$ and is approximately the average stress in the concrete stress diagram in Fig. 3.5(c).

For a member loaded in axial tension Beeby [7] also used Eqn. 3.30 to predict the average crack width with s_m given by Eq. 3.19. The term ε_m was given as [5]:

$$\varepsilon_m = \varepsilon_{s2} - \frac{K\, f_t'\, f_{s2,cr}}{E_s\, \rho\, f_{s2}} \tag{3.32}$$

K is a constant depending on the type of bar.

Leonhardt [4] has presented a detailed procedure for computing the mean strains and crack widths. The crack spacing is assumed to be:

$$s = \ell_o + \ell_t \tag{3.33}$$

where ℓ_o is the unbonded length next to the crack (Eq. 3.17) and ℓ_t is the bond transfer length (Eq. 3.18).

Figure 3.6 is a load deformation diagram for an axially loaded reinforced concrete prism. The steel alone would develop strains, ε_{s2} corresponding to the dashed line (See Eq. 3.6a). The average strain over the entire length, ε_m is somewhat less, especially just after cracking. The difference between ε_m and ε_{s2} is referred to as "tension stiffening". If the cracking strain of the concrete, ε_{cr} is ignored as being very small, ε_m can be approximated by:

$$\varepsilon_m = \varepsilon_{s2}\left[1 - \left(\frac{f_{s2,cr}}{f_{s2}}\right)^2\right] \tag{3.34}$$

The crack width is computed as:

$$w = \varepsilon_{s2} \ell_o + \varepsilon_m \ell_t \tag{3.35}$$

This calculation is illustrated in Fig. 3.7. In the "almost unbonded" region, ℓ_o, adjacent to the cracks the steel elongates independently of the concrete. Between these regions the steel strain is lower.

(d) Empirical Cracking Relationships

Two other crack width studies should be mentioned.

Gergely and Lutz [17] statistically studied all available beam test results and concluded:

1. Steel stress was the most important variable.
2. Other important variables are the effective area around the bar, A, the side or bottom cover, c, and in beams, the ratio of the distance from the neutral axis to the bottom of the beam to the distance from the neutral axis to the reinforcement, R.
3. The bar diameter d_b was not a major variable.

It is interesting to note that all of the equations presented in this section include some of these variables. Based on their statistical analysis, Gergely and Lutz proposed:

$$w_{max}\text{(at level of steel)} = 0.091 \sqrt[3]{(c + d_b/2)\ A}\ (f_s - 5 \text{ ksi}) \times 10^{-3} \text{ in.} \tag{3.36}$$

Based on studies of floor slabs with orthogonal reinforcement in a given face, Nawy [15] proposed that the crack width be expressed as:

$$w_{max} = KRf_s \sqrt{I} \tag{3.37}$$

where I = grid index = $(d_{b1} \cdot t_2)/\rho_{e1}$

where 1 refers to bars in layer closest to surface, 2 refers to bars in inner layer, t is bar spacing.

This expression is of interest since it relates the crack width to the spacing of the bars in both directions.

3.5 Similitude of Crack Widths

If models are used to study structural behavior, certain rules of dimensional analysis must be considered in designing the tests and interpreting the results. If model and prototype have the same material properties the two structures are related only by a geometric scale factor (SF) and lengths and deflections scale accordingly. On the other hand, concentrated loads scale as SF^2, while stresses and strains have a scale factor of 1.

Ferry-Borges and Lima [12] concluded that similitude of flexural crack formation does exist and hence crack widths in a relatively large scale model would be SF times those in the prototype.

Kaar [18] tested quarter, half and full scale models of a 40 inch deep beam. He reported that the total number of cracks decreased with decreasing model size although the overall crack patterns were of the same general nature. He suggested that the crack widths were proportional to the square root of SF.

From tests of slabs with thicknesses ranging 4.5 in. to 15 in., Beeby [19] concluded that if the effects of bond, aggregate interlock and internal cracking all scale, the crack width should scale but the crack spacing would not.

Filho [20] carried out dimensional analyses of Beeby's crack width equation Eq. 3.32 and the Gergely-Lutz crack width equation, Eq. 3.36. In both cases the analyses showed that the crack widths were proportional to the scale factor. He also reported tests of 3/8 scale models of bridge pier caps and concluded that the crack widths scaled as SF and not as the square root of SF.

Although the literature is somewhat contradictory on the subject, Beeby's tests of cracking similitude and Filho's work both confirm that crack widths scale in the same proportion as dimensions. Filho cautions that one must consider relatively large scale models, however, and Beeby warns that the reinforcement must be similar to the prototype.

4. CRACKING IN WALL SEGMENT TESTS

4.1 Typical Sequence of Crack Development in Wall Segment Tests

The development of cracks in Specimen 2 will be described in this section. Specimen 2 was biaxially loaded with a loading ratio of 2:1, the vertical loads being largest. The crack development in this specimens was typical of other tests.

Prior to testing this specimen had several shrinkage cracks on Face A which was the top surface during casting. These are shown in Fig. 4.1. There were no such cracks on Face B. At a vertical load of 287 kips the first cracks developed in a horizontal direction on Face A. Fig. 4.2(a) and (b) show the extent of cracking at a vertical load of 300 kips. The first significant cracks on each face were roughly along reinforcing bars and coincided with the locations of the three transverse tendons.

Vertical cracks occurred on Faces A and B at horizontal loads of 183K and 200K, respectively. These cracks also occurred along reinforcing bars, especially on Face A as shown in Fig. 4.3(a). On Face B (Fig. 4.3(b)) the most pronounced vertical cracks followed the two outside vertical tendons which were close to this face.

The crack patterns at the end of the test are shown in Fig. 4.4. Vertical and horizontal cracks have formed at almost every reinforcing bar.

Although a few cracks extended straight through the specimens, most cracks tended to converge on a tendon. Figure 4.5(a) shows a section cut through the companion specimen, Segment 1, in a vertical direction. The cracks crossing this section are horizontal cracks. Two types of cracks can be seen. The cracks adjacent to the tendons converged on the tendons and penetrated the segment. A comparison of Fig. 4.2(a) and 4.5(a) indicates that the first horizontal cracks to form penetrated through the wall adjacent to the tendons. The cracks that formed away from the tendons penetrated into the segment as far as the steel and stopped there. Figure 4.5(b) shows a section cut through Segment 2 in the horizontal direction to intersect the vertical cracks. Again, the cracks converge on the tendons and penetrate the wall at roughly the tendon spacing. The cracks at the two end tendons were strongly affected by the load introduction zone.

Another cracking phenomenon noted in quite a few tests is shown in Fig. 4.6. Here the initial crack has formed parallel to the reinforcing bar as shown by the number 350 (referring to the load at which this crack was first observed). With further loading the two diagonal cracks marked 550 occurred. The transfer of force from a deformed bar to concrete is accomplished primarily by the bearing of the bar deformations on the concrete around the bar. This results in a wedging action which leads to splitting cracks which isolate wedge shaped pieces of concrete as shown in Fig. 4.6. At very high strains these pieces could come loose from the surface and fall. This would be especially true near lap splices or bar cutoffs.

4.2 Strains Measured in Wall Segment Tests

Strains were measured in three ways in the wall segment tests. Mechanical gages referred to as Demec gages were used to measure strains at the surface of the concrete on both faces. These gages had a 5 inch gage length and hence the "strains" measured in this way included strain in the concrete itself plus the opening of the cracks falling within the gage lengths. In a similar manner Demec gages were used to measure average steel strains on a series of 5 inch gage lengths. These measured the changes in length between plugs extending from the surface of the bar to the surface of the concrete. In addition, up to 12 electric resistance strain gages were mounted on the reinforcing bars in the specimens. These gave spot measurements of the reinforcement strains in isolated points in the specimens. The readings from the embedded gages on the steel have not been used in this report although a correlation of these readings and the Demec readings is given in Ref. 1.

The wall segment specimens were 31.5 by 31.5 by 10.5 in. in size. Loads were transferred to the edges of the specimens through tendons and reinforcing bars extending from these edges. To avoid the possibility that stress concentrations resulting from the load transfer caused atypical cracking or strains in the edge regions, all measurements taken within half the thickness from the edges were disregarded. As a result of the Demec strain gage placement, only the center 15 by 15 in. area of each face was considered in the analysis of crack width and strain data for specimens 1 to 3, and the center 20 by 20 in. area for specimens 5 to 13. Specimen 4 had measurements taken on a 15 by 15 in. area on one side and a 20 by 20 in. area on the other.

A typical load vs strain graph is shown in Fig. 4.7. Several things should be noted. The Demec gage had a dial gage graduated to 0.0001 in. Readings were reproducable by about 5 dial divisions, hence the strains were reliable to the nearest 0.0001 in/in (100 μ in/in strain). The strains on the two faces and on the steel and concrete differed due to the differing crack patterns on the two faces, round-off errors in reading the dial gages, and slight eccentricities in the loading system. At a load of 380 kips, corresponding roughly to the yield of the reinforcing bars, the differences between the three sets of Demec strains ranged from a low of 88 percent to a high of 114 percent of the average strain.

Throughout this report, the strains referred to are the averages of the concrete Demec strains for the two faces based on the 15 or 20 in. spaces referred to in the last paragraph. The procedures used to compute average strains are presented in Ref. 1 and extensive plots of these strains are given there.

4.3 Crack Widths Measured in Wall Segment Tests

(a) Method and Location of Measurements

During the tests, the widths of all the cracks crossing two horizontal and two vertical lines on each face of each specimen were measured using a hand microscope with a graduated optical scale. The microscope used for specimens 1, 2 and 3 was graduated to 0.1 mm (0.004 in.). The microscope used in the balance of the tests was graduated to 0.001 in. Readings were estimated to the nearest 0.5 division for crack widths greater than 1 division and to the nearest 0.2 division for smaller widths. Taking account of the crookedness of the cracks and the need for repeatedly measuring at the same point and in the same direction, it is believed the readings were reproducable to the nearest 0.5 division.

The measuring lines used were either directly over a reinforcing bar or halfway between two bars, typically at 5.25 in. and 9.75 in. from the top of the segment or a vertical edge of the segment.

(b) Reduction of Crack Width Data

To remove effects of the load transfer zone from the strain data, average strains were computed for the center 15 or 20 inches of each face of each segment as described in Section 4.2. A similar technique was used in reducing the crack width data. The technique used will be illustrated using Segment 2 as an example.

The locations of the cracks crossing the two horizontal lines and the two vertical lines on Face A (top face when specimen was cast) of Specimen 2 are plotted in Fig. 4.8 and 4.9, respectively. The cracks are numbered to show the sequence of formation. The letters V1 to V10 and H1 to H10 show the locations of the vertical and horizontal reinforcement. The shaded areas represent the tendon locations. The close relationship between the cracks and reinforcement locations can be seen in these figures.

Strain measurements were made in the 15 inch spaces between bars V3 and V8 and between H3 and H8. The crack widths and spacings reported in this section are also referred to this space. For cracks near the end of the measuring zone, such as crack 2 on line AH2 in Fig. 4.8, only a portion of the crack width was assumed to result from strains in the measuring zone. It was assumed that strains occurring in the zone extending from halfway between cracks 5 and 2 to halfway between cracks 2 and 3 would contribute to the width of crack 2. This total width is 3.1 inches of which 1.53 inches falls within the length over which strains were measured. Therefore, in computing the total width of cracks related to strains in the 15 inch measuring zone, (1.53/3.1) times the width of crack 2 was included. Thus, the total width of crack related to the strains was calculated by adding the widths of:

Crack 1 + (1.53/3.10) x Crack 2 + Crack 3 + (1.70/5.63) x
Crack 4 + Crack 6 + Crack 7 + similar quantity for Face B

The resulting width will be referred to as the "total crack width" or Σw. The term $\Sigma w/L$, where L was the total length considered in computing Σw (in this case 2 x 15 = 30 in.) is referred to as the average "crack strain".

The number of cracks in the measuring zones, in this case:

4 + (1.53/3.10) + (1.70/5.63) = 4.8 for Face A plus
a similar quantity for Face B

This number will be referred to as the "total number of cracks", n. The "average spacing" is computed as L/n. Finally, the average crack width is $\Sigma w/n$.

(c) Presentation of Crack Width Data The cracking loads and tensile stresses at first cracking are given in Table 4.1. The method of calculation used is discussed in Ref. 2. Values of load, average Demec strain, crack widths and average crack strain are given in Tables 4.2.1 to 4.2.13 for each of the walls. All measured cracks are included in these tables regardless of whether crack widths were measured directly over a bar or half way between two bars. The third number in the Table number is the segment number. Tables 4.2.1, 4.2.2 and 4.2.8 also report average crack spacing for segments 1, 2 and 8. on the lines located over the bars and those measured on the lines located between the bars. The strains are those measured on gage lines perpendicular to the cracks in each case.

Figures 4.10.1 to 4.10.13 show the crack patterns at the end of testing each of the segments. The third number in the figure number refers to the segment number. Figures 4.11.1 to 4.11.13 are histograms of the crack widths at various strains. With the exception of Segments 12 and 13, these diagrams present the combined data for cracks measured over the bars and those between the bars on Faces A and B. Since Segments 12 and 13 had moment about one or both axes of the specimen, separate plots are given for Faces A and B for these segments. The radial lines in these drawings represent the 50th and 75th percentile values.

5. DISCUSSION OF CRACK WIDTH DATA FROM WALL SEGMENT TESTS

Various procedures for computing crack widths and crack spacings are presented in Chapter 3. In general these theories indicate that the average crack width can be computed if the average spacing and average strains are known. These two quantities are discussed in Sections 5.1 and 5.2. The overall procedure used to calculate crack widths is given in Section 5.3 where it is compared to test data.

5.1 Crack Spacing and Sequence of Formation

(a) Cracks at Surface of Specimen

In Section 3.3 several procedures for estimating the crack spacing were discussed. These relate the mean spacing to:

1. the ratio of bar diameter, d_b, to the reinforcement ratio, ρ (Eq. 3.12);
2. the minimum cover to the surface of the bar, c, or the cover a_{cr} measured radially from the surface of the bar to the point where the cracks are being observed (Eq. 3.13);
3. some combination of 1. and 2. (Eq. 3.15);
4. the spacing of the bars which are parallel to the direction of the cracks.

The two extremes of bar cover in the tests were the cover of 0.5 in. on the vertical bars in Segments 1 and 2 and the cover of 1.63 in. on the horizontal bars in Segment 8. Figure 5.1 shows the change in average crack spacing in these segments (defined as n/L in Section 4.3(b)) as a function of strain. The average spacing decreases as more cracks form until the strain reaches about 0.0015 to 0.002 and then remains constant for the rest of the test. In the analysis that follows it will be assumed that the crack pattern has reached its final stage when ε equals 0.002.

Figure 5.2 compares the average crack spacing at 0.002 strain for all the specimens with 3 inch spacing of bars. The horizontal line represents the bar spacing and sets a lower bound on the data. The sloping lines are the crack spacings predicted by Eq. 3.19 modified to account for crack measurements taken at points not directly over the bars. There is no relationship between these lines and the data.

Figures 5.3 and 5.4 are similar plots for specimens with 4 in. and 6 in. bar spacings. Again the bar spacing is the lower limit on the crack spacing and again Eq. 3.19 does not fit the data.

A reinforcing bar has a modulus of elasticity 7 to 10 times that of the surrounding concrete. When a bar is embedded perpendicular to the direction of applied stress in a softer elastic medium, as shown in Fig. 5.5, the tensile stresses at A and B increase and those at C and D decrease slightly. If, however, the bond is broken at A and B, the stresses at C and D increase significantly, approaching those found adjacent to a circular hole. This stress concentration probably tends to reduce the average tensile stress required to crack the concrete. As a result, if a crack is expected in a given region, it will often occur at a transverse reinforcing bar. This is particularly true if the bar spacing is similar to the expected crack spacing. For bar spacings between a half and one times the minimum expected crack spacings the stress concentrations at the bars should be enough to cause cracking at the bar locations. For bar spacings between one and two times the minimum expected spacings, the formation of cracks along the bars should make additional cracks between the bars unlikely. Thus, cracks should be expected to follow bars if the bar spacing is between a half and two times the expected spacing.

As shown in Fig. 5.2 to 5.4 there was no significant difference between the crack spacings directly over the bars or those spacings measured half way between two cracks. Once a crack has occurred at one point along a transverse reinforcing bar, say directly over a perpendicular bar, it can be expected to propagate along the length of the transverse bar. As a result, the number of cracks at points between the perpendicular bars is essentially the same as it is over these bars.

(b) Through-the-Wall Cracks

The photographs of the faces of Segments 1, 2, 4, 5 and 12 and the sections cut through them in Fig. 4.10.1, 4.10.2, 4.10.4, etc. show that roughly one-half the cracks in the segments extended through the segments. In most cases the through the wall cracks divided near the surface to form two surface cracks. In all the wall segments which had prestressing tendons parallel to the cracks, the through-the-wall cracks occurred at prestressing tendons.

(c) Sequence of Crack Formation

As load was applied, the specimens initially cracked at one location. With further loading more cracks occurred reducing the crack spacing as shown in Fig. 5.1. The first cracks to form were through-the-wall cracks. The next stage of cracking saw these cracks dividing to form two cracks at the surface. At the surface the cracks coincided with reinforcing bar locations. The final stage of cracking involved surface cracks between the through-the-wall cracks. The surface cracks penetrated roughly as far as the reinforcement layer perpendicular to the cracks. The surface cracks developed at strains greater than about 80 percent of the yield strain of the reinforcing bars.

(d) Assumed Model of Crack Formation and Spacing

As a result of these observations, a series of rules were developed for use in computing the mean crack widths in the wall segment specimens. It is expected that the same rules would apply in the prototype structure.

1. If the spacing of transverse bars is between 0.5 and 2 times the crack spacing computed from Eq. 3.19, cracks will form along each of the transverse bars by the end of the test. The cracking will be limited to these cracks.
2. The spacing of cracks at the surface of the specimen is independent of the radial distance from the longitudinal bars (bars perpendicular to the cracks) to the point on the surface where the cracks are observed.
3. In walls containing prestressing tendons parallel to the direction of cracking, through-the-wall cracks will occur at the same spacing as the tendons. Each of these cracks will eventually subdivide into two surface cracks.
4. In walls without prestressing tendons parallel to the direction of cracking, through-the-wall cracks will occur at every second reinforcing bar and not further apart than the wall thickness.

5. The number of through-the-wall cracks will stabilize by the time the strain reaches 0.002. At any given strain less than 0.002 the number of through-the-wall cracks can be given as:

$$N = N_{twc} \left(\frac{\varepsilon_{s2} - \varepsilon_{s2,cr}}{0.002 - \varepsilon_{s2,cr}}\right) \qquad (5.1)$$

where N is the number of through the wall cracks at the load in question; N_{twc} is the final number of through-the-wall cracks according to assumptions 3 or 4; ε_{s2} is the strain in the reinforcing bars at the crack; ε_{cr} is the average strain at the onset of cracking.

6. At a strain of 0.002, surface cracks form so that the final spacing agrees with assumptions 1 and 2.

5.2 Mean Strain

As shown in Fig. 3.6 the mean strain, ε_m, measured over a gage length including several cracks is less than the strain in the reinforcement at the cracks. Leonhardt [4] has presented Eq. 3.34 to calculate the mean strain after cracking. This is compared to the measured mean strains and the mean strains from the BOSOR5 analyses in Fig. 5.6.1 through 5.6.11 (the third number refers to the Segment number). As can be seen the prediction of ε_m by either method is adequate to good depending on the specimen. It is interesting to note that Eq. 3.34 gives a satisfactory prediction of strains for Segments 9 and 11 which contained splices.

For the purposes of computing mean crack widths in the segment specimens the mean strain, ε_m, will be based on Eq. 3.34. To estimate the crack widths in the prototype, similar calculations can be carried out based on the strains from the BOSOR5 analyses.

5.3 Mean Crack Widths

(a) Calculation Procedure

Although many authors present relationships for the maximum crack widths, only mean crack width will be considered here. In view of the vast area of concrete surface which would crack in a containment vessel the mean width best represents the cracks governing potential leakage. In the analysis of crack widths it is necessary to distinguish between through-the-wall cracks which result in paths for leakage, and surface cracks which do not. In the calculations for comparison with test results both types must be considered. In leakage calculations the surface cracks can be ignored.

The calculation of the mean width of the through-the-wall cracks is based on Eq. 3.35 using the crack spacing model given in Section 5.1(d), and the mean strain based either on Eq. 3.34 or the mean strains from a BOSOR5 analysis. For comparison with the test data the following steps were involved:

1. The total number, N_{twc}, of through-the-wall cracks anticipated at the end of the test in the gage length, L, in which cracks were observed was taken as:

$$N_{twc} = \frac{n}{31.5} \times L \qquad (5.2)$$

where 31.5 in. was the total width of the specimen and n was taken as 3 if cracks were developing parallel to the 3 tendon direction (vertical cracks). In specimens without tendons parallel to the cracks n was taken as 5 if the bar spacing was 3 in., 4 if it was 4 in. and 3 for 6 in. bar spacings.

2. The stress and load-induced strain in the reinforcing bars at a through-the-wall crack at the cracking load were computed as:

$$f_{s2,cr} = \frac{P_{cr} - F_{se}}{A_s + A_p} \tag{5.3}$$

and

$$\varepsilon_{s2,cr} = f_{s2,cr}/E_s \tag{5.4}$$

where P_{cr} is the cracking load, F_{se} is the effective prestressing force after losses and A_s and A_p are the areas of reinforcing bars and prestressing tendons respectively. Leonhardt's relationship (Eq. 3.17) was used to calculate the effective unbonded length of bar at the cracks, ℓ_o. This was based on the diameter of a bar having the same cross-sectional area as the wires in the tendons (0.73 in. for 7 wire tendons, 0.68 for 6 wire tendons).

3. The bond transfer length, ℓ_t, was taken as:

$$\ell_t = s - \ell_o \tag{5.5}$$

where s was taken as the final spacing of the cracks at the end of the test, taken equal to the spacing of the tendons parallel to the crack or, in specimens without such tendons, as two times the surface bar spacing.

At each load level, P, at which crack widths were computed the following steps were carried out:

4. The stress and load-induced strain in the deformed bar reinforcement at a crack were calculated as:

$$f_{s2} = \frac{P - F_{se}}{A_s + A_p} \tag{5.6}$$

and

$$\varepsilon_{s2} = f_{s2}/E_s \tag{5.7}$$

If f_{s2} exceeded the yield strength of the reinforcing bars, the stress in the prestressing tendons was calculated from:

$$f_{p2} = \frac{P - A_s f_y}{A_p} \tag{5.8}$$

In this case the total strain in the tendons, was calculated from the stress-strain curve of the tendons.

5. The mean strain, ε_m, was calculated using Eq. 3.34.

6. The width w_{twc}, of a through-the-wall crack was calculated using Eq. 3.35. This width was assumed to be divided evenly between the two cracks which converge on a given tendon.

Surface cracks were assumed to occur after the through-the-wall cracks to relieve the tension built up in the concrete between the through-the-wall cracks. In the tests these cracks generally did not occur until the reinforcing bars had yielded at through-the-wall cracks. In the calculation of their width it was assumed that Eq. 3.17, 3.34 and 3.35 would be applied in a slightly modified form:

6. The tensile force at cracking in a reinforcing bar crossing a surface crack was taken equal to the tension force required to crack the concrete concentric to that bar. Thus:

$$f_{s,cr} = f'_t \, A/A_b \tag{5.9}$$

where $A = (2c + d_b)$(bar spacing)

7. The effective unbonded length at a surface crack was taken as:

$$\ell_{os} = \frac{f_{s,cr} \, d_b}{6500} \tag{5.10}$$

where $f_{s,cr}$ is in psi and d_b is the diameter of a surface bar.

8. The bond transfer length at such a crack was taken as:

$$\ell_{ys} = \text{(bar spacing)} - \ell_{os} \tag{5.11}$$

9. The width of the surface cracks was then computed using Eq. 3.35:

$$w_s = \varepsilon_{s2} \, \ell_{os} + \varepsilon_m \, \ell_{ts} \tag{5.12}$$

using ε_{s2} and ε_m from steps 4 and 5.

Once the mean widths of the through-the-wall cracks and surface cracks were known for a given load, the total width of cracks in the gage length L was calculated as follows:

10. The number of through-the-wall cracks, N was calculated using Eq. 5.1.

11. Before the reinforcing bars yielded, the total crack width was computed as:

$$\Sigma w = N \cdot w_{twc} \tag{5.13}$$

After yield of the reinforcing bars the total crack width was computed as:

$$\Sigma w = N \cdot w_{twc} + N_s \cdot w_s \tag{5.14}$$

(b) Comparison of Computed and Measured Crack Widths

Figures 5.7.1 to 5.7.13 compare the measured and computed crack widths. Here, as in the case of the mean strain, the agreement of measured and computed crack widths is adequate to good. In the range of loading from a strain of 0.0005 to 0.002, during the period that cracks are growing and extending, the mean ratio of measured to computed $\Sigma w/L$ was 1.07 with a coefficient of variation of 0.347 for axially loaded specimens without splices (Segments 1 to 6 and 8). This comparison was not made for very high strains due to yielding of the mild steel reinforcing at strains greater than about 0.0015 and the gradual loss of bond on the prestressing tendons.

Segment 7 was not included in the average quoted. The computed widths for this specimen were consistently lower than the measured ones. This is due primarily to the extensive shrinkage cracking in this specimen prior to testing. Several of these cracks did not extend during the test. If the measured crack width at zero load is added to the calculated widths, the resulting values agree quite well with the measured values.

5.4 Effects of Variables on Crack Widths

The effects of a series of variables are considered in the following sections. The discussion of the effects is limited to the range of mean strains, ε_m, from 0 to 0.002. The latter strain corresponds well developed yielding of the reinforcing bars coupled with some loss of bond on the tendons. Since this stage would represent an advanced stage of damage to the containment it was assumed that designs would be carried out to limit deformations to less than this value.

(a) Effect of Scale

The specimens tested were one-quarter scale models of segments cut from the containment walls. In Section 3.5, a number of studies the effect of scale on crack widths were reviewed. These concluded that in properly scaled models, crack widths should scale in the same ratio as the dimensions.

Segments 4 and 7 were tested to examine the scale effect. With the exception of the overall width and height of the specimens which remained at 31.5 in. in both cases, all dimensions in Segment 7 were 1.5 times the corresponding ones in Segment 4.

Figure 5.8 plots the median crack widths in Segments 4 and 7 as a function of the mean strains. The data exhibits a very large scatter, particularly in the case of Segment 4. Linear regression lines through the data are also plotted. The slope of the line for Segment 7 is 1.46 times that for Segment 4, suggesting that the crack widths increase in proportion to the scale as suggested in Section 3.5.

(b) Effect of Biaxial State of Stress at Cracking

Several of the segments had different levels of prestress in the two directions and were loaded at different rates in the two directions. As a result, the ratio of the stresses in the two directions varied during the test. This was further complicated by different cracking loads in the two directions. When a crack forms the tensions causing the crack are dissipated adjacent to the crack.

The effect of the biaxial stress state on cracking is examined in Fig. 5.9. The lines plotted in this figure are linear regression lines to each set of data. Although the lines are roughly parallel, their initial ordinates vary. The data falls into two groups:

1. The segments represented by solid points (Lines 2 and 3) had loads parallel to the crack equal to 0.5 or 1.0 times the loads causing the cracks considered in this plot. At the time the first cracks formed, the stresses parallel to the cracks were tensile in both cases and were about 30 percent of the cracking stress for the segments represented by solid circles (Line 2) and were about 100 percent of the cracking stress for the segments represented by solid triangles (Line 3).
2. The open symbols represent cracks in segments with zero loads and zero prestress parallel to the cracks (open triangles, Line 1), and segments in which the applied tensions parallel to the cracks had been dissipated by previous cracking perpendicular to the cracks plotted in Fig. 5.9 (open circles, Line 4).

Although it appears the transverse state of stress at the time of cracking affects the crack width, this effect is not large and has not been explained as yet. When a crack occurs in a homogeneous elastic body subjected to biaxial stress, the strain perpendicular to the crack, which would contribute to crack opening, changes from

$$\varepsilon = \frac{\sigma_1}{E} - \frac{\mu \sigma_2}{E}$$

before cracking to

$$\varepsilon = -\mu \frac{\sigma_2}{E}$$

after cracking. The total change in strain is the same regardless of the value of σ_2. The crack width model presented in Eq. 3.35 is a function on the equivalent unbonded length of bar adjacent to a crack. Although this would be expected to be larger if the transverse stress is tensile, the cracks appeared to open more slowly in this case.

The effect of the transverse stresses was ignored in the crack width calculations with relatively little error.

(c) Effect of Bar Splices

At strains up to 0.002, the presence of bar splices did not appear to affect the crack widths significantly as shown in Fig. 5.10. Every horizontal bar in Segment 9 was lap spliced and alternate horizontal bars were lap spliced in Segment 11. The crack widths in these segments are compared in Fig. 5.10 to the crack widths observed in Segments 1 and 2 which were similar in construction and loading. Regression lines are plotted in Fig. 5.10(b) to aid in the comparison. At high strains, large cracks opened up near the ends of the lapped splice.

It is important to note that the spliced bars were the inside layer and, as a result, had a layer of bars outside them to restrain the opening of cracks.

(d) Effect of Moments

Segment 12 was loaded axially in the vertical direction and subjected to an eccentrically applied horizontal load which caused Face A to be in tension while Face B was near zero strain. As a result, vertical cracks appeared only on Face A while horizontal cracks appeared on both faces. Figure 5.7.12(a) shows that the calculation procedure used in this report gives a reasonable estimate of crack widths in segments subjected to moment. The widths of the horizontal cracks are also closely estimated as shown in Fig. 5.7.12(b) and (c). The computed crack widths plotted in these diagrams were based on the average Demec strains. It is important to note that moment about one axis had little effect on the widths of cracks perpendicular to that axis.

Segment 13 was loaded with eccentrically applied loads in both directions. The loads were applied in such a manner that Face B was in tension and Face A near zero strain. Again the computed crack widths based on the measured surface strains are a reasonable estimate of the crack widths as shown in Fig. 5.7.13.

5.5 Closing of Cracks on Unloading

Several of the specimens were partially unloaded after cracking had occurred to observe the degree to which cracks closed on unloading. Except after the test was finished, the load was never completely removed due to the need to maintain alignment of the specimen, etc. In the prestressed specimens, the loads after unloading were chosen to be less than the effective prestress force so that compression existed across the cracks after unloading.

In no case did all the cracks close completely. This is believed to be a result of the internal cracking adjacent to the bars and possible slight misalignments of the crack surfaces. Cracks of 0.0001 to 0.0057 in. were observed after unloading with the average width being roughly 0.0013 in. If the specimens had been completely unloaded it is likely these widths would have been smaller. The change the crack strain, $\Sigma w/L$, corresponding to a change in average Demec strain is plotted in Fig. 5.11. The change in crack strain is roughly equal to:

$$\Delta(\Sigma w/L) = 0.5\Delta\varepsilon$$

The residual crack strain after unloading is plotted in Fig. 5.12 as a function of the strain before unloading. For average strains up to that corresponding to yield of the reinforcement, an upper bond to the residual strain was given by

$$\Delta\varepsilon - \Delta(\Sigma w/L) = \frac{\text{Strain Before Unloading}}{3}$$

5.6 Effect of Attachments

Although the presence or absence of attachments was not a variable per se, Segments 4 to 13 had 3/8 in. diameter holes extending into the specimen as far as the reinforcement on Face A. Segments 4, 6, 7, 10, 11 and 12 cracked first on face A with the initial cracks close to or at the holes. Segments 1, 2, 3, 5, 8 and 9 developed first cracking in regions without such holes. No significant difference was observed at the 5 percent level in the tensile stresses at the time of cracking in these two groups of specimens.

6. CALCULATION OF CRACK WIDTHS IN CONTAINMENT STRUCTURE

The calculation procedure used in Chapter 5 to calculate crack widths in the wall segment specimens can be applied with suitable modifications to the prototype structure. It is assumed in the following that the strains, ε_m, on the two surfaces are known from a BOSOR5 analysis of the structure. Since the results of a crack width analysis would be used to estimate leakage, the following calculation ignores surface cracks. The following steps are then required:

1. Determine the final pattern of through-the-wall cracks in each direction. This involves the following steps:

   (a) In walls containing prestressing tendons parallel to the direction of cracking, through-the-wall cracks will occur at the same spacing as the tendons but not farther apart than the wall thickness. Each of these cracks will eventually subdivide into two surface cracks.

   (b) In walls without prestressing tendons parallel to the direction of cracking, through-the-wall cracks will occur at every second reinforcing bar and not farther apart than the wall thickness.

   (c) In a Gentilly-2 type of structure the "circumferential" cracks in the dome are assumed to form along tendons forming hexagons concentric about the center of the dome. "Meridional" cracks are assumed to form along all other tendons in the dome.

2. Determine the number of cracks in each region in the wall as

$$N = \frac{\varepsilon_m}{0.002} \text{ x (Number of cracks from step 1)}$$

but not less than one fifth the final number of cracks from step 1, where ε_m is the strain from a BOSOR5 analysis for the surface in question. If this differs on the two faces, the larger number (larger surface strain) governs, except that if one face has not cracked there are no through-the-wall cracks in that region.

3. Compute the crack width as

$$w = \varepsilon_m \cdot s$$

where ε_m is the strain from a BOSOR5 analysis for the surface having the smaller strain perpendicular to the crack direction at the load under consideration.

4. Using the numbers of cracks from step 2 and the widths from step 3, it is possible to estimate the total length of crack of each width that exists at each load level.

7. SUMMARY AND CONCLUSIONS

The following observations and conclusions were drawn from the cracking behavior in the wall segment tests:

1. The initial load-induced cracks extend through the wall. The spacing of such cracks is governed primarily by the spacing of tendons parallel to the cracks.
2. The number of through-the-wall cracks increases as the strain increases. A fully developed pattern of through-the-wall cracks is reached at a strain of about 0.002.
3. When the through-the-wall cracking is fully developed subsequent loading causes surface cracks which penetrate roughly as far as the surface layer of reinforcement. The spacing of these cracks is governed primarily by the spacing of reinforcement near the surface.
4. The crack width can be calculated using Leonhardt's procedure using a calculated mean strain or the mean strain from a BOSOR5 Analysis.
5. In geometrically similar specimens the crack widths scale in proportion to lengths.
6. Biaxial tension stresses in uncracked concrete had a small effect on crack widths. This effect was ignored in the crack width calculations with very little error.
7. Lapped bar splices had no effect on crack widths at strains up to 0.002. At high strains, large cracks developed near the ends of the splices.

8. Although relatively little data is available, in no case did all the cracks close completely on unloading. The change in crack strain on unloading was about half the total change in strain. The residual crack strain that remained after unloading increased as the strain before unloading increased.

9. Holes in the surface of the specimen had no significant effect on the tensile strength at first cracking.

REFERENCES

1. Simmonds, S.H.; Rizkalla, S.H. and MacGregor, J.G.; "Tests of Wall Segments from Reactor Containments," Structural Engineering Report No. 81, Department of Civil Engineering, University of Alberta, Edmonton, Canada, November 1979.

2. Chitnuyanondh, L.; Rizkalla, S.; Murray, D.W. and MacGregor, J.G.; "An Effective Uniaxial Tensile Stress-Strain Relationship for Prestressed Concrete", Structural Engineering Report No. 74, Department of Civil Engineering, University of Alberta, Edmonton, Canada, February 1979.

3. Rizkalla, S.H.; Simmonds, S.H. and MacGregor, J.G.; "Leakage Tests of Wall Segments of Reactor Containments", Structural Engineering Report No. 80, Department of Civil Engineering, University of Alberta, Edmonton, Canada, October 1979.

4. Leonhardt, F.; "Crack Control in Concrete Structures", IABSE Surveys, S-4/77, IABSE Periodica 3/1977, International Association for Bridge and Structural Engineering, Zurich, August 1977.

5. Beeby, A.W., "The Prediction of Crack Widths in Hardened Concrete", The Structural Engineer, Vol. 57A, No. 1, Jan. 1979, pp. 9-17.

6. Reis, E.E. Jr.; Mozer, J.D.; Bianchini, A.C. and Kesler, C.E.; "Causes and Control of Cracking in Concrete Reinforced with High-Strength Steel Bars - A Review of Research", Engineering Experiment Station Bulletin 479, University of Illinois, Urbana, Illinois, Aug. 1965.

7. Beeby, A.W., "A Study of Cracking in Reinforced Concrete Members Subjected to Pure Tension", Technical Report 42.468, Cement and Concrete Association, London, June 1972.

8. Goto, Y.; "Cracks formed in Concrete around Deformed Tension Bars", Journal American Concrete Institute, Proc. Vol. 68, No. 4, April 1971, pp. 244-251.

9. Saliger, R.; "High Grade Steel in Reinforced Concrete", Preliminary Publication, 2nd Congress, International Association Bridge and Structural Engineering, Berlin-Munich, 1936, pp. 293-315.

10. Base, G.D.; Read, J.B.; Beeby, A.W. and Taylor, H.P.J.; "An Investigation of the Crack Concrol Characteristics of Various Types of Bar in Reinforced Concrete Beams", Research Report No. 18, Parts I and II, Cement and Concrete Association, London, Dec. 1966.

11. Broms, B.B.; "Crack Width and Crack Spacing in Reinforced Concrete Members", Journal of the American Concrete Institute, Vol. 62, No. 10, Oct. 1965, pp. 1237-1255.

12. Ferry-Borges, J. and Lima, J.A., "Crack and Deformation Similitude in Reinforced Concrete," RILEM Bulletin, No. 7, Paris, June 1960, pp. 79-90.

13. Welch, G.B. and Janjua, M.A., "Width and Spacing of Tensile Cracks in Reinforced Concrete", Uniciv Report No. R-76, School of Civil Engineering, University of New South Wales, Kensington, NSW, Australia, Dec. 1971.

14. Beeby, A.W., "An Investigation of Cracking on the Side Faces of Beams", Technical Report 42.466, Cement and Concrete Association, Slough, England, Dec. 1971.

15. Nawy, E.G. and Blair, K.W., "Further Studies on Flexural Crack Control in Structural Slab Systems", Cracking, Deflection and Ultimate Load of Concrete Slab Systems, SP-30, American Concrete Institute, Detroit, 1971, pp. 1-42.

16. Thomas, F.G., "Cracking in Reinforced Concrete," The Structural Engineer, Vol. 14, No. 7, July 1936, pp. 298-320.

17. Gergely, P. and Lutz, L.A., "Maximum Crack Width in Reinforced Concrete Flexural Members," Causes, Mechanism, and Control of Cracking in Concrete, SP-20, American Concrete Institute, Detroit, 1968, pp. 87-117.

18. Kaar, P.H., "An Approach to the Control of Cracking in Reinforced Concrete," Causes, Mechanism and Control of Cracking in Concrete, SP-20, American Concrete Institute, Detroit, 1968, pp. 141-157.

19. Beeby, A.W., "An Investigation of Cracking in Slabs Spanning One Way," Technical Report TRA 443, Cement and Concrete Association, London, April 1970.

20. Filho, F.M.G., "A Simplified Test Method for Determination of Reinforced Concrete Side Face Crack Profiles", M.S. Thesis, University of Texas at Austin, May 1977.

Table 2.1 - Overview of Variables Considered in Wall Segment Tests

Specimen*	Prestressed	Non-Prestressed Reinforcement per Layer, 1**	Min. Concrete Cover in.	Loading Ratio H/V	Applied Moment	Thickness in.	Lap Splices
1	two	10 #3 @ 3 in.	0.5	1:2		10.5	
2	two	10 #3 @ 3 in.	0.5	1:2		10.5	
3	two	10 #3 @ 3 in.	0.5	1:1		10.5	
4	none	8 #4 @ 4 in.	0.5	1:1		10.5	
5	one***	10 #3 @ 3 in.	0.5	1:0		10.5	
6	one***	8 #4 @ 4 in.	0.5	1:0		10.5	
7	none	6 #6 @ 6 in.	0.75	1:1		15.75	
8	two	10 #3 @ 3 in.	1.25	1:2		10.5	
9	two	10 #3 @ 3 in.	0.5	1:2		10.5	yes
11	two	10 #3 @ 3 in.	0.5	1:2		10.5	yes
12	two	10 #3 @ 3 in.	0.5	1:2	yes	10.5	
13	two	10 #3 @ 3 in.	0.5	1:2	yes	10.5	

* Two additional tests involving air leakage (Specimens 10 and 14) are presented in Reference (3).

** Each face of the specimen had one such layer in each direction.

*** Three tendon direction only, other tendons omitted.

Table 2.2 Prestress in Tendons

Specimen	Vertical Tendons (4 Tendon Direction)			Vertical Tendons (3 Tendon Direction)		
	Initial	Effective after Losses		Initial	Effective after Losses	
	Stress, ksi	Stress, ksi	Force, ksi	Stress, ksi	Stress, ksi	Force, kips
1	153.5	135.1	226.3	134.0	123.3	132.7
2	151.6	133.4	223.5	134.9	124.1	133.6
3	153.3	134.9	226.0	135.2	124.3	133.9
4	-	-	-	-	-	-
5	-	-	-	132.0	121.4	130.8
6	-	-	-	138.0	126.9	136.7
7	-	-	-	-	-	-
8	154.0	135.6	227.1	139.9	128.7	138.6
9	150.6	132.6	222.1	134.3	123.6	133.1
10	152.4	134.1	225.3	134.0	123.3	132.8
11	151.5	133.3	223.3	135.0	124.2	133.8
12	152.8	134.5	225.2	135.8	124.9	134.6
13	152.4	134.1	225.3	134.0	123.3	133.1
14	-	-	-	134.0	123.3	133.1

Table 2.3 Strengths and Modulus of Elasticity of Concrete

			From Cylinder Tests					From Specimen	
Specimen No.	Age At Prestress Days	Age At Test Days	Compressive Strength psi	Split Tensile Strength psi	$f_t/\sqrt{f'_c}$	Modulus of Elasticity 10^3 ksi	$E_c/\sqrt{f'_c}$	Modulus of Elasticity 10^3 ksi	$E_c/\sqrt{f'_c}$
1	30	84	5093	490	6.87	-	-	3.76	52.7
2	30	92	4456	436	6.53	-	-	3.92	58
3	35	99	5690	426	5.65	-	-	3.22	42
4	-	109	5590	536	7.17	3.23	43.2	3.47	46.4
5	63	109	5690	444	5.89	4.22	55.9	3.51	46.5
6	57	127	4540	325	4.82	3.53	52.4	3.37	50.0
7	-	104	2390 (A)*	312 (A)	5.44 (A)	-	-	4.05	68.5
			3720 (B)*	365 (B)	5.99 (B)				
8	42	92	4920	424	6.04	3.82	54.5	5.56	50.8
9	76	159	3920	437	6.98	3.08	49.2	3.57	57.0
11	-	186	4920	411	5.86	3.10	44.2	4.11	70.1
12	131	372	5930	486	6.31	3.52	45.7	-	-
13	63	391	6130	566	7.23	-	-	-	-

* Specimen 7 was made from two batches, one on face A, and the other on face B.

Table 4.1 Load and Tensile Stress at First Cracking

Segment	Vertical Load at First Horizontal Cracking, kips		Horizontal Load at First Vertical Cracking kips		Tensile Stress at First Cracking, psi
	Face A	Face B	Face A	Face B	
1	300.0	325.0	194.0	179.3	307
2	287.5	300.0	183.5	200.0	174
3	350.0	300	206.8	206.8	229
4	80.3	60	60	60	259
5	--	--	280.2	255.5	389
6	--	--	185.0	196.0	223
7	75.1	100.0	82.1	82.1	168
8	350.0	350.0	175.0	175.0	321
9	350.0	300.0	181.8	181.8	221
11	284	300	175	175	170
12	300	340	170	--	292
13	--	175	--	150	300

The underlined values indicate the loads and faces corresponding to the reported tensile stresses at first cracking.

TABLE 4.2.1

Crack Width and Average Strain Data for Segment 1

Load, kips V:H	Strain in.x10^3	No. of Cracks	Crack Widths, in.x10^3 Mean	50%ile	75%ile	Maximum	Average Crack Strain $(\Sigma w/L)$x10^3	Average Crack Spacing in.
(a) Horizontal Cracks								
350.5:179.3	.7015	5	1.7	1.2	1.9	3.94	.132	17.43
400:202.7	1.252	10	3.3	2.0	3.7	7.87	.514	10.97
450.5:228.1	1.830	13	3.4	2.6	3.9	7.1	.713	6.15
150:75	.5233	4	0.6	.4	.8	.8	.04	--
500.7:253.8	2.603	21	4.4	3.3	4.9	11.8	1.394	4.22
547.3:275.4	4.587	24	9.3	4.3	7.0	35.4	3.514	3.82
547.5:328.2	4.965	25	9.6	5.2	10.7	39.4	3.526	3.82
5:5	3.292	22	6.9	2.0	7.5	29.52	2.37	--
(b) Vertical Cracks								
350.5:179.3	.2288	7	1.2	1.2	1.7	3.93	.135	12.62
400:202.7	.5000	11	3.2	2.4	3.2	3.93	.357	7.74
450.5:228.1	.9100	9	3.9	3.3	3.9	4.72	.547	7.74
500.7:253.8	1.305	12	3.1	2.5	4.0	5.90	.514	6.71
547.3:275.4	1.917	12	3.9	3.5	5.0	6.30	.728	6.71
547.5:328.2	2.257	17	5.2	3.4	5.2	15.75	1.331	5.23
5:5	.3917	10	3.0	2.0	3.2	7.87	.48	--

TABLE 4.2.1 (continued)

Crack Width and Average Strain Data for Segment 1

Load, kips V:H	Strain in.x10^3	No. of Cracks	Mean	Crack Widths, in.x10^3 50%ile	75%ile	Maximum	Average Crack Strain $(\Sigma w/L)$x10^3	Average Crack Spacing in.
(c) Horizontal Cracks (Measured Over Bars)								
350.5:179.3	.7015	2	0.6	1.0	1.5	2.0	.0286	18.87
400:202.7	1.252	4	2.7	1.3	2.0	6.0	.3123	8.36
450.5:228.1	1.83	8	3.1	1.6	4.0	8.0	.7651	4.10
150:75	.5233	2	0.6	1.0	1.5	2.0	.04	--
500.7:253.8	2.603	10	4.4	3.2	5.0	12.0	1.356	3.4
547.3:275.4	4.587	10	11.3	5.0	9.0	36.0	3.566	3.4
547.5:328.2	4.965	11	10.2	5.2	12.5	32.0	3.348	3.4
5:5	3.292	10	7.6	2.0	16.5	24.0	2.37	--
(d) Vertical Cracks (Measured Over Bars)								
350.5:179.3	.2288	4	1.6	1.3	2.0	4.0	.2008	8.11
400:202.7	.5000	6	3.3	2.5	3.2	4.0	.6168	5.26
450.5:228.1	.9100	4	3.7	3.0	3.5	4.0	.4593	5.26
500.7:253.8	1.305	6	2.9	2.7	3.7	6.0	.5131	4.78
547.3:275.4	1.917	6	3.2	2.7	3.7	6.0	.5814	4.78
547.5:328.2	2.257	7	5.4	3.7	5.2	12.0	1.084	4.38
5:5	.3917	4	4.2	3.0	4.0	8.0	.45	--

TABLE 4.2.1 (continued)

Crack Width and Average Strain Data for Segment 1

Load, kips V:H	Strain in.x10^3	No. of Cracks	Crack Widths, in.x10^3 Mean	50%ile	75%ile	Maximum	Average Crack Strain $(\Sigma w/L)x10^3$	Average Crack Spacing in.
(e) Horizontal Cracks (Measured Between Bars)								
350.5:179.3	.7015	3	2.4	1.5	2.5	4.0	.2362	10.0
400:202.7	1.252	6	3.8	2.7	3.7	8.0	.7152	5.26
450.5:228.1	1.83	5	3.9	3.2	3.9	6.0	.6601	5.26
150:75	.5233	2	0.6	1.0	1.0	1.0	.04	--
500.7:253.8	2.603	11	4.4	3.4	4.8	10.0	1.433	2.96
547.3:275.4	4.587	14	7.8	3.6	6.5	36.0	3.463	2.48
547.5:328.2	4.965	14	9.0	5.0	9.0	40.0	3.705	2.48
5:5	3.292	12	6.4	2.0	7.0	30.0	1.28	--
(f) Vertical Cracks (Measured Between Bars)								
350.5:179.3	.2288	3	0.8	1.0	1.5	2.0	.0696	1.36
400:202.7	.5000	5	3.1	2.3	3.2	4.0	.4777	6.47
450.5:228.1	.9100	5	4.1	3.7	4.7	6.0	.6352	6.47
500.7:253.8	1.305	6	3.4	2.0	4.5	6.0	.6352	5.32
547.3:275.4	1.917	6	4.7	4.7	5.7	8.0	.8753	5.32
547.5:328.2	2.257	10	5.1	3.0	5.0	16.0	1.577	5.32
5:5	.3917	6	2.1	1.5	2.5	4.0	.210	--

TABLE 4.2.2

Crack Width and Average Strain Data for Segment 2

Load, kips V:H	Strain in.x10^3	No. of Cracks	Crack Widths, in.x10^3 Mean	50%ile	75%ile	Maximum	Average Crack Strain $(\Sigma w/L)x10^3$	Average Crack Spacing in.
(a) Horizontal Cracks								
298.5:154.4	.8233	7	2.5	2.2	3.1	3.94	.2887	11.43
350.6:181.2	1.572	19	2.3	1.9	3.1	4.72	.6824	4.52
200:100	.6667	17	1.3	1.1	1.6	4.72	.3185	--
348.7:183.6	1.538	19	2.1	1.9	3.1	4.72	.5906	4.52
400.5:202.7	1.837	18	3.1	2.7	3.5	7.1	.8727	4.32
453.4:230.9	2.33	22	3.5	3.0	3.9	7.87	1.122	4.32
200:101	.7933	20	2.5	2.3	3.2	3.94	.731	--
450.9:230.8	2.34	23	3.5	3.0	3.7	7.87	1.1352	4.01
498.4:255.2	3.6	23	4.6	3.9	5.3	13.0	1.5354	4.01
546:279.2	7.12	22	14.1	12.0	19.7	31.5	4.3924	4.01
545.6:354.3	9.16	22	22.0	22.7	29.0	39.4	6.7421	4.01
545.9:389.8	9.625	16	26.8	28.0	36.0	51.2	6.3360	4.01
1.7:7.0	7.65	9	16.4	17.0	21.5	25.6	6.24	--
(b) Vertical Cracks								
298.5:154.4	.2133	0	0.0	0.0	0.0	0.0	0.0	--
350.6:181.2	.2967	5	2.1	1.7	2.7	3.2	.1706	17.82
200:100	.1983	5	1.9	1.2	1.9	3.2	.153	--
348.7:183.6	.35	5	2.3	2.3	3.2	3.2	.1831	17.82
400.5:202.7	.4583	7	3.2	3.0	3.7	4.3	.2638	17.74
453.4:230.9	.725	10	3.8	2.7	4.5	5.9	.4738	11.43
200:101	.2683	10	2.4	1.7	2.7	3.2	.248	--
450.9:230.8	.7317	17	3.1	2.4	3.6	5.1	.7828	5.97
498.4:255.2	.920	16	4.0	3.4	5.3	7.87	.9731	5.56
546.0:279.2	1.640	16	3.6	2.0	5.0	9.84	.9738	5.56
545.6:354.3	2.39	17	8.5	5.0	15.5	19.7	2.157	5.2
545.9:389.8	4.264	13	22.0	16.5	21.5	80.7	5.155	5.2
1.7:7.0	2.592	15	10.1	7.0	14.5	31.5	3.197	--

TABLE 4.2.2 (continued)

Crack Width and Average Strain Data for Segment 2

Load, kips V:H	Strain in.x10^3	No. of Cracks	Crack Widths, in.x10^3 Mean	50%ile	75%ile	Maximum	Average Crack Strain $(\Sigma w/L)$x10^3	Average Crack Spacing in.
(c) Horizontal Cracks (Measured Over Bars)								
298.5:154.4	.8233	4	2.0	1.3	2.0	4.0	.2625	7.5
350.6:181.2	1.572	9	2.2	2.2	3.1	4.0	.6037	3.6
200:100	.6667	7	1.0	1.0	1.5	2.0	.1166	--
348.7:183.6	1.538	9	1.7	1.5	2.5	4.0	.4331	3.6
400.5:202.7	1.837	8	2.6	2.0	3.0	4.0	.6430	3.42
453.4:230.9	2.330	11	3.0	2.6	3.7	6.0	.9318	3.07
200:101	.7933	11	2.3	1.8	2.9	4.0	.4216	--
450.9:230.8	2.340	12	3.1	2.9	3.7	6.0	1.037	2.94
498.4:255.2	3.600	12	3.8	4.0	5.0	6.0	1.260	2.94
546:279.2	7.120	11	10.4	7.0	12.5	32.0	3.509	2.94
545.6:354.3	9.160	11	20.6	21.0	26.5	36.0	6.581	2.94
545.9:389.8	9.625	7	23.6	23.0	34.5	40.0	5.008	2.94
1.7:7.0	7.650	5	14.6	11.0	17.5	24.0	2.433	--
(d) Vertical Cracks (Measured Over Bars)								
298.5:154.4	.2133	0	0.0	0.0	0.0	0.0	0.0	--
350.6:181.2	.2967	2	3.1	3.0	3.5	4.0	.21	15.0
200:100	.1983	2	2.6	2.0	3.0	4.0	.087	--
348.7:183.6	.3500	2	3.0	3.0	3.5	4.0	.1969	15.0
400.5:202.7	.4583	4	3.5	3.3	4.0	6.0	.2782	14.85
453.4:230.9	.7250	5	4.6	3.5	5.5	8.0	.4882	11.9
200:101	.2683	5	3.0	2.7	3.4	4.0	.1875	--
450.9:230.8	.7317	8	3.5	3.0	4.0	8.0	.7782	5.36
498.4:255.2	.9200	8	3.9	3.3	5.0	8.0	.8832	5.36
546:279.2	1.640	8	3.8	2.0	5.3	10.0	1.003	5.36
545.6:354.3	2.390	9	9.9	5.5	16.7	20.0	2.476	4.55
545.9:389.8	4.264	7	31.2	19.0	39.2	82.0	4.55	4.55
1.7:7.0	2.592	7	14.5	12.5	24.5	32.0	1.692	--

TABLE 4.2.2 (Continued)

Crack Width and Average Strain Data for Segment 2

Load, kips V:H	Strain in.x10^3	No. of Cracks	Crack Widths, in.x10^3 Mean	50%ile	75%ile	Maximum	Average Crack Strain $(\Sigma w/L)x10^3$	Average Crack Spacing in.
(e) Horizontal Cracks (Measured Between Bars)								
298.5:154.4	.8233	3	3.1	3.0	3.5	4.0	.3150	10.0
350.6:181.2	1.572	10	2.4	1.7	3.0	6.0	.7612	3.21
200:100	.6667	10	1.5	1.1	1.7	6.0	.250	--
348.7:183.6	1.538	10	2.4	2.4	3.4	6.0	.7480	3.21
400.5:202.7	1.837	10	3.6	3.1	3.9	8.0	1.102	3.08
453.4:230.9	2.330	11	4.0	3.3	4.2	8.0	1.312	3.08
200:101	.7933	9	2.6	2.7	3.4	4.0	.390	--
450.9:230.8	2.340	11	3.8	3.1	3.6	8.0	1.234	3.08
498.4:255.2	3.600	11	5.4	3.8	6.5	14.0	1.811	3.08
546:279.2	7.120	11	17.9	19.0	22.8	32.0	5.276	3.08
545.6:354.3	9.160	11	23.3	26.5	32.2	40.0	6.903	3.08
545.9:389.8	9.625	9	29.3	33.0	39.5	52.0	7.664	3.08
1.7:7.0	7.650	4	18.7	20.0	22.0	28.0	1.247	--
(f) Vertical Cracks (Measured Between Bars)								
298.5:154.4	.2133	0	0.0	0.0	0.0	0.0	0.0	--
350.6:181.2	.2967	3	1.4	1.0	1.5	2.0	.1312	12.05
200:100	.1983	3	1.4	1.0	1.5	2.0	.070	--
348.7:183.6	.3500	3	1.8	1.5	2.5	4.0	.1706	12.05
400.5:202.7	.4583	3	2.8	2.5	3.3	4.0	.2493	12.05
453.4:230.9	.7250	5	3.0	1.7	3.5	6.0	.4593	6.7
200:101	.2683	5	1.8	1.0	1.5	2.0	.150	--
450.9:230.8	.7317	9	2.8	1.8	3.2	6.0	.7874	3.85
498.4:255.2	.9200	8	4.0	3.5	6.0	8.0	1.063	3.41
546:279.2	1.640	8	3.3	2.0	4.0	8.0	.9449	3.41
545.6:354.3	2.390	8	6.8	4.0	8.0	20.0	1.837	3.41
545.9:389.8	4.264	6	11.2	8.0	17.0	22.0	3.806	3.41
1.7:7.0	2.592	8	6.2	2.0	8.0	18.0	.826	--

TABLE 4.2.3

Crack Width and Average Strain Data for Segment 3

Load, kips V:H	Strain in.x10^3	No. of Cracks	Crack Widths, in.x10^3 Mean	50%ile	75%ile	Maximum	Average Crack Strain $(\Sigma w/L)x10^3$
(a) Horizontal Cracks							
206.6:206.8	.1067	0	0.0	0.0	0.0	0.0	0.0
255.1:255.5	.1617	0	0.0	0.0	0.0	0.0	0.0
304.1:307.5	.2767	1	.8	.8	0.8	0.8	.0197
105.4:106.3	.0883	1	.8	.8	0.8	0.8	.019
300:306.3	.315	1	1.2	1.0	1.2	1.2	.0262
354.3:356.3	.575	4	1.9	1.3	2.0	3.93	.1312
403.9:354	1.087	9	2.1	1.5	2.7	5.11	.2625
378.8:378.4	1.043	8	2.8	2.8	3.6	6.3	.2396
454:380.8	1.632	11	3.6	3.2	3.8	7.87	.5184
105.8:107.9	.23	6	.6	1.0	1.5	2.76	.114
453.7:375	1.715	12	3.6	3.1	4.0	7.87	.5643
503.6:375	2.242	12	4.8	4.0	6.0	9.84	.7415
530:375	2.455	11	5.8	5.	6.5	9.84	.8268
4.5:5.7	.66	10	2.2	1.4	2.5	7.87	.2261
(b) Vertical Cracks							
206.6:206.8	.080	6	3.0	2.7	3.7	3.94	.265
255.1:255.5	.8267	16	2.6	2.5	3.5	5.5	.723
304.1:307.5	1.397	19	3.8	3.3	4.1	7.87	1.0613
105.4:106.3	.3467	14	1.9	1.4	2.3	5.9	1.0136
300:306.3	1.455	21	4.3	3.6	5.1	7.87	1.376
354.3:356.3	2.118	22	4.5	4.6	5.7	7.87	1.6
403.9:354	2.292	25	4.9	4.9	6.5	8.66	1.738
378.8:378.4	2.45	16	5.3	4.4	6.0	9.84	1.68
454:380.8	2.635	14	6.1	5.5	7.7	9.84	1.77
105.8:107.9	1.09	8	3.7	3.0	4.0	7.87	.9436
453.7:375	2.70	17	6.8	6.2	7.6	11.8	2.01
503.6:375	2.91	19	7.6	6.9	8.2	11.8	2.065
530:375	2.91	16	8.5	8.0	10.0	15.75	2.45
4.5:5.7	1.173	13	5.4	5.0	6.7	7.87	1.355

TABLE 4.2.4

Crack Width and Average Strain Data for Segment 4

Load, kips V:H	Strain in.x10^3	No. of Cracks	Crack Widths, in.x10^3 Mean	50%ile	75%ile	Maximum	Average Crack Strain $(\Sigma w/L)$x10^3
(a) Horizontal Cracks							
80.2:84.9	.5537	4	4.2	4.0	6.0	7.0	.2417
100.1:105.5	.845	10	3.3	1.7	6.5	9.0	.45
1.7:5.6	.3683	7	1.6	1.7	2.8	3.0	.1594
100.1:106	.959	19	2.6	2.6	3.8	8.0	.441
120.6:124.6	1.209	20	3.4	3.1	4.0	11.0	.6164
140.6:143.7	1.472	21	4.1	3.9	5.6	12.0	.7637
160.7:159.9	2.667	23	18.3	7.5	31.5	56.0	3.639
(b) Vertical Cracks							
80.2:84.9	.8483	10	4.1	4.0	5.7	10.0	.3581
100.1:105.5	1.162	13	5.0	5.5	7.4	10.0	.5066
1.7:5.6	.506	12	2.4	3.0	3.7	4.0	.24
100.1:106	1.248	21	5.2	4.8	8.7	12.0	.7746
120.6:124.6	1.461	24	5.9	5.3	10.4	14.0	.8480
140.6:143.7	1.907	27	5.3	3.7	9.2	15.0	1.04
160.7:159.9	5.087	26	21.2	6.0	37.0	60.0	3.357

TABLE 4.2.5

Crack Width and Average Strain Data for Segment 5

Load, kips V:H	Horizontal Strainx10^3	No. of Cracks	Crack Widths, in.x10^3 Mean	50%ile	75%ile	Maximum	Average Crack Strain $(\Sigma w/L)x10^3$
(b) Vertical Cracks							
0:280.2	.5721	19	3.2	3.4	4.6	7.0	.435
0:305	1.099	29	4.1	3.6	6.2	10.0	.871
0:330	1.291	31	5.2	4.9	6.9	12.0	1.24
0:8.5	.1496	19	0.8	1.2	1.8	2.0	.104
0:105.3	.2575	29	0.7	1.2	1.7	3.0	.222
0:208.1	.6954	31	2.4	2.9	3.6	6.0	.6096
0:330.4	1.454	31	4.8	4.6	6.6	12.0	1.186
0:354.9	1.502	31	6.2	6.3	7.7	15.0	1.521
0:379.2	1.617	31	6.2	5.7	8.8	15.0	1.85
0:399.7	2.767	31	12.3	9.5	15.7	35.0	2.891
0:411.9	4.358	16	12.6	10.0	21.0	24.0	3.623
0:5.4	4.171	28	21.8	21.7	30.0	50.0	4.382

TABLE 4.2.6

Crack Width and Average Strain Data for Segment 6

Load, kips V:H	Horizontal Strain$\times 10^3$	No. of Cracks	Crack Widths, in.$\times 10^3$ Mean	50%ile	75%ile	Maximum	Average Crack Strain $(\Sigma w/L) \times 10^3$
(b) Vertical Cracks							
0:155.9	.0879	4	1.2	1.3	2.0	2.0	.0296
0:204.2	.3442	10	2.9	2.7	5.0	7.0	.1832
0:229.5	.6512	24	2.7	3.0	4.4	7.0	.3904
0:280.8	1.125	36	3.4	3.3	4.9	9.0	.7584
0:330.8	1.529	36	4.2	3.9	5.6	10.0	.9465
0:381.2	1.822	38	5.4	5.7	7.1	10.0	1.3015
0:406.0	1.982	38	6.5	6.8	7.8	15.0	1.5332
0:304.6	1.460	38	3.9	4.4	5.5	8.0	.9788
0:203.9	.8571	38	2.0	2.3	3.2	5.0	.4941
0:5.98	.264	38	1.0	1.2	1.8	2.0	.226

TABLE 4.2.7

Crack Width and Average Strain Data for Segment 7

Load, kips V:H	Strain in.x10^3	No. of Cracks	Crack Widths, in.x10^3 Mean	50%ile	75%ile	Maximum	Average Crack Strain $(\Sigma w/L)$x10^3
(a) Horizontal Cracks							
3.4:5.0	0.0	7	1.8	1.4	2.5	4.0	.1209
25.2:29.8	.0671	7	1.6	1.4	2.5	4.0	.1050
50.1:55.2	.1900	7	1.7	1.2	1.7	5.0	.1100
75.1:82.1	.2858	7	2.8	2.7	3.6	7.0	.1834
100:105.1	.4825	8	2.9	2.7	4.0	7.0	.2241
125.4:130.2	.8025	12	4.5	3.3	5.0	13.0	.5884
150.6:154.9	.9991	12	4.0	3.2	3.8	12.0	.5414
175.8:180.9	1.145	13	5.2	4.3	7.5	13.5	.7754
200.6:205	1.342	13	5.5	5.2	8.5	12.0	.8264
225.7:229.9	1.545	13	7.3	6.7	8.7	19.0	1.108
250.4:256.3	1.711	12	7.4	6.0	8.0	22	1.037
275.5:278	1.747	13	8.7	8.3	10.7	24	1.328
285.5:288.8	1.812	13	10.2	9.0	11.7	26	1.568
1.69:4.64	.515	13	3.9	3.4	5.7	13	.595
(b) Vertical Cracks							
3.4:5.0	0.0	13	2.5	2.8	3.9	6.0	.3149
25.2:29.8	.0637	13	2.6	2.7	3.6	6.0	.3364
50.1:55.2	.1675	13	3.1	3.8	5.1	6.0	.3920
75.1:82.1	.2412	13	3.5	4.2	5.2	6.0	.4421
100:105.1	.5637	16	4.4	4.9	5.8	7.5	.7215
125.4:130.2	.9312	16	5.2	5.3	6.8	14.0	.8801
150.6:154.9	1.114	16	6.3	6.0	8.0	15.0	1.065
175.8:180.9	1.267	16	6.8	6.7	9.3	16.0	1.151
200.6:205	1.456	17	7.1	7.0	10.5	17.0	1.286
225.7:229.9	1.651	17	8.6	7.7	12.5	25.0	1.571
250.4:256.3	1.857	17	10.1	7.5	15.7	30	1.878
275.5:278	2.117	17	12.5	13.0	15.9	32.0	2.287
285.5:288.8	3.972	18	18.7	10.0	19.0	65.0	3.690
1.69:464	1.814	18	12.1	6.0	13.0	40.0	2.49

TABLE 4.2.8

Crack Width and Average Strain Data for Segment 8

Load, kips V:H	Strain in.x10^3	No. of Cracks	Crack Widths, in.x10^3 Mean	50%ile	75%ile	Maximum	Average Crack Strain $(\Sigma w/L)$x10^3	Average Crack Spacing in.
(a) Horizontal Cracks								
350.4:178.9	.2969	2	2.0	2.0	2.0	2.0	.0563	34.04
375.4:193.2	.4825	5	3.1	2.0	6.0	6.0	.2213	14.26
425.2:216.7	1.046	8	4.5	5.0	6.7	7.0	.5475	8.37
475.6:242.9	1.704	13	4.5	3.8	7.7	10.0	.8613	4.57
525.3:268.4	2.349	19	8.1	5.5	11.2	30.0	2.096	3.4
571:290.6	8.143	29	38.1	37.7	55.8	75.0	14.935	2.54
570:354.3	---	29	38.2	41.0	55.8	75.0	15.039	2.54
570.2:391.9	---	29	43.8	44.5	61.2	100.0	17.270	2.54
0:0	---	29	36.6	31.7	51.2	75.0	14.42	2.54
(b) Vertical Cracks								
350.4:178.9	.2081	7	3.4	3.4	4.2	5.0	.2888	11.17
375.4:193.2	.405	7	5.0	5.5	7.2	8.5	.4238	11.17
425.2:216.7	.6612	12	5.2	4.5	6.0	13.0	.7288	6.88
475.6:242.9	.9287	13	7.3	5.2	13.5	20.0	1.161	6.04
525.3:268.4	1.181	18	5.6	4.7	7.2	20.0	1.208	4.48
571:290.6	1.606	18	9.9	5.6	10.5	65.0	2.125	4.48
570:354.3	2.779	18	16.4	9.0	17.0	105.0	3.604	4.48
570.2:391.9	7.292	20	37.5	26.0	52.0	170.0	9.771	4.03
0:0	---	20	29.2	16.0	35.0	150.0	6.925	4.03

TABLE 4.2.8 (Continued)

Crack Width and Average Strain Data for Segment 8

Load, kips V:H	Strain in.x10^3	No. of Cracks	Crack Widths, in.x10^3 Mean	50%ile	75%ile	Maximum	Average Crack Strain $(\Sigma w/L)x10^3$	Average Crack Spacing in.
(c) Horizontal Cracks (Measured Over Bars)								
350.4:178.9	.2969	1	2.0	2.0	2.0	2.0	.0625	29.63
375.4:193.2	.4825	3	2.8	3.0	6.5	8.0	.2675	11.08
425.2:216.7	1.046	5	3.7	4.5	5.7	8.0	.5850	6.68
475.6:242.9	1.704	5	4.3	3.5	7.5	12.0	.6775	4.72
525.3:268.4	2.349	10	7.2	5.2	10.5	26.0	1.965	2.97
571:290.6	8.143	16	33.8	30.0	51.0	66.0	14.265	2.29
570:354.3	---	16	35.4	32.0	52.0	72.0	14.958	2.29
570.2:391.9	---	16	38.5	32.0	46.0	102.0	16.268	2.29
0:0	---	16	32.4	28.0	45.0	76.0	6.48	--
(d) Vertical Cracks (Measured Over Bars)								
350.4:178.9	.2081	5	2.9	3.0	3.5	4.0	.3825	7.39
375.4:193.2	.4050	5	4.3	5.0	6.7	8.0	.5625	7.39
425.2:216.7	.6612	7	4.6	4.3	5.5	12.0	.8525	5.4
475.6:242.9	.9387	7	7.1	5.5	14.2	16.0	1.313	4.99
525.3:268.4	1.181	9	5.7	4.5	6.7	22.0	1.320	4.02
571:290.6	1.606	9	12.2	5.7	9.5	66.0	2.830	4.02
570:354.3	2.779	9	17.7	9.0	11.7	106.0	4.138	4.02
570.2:391.9	7.292	10	35.9	20.0	41.0	172.0	10.555	3.66
0:0	---	10	27.3	12.0	31.0	152.0	3.412	--

TABLE 4.2.8 (Continued)

Crack Width and Average Strain Data for Segment 8

Load, kips V:H	Strain in.x10^3	No. of Cracks	Crack Widths, in.x10^3 Mean	50%ile	75%ile	Maximum	Average Crack Strain $(\Sigma w/L)x10^3$	Average Crack Spacing in.
(e) Horizontal Cracks (Measured Between Bars)								
350.4:178.9	.2969	1	2.0	2.0	2.0	2.0	.05	40
375.4:193.2	.4825	2	3.5	2.0	7.0	8.0	.175	20
425.2:216.7	1.046	3	5.8	6.5	7.2	8.0	.510	1.2
475.6:242.9	1.704	8	4.7	4.0	8.0	12.0	1.045	4.43
525.3:268.4	2.349	9	9.1	6.5	13:5	32.0	2.228	3.99
571:290.6	8.143	13	43.4	45.0	64.7	76.0	16.605	2.85
570.354.3	---	13	41.6	45.0	60.7	76.0	15.120	2.85
570.2:391.9	---	13	50.4	60.2	61.9	82.0	18.273	2.85
0:0	---	13	41.7	41.5	54.7	72.0	6.776	-
(f) Vertical Cracks (Measured Between Bars)								
350.4:178.9	.2081	2	4.5	5.0	5.5	6.0	.195	22.86
375.4:193.2	.4050	2	6.7	6.0	9.0	10.0	.285	22.86
425.2:216.7	.6612	5	6.2	5.0	9.5	14.0	.605	9.48
475.6:242.9	.9387	6	7.5	5.0	13.0	22.0	1.010	7.66
525.3:268.4	1.181	9	5.6	5.0	7.7	14.0	1.095	5.06
571:290.6	1.606	9	7.6	5.5	11.5	22.0	1.420	5.06
570:354.3	2.779	9	15.2	9.0	19.5	62.0	3.070	5.06
570.2:391.9	7.292	10	39.1	36.0	61.0	82.0	8.988	4.49
0:0	---	10	31.1	31.0	55.0	66.0	3.887	--

TABLE 4.2.9

Crack Width and Average Strain Data for Segment 9

Load, kips V:H	Strain in.x10^3	No. of Cracks	Crack Widths, in.x10^3 Mean	50%ile	75%ile	Maximum	Average Crack Strain $(\Sigma w/L)$x10^3
(a) Horizontal Cracks							
350:179	.6662	6	1.2	1.2	1.8	2.0	.0875
400.7:205.9	1.252	17	2.6	3.0	3.8	5.0	.5375
449.6:233.1	1.804	19	3.4	3.9	5.2	6.0	.8150
500.5:255.7	2.669	23	4.8	3.9	8.2	14.0	1.395
561.4:284.9	7.462	23	18.7	15.7	30.8	50.0	5.306
562.2:304.7	9.249	24	23.4	22.0	40.8	60.0	7.094
0:0	---	24	19.8	16.0	30.7	65.0	2.468
(b) Vertical Cracks							
350:179	.2037	0.	0.0	0.0	0.0	0.0	0
400.7:205.9	.4625	6.	1.3	1.5	2.0	2.0	.1013
449.6:233.1	.6750	6	1.8	2.5	3.0	3.0	.1825
500.5:255.7	.8425	9	2.3	2.3	3.8	7.0	.3413
561.4:284.1	1.317	9	7.2	5.0	11.5	20.0	.9113
562.2:304.7	1.639	10	8.2	6.0	13.0	20.0	1.169
560.7:355.3	2.705	12	11.6	5.6	19.0	35.0	1.811
560.7:379.5	---	15	16.6	11.0	30.5	55.0	2.796
0:0	---	15	9.9	5.7	12.5	40.0	.699

TABLE 4.2.11

Crack Width and Average Strain Data for Segment 11

Load, kips V:H	Strain in.x10^3	No. of Cracks	Mean	Crack Widths, in.x10^3 50%ile	75%ile	Maximum	Average Crack Strain $(\Sigma w/L)$x10^3
(a) Horizontal Cracks							
300.9:155.8	.4325	4	1.2	1.3	2.0	2.0	.1175
351:180.8	.935	12	2.5	2.0	4.0	6.0	.36
426:218.1	1.549	26	2.0	2.3	3.3	6.0	.6525
450.8:230.8	2.131	29	3.1	3.0	3.8	12.0	1.119
498.2:254.1	3.09	32	5.4	4.6	7.5	23.0	2.116
498.2:305.1	3.385	33	5.5	4.9	7.1	20.0	2.244
498.2:354.5	3.554	33	6.2	4.7	8.4	28.0	2.486
498.2:384.4	3.74	33	5.7	4.6	8.3	23.0	2.290
(b) Vertical Cracks							
300.9:155.8	.2113	2	1.5	1.0	2.0	2.0	.15
351:180.8	.2975	4	1.2	1.3	2.0	2.0	.0733
426:218.1	.4512	8	1.2	1.3	2.0	2.0	.1075
450.8:230.8	.7325	11	2.1	1.8	3.5	4.0	.255
498.2:254.1	1.017	13	2.5	2.3	4.4	4.5	.3825
498.2:305.1	1.484	14	3.2	3.4	5.0	7.0	.54
498.2:354.5	2.047	19	3.6	3.3	5.5	8.0	.7763
498.2:384.4	2.08	19	3.7	3.4	5.5	8.0	.8338
498.2:404.5	3.301	19	14.0	6.2	28.5	55.0	1.356

TABLE 4.2.12

Crack Width and Average Strain Data for Segment 12

Load, kips V:H	Strain in.x10^3	No. of Cracks	Crack Widths, in.x10^3 Mean	50%ile	75%ile	Maximum	Average Crack Strain $(\Sigma w/L)$x10^3
(a) Horizontal Cracks (Face A)							
251.1:129.3	.3112	2	1.5	1.0	2.0	2.0	.075
301.1:154.4	.4375	3	2.0	2.0	3.0	3.0	.15
350.6:179.1	1.156	9	2.2	1.5	3.5	6.0	.495
400.5:203.8	1.844	12	3.2	4.0	5.2	7.0	.90
460.8:228.6	2.426	14	5.1	5.7	7.0	8.0	1.688
535.5:280.1	4.335	14	8.2	8.0	11.5	30.0	2.878
535.5:303.6	4.882	14	8.8	8.0	13.0	29.0	3.233
535.5:319.4	5.257	14	9.0	8.0	11.7	30.0	3.348
(b) Vertical Cracks (Face A)							
251.1:129.3	.1012	0	0.0	0.0	0.0	0.0	0
301.1:154.4	.1725	0	0.0	0.0	0.0	0.0	0
350.6:179.1	.3962	3	1.5	1.5	2.0	2.0	.1125
400.6:203.8	.8237	8	2.2	2.8	3.6	4.0	.4050
460.8:228.6	1.266	10	3.3	3.7	4.7	5.0	.8075
535.5:280.1	2.054	11	4.8	4.5	8.6	9.0	1.295
535.5:303.6	2.376	11	5.5	5.5	8.5	11.0	1.5
535.5:319.4	2.639	12	5.5	6.0	10.0	11.0	1.623

TABLE 4.2.12

Crack Width and Average Strain Data for Segment 12

Load, kips V:H	Strain in.10^3	No. of Cracks	Mean	Crack Widths, in.x10^3 50%ile	75%ile	Maximum	Average Crack Strain $(\Sigma w/L)$x10^3
(a) Horizontal Cracks (Face B)							
251.1:129.3	.0875	0	0.0	0.0	0.0	0.0	0
301.1:154.4	.1200	0	0.0	0.0	0.0	0.0	0
350.6:179.1	.3900	2	1.5	2.0	2.0	2.0	.08
400.6:203.8	1.147	11	2.3	2.5	3.4	4.0	.64
460.8:228.6	1.807	14	3.0	3.2	4.2	5.0	1.068
535.5:280.1	2.437	16	5.0	4.5	6.7	11.0	2.003
535.5:303.6	3.452	16	7.3	4.0	14.0	17.0	2.855
535.5:319.4	4.397	16	16.3	5.5	32.0	59	6.305
(b) Vertical Cracks (Face B)							
251.1:129.3	.0225	0	0.0	0.0	0.0	0.0	0
301.1:154.4	.0025	0	0.0	0.0	0.0	0.0	0
350.6:179.1	-.055	2	1.2	2.0	2.0	2.0	.05
400.6:203.8	-.0525	2	1.8	2.0	2.0	2.0	.07
460.8:228.6	.0675	2	1.5	2.0	2.0	2.0	.06
535.5:280.1	.0625	2	1.5	2.0	2.0	2.0	.06
535.5:303.6	-.0625	2	1.8	2.0	2.0	2.5	.07
535.5:319.4	-.0875	2	1.5	2.0	2.0	2.0	.06

TABLE 4.2.13

Crack Width and Average Strain Data for Segment 13

Load, kips V:H	Strain in.x10^3	No. of Cracks	Crack Widths, in.x10^3 Mean	50%ile	75%ile	Maximum	Average Crack Strain $(\Sigma w/L)$x10^3
(a) Horizontal Cracks (Face A)							
201.9:106.7	-.3300	2	1.3	1.0	1.5	1.5	.0575
252.1:130.8	-.5075	3	1.5	1.5	2.0	2.0	.0875
302.6:155.6	-.42	3	2.0	2.5	3.0	3.0	.1125
337.4:172.2	-.3175	3	3.0	3.0	6.0	6.0	.1575
337.4:205.4	-.37	3	3.0	3.0	4.5	5.0	.1650
337.4:229.8	-.36	3	3.7	3.0	6.5	7.0	.1950
337.4:256.3	-.355	3	4.3	5.0	6.5	7.0	.2375
337.4:280.9	-.365	3	4.3	5.0	6.5	7.0	.2375
337.4:305.9	-.35	3	4.3	5.0	6.5	7.0	.2375
337.4:329.4	-.44	3	4.3	5.0	6.5	7.0	.2375
337.4:345.6	-.4025	3	4.3	5.0	6.5	7.0	.2375
(b) Vertical Cracks (Face A)							
201.9:106.7	.045	0	0.0	0.0	0.0	0.0	0
252.1:130.8	.085	1	2.5	2.5	2.5	2.5	.0625
302.6:155.6	.12	1	2.5	2.5	2.5	2.5	.0625
337.4:172.2	.285	3	1.7	1.5	2.5	2.5	.125
337.4:205.4	.35	5	2.7	3.0	3.5	3.0	.3375
337.4:229.8	.605	5	2.4	3.0	3.5	3.0	.30
337.4:256.3	.64	7	3.3	3.4	4.2	5.0	.5525
337.4:280.9	.67	7	3.1	3.4	4.2	5.0	.5225
337.4:305.9	.61	7	2.9	3.2	3.7	4.0	.4875
337.4:329.4	.505	7	2.9	3.2	3.7	4.0	.4750
337.4:345.6	.38	7	2.6	3.2	3.7	4.0	.430

TABLE 4.2.13

Crack Width and Average Strain Data for Segment 13

Load, kips V:H	Strain in.x10^3	No. of Cracks	Crack Widths, in.x10^3 Mean	50%ile	75%ile	Maximum	Average Crack Strain $(\Sigma w/L)x10^3$
(a) Horizontal Cracks (Face B)							
201.9:106.7	.495	10	1.2	1.0	1.5	1.5	.3
252.1:130.8	1.125	12	3.0	3.2	4.0	4.5	.8875
302.6:155.6	1.115	12	3.0	3.3	4.5	5.0	.90
337.4:172.2	1.06	13	3.5	3.8	4.9	5.0	1.125
337.4:205.4	1.16	13	3.7	3.8	5.1	10.0	1.20
337.4:229.8	1.11	13	3.3	3.6	4.9	6.0	1.163
337.4:256.3	1.05	13	3.3	4.1	5.0	5.0	1.08
337.4:280.9	1.155	16	2.9	3.5	4.7	5.0	1.113
337.4:305.9	1.05	16	3.8	3.7	5.5	6.0	1.498
337.4:329.4	1.08	16	4.3	4.4	6.0	7.5	1.775
337.4:345.6	1.165	17	4.6	3.8	5.0	5.0	1.848
(b) Vertical Cracks (Face B)							
201.9:106.7	.005	0	0.0	0.0	0.0	0.0	0
252.1:130.8	.105	0	0.0	0.0	0.0	0.0	0
302.6:155.6	.14	0	0.0	0.0	0.0	0.0	0
337.4:172.2	.31	4	1.7	2.0	3.0	3.0	.27
337.4:205.4	.71	7	2.9	3.0	5.2	7.0	.6275
337.4:229.8	1.14	10	3.1	3.3	5.0	6.0	.97
337.4:256.3	1.4	10	3.9	4.0	5.7	8.0	1.14
337.4:280.9	1.615	10	4.1	4.8	5.8	6.0	1.243
337.4:305.9	1.615	10	5.9	6.0	9.0	11.0	1.693
337.4:329.4	1.92	10	6.6	6.7	10.5	13.0	1.978
337.4:345.6	4.425	11	12.0	7.5	22.5	31.0	4.045

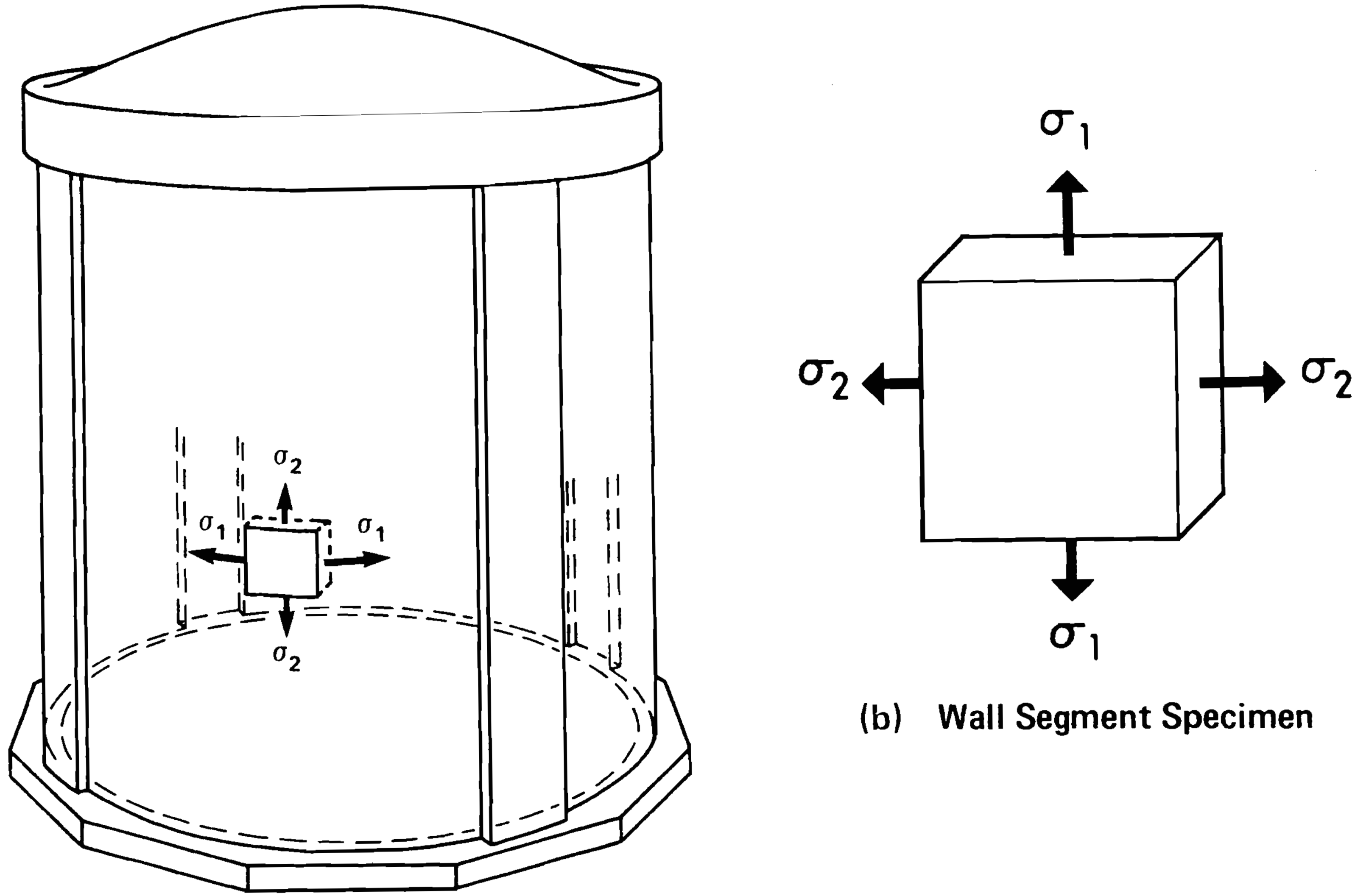

(a) Element in Prototype

(b) Wall Segment Specimen

Fig. 1.1 Relationship between Specimen and Prototype

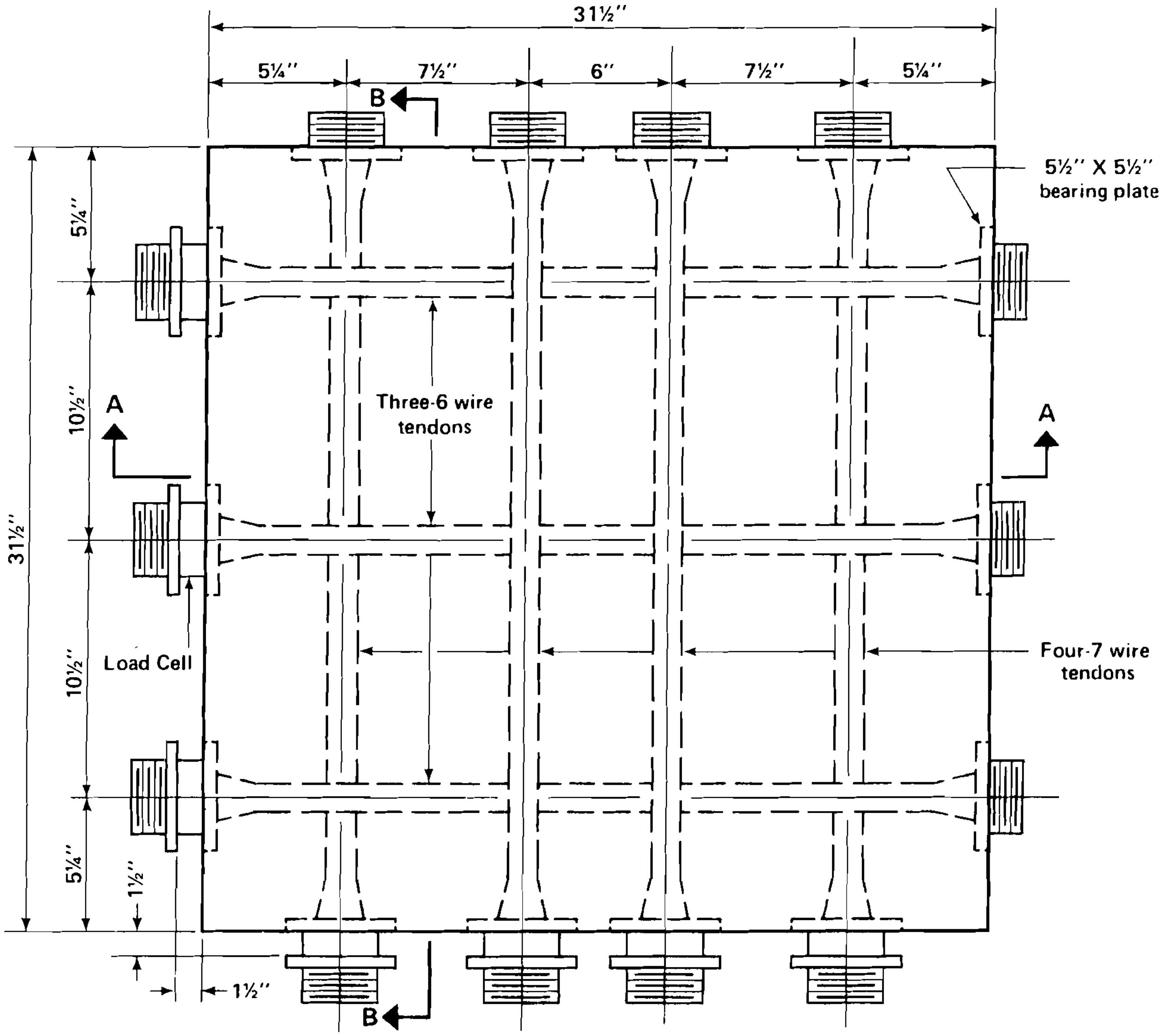

Figure 2.1 Side View of Wall Segment Specimen

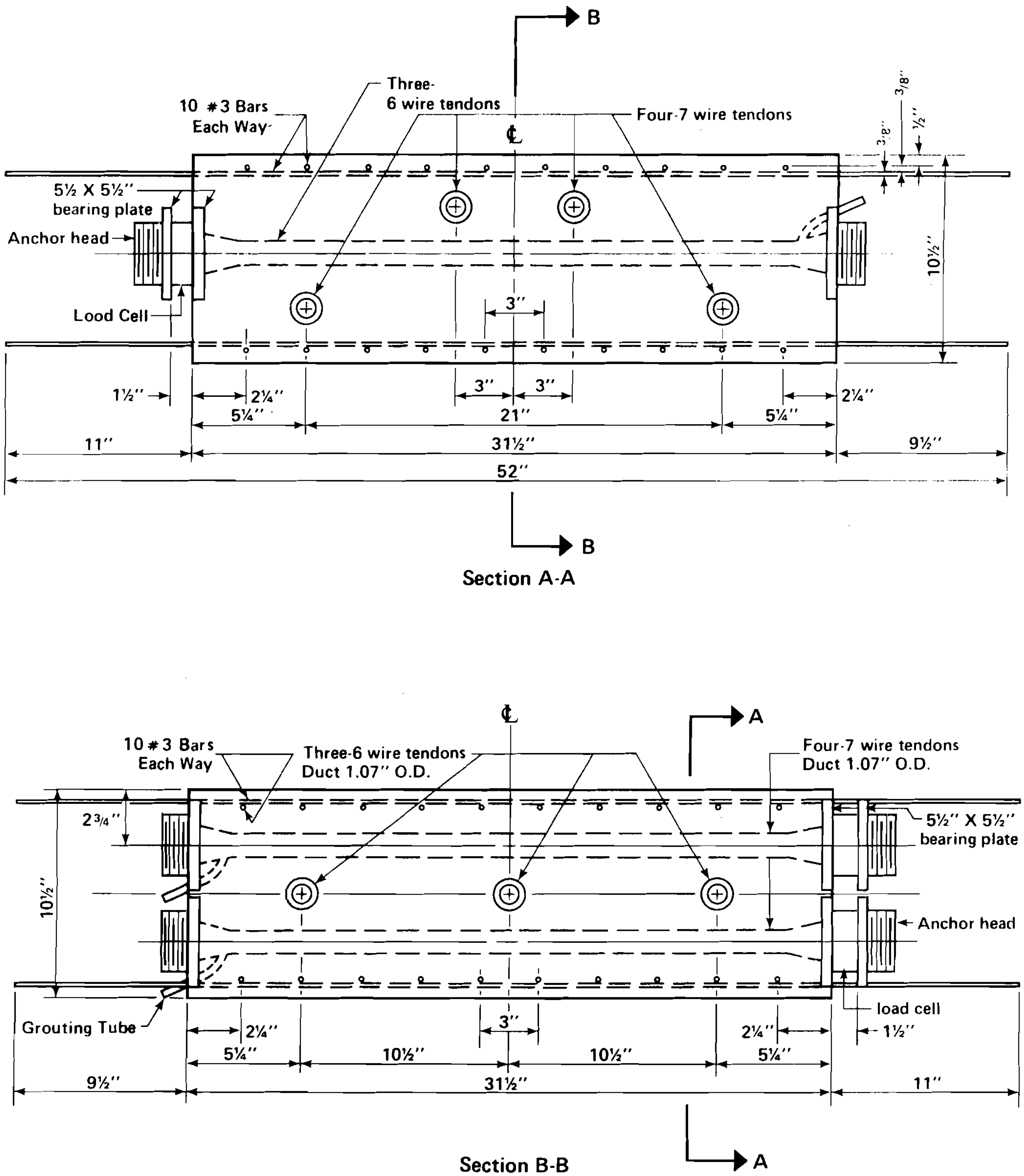

Figure 2.2 Sections Through Wall Segment Specimen

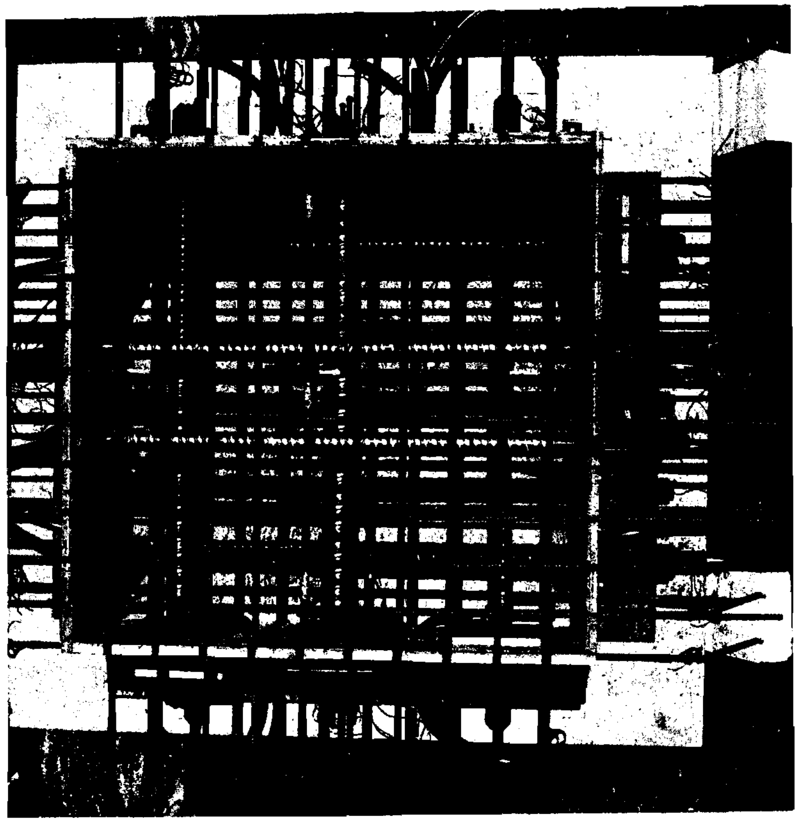

Figure 2.3 Specimen 2 Before Concreting

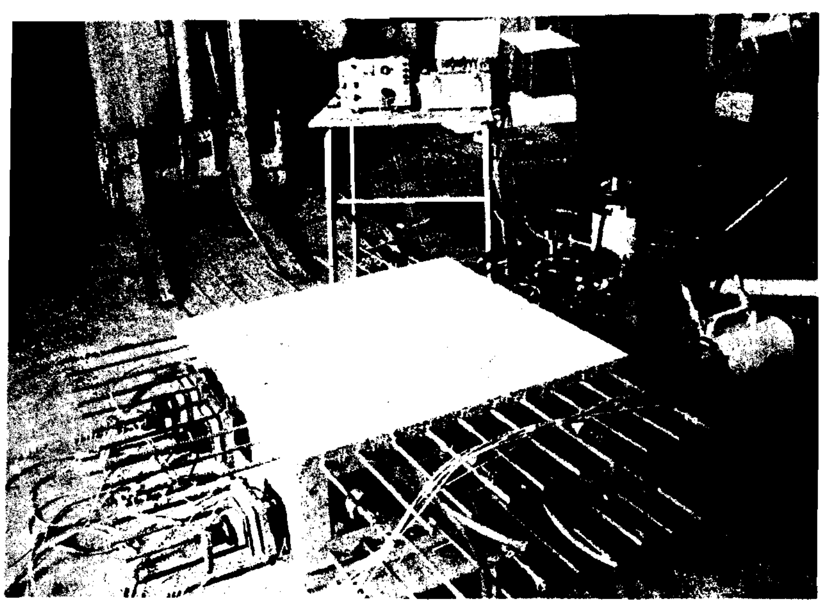

Figure 2.4 Specimen 2 After Testing

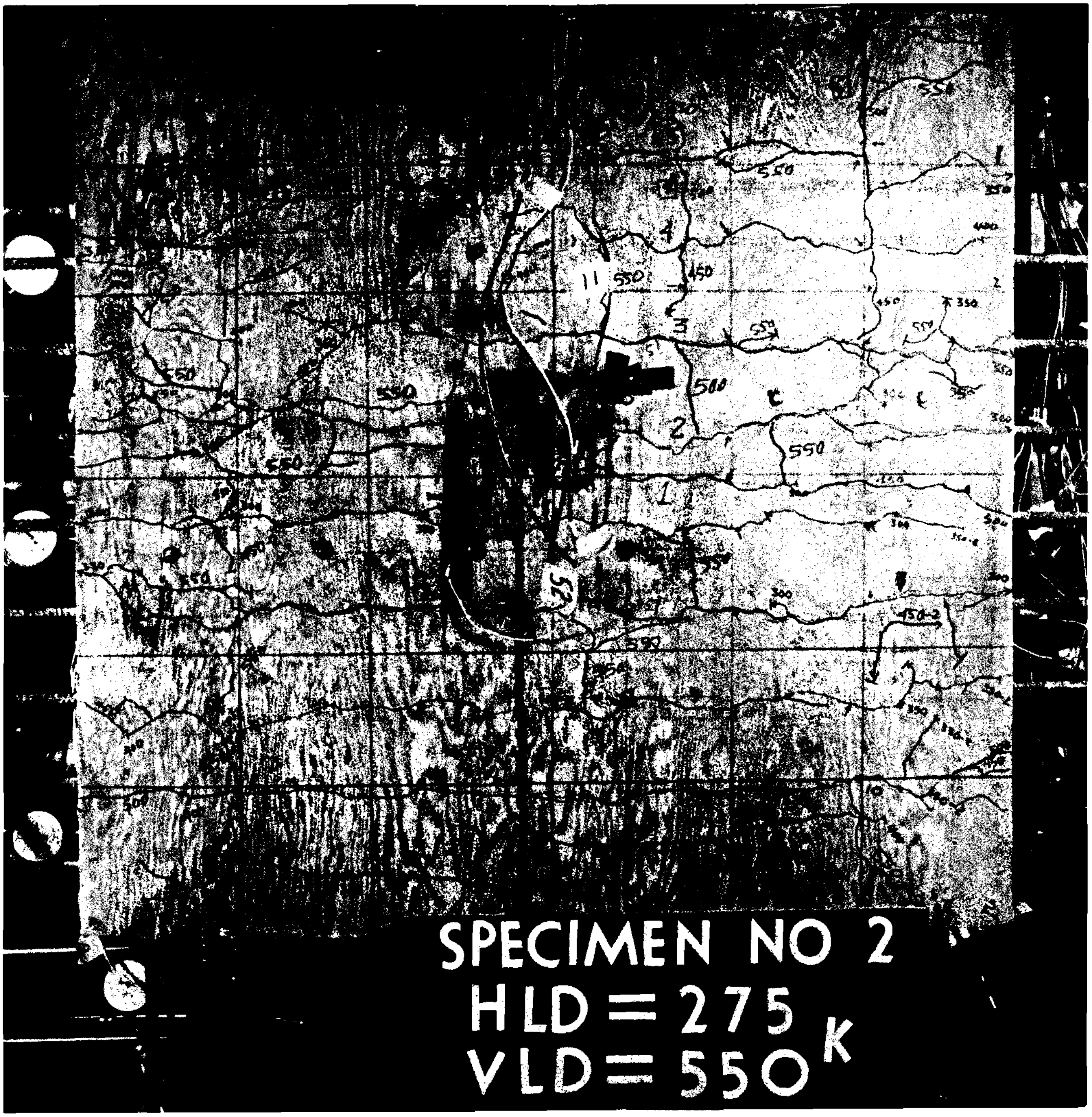

Figure 2.5 Specimen 2 After Testing

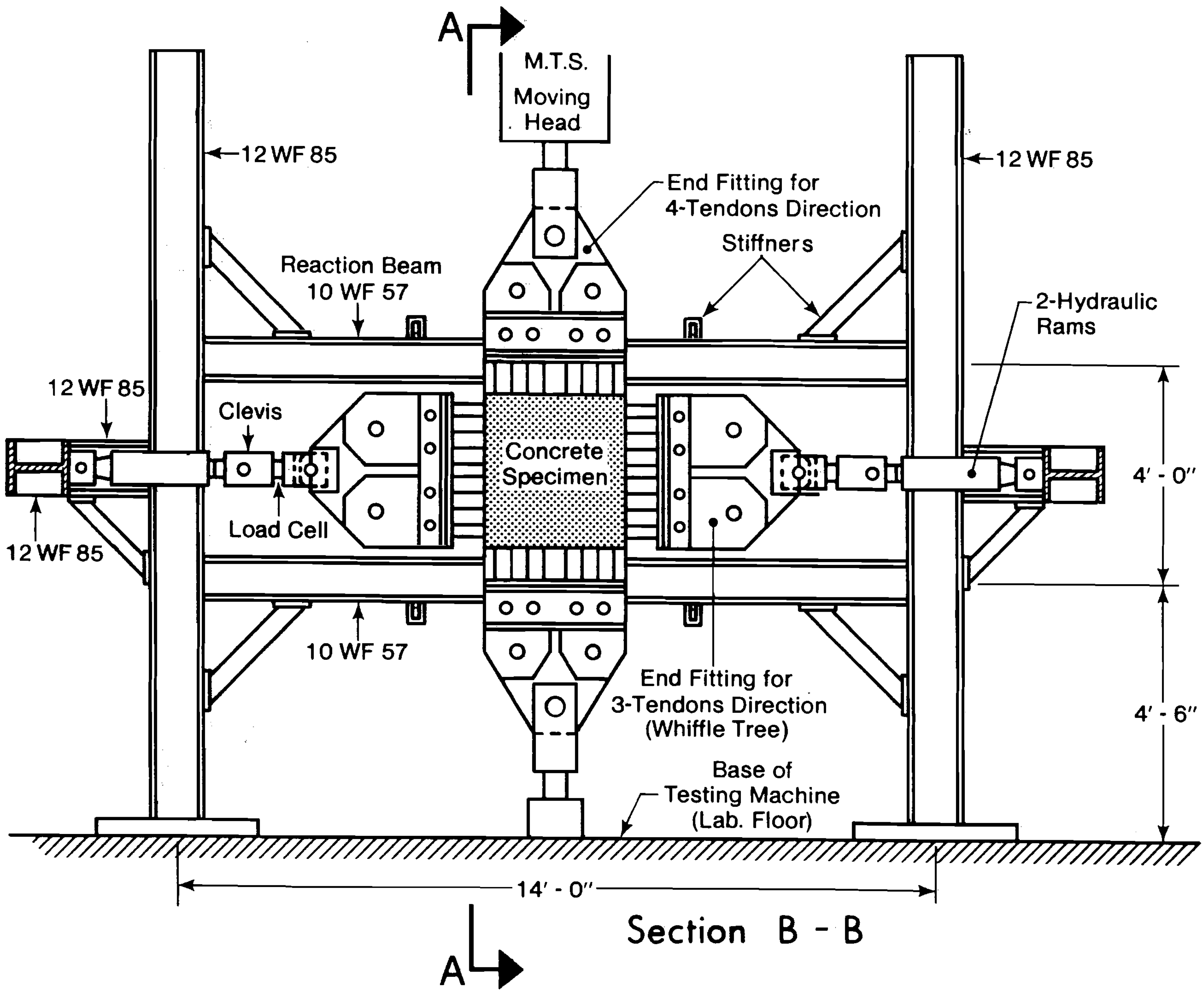

Figure 2.6 East-West Section Through Loading Frame

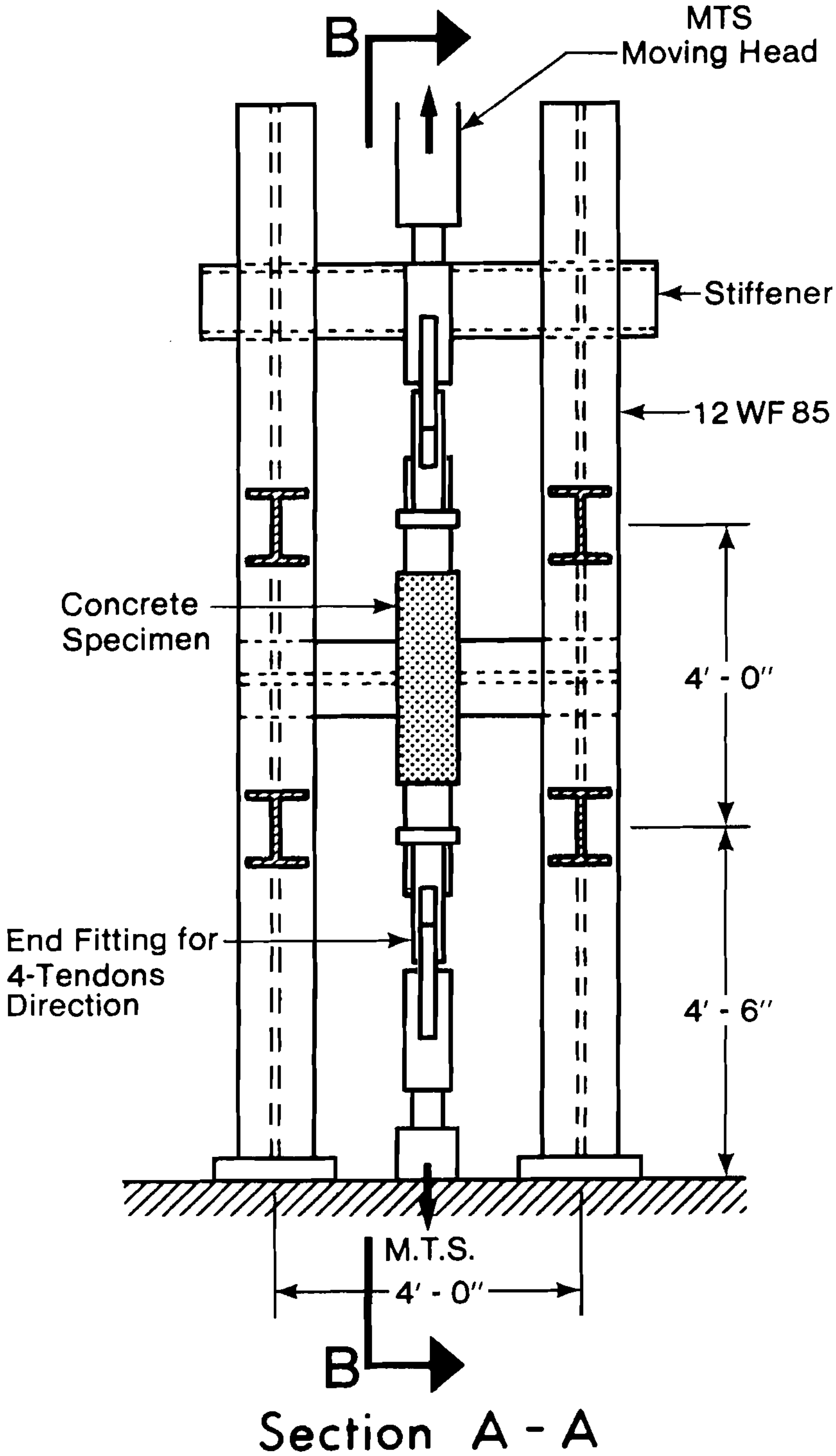

Figure 2.7 North-South Section Through Loading Frame

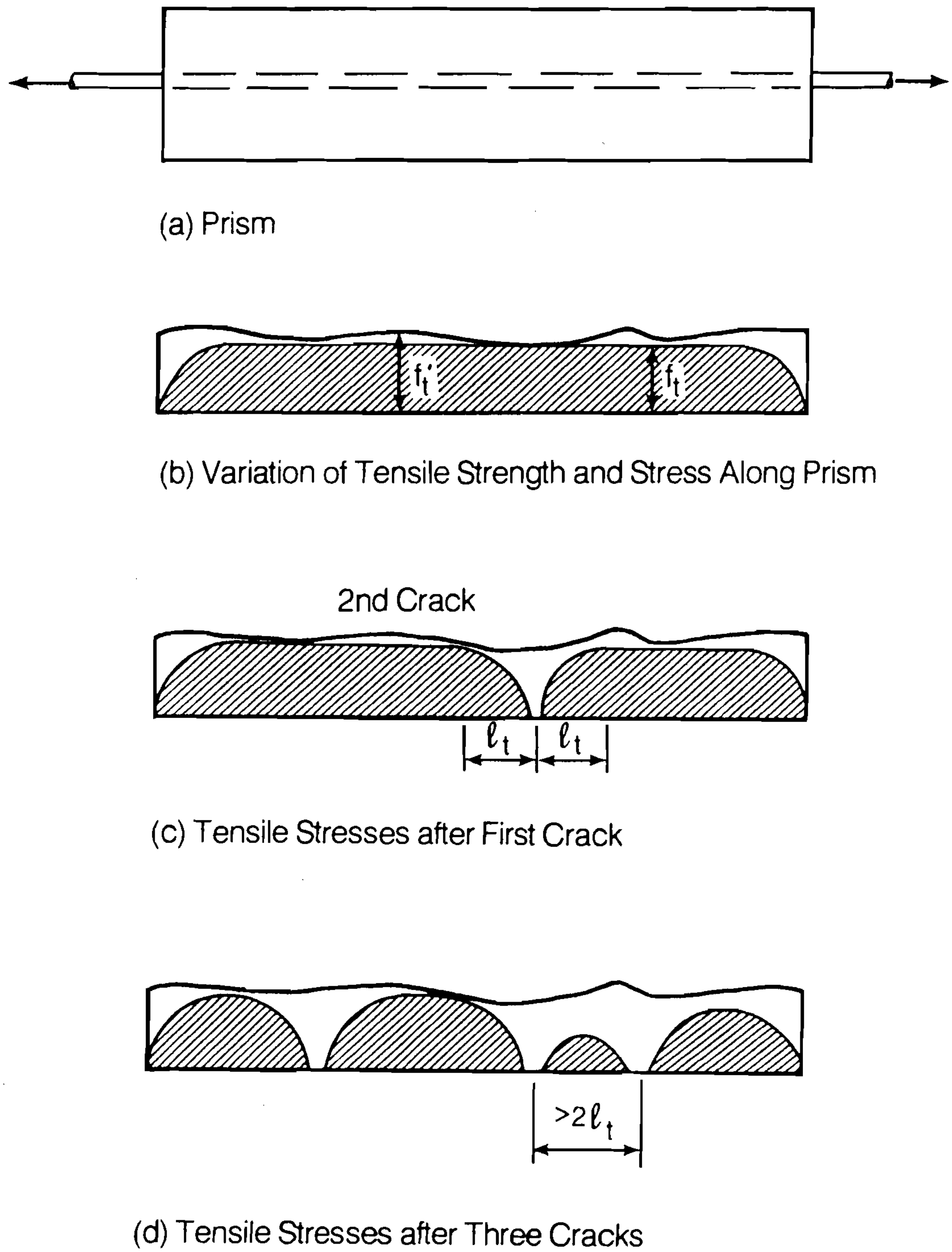

Figure 3.1 Cracking of an Axially Loaded Prism

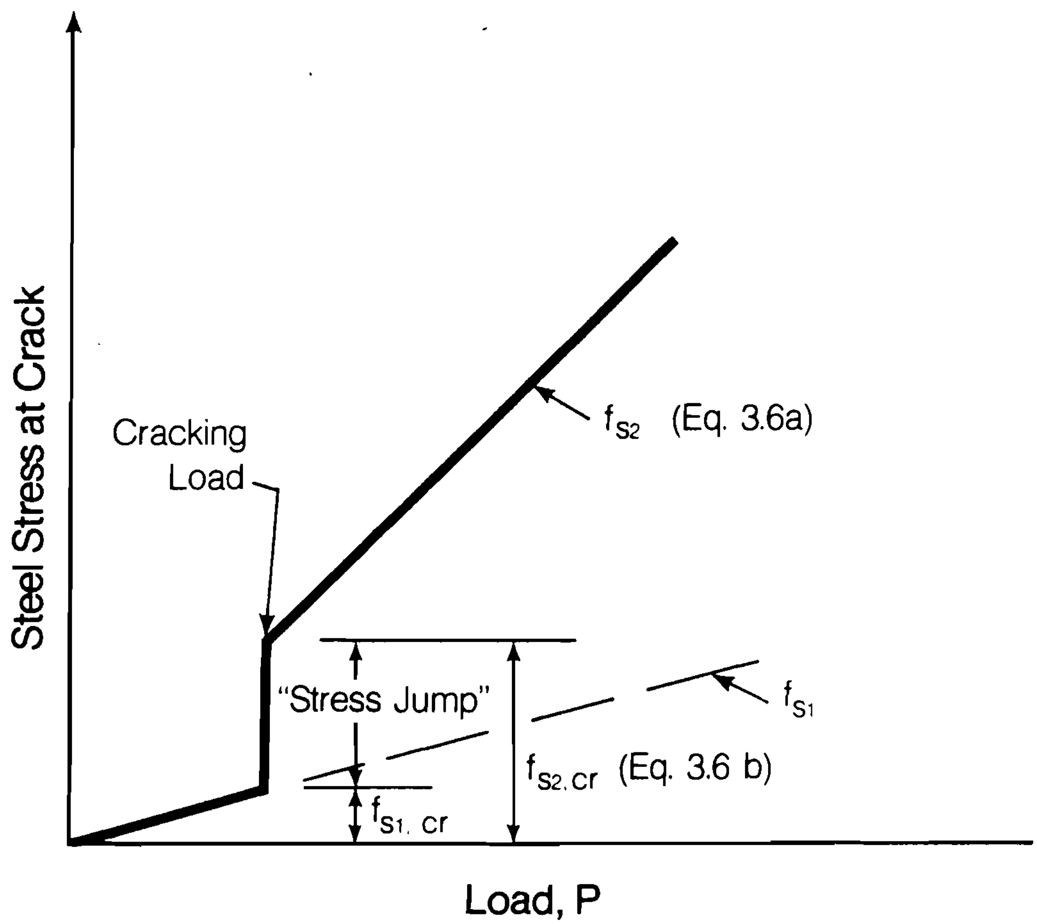

Figure 3.2 Jump in Steel Stress at Cracking

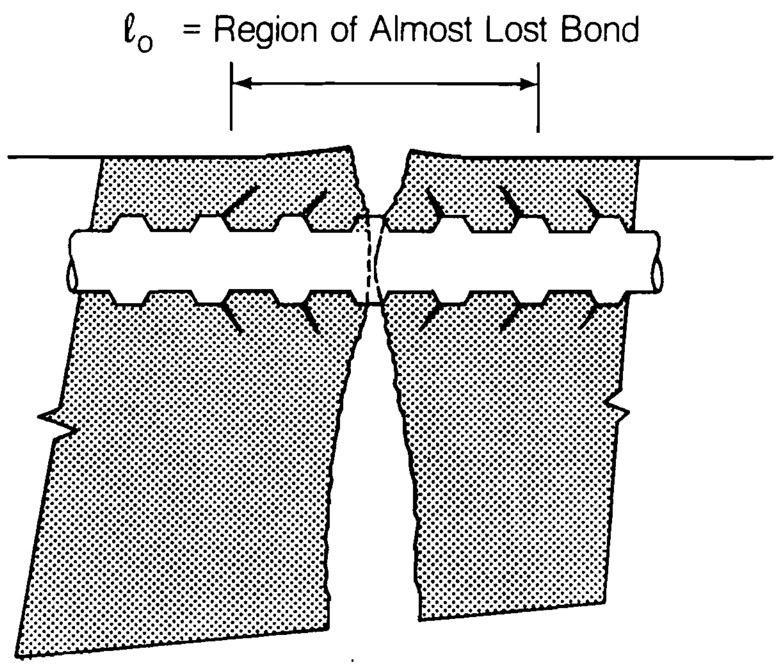

Figure 3.3 Internal Cracks at Bar Deformations

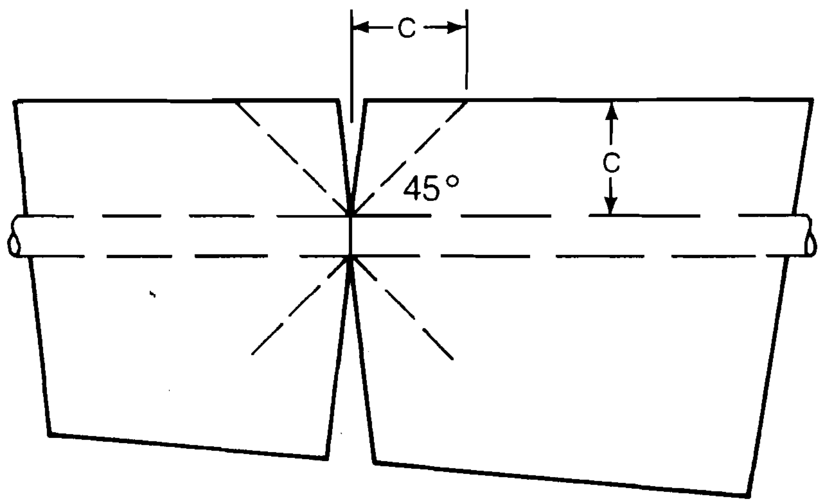

Figure 3.4 Spread of Tensile Stresses Adjacent to a Crack

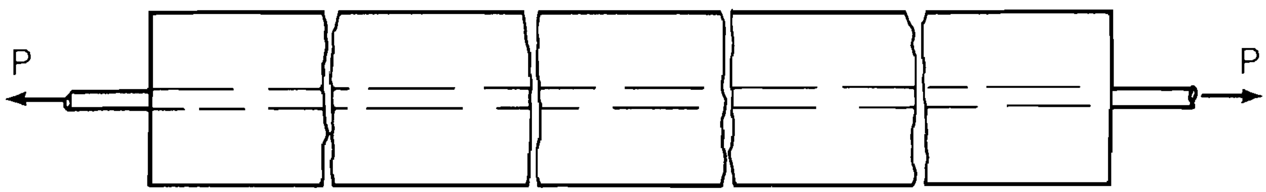

(a) Cracked Prism

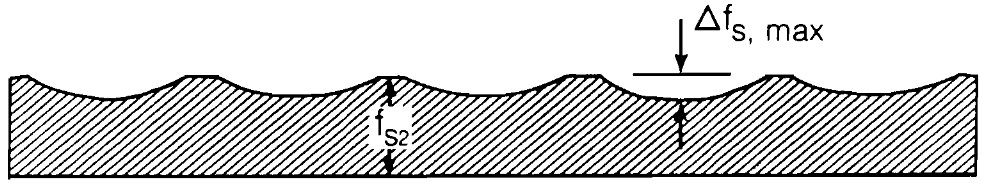

(b) Variation of Steel Stress along Bar

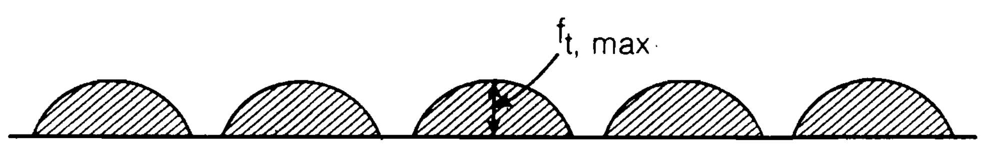

(c) Variation of Concrete Stress along Prism.

Figure 3.5 Stresses in Concrete and Steel in a Cracked Prism

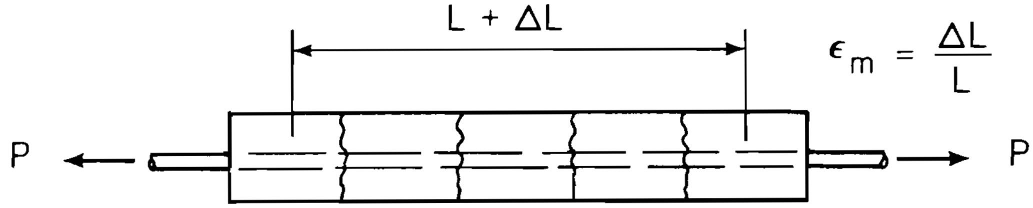

(a) Definition of ϵ_m

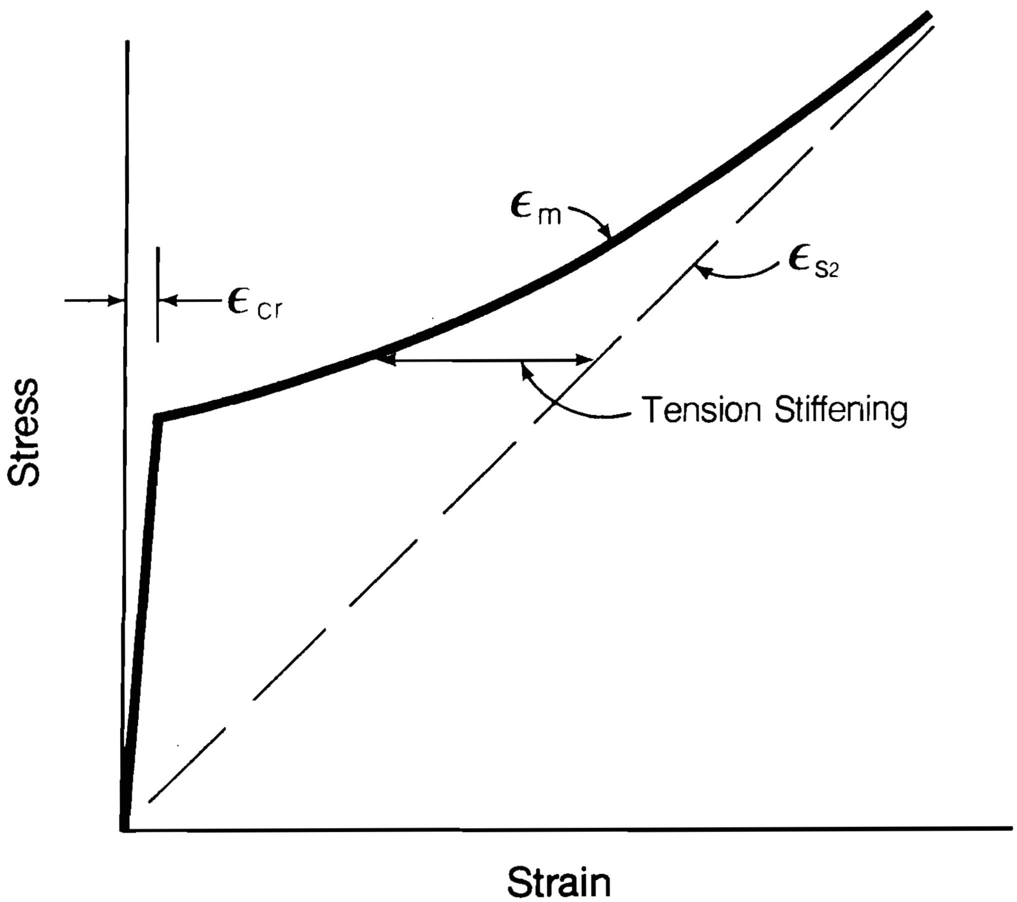

(b) f_s - ϵ_m Diagram

Figure 3.6 Load-Deformation Diagram for an Axially Loaded Reinforced Concrete Prism

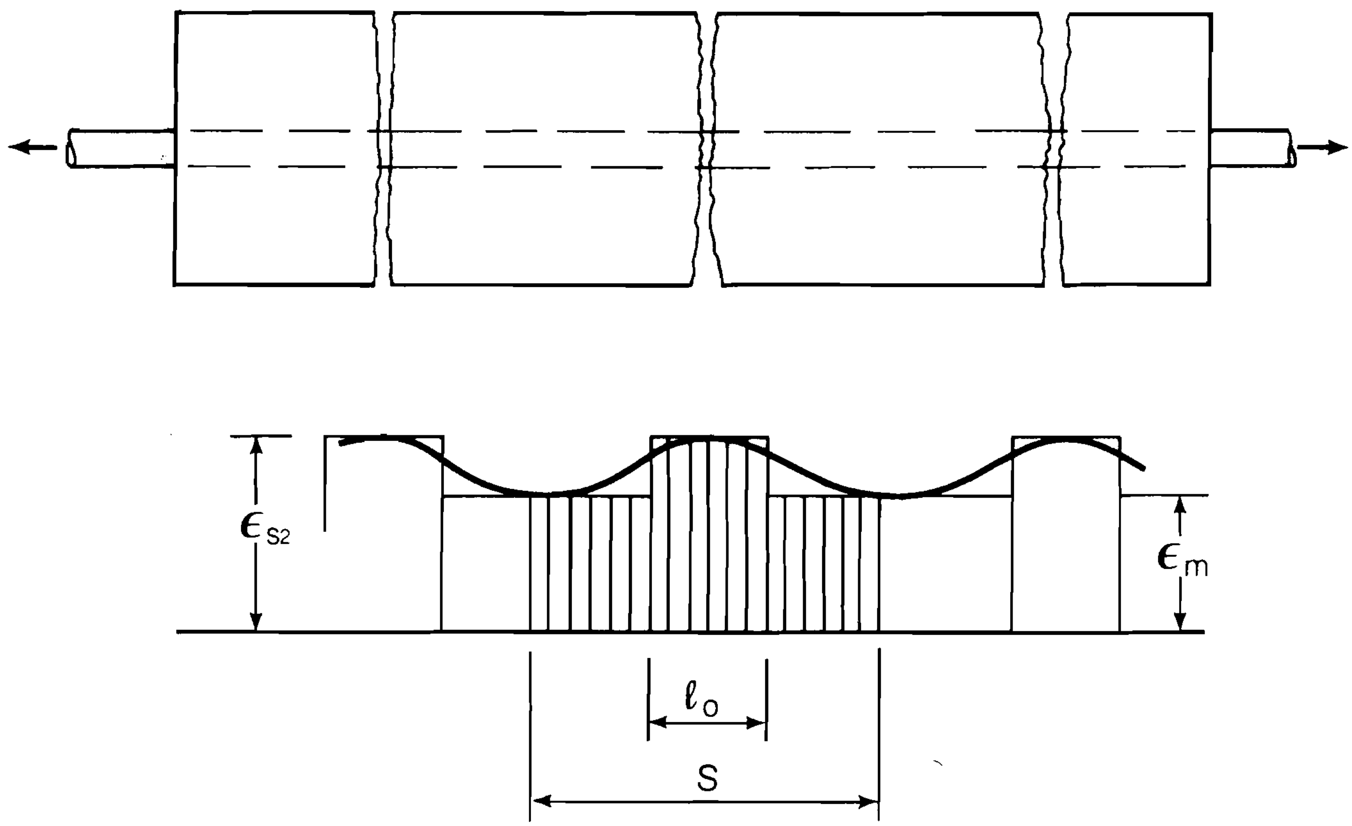

Figure 3.7 Strain Diagram Assumed in Crack Width Calculations

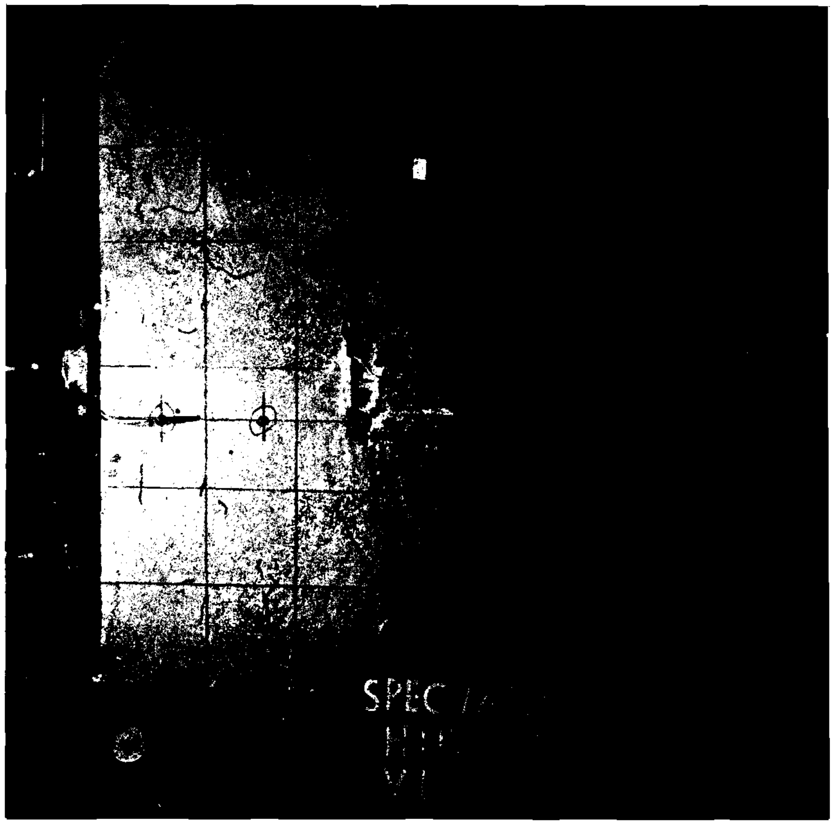

(a) Face A

(b) Face B

Figure 4.1 Shrinkage Cracks in Segment 2 Prior to Test

(a) Face A

(b) Face B

Figure 4.2 First Horizontal Cracks in Segment 2

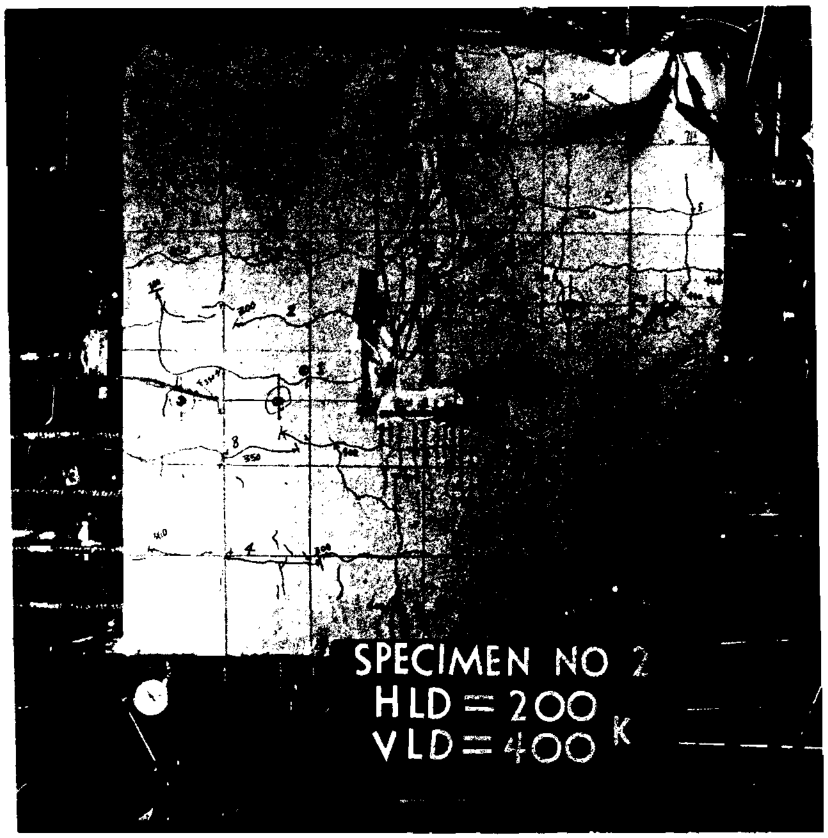

(a) Face A

(b) Face B

Figure 4.3 First Vertical Cracks in Segment 2

(a) Face A

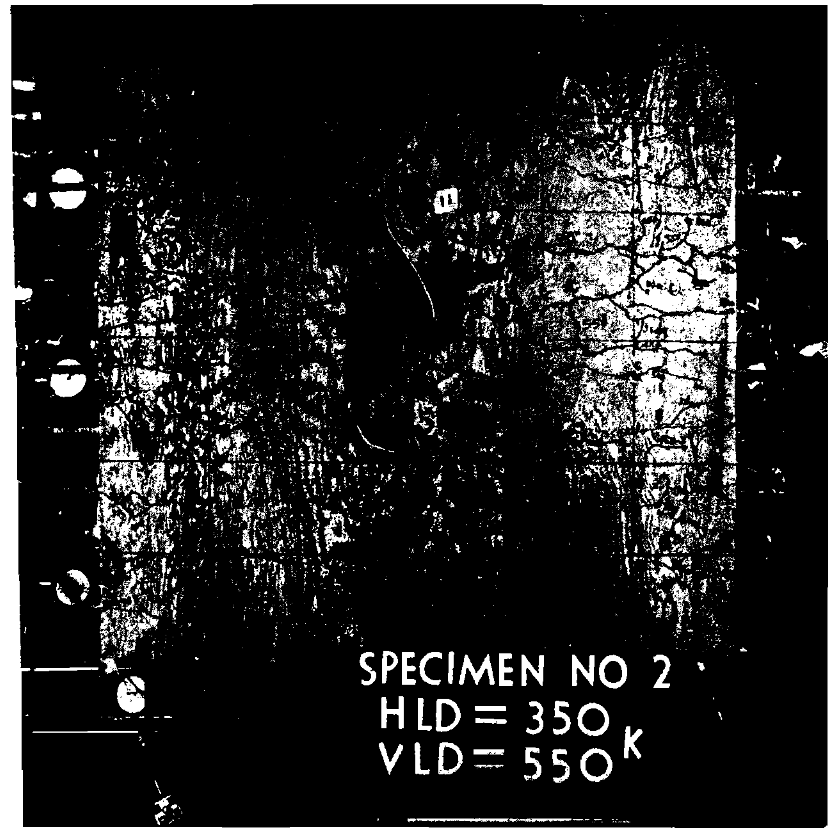

(b) Face B

Figure 4.4 Cracks in Segment 2 at End of Test

(a) Horizontal Cracks in Segment 1 (Face A Upwards)

(b) Vertical Cracks in Segment 2 (Face A Upwards)

Figure 4.5 Sections through Segments 1 and 2 at Ends of Tests

Figure 4.6 Development of Cracks along Bars

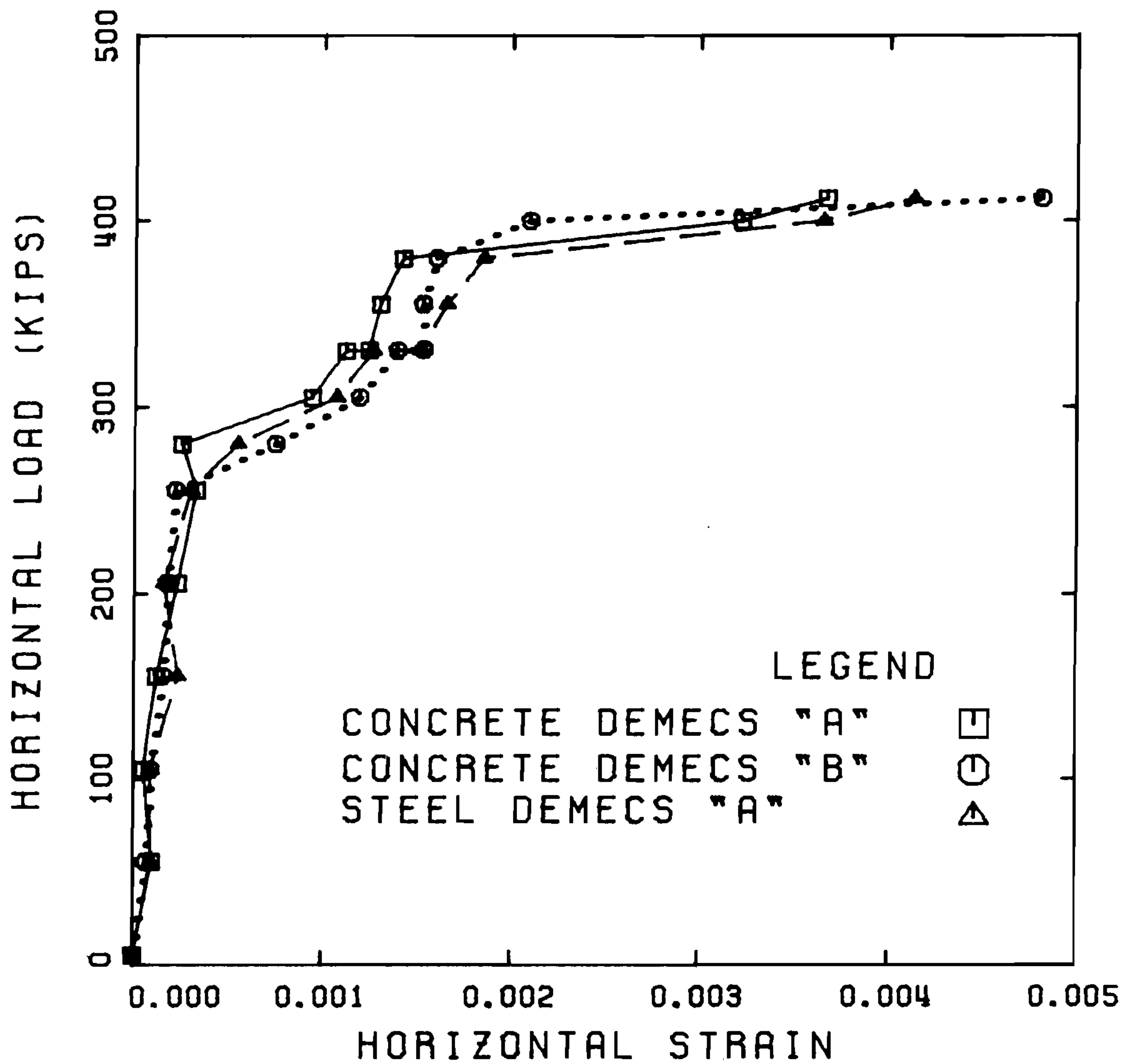

Horizontal Direction

Figure 4.7 Load-Average Strain Curves, Segment 5

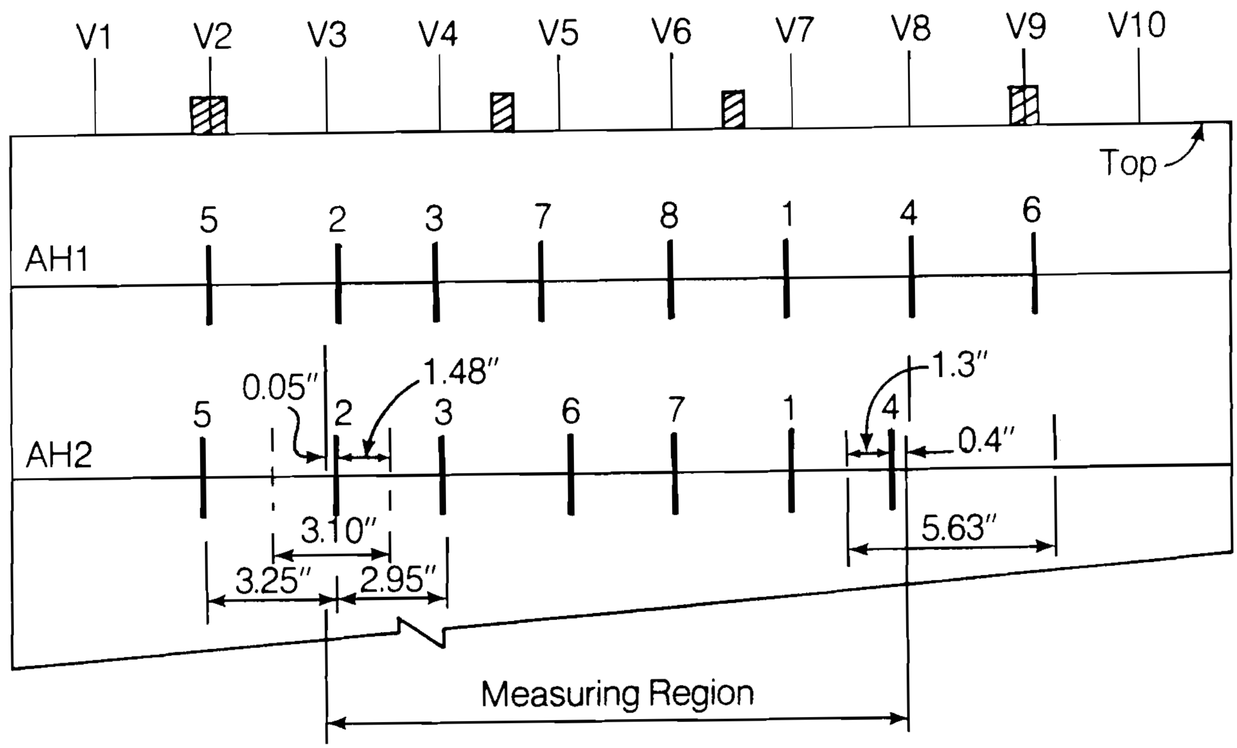

Figure 4.8 Locations of Cracks Crossing Horizontal Measuring Lines, Face A, Segment 2

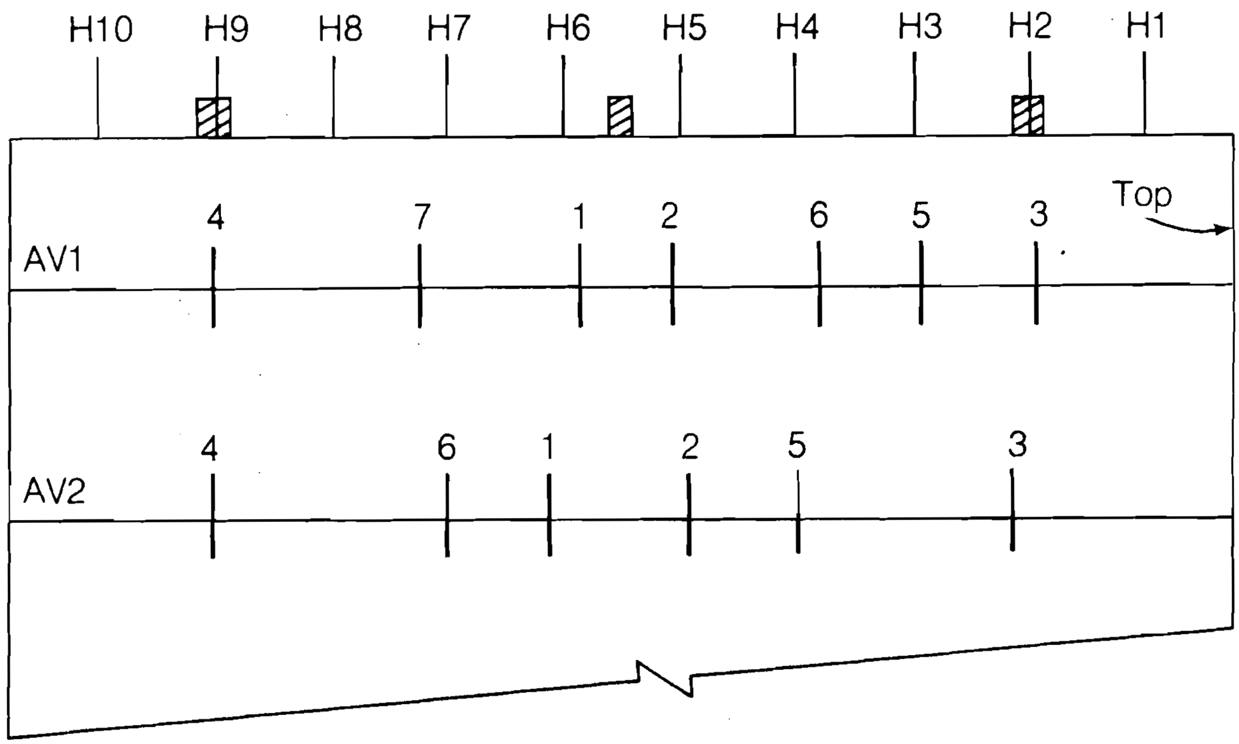

Figure 4.9 Locations of Cracks Crossing Measuring Lines, Face A, Segment 2

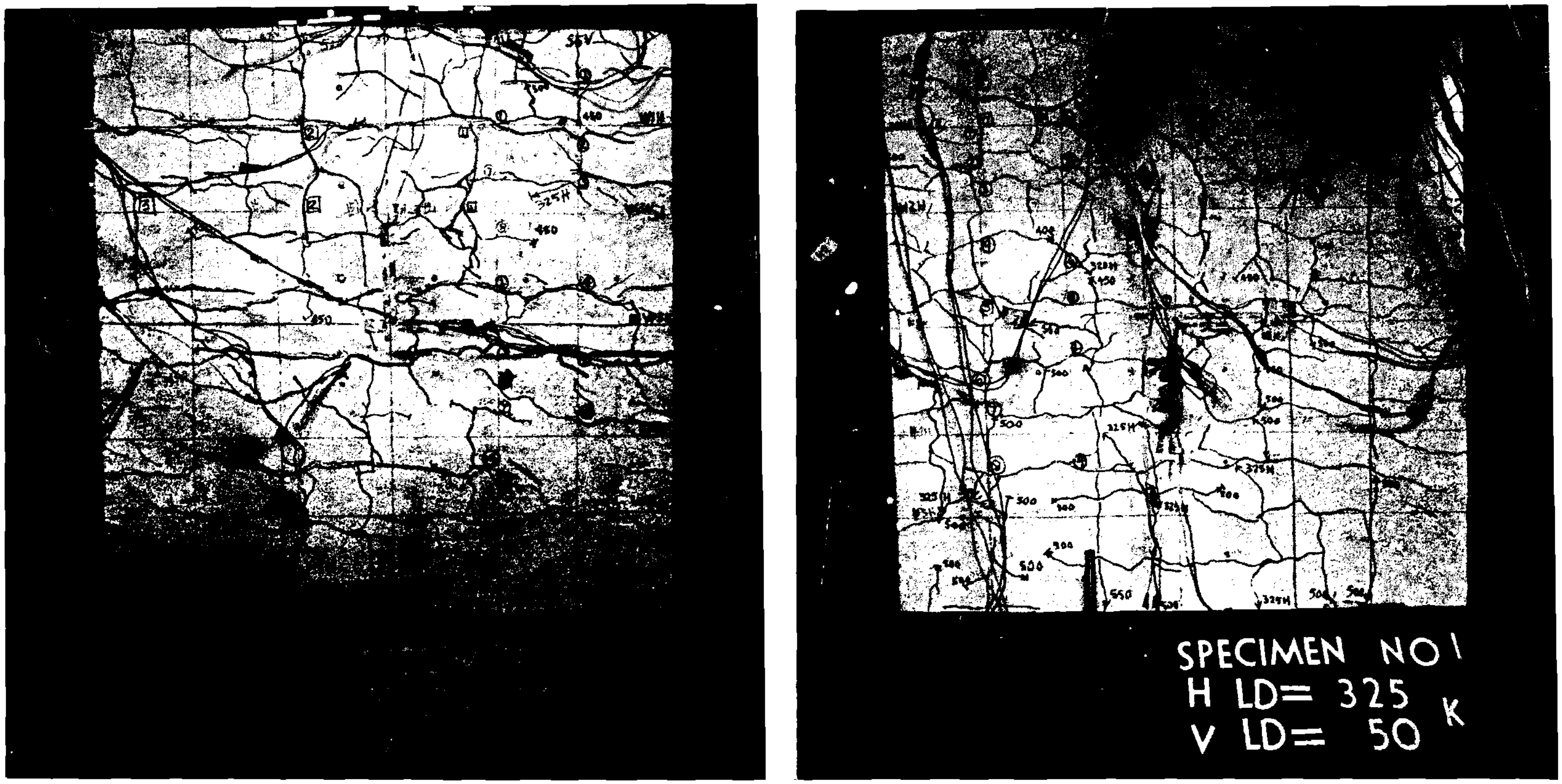

(a) Face A

(b) Face B

Figure 4.10.1 Cracks in Segment 1 at End of Test

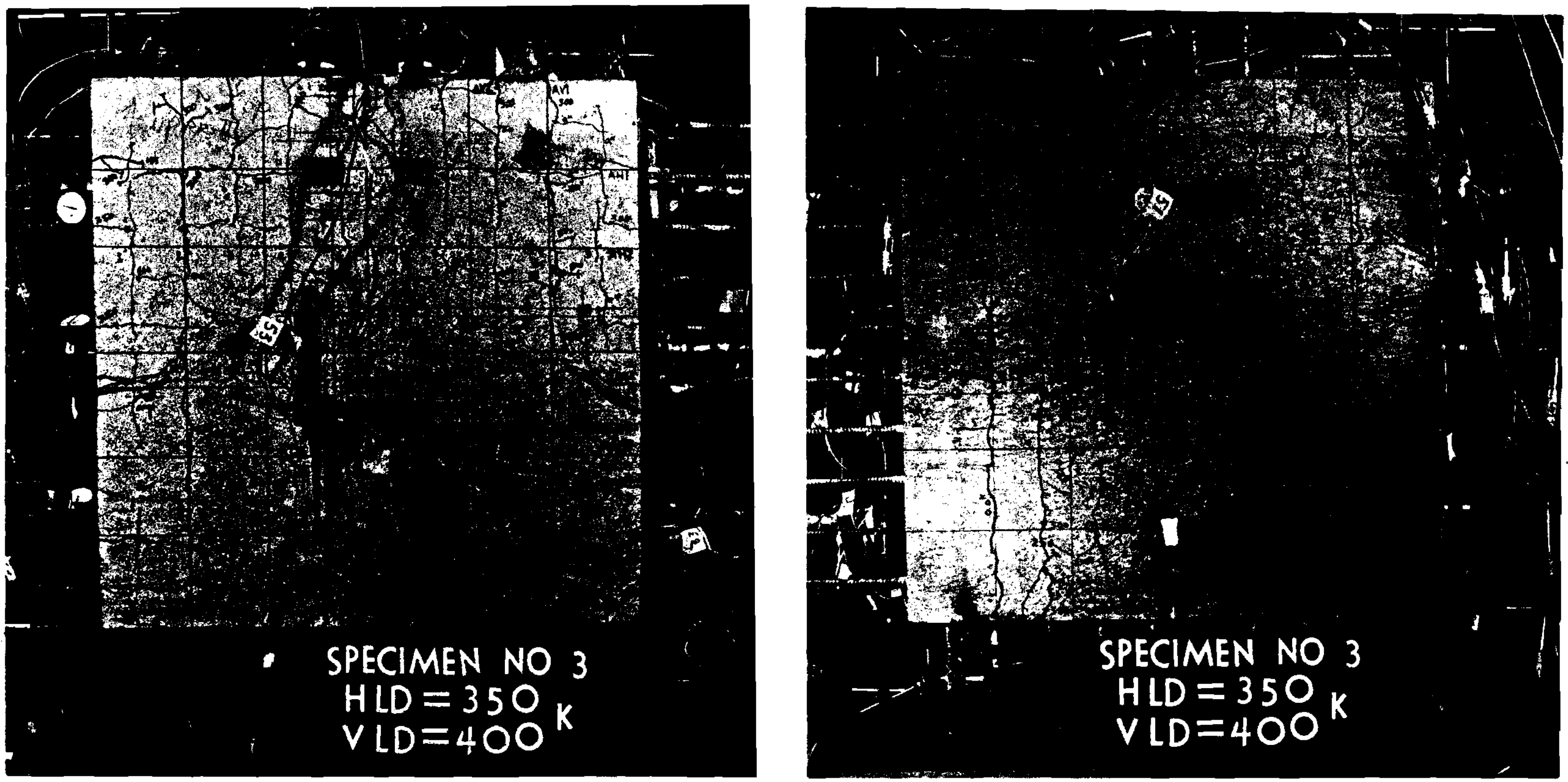

(a) Face A

(b) Face B

Figure 4.10.3 Cracks in Segment 3 at End of Test

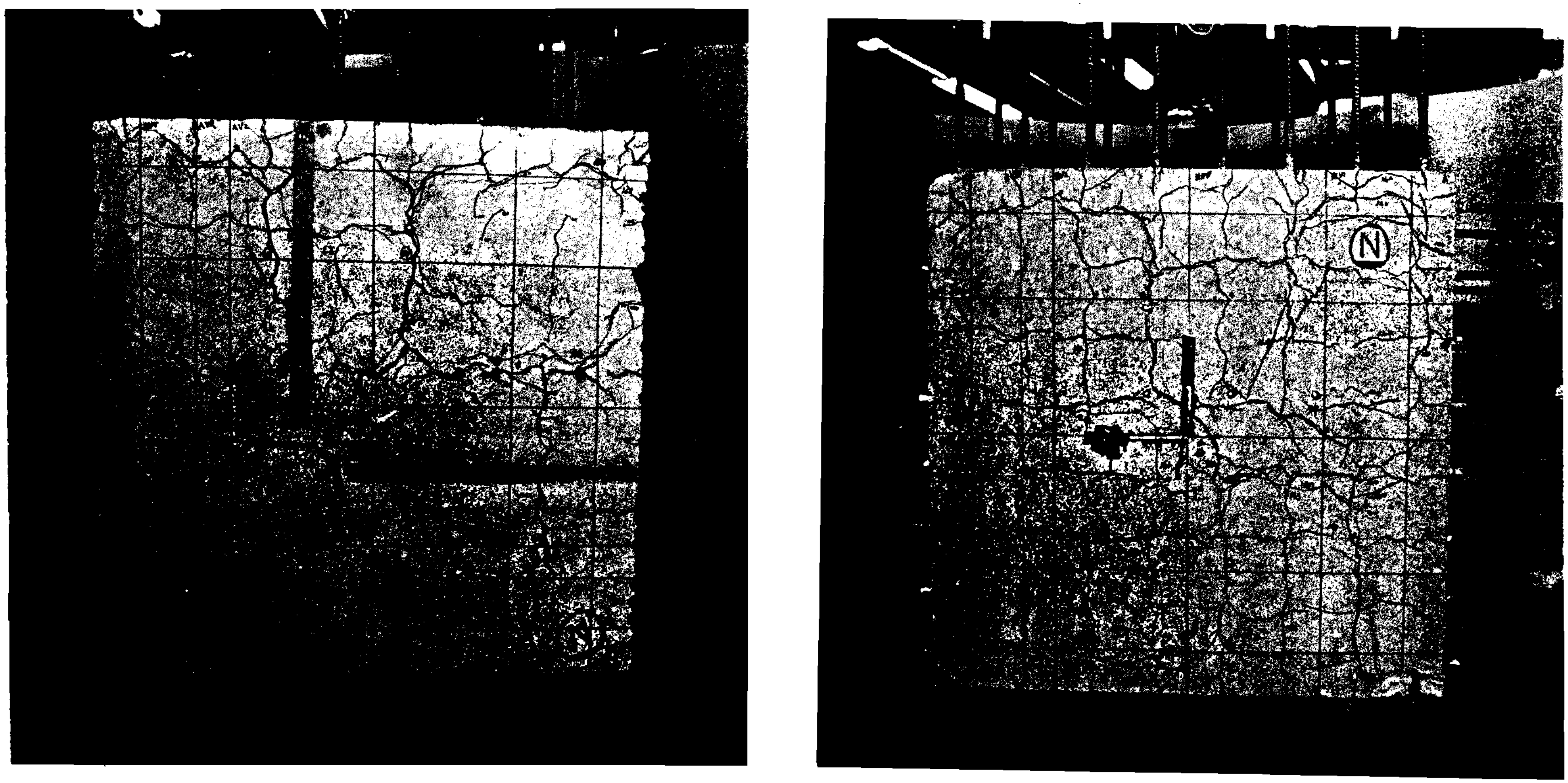

(a) Face A

(b) Face B

Figure 4.10.4 Cracks in Segment 4 at End of Test

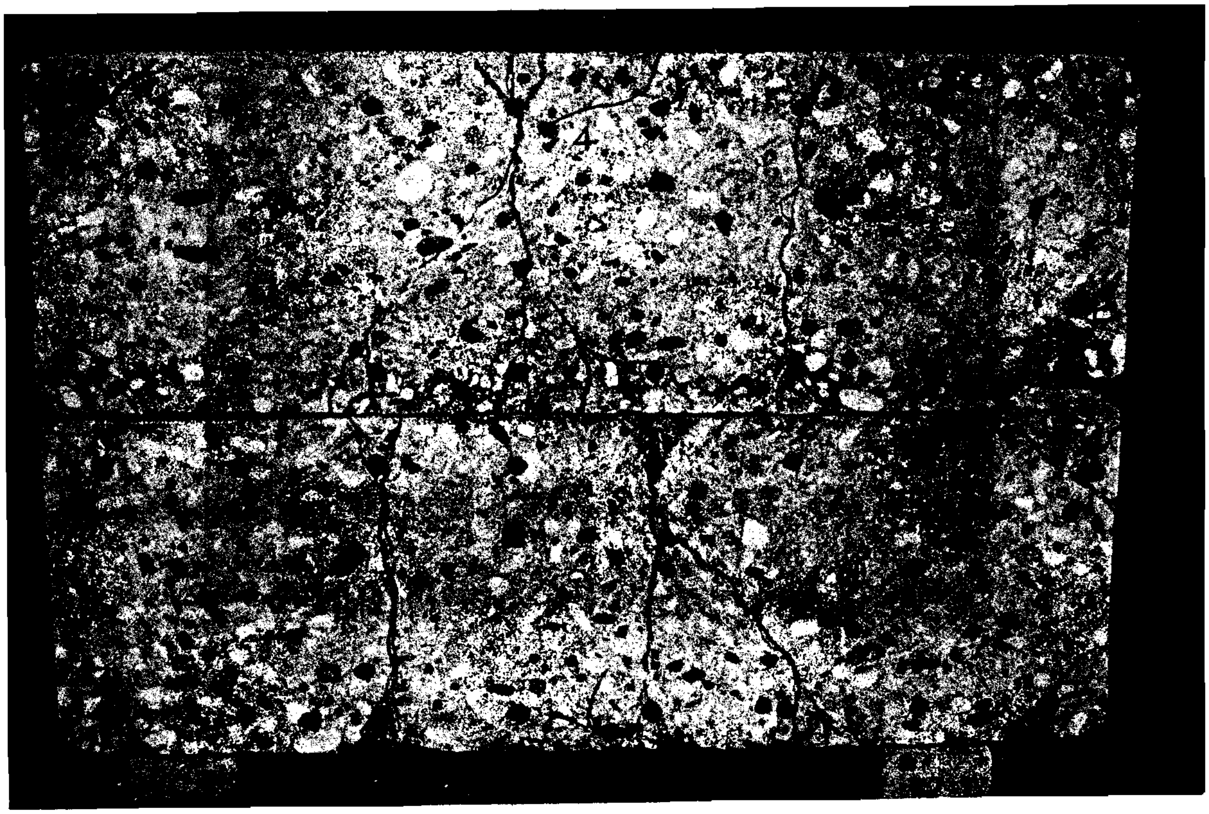

(c) Horizontal Section (Face A Upward)

Figure 4.10.4 Cracks in Segment 4 at End of Test

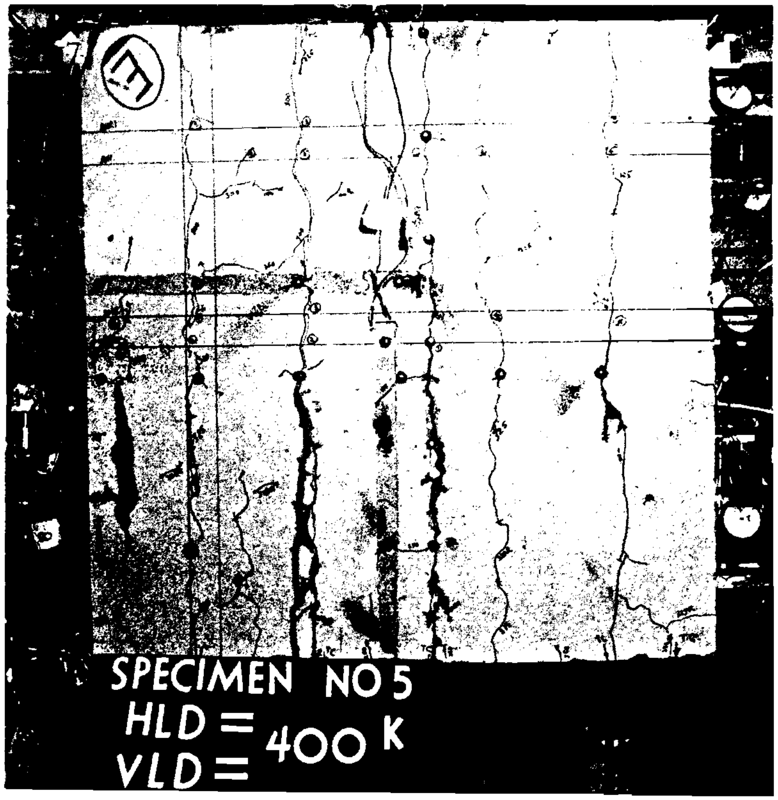

(a) Face A

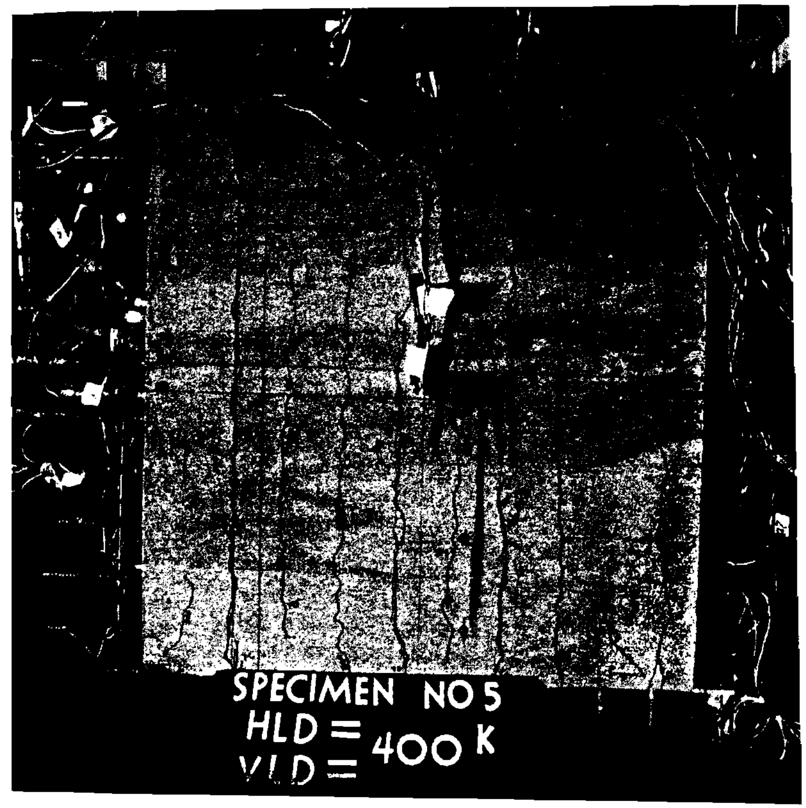

(b) Face B

Figure 4.10.5 Cracks in Segment 5 at End of Test

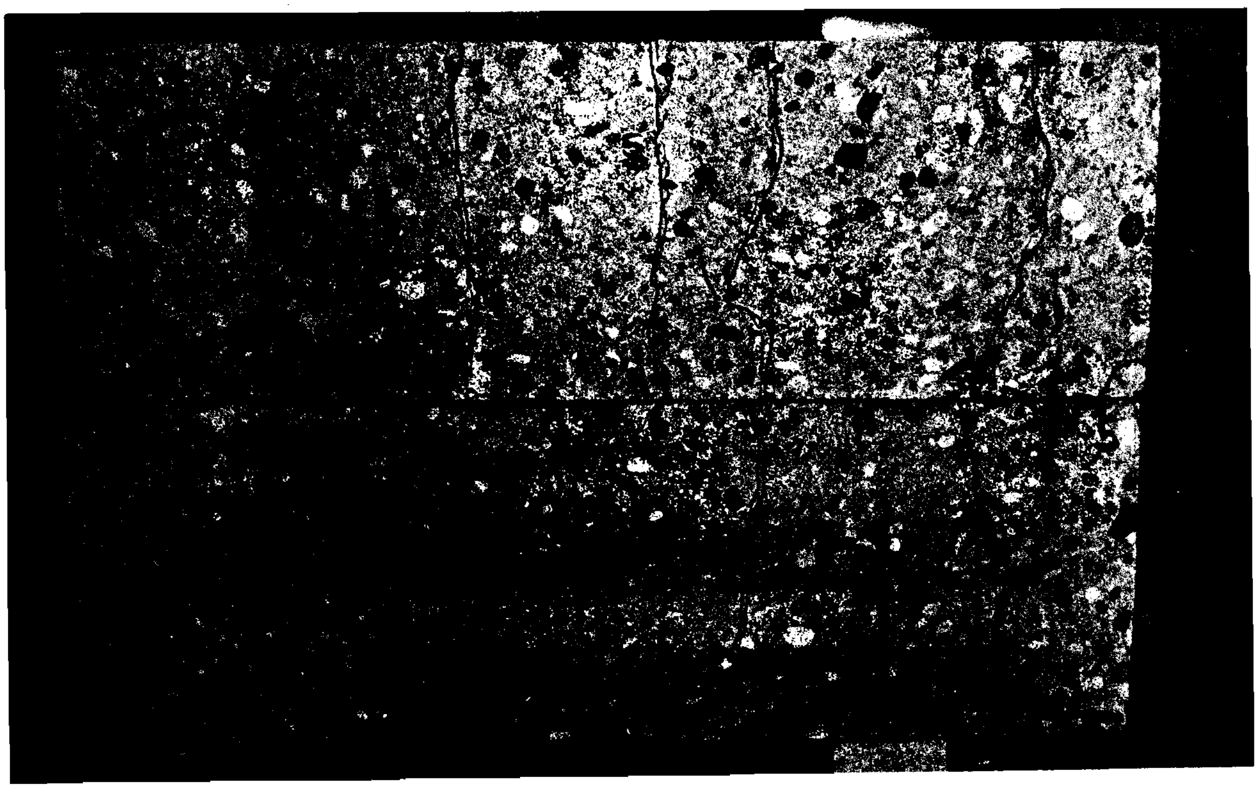

(c) Horizontal Section (Face A Upward)

Figure 4.10.5 Cracks in Segment 5 at End of Test

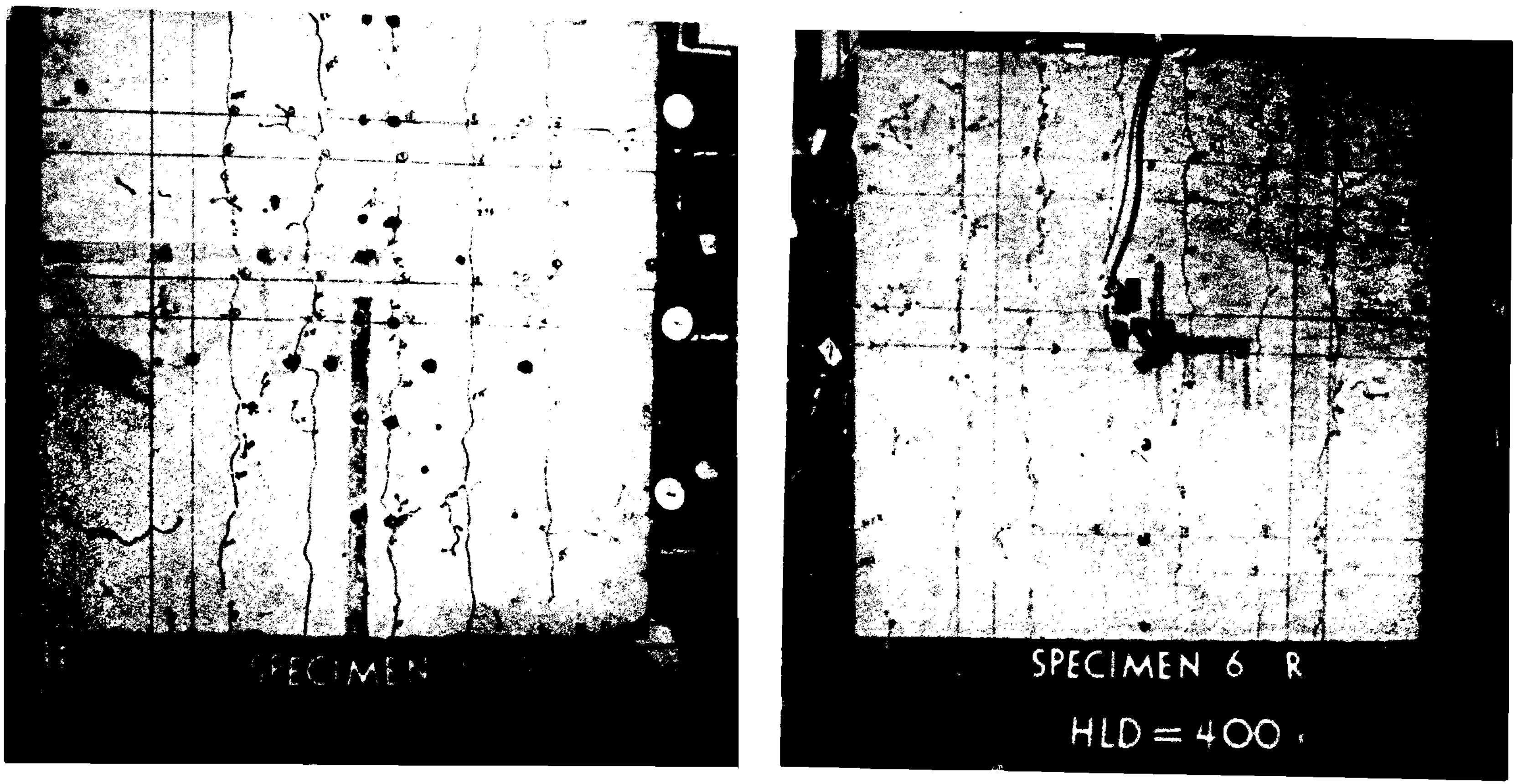

(a) Face A

(b) Face B

Figure 4.10.6 Cracks in Segment 6 at End of Test

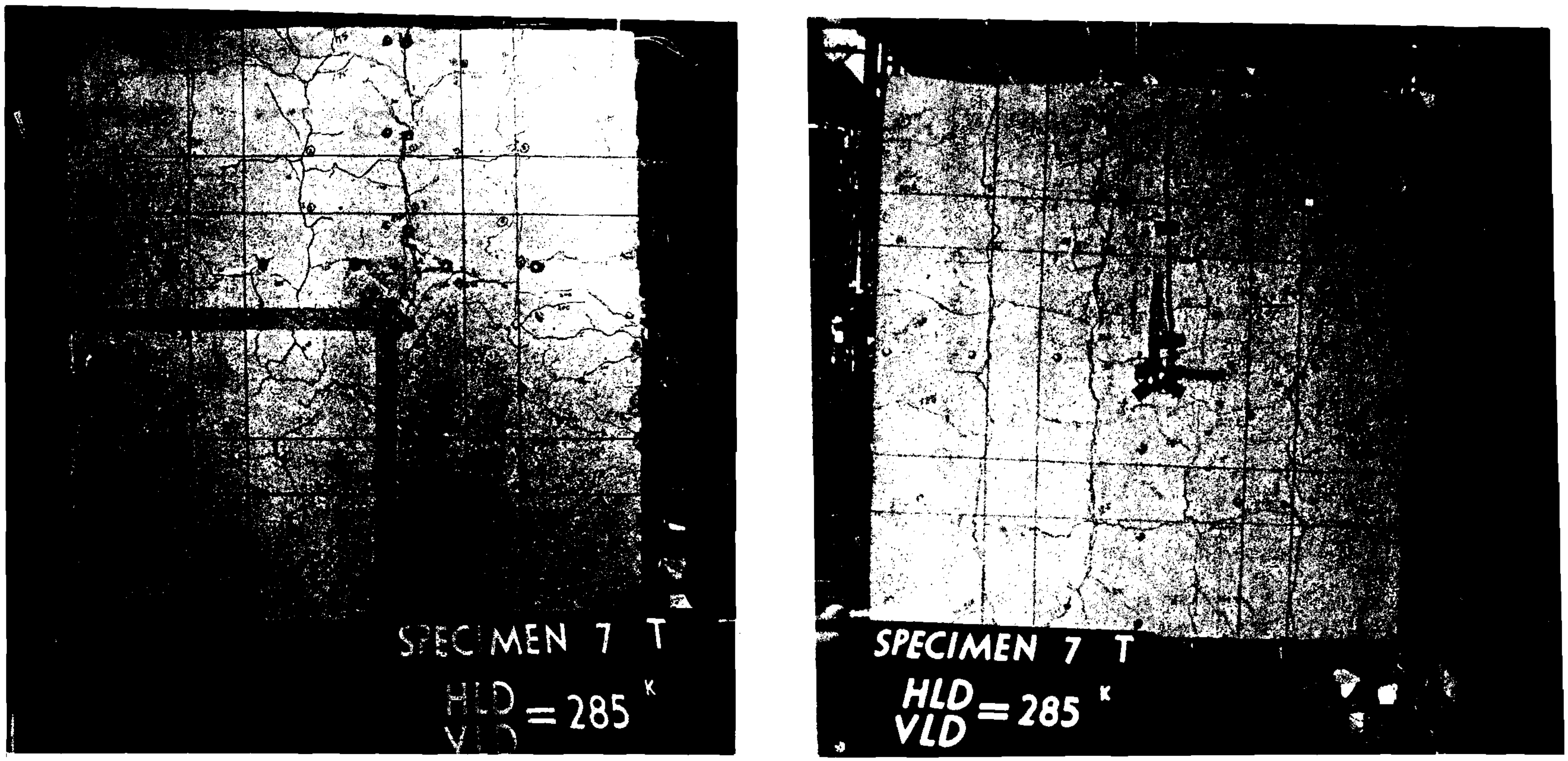

(a) Face A

(b) Face B

Figure 4.10.7 Cracks in Segment 7 at End of Test

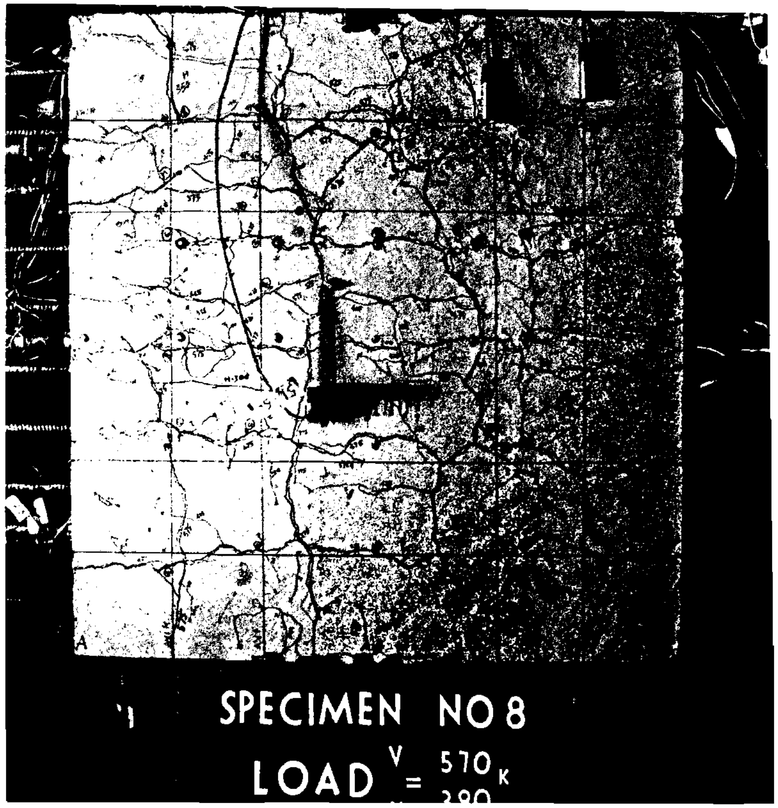

(a) Face A

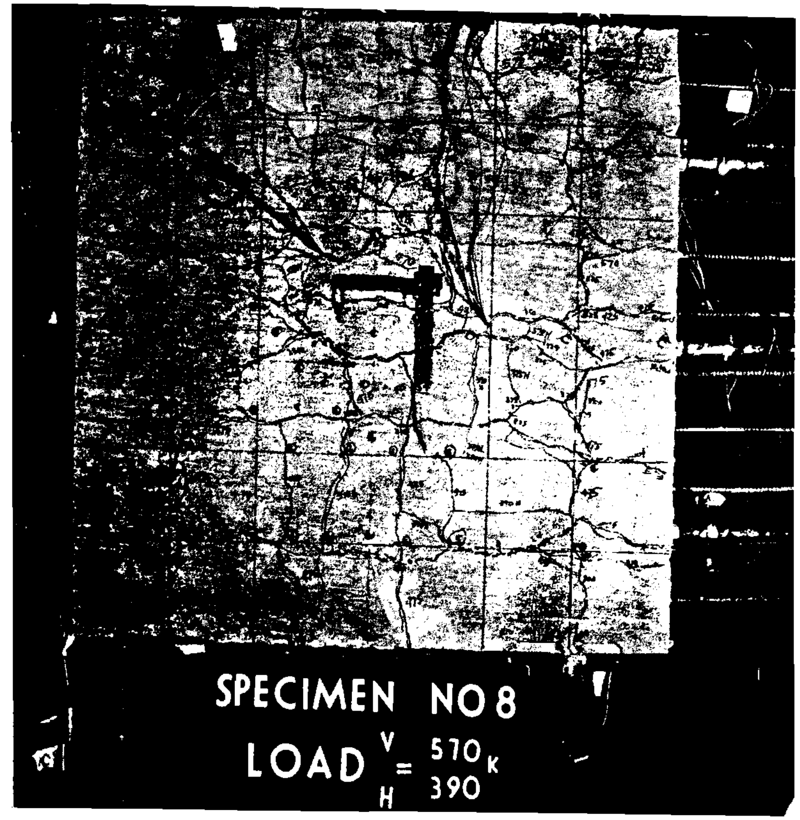

(b) Face B

Figure 4.10.8 Cracks in Segment 8 at End of Test

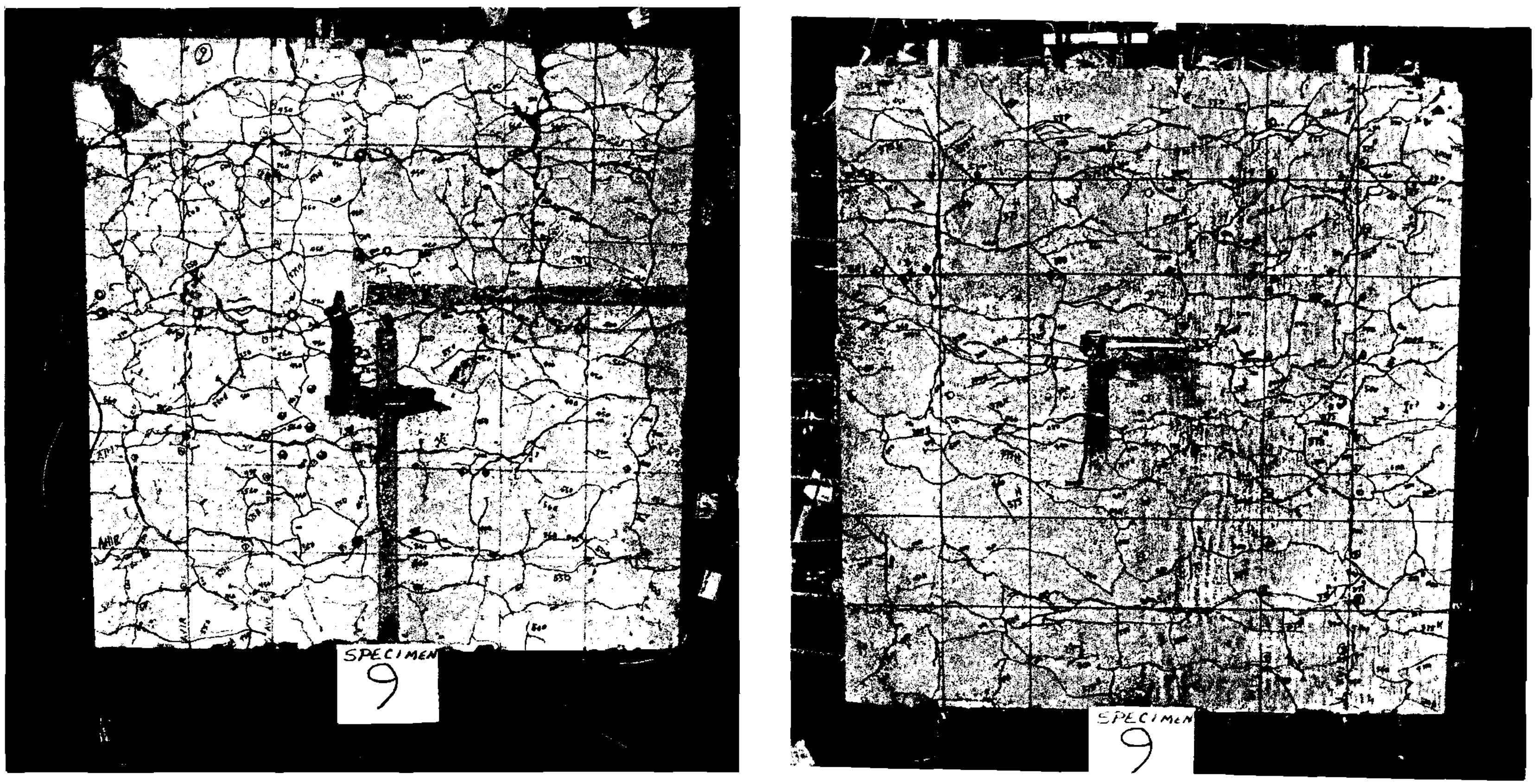

(a) Face A

(b) Face B

Figure 4.10.9 Cracks in Segment 9 at End of Test

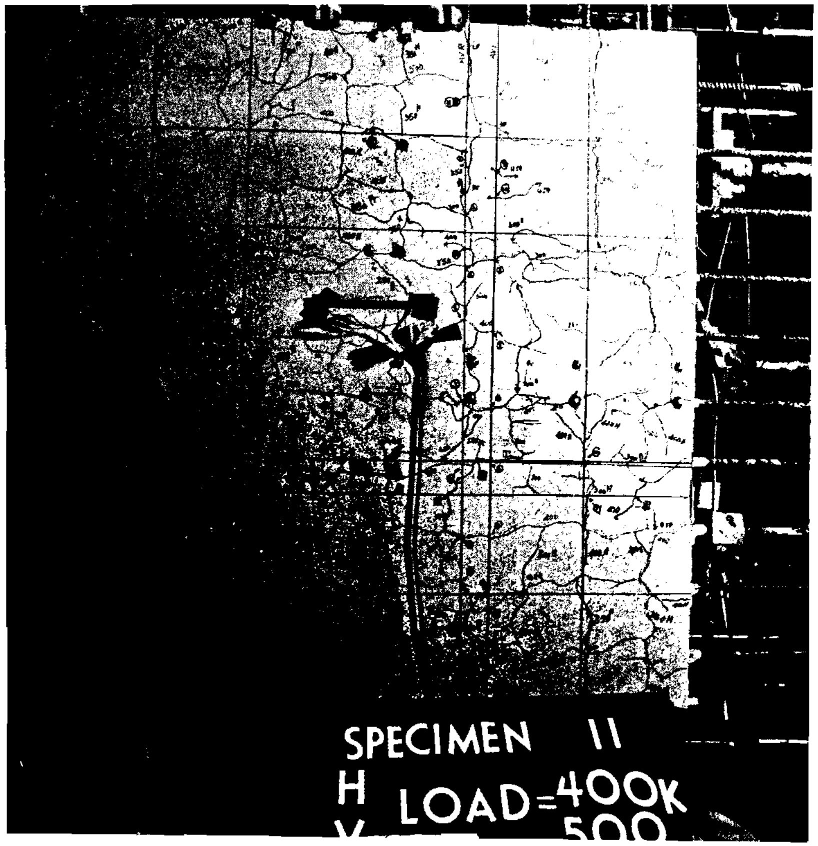

(a) Face A

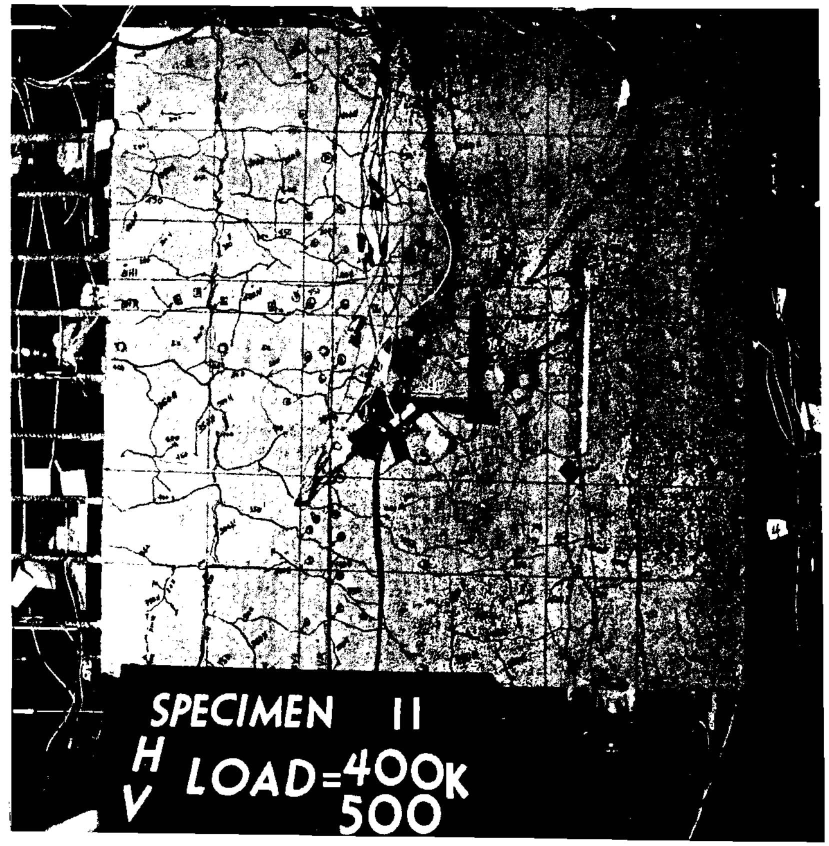

(b) Face B

Figure 4.10.11 Cracks in Segment 11 at End of Test

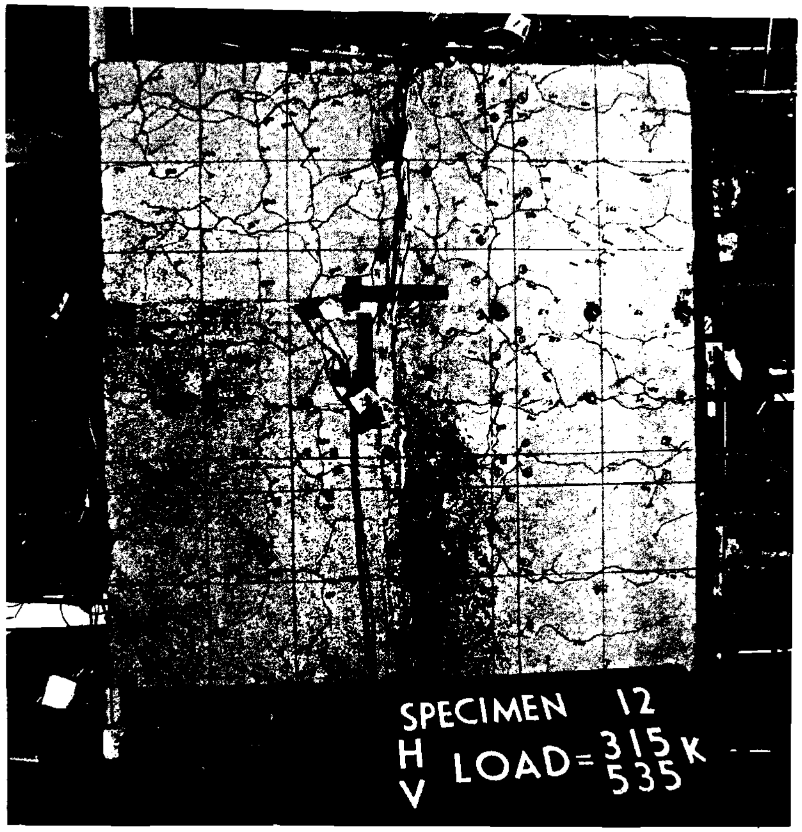

(a) Face A

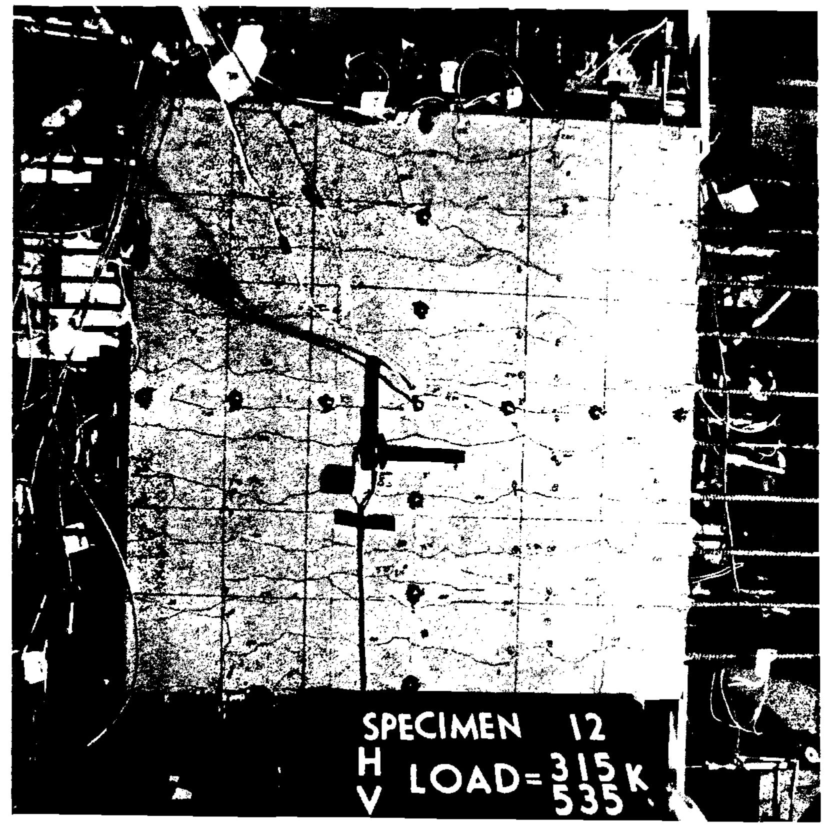

(b) Face B

Figure 4.10.12 Cracks in Segment 12 at End of Test

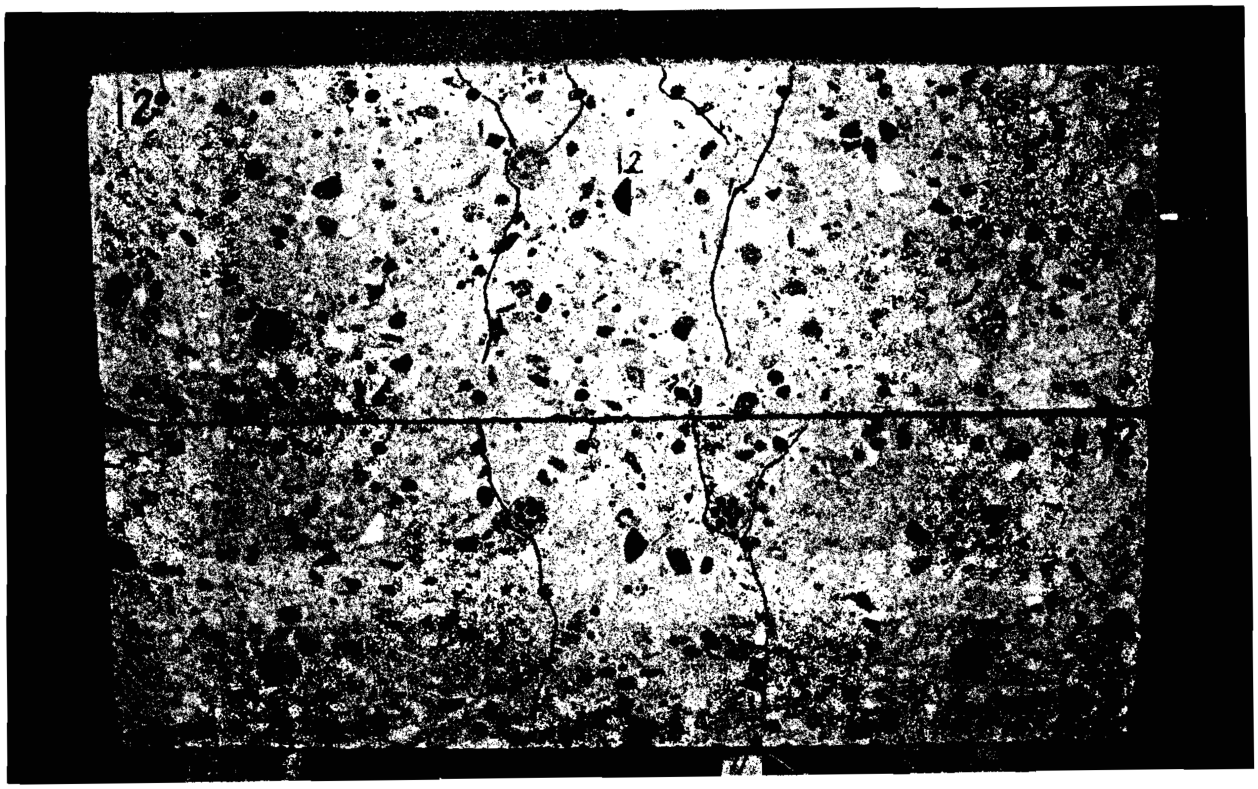

(c) Horizontal Section (Face A Upward)

Figure 4.10.12 Cracks in Segment 12 at End of Test

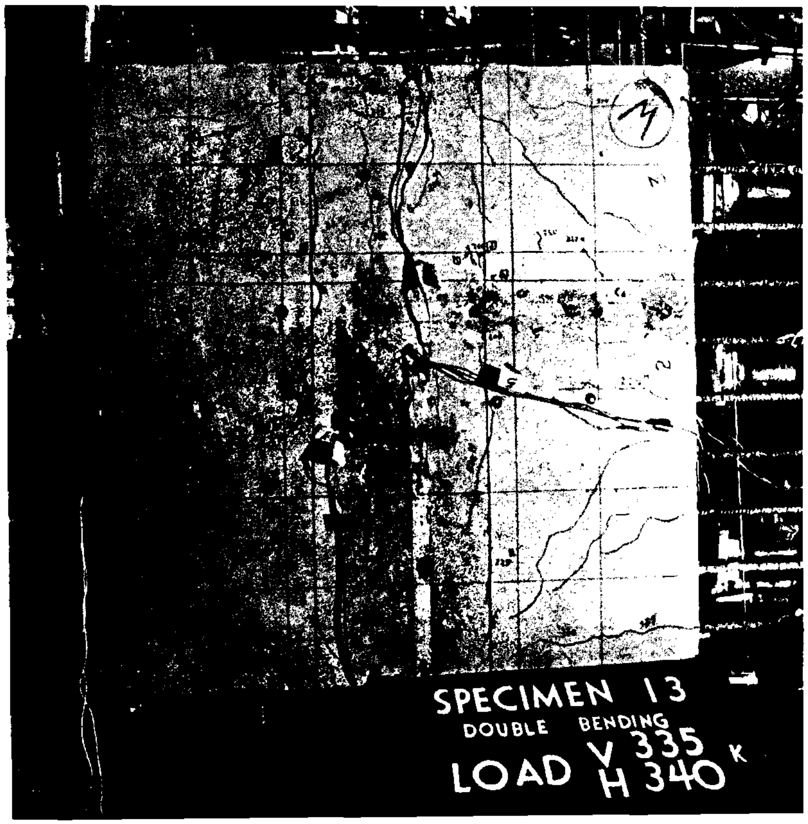

(a) Face A

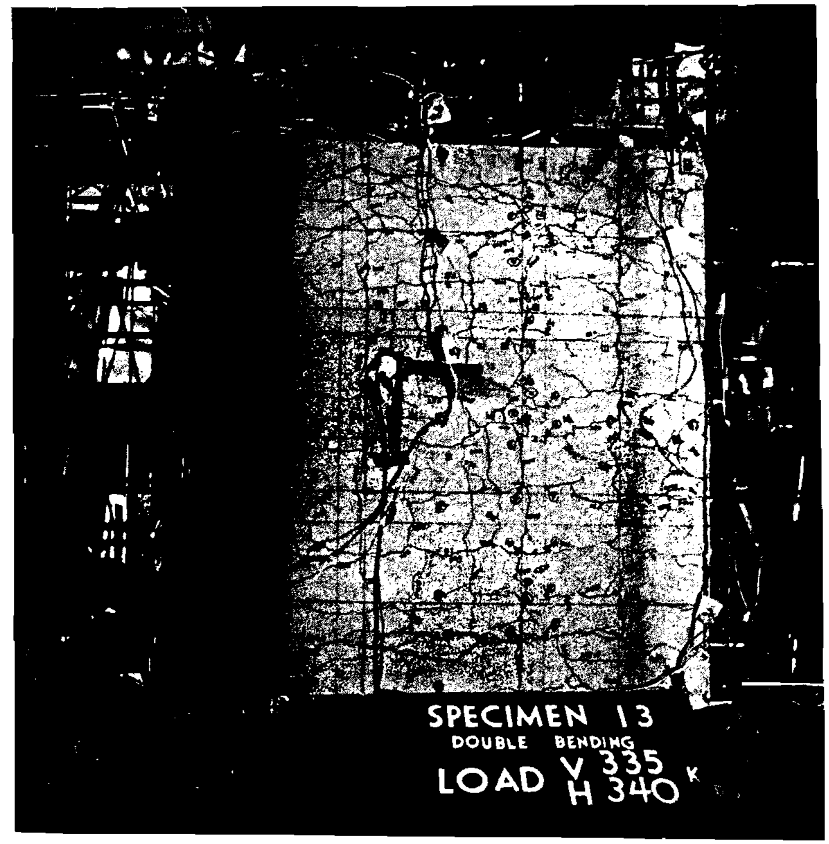

(b) Face B

Figure 4.10.13 Cracks in Segment 13 at End of Test

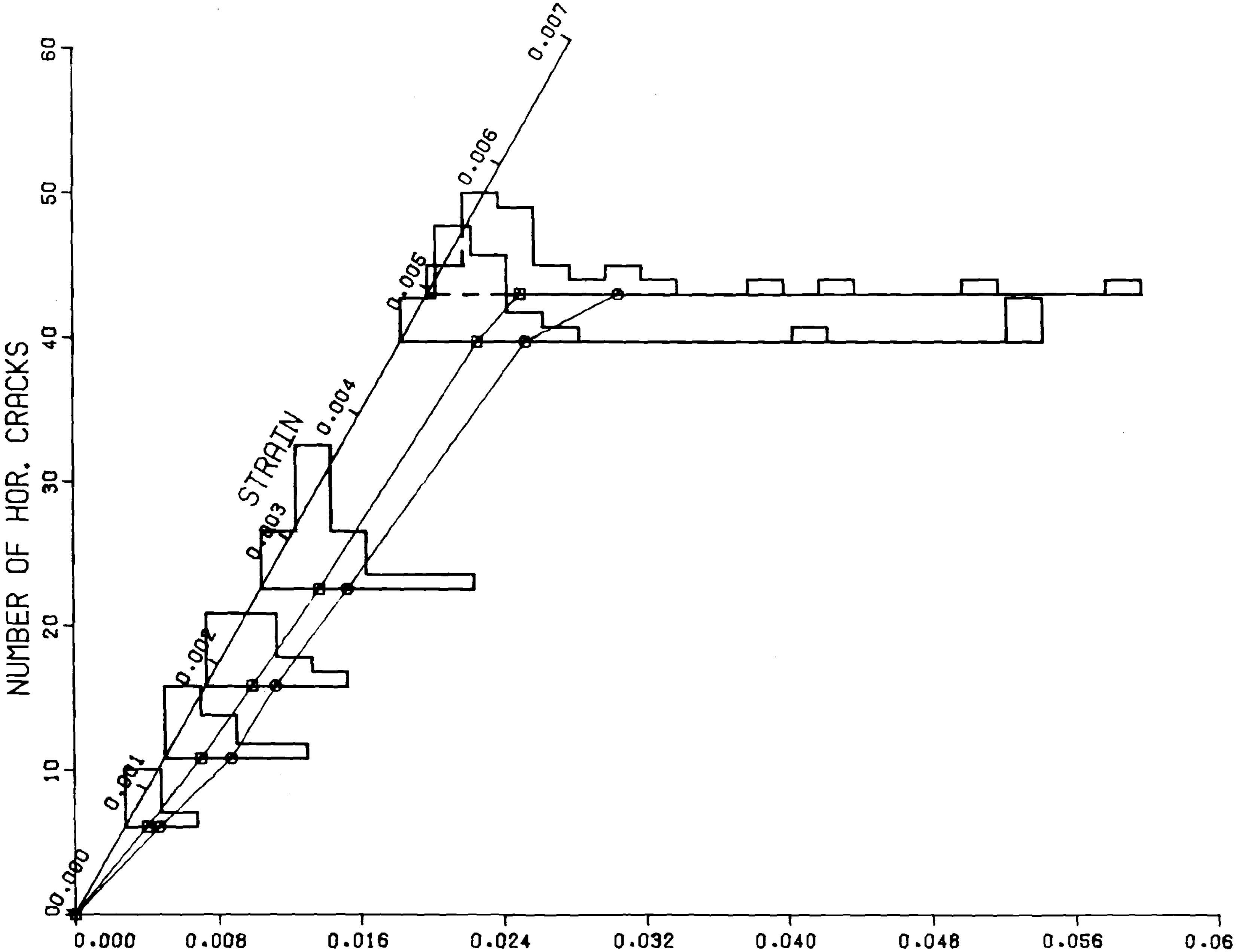

(a) Horizontal Cracks

Figure 4.11.1 Distribution of Crack Widths, Segment 1

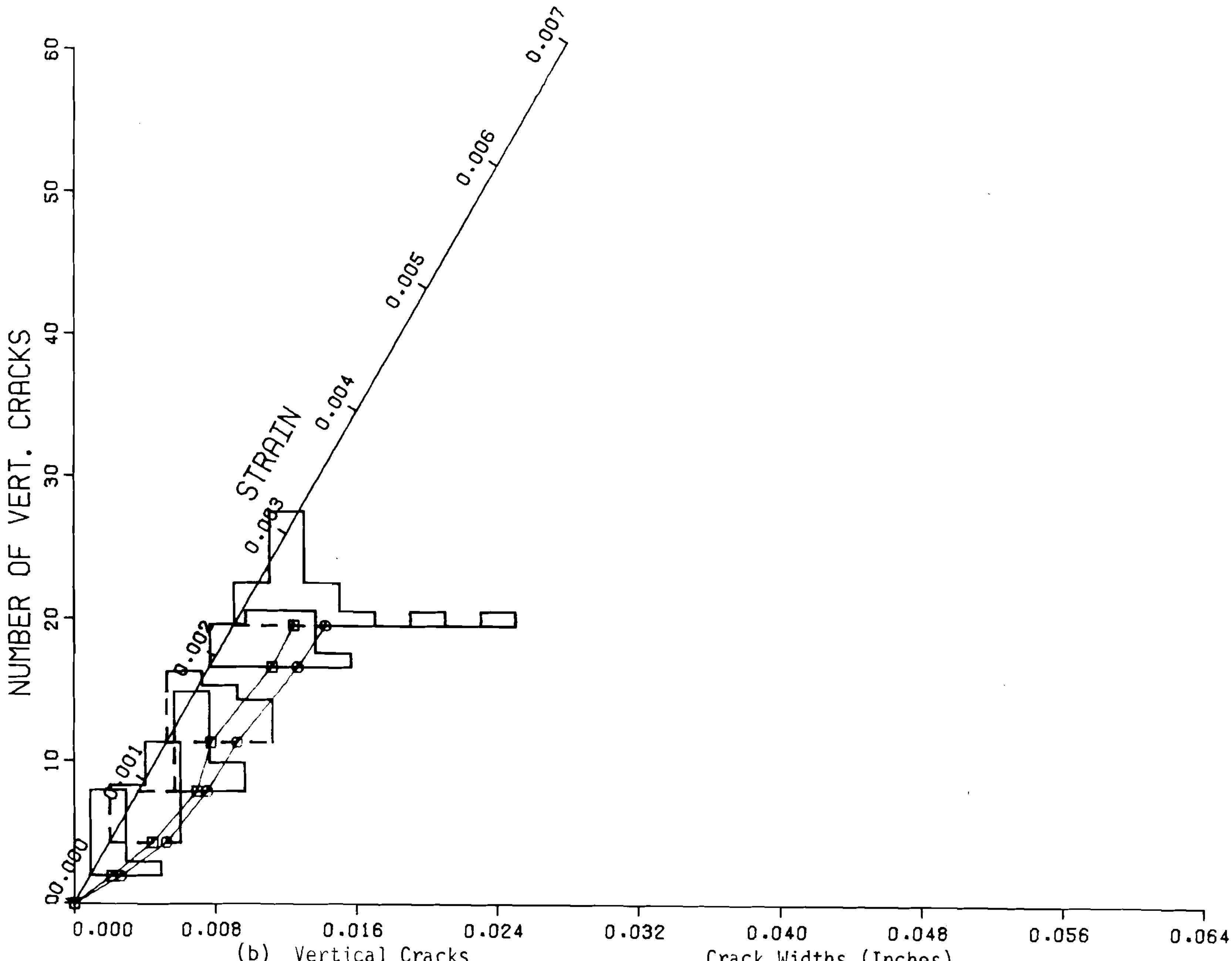

(b) Vertical Cracks

Figure 4.11.1 Distribution of Crack Widths, Segment 1

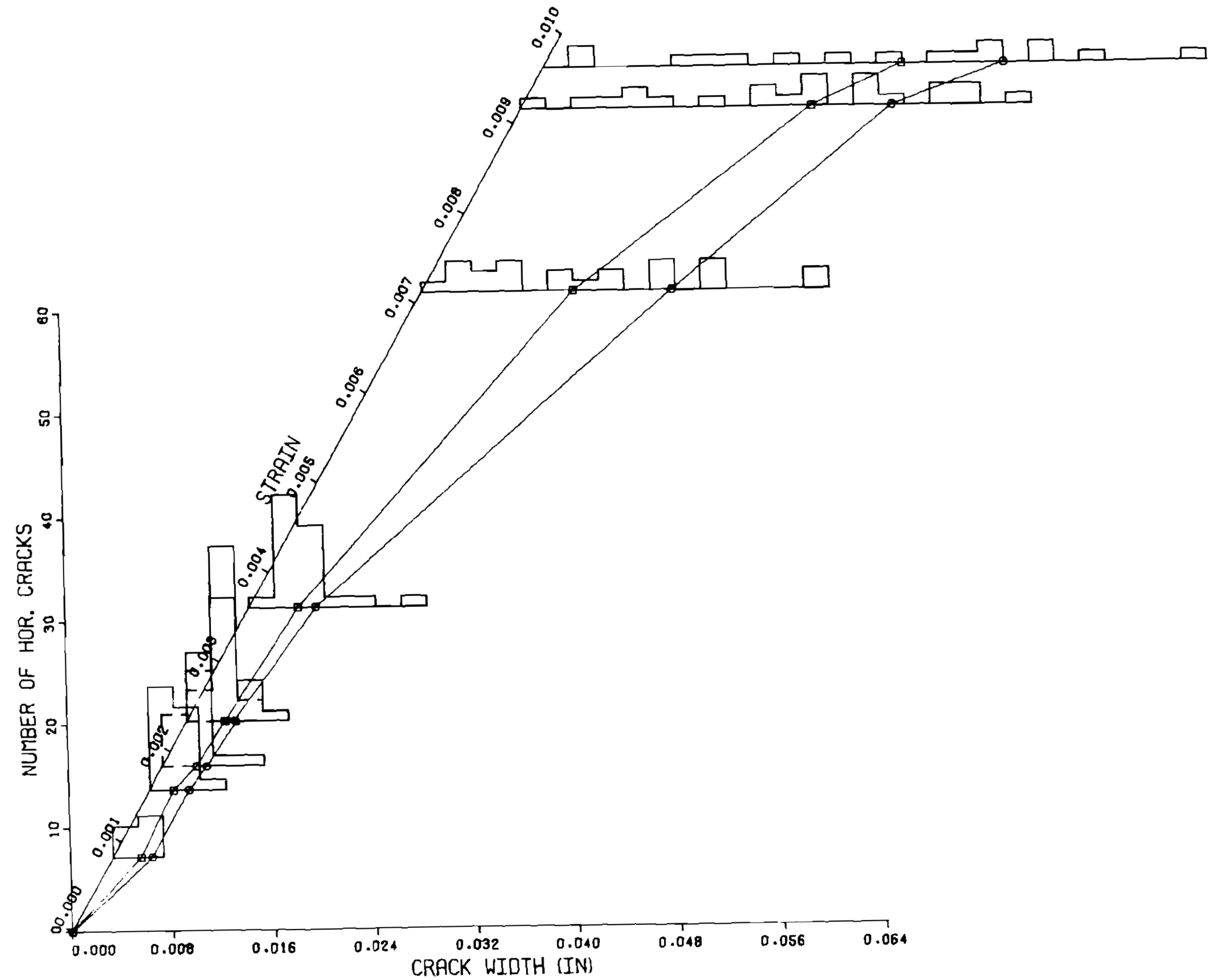

(a) Horizontal Cracks

Figure 4.11.2 Distribution of Crack Widths, Segment 2

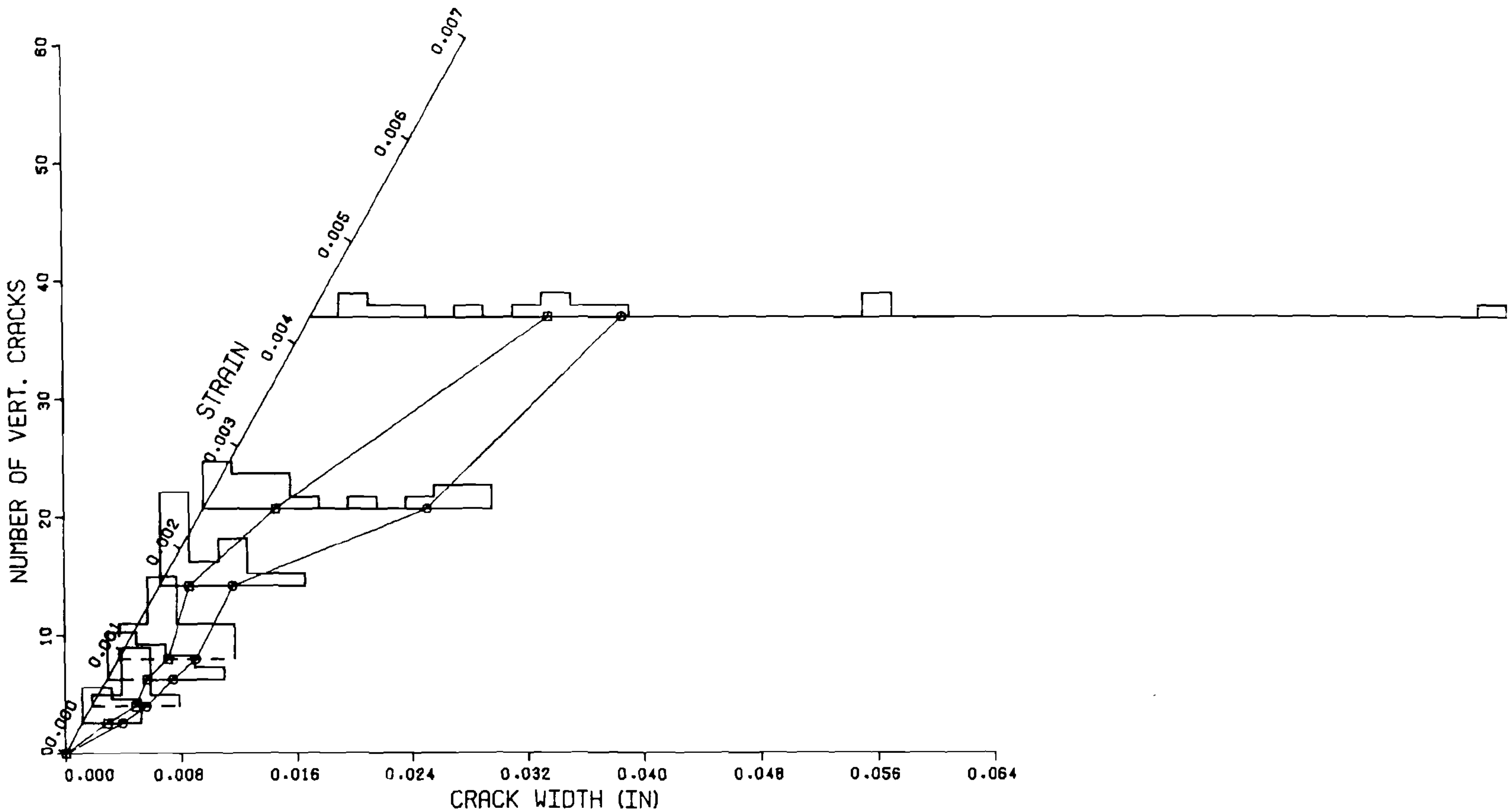

(b) Vertical Cracks

Figure 4.11.2 Distribution of Crack Widths, Segment 2

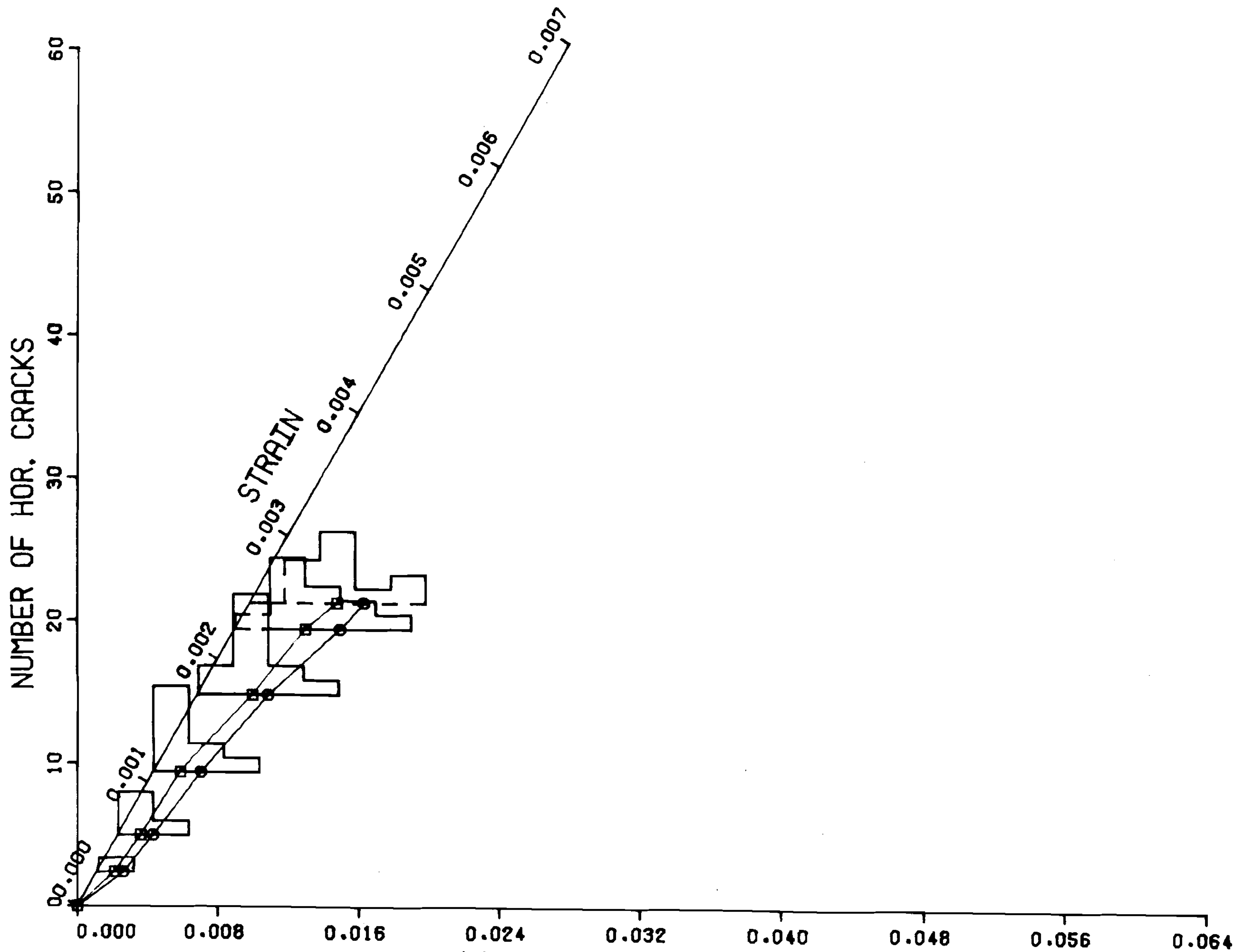

(a) Horizontal Cracks

Figure 4.11.3 Distribution of Crack Widths, Segment 3

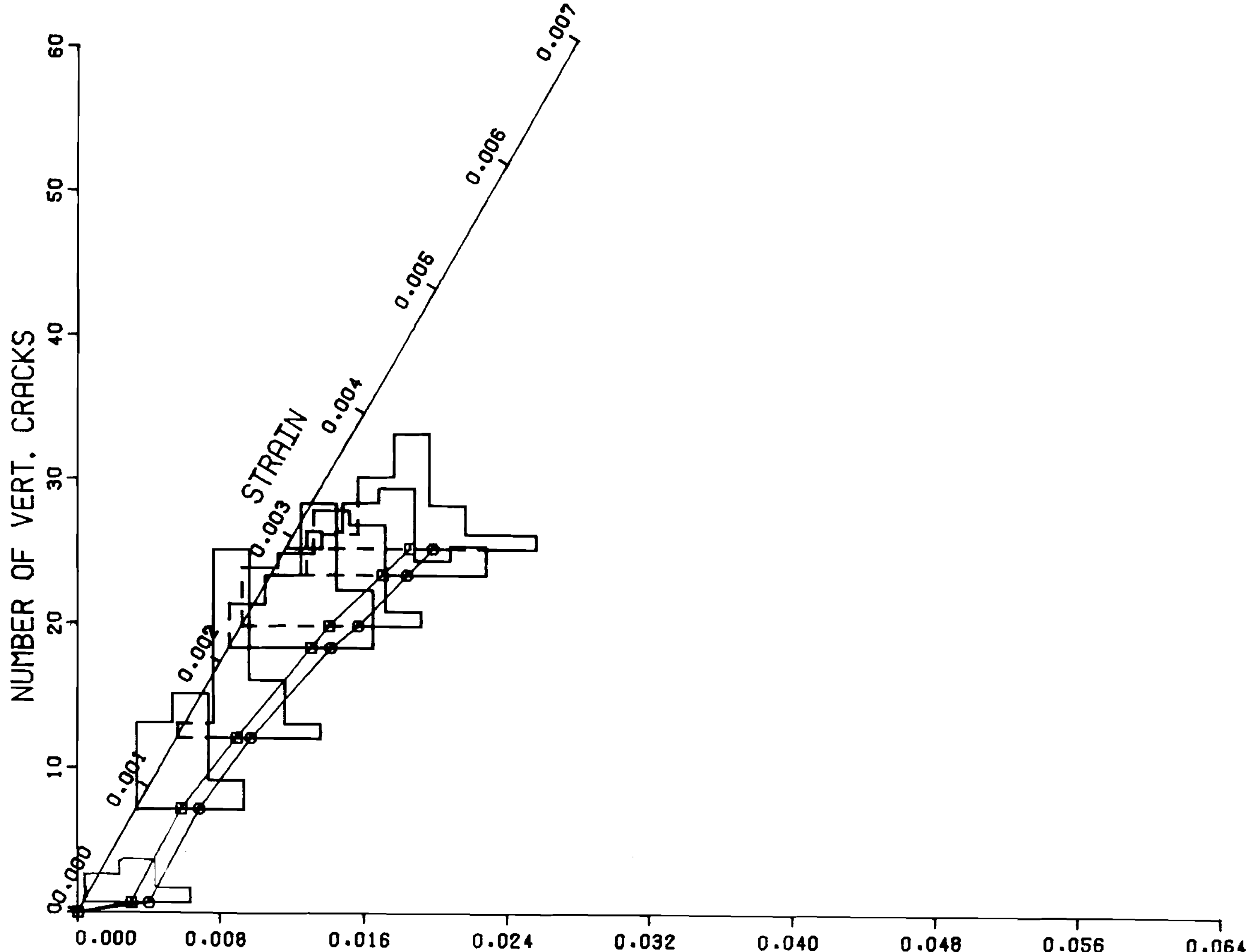

(b) Vertical Cracks

Figure 4.11.3 Distribution of Crack Widths, Segment 3

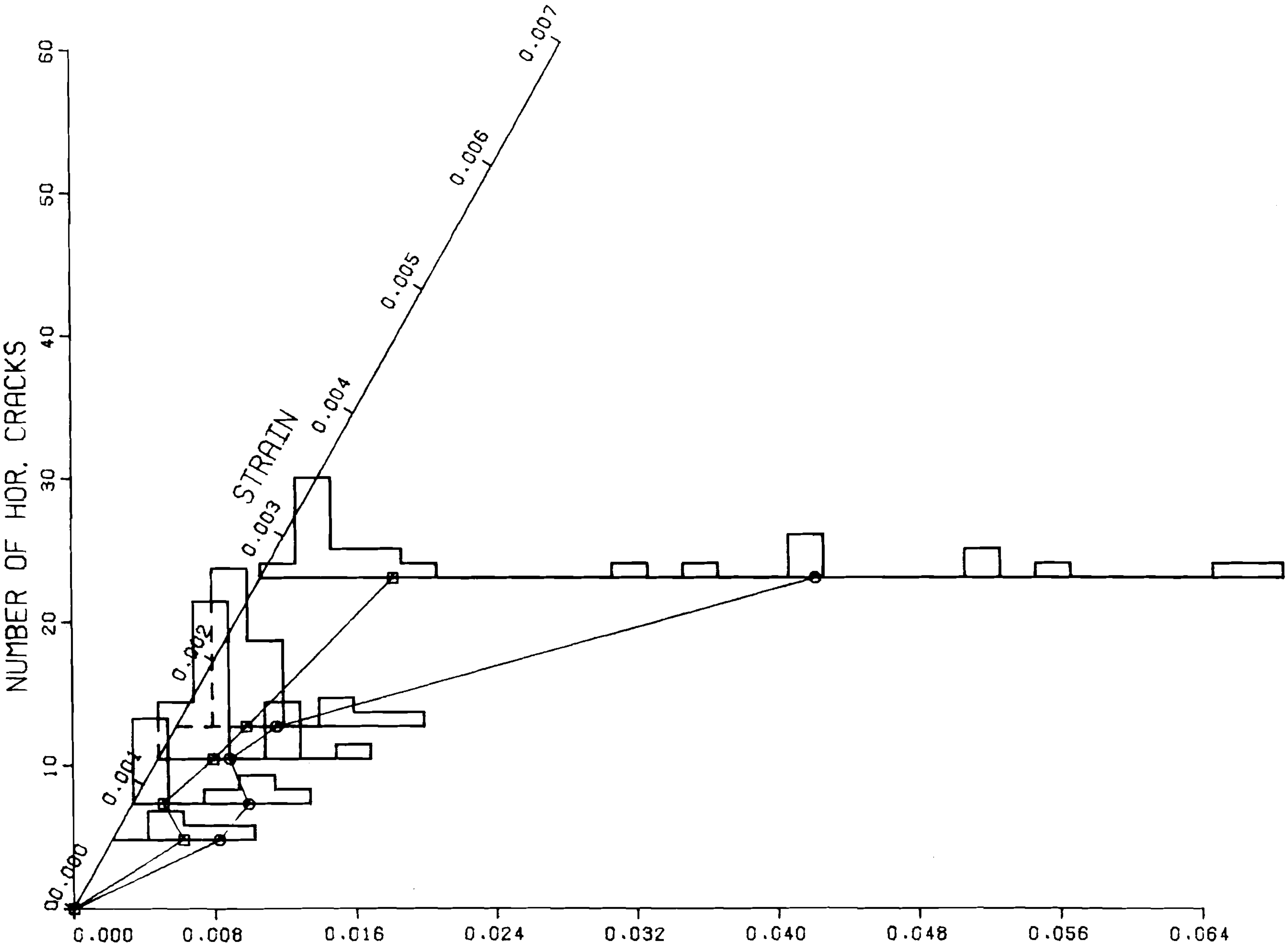

(a) Horizontal Cracks

Figure 4.11.4 Distribution of Crack Widths, Segment 4

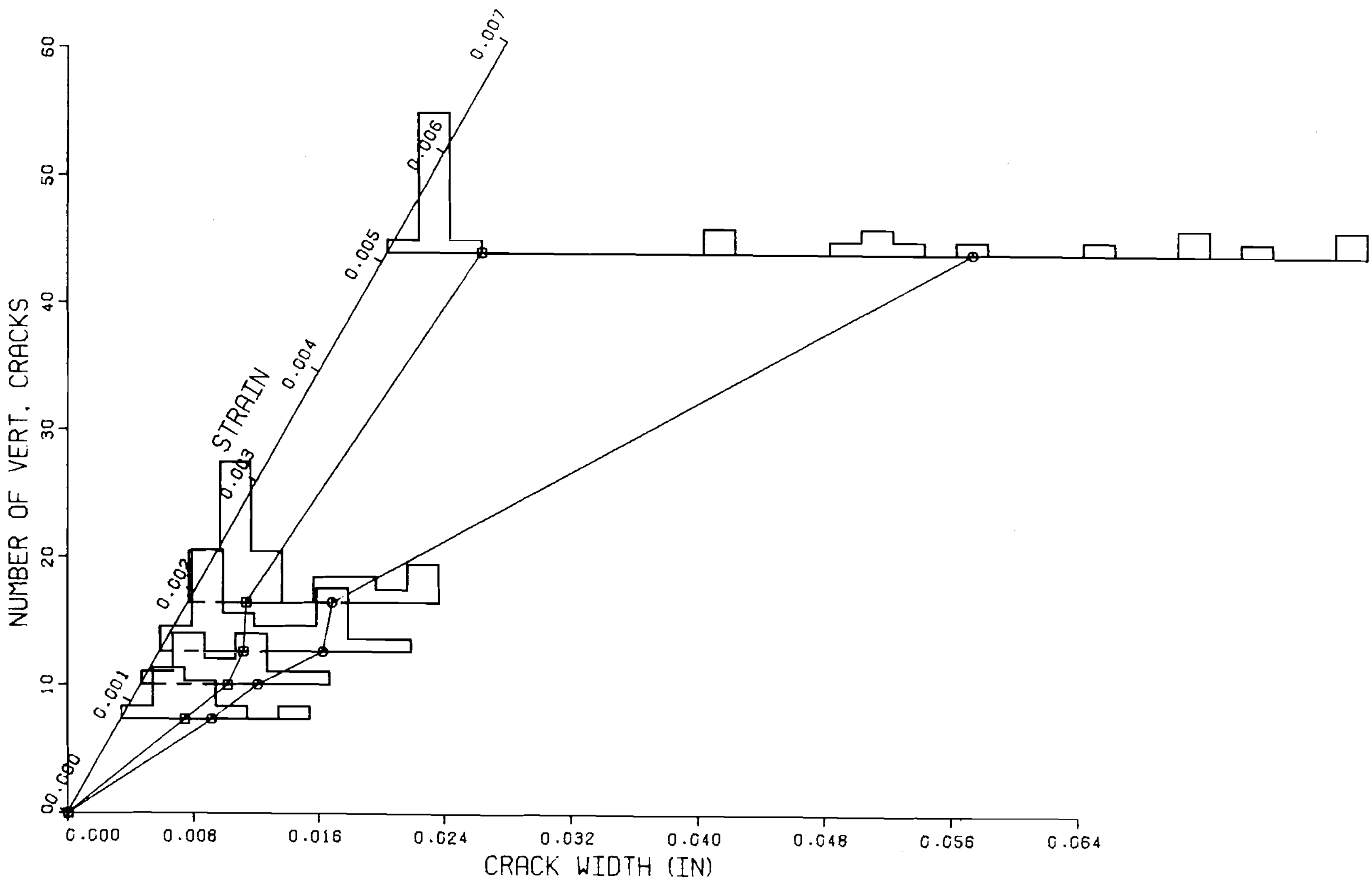

(b) Vertical Cracks

Figure 4.11.4 Distribution of Crack Widths, Segment 4

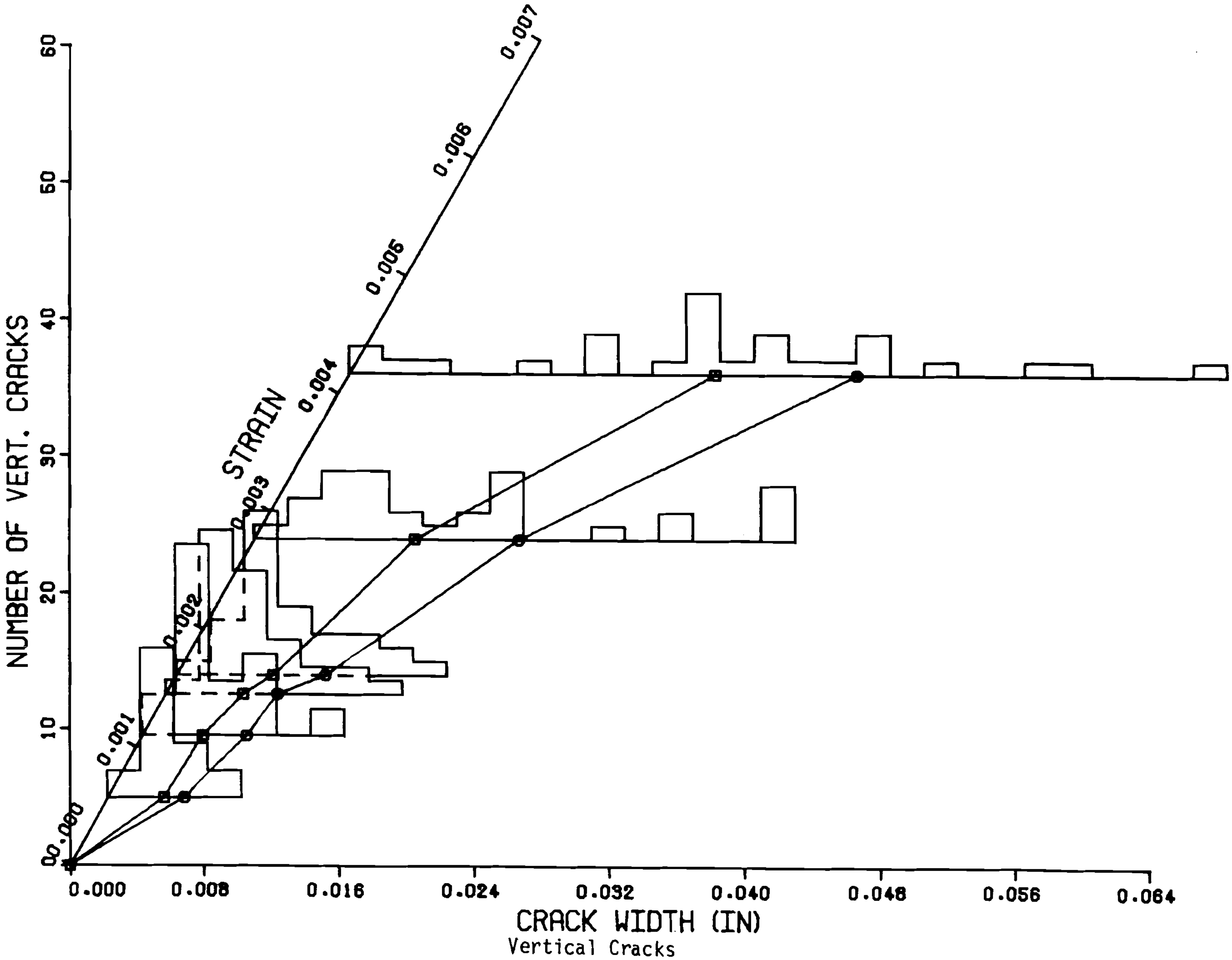

Figure 4.11.5 Distribution of Crack Widths, Segment 5

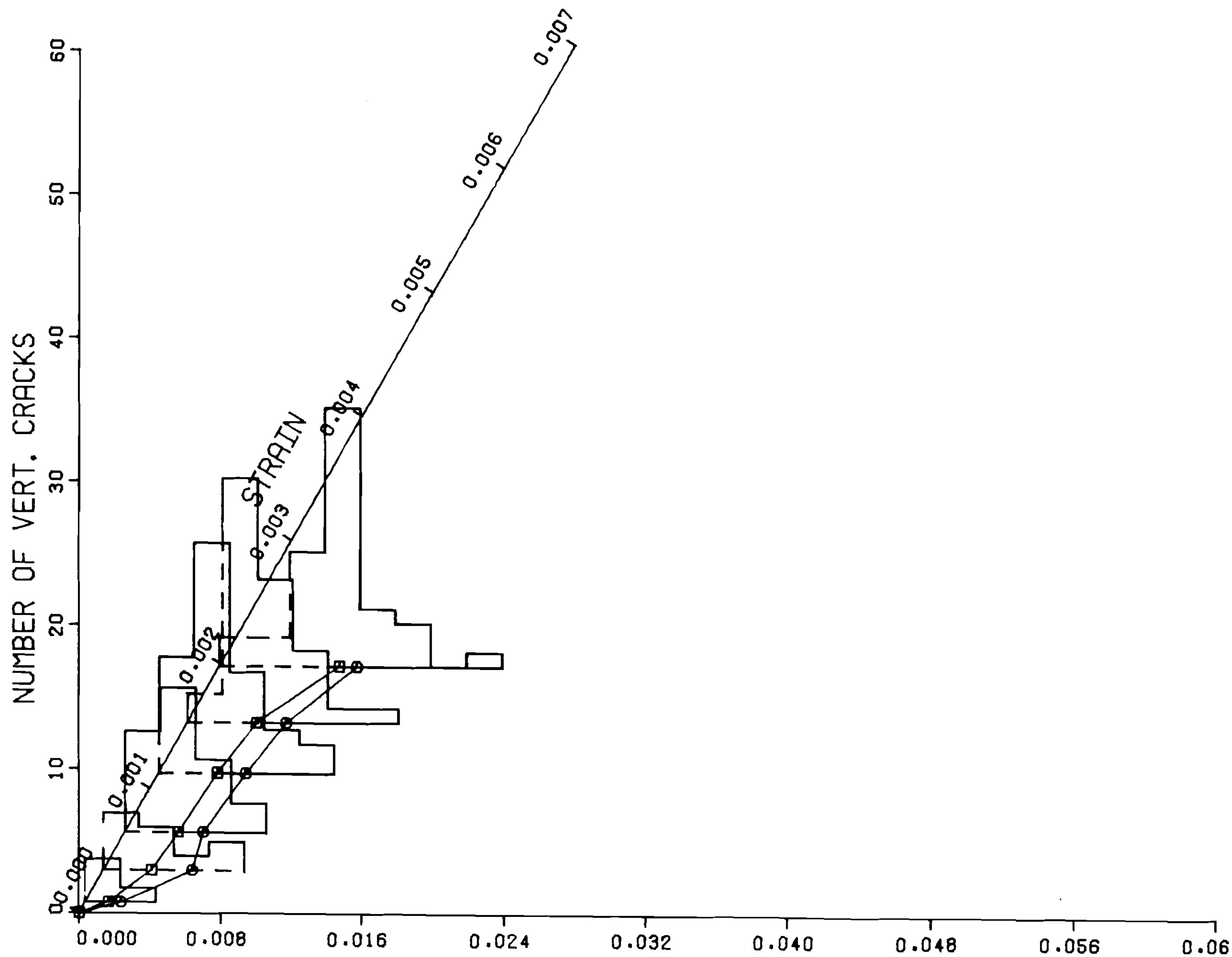

Vertical Cracks

Figure 4.11.6 Distribution of Crack Widths, Segment 6

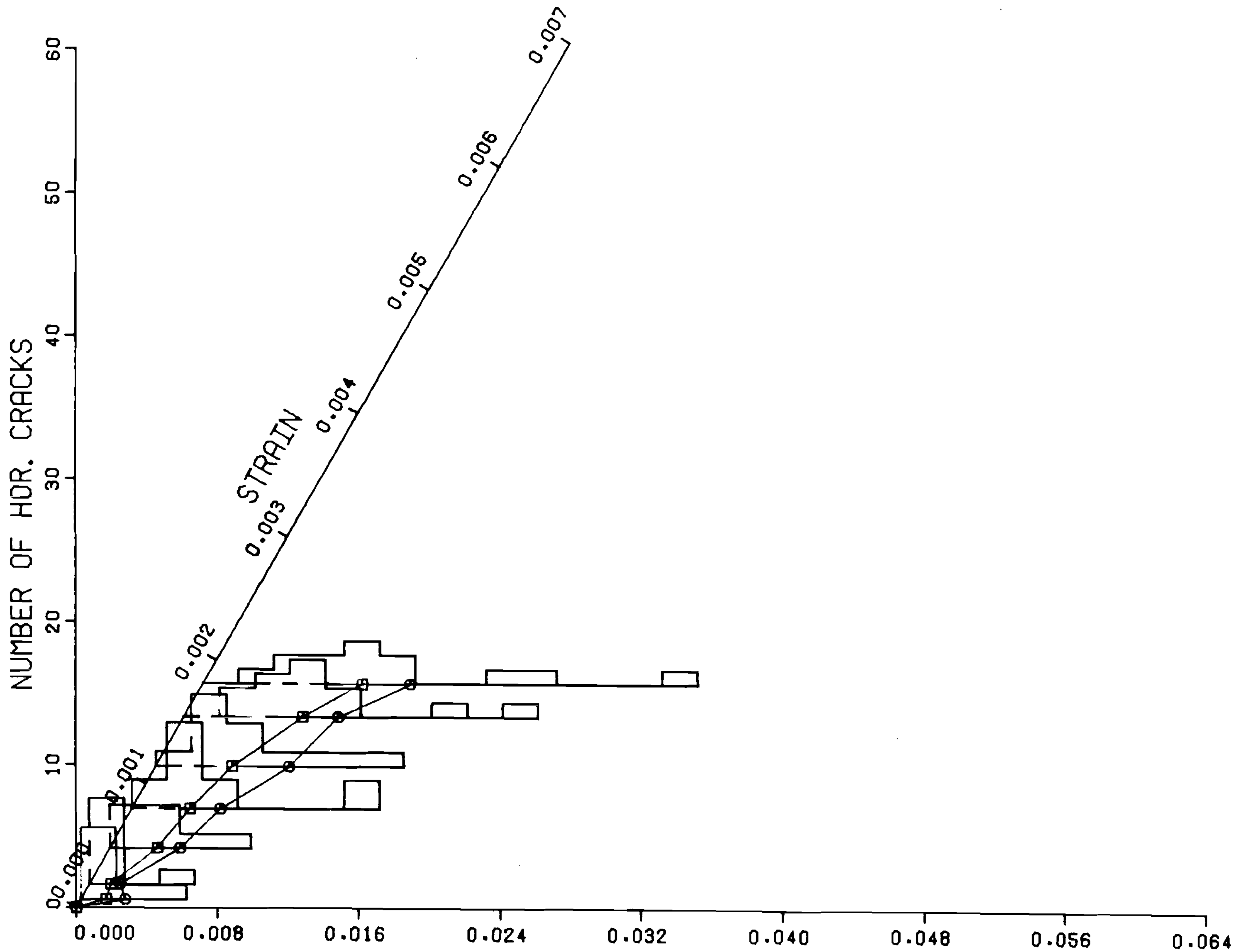

(a) Horizontal Cracks

Figure 4.11.7 Distribution of Crack Widths, Segment 7

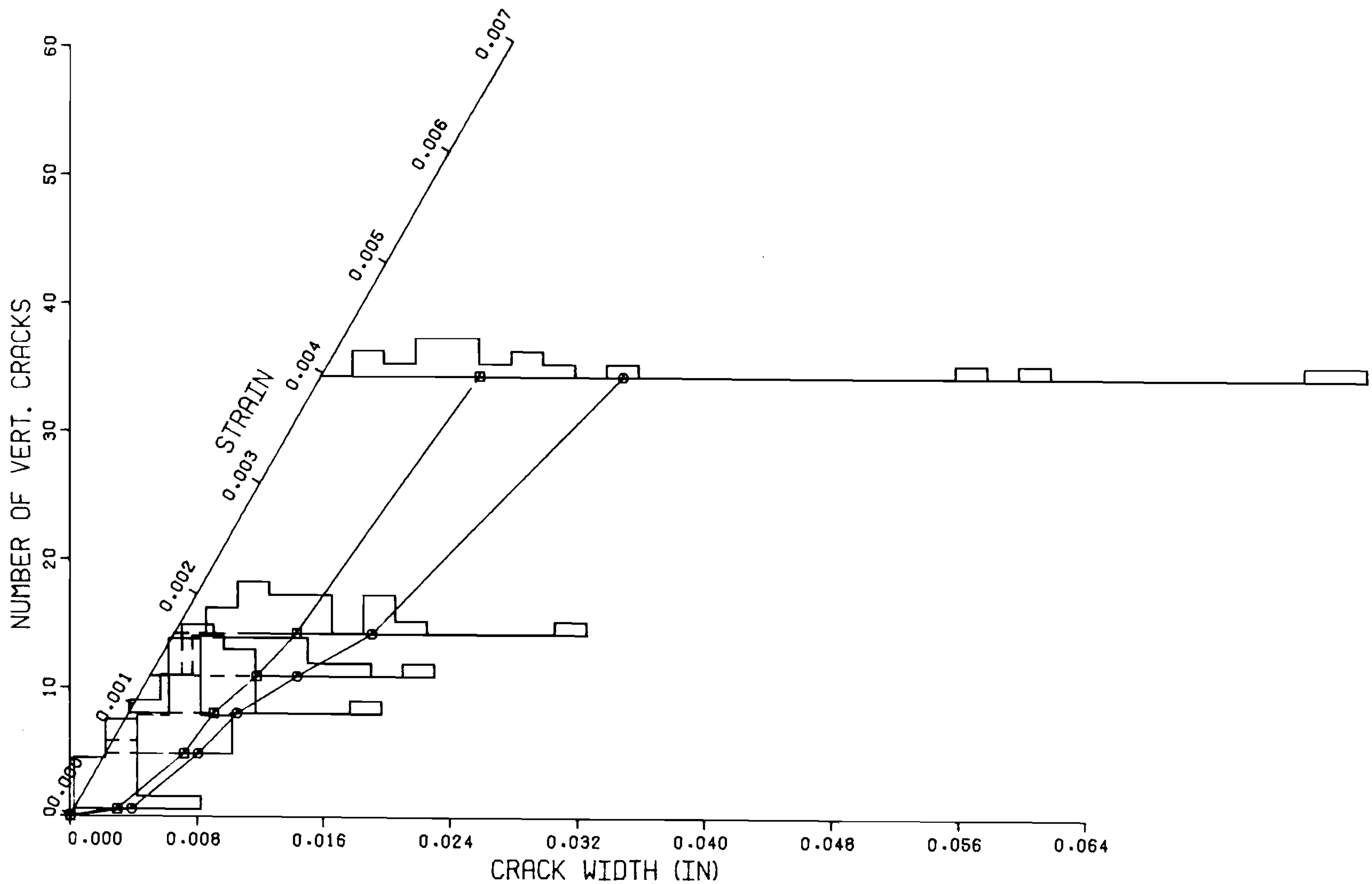

(b) Vertical Cracks

Figure 4.11.7 Distribution of Crack Widths, Segment 7

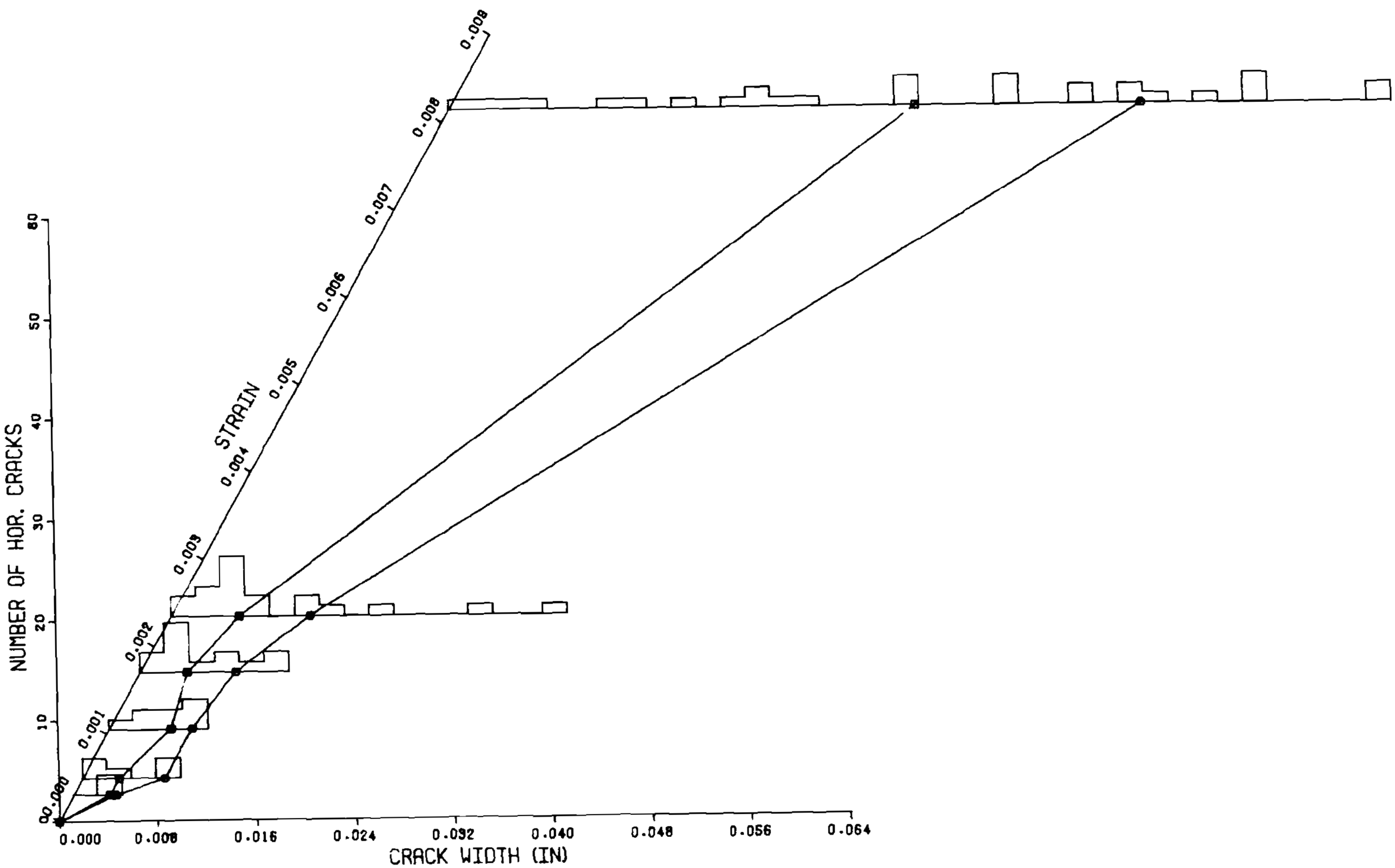

(a) Horizontal Cracks

Figure 4.11.8 Distribution of Crack Widths, Segment 8

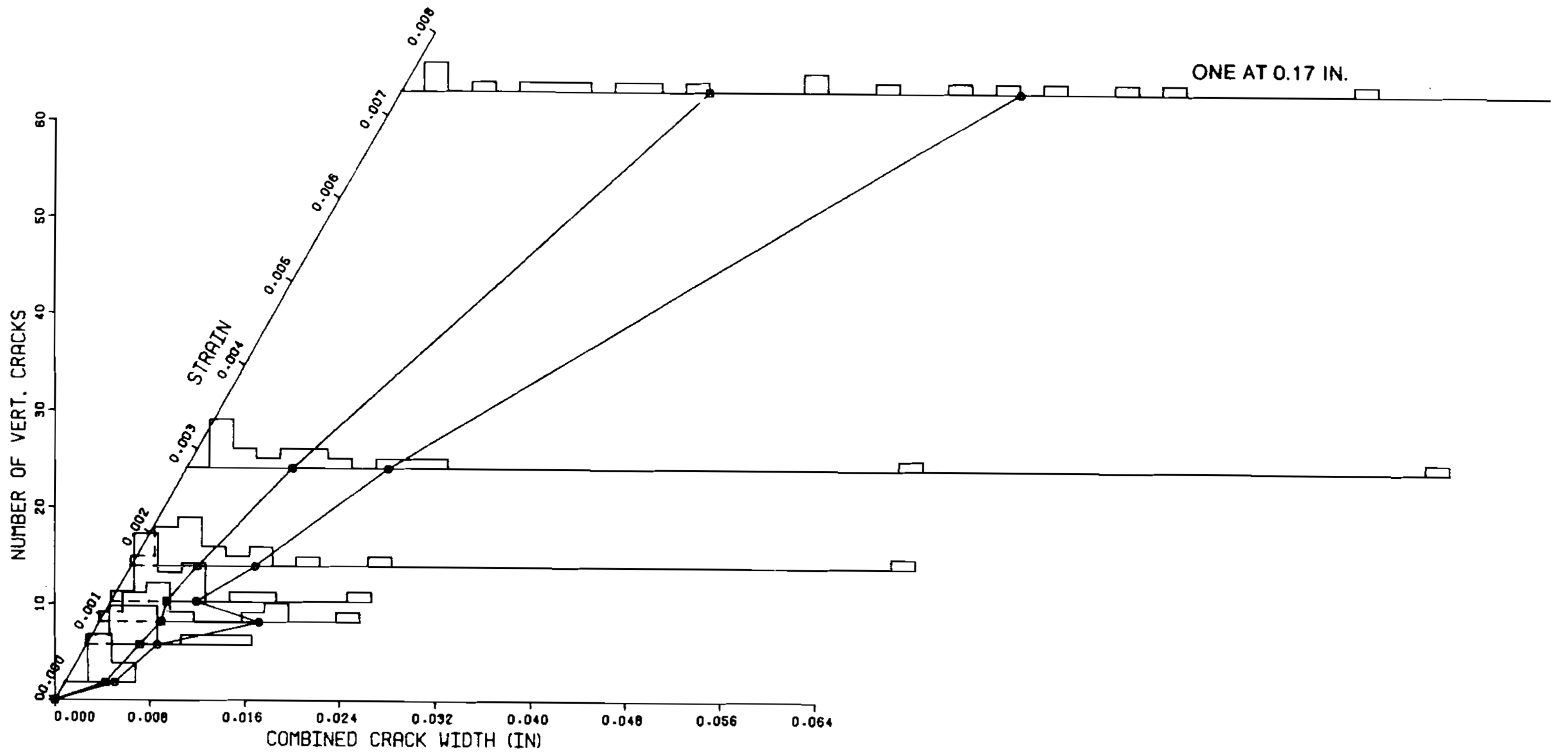

(b) Vertical Cracks

Figure 4.11.8 Distribution of Crack Widths, Segment 8

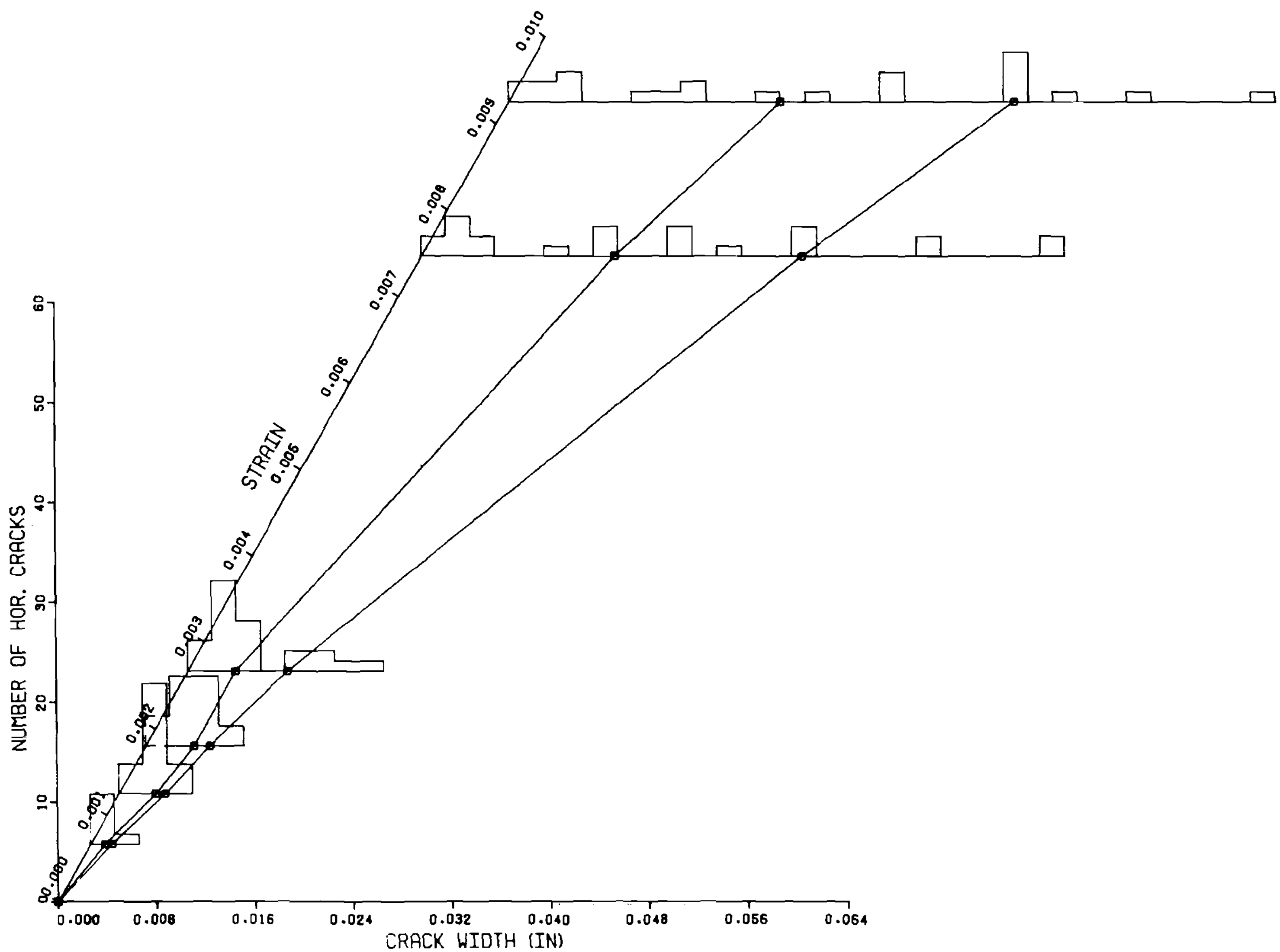

(a) Horizontal Cracks

Figure 4.11.9 Distribution of Crack Widths, Segment 9

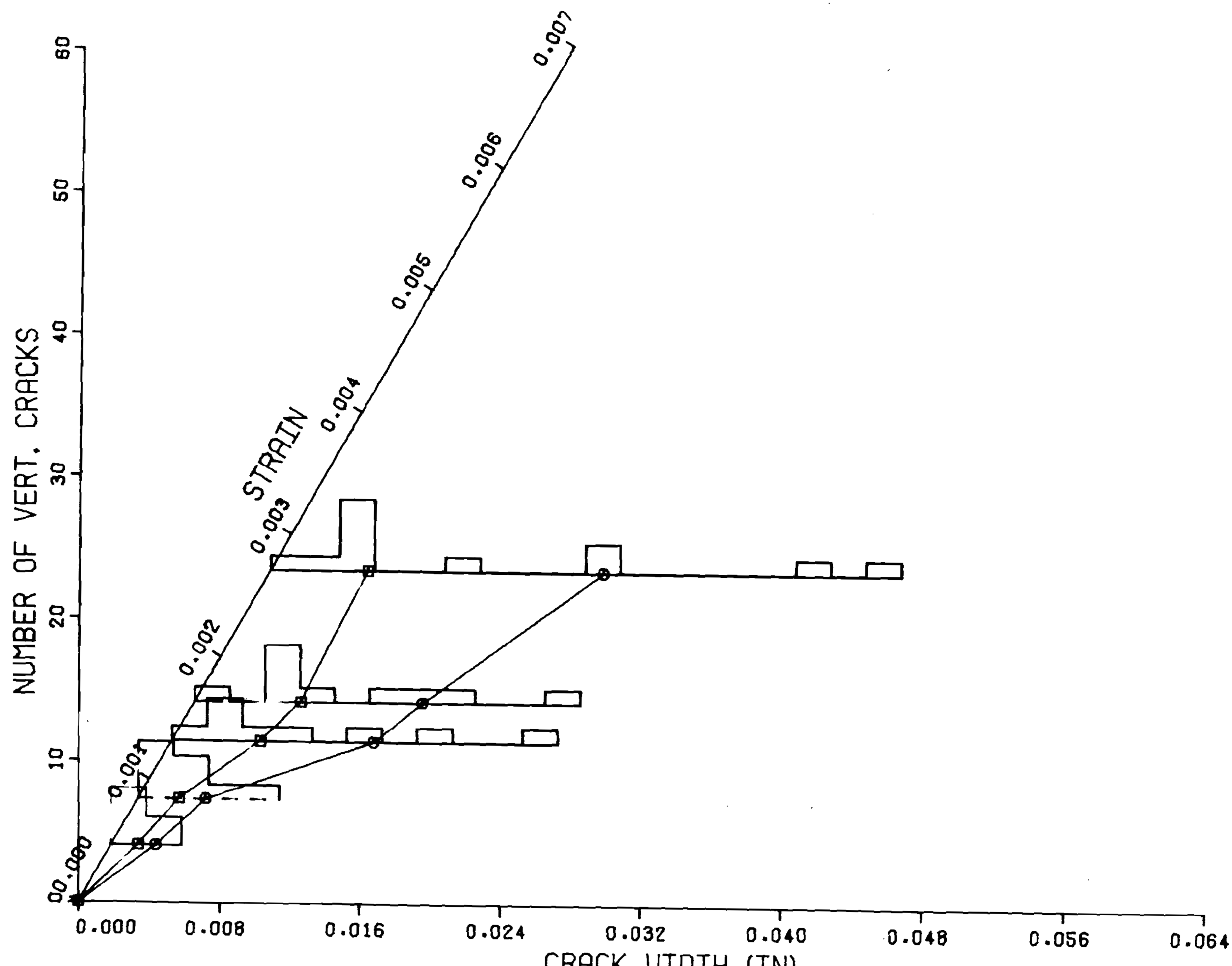

(b) Vertical Cracks

Figure 4.11.9 Distribution of Crack Widths, Segment 9

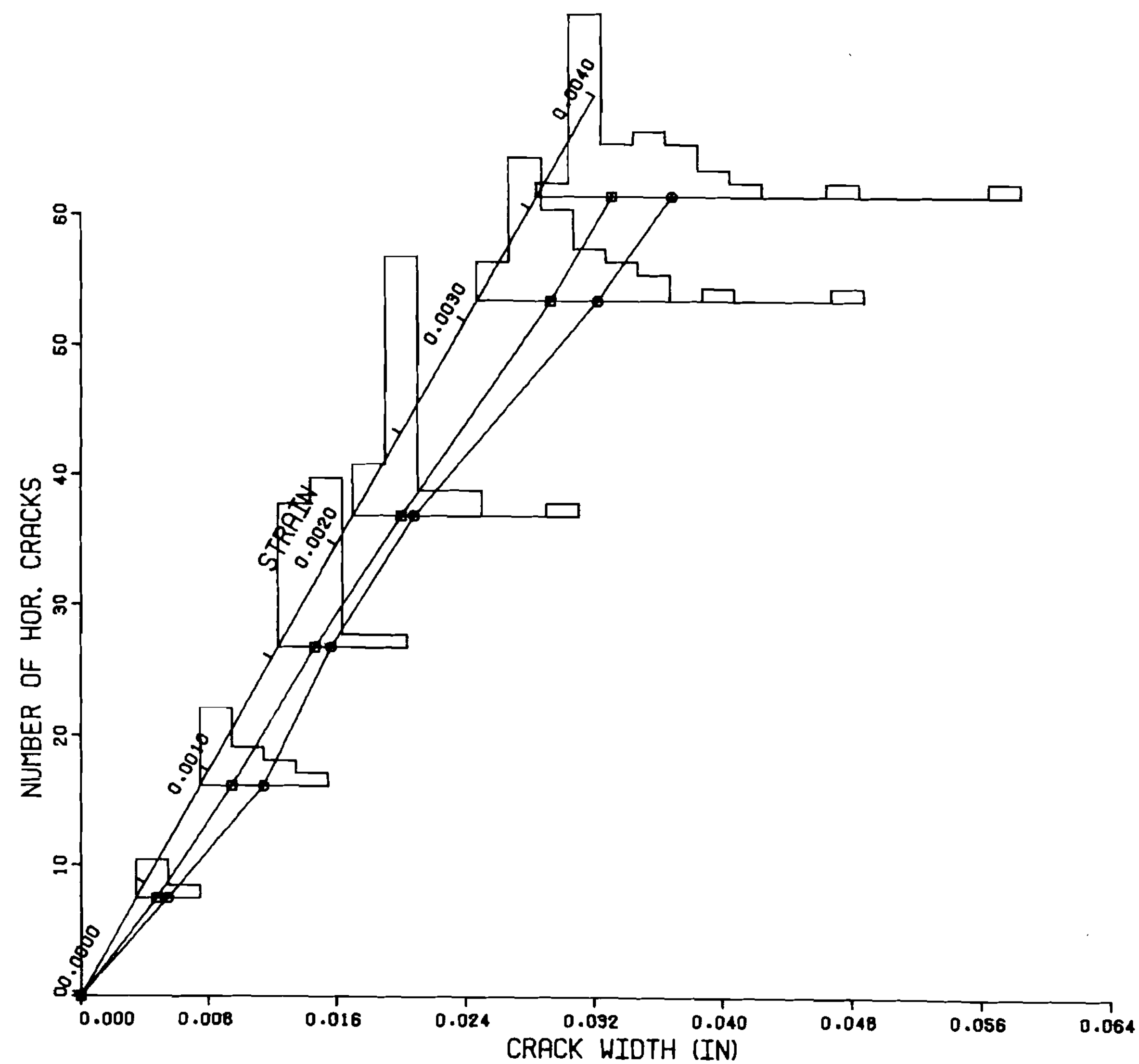

(a) Horizontal Cracks

Figure 4.11.11 Distribution of Crack Widths, Segment 11

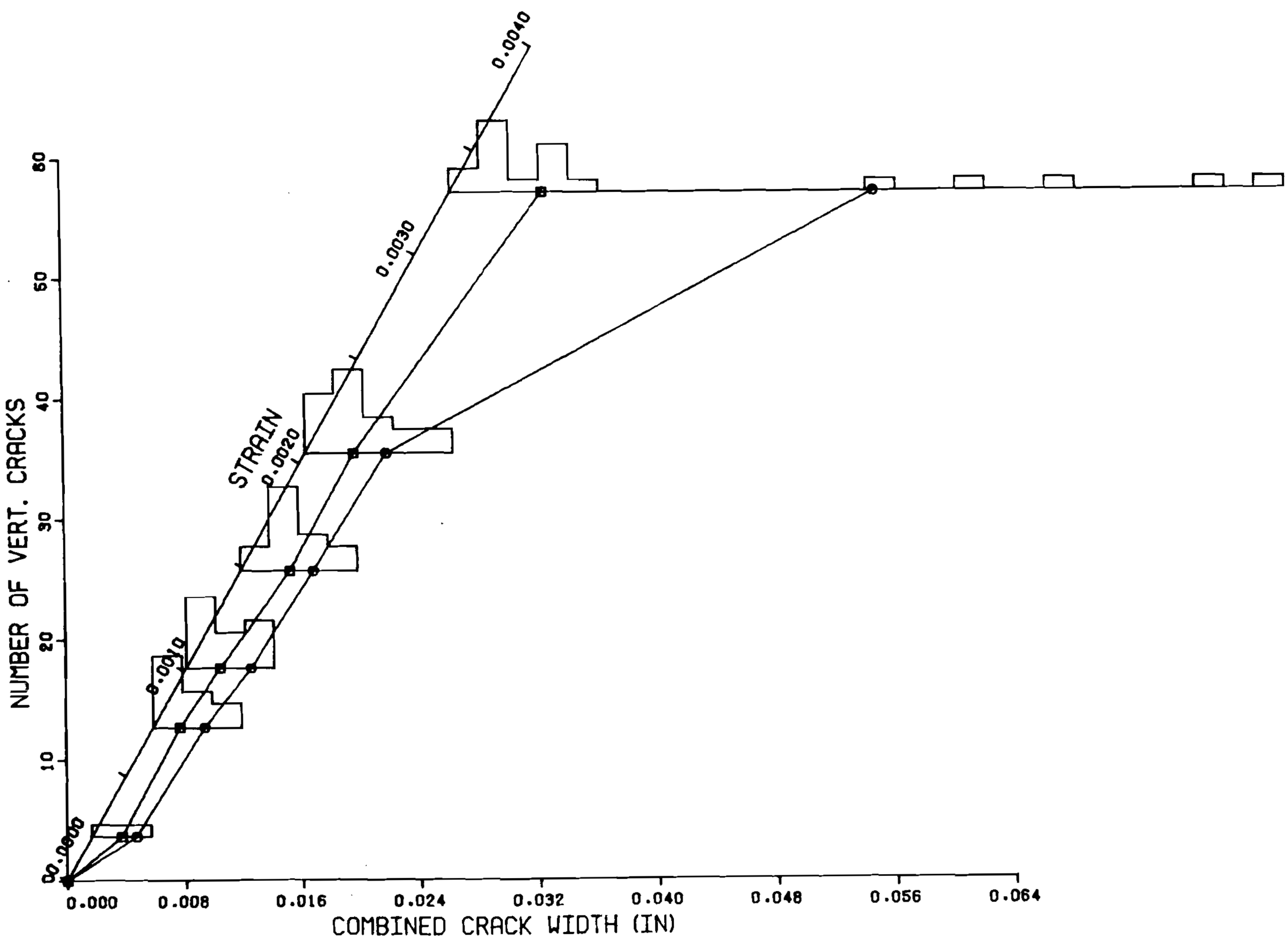

(b) Vertical Cracks

Figure 4.11.11 Distribution of Crack Widths, Segment 11

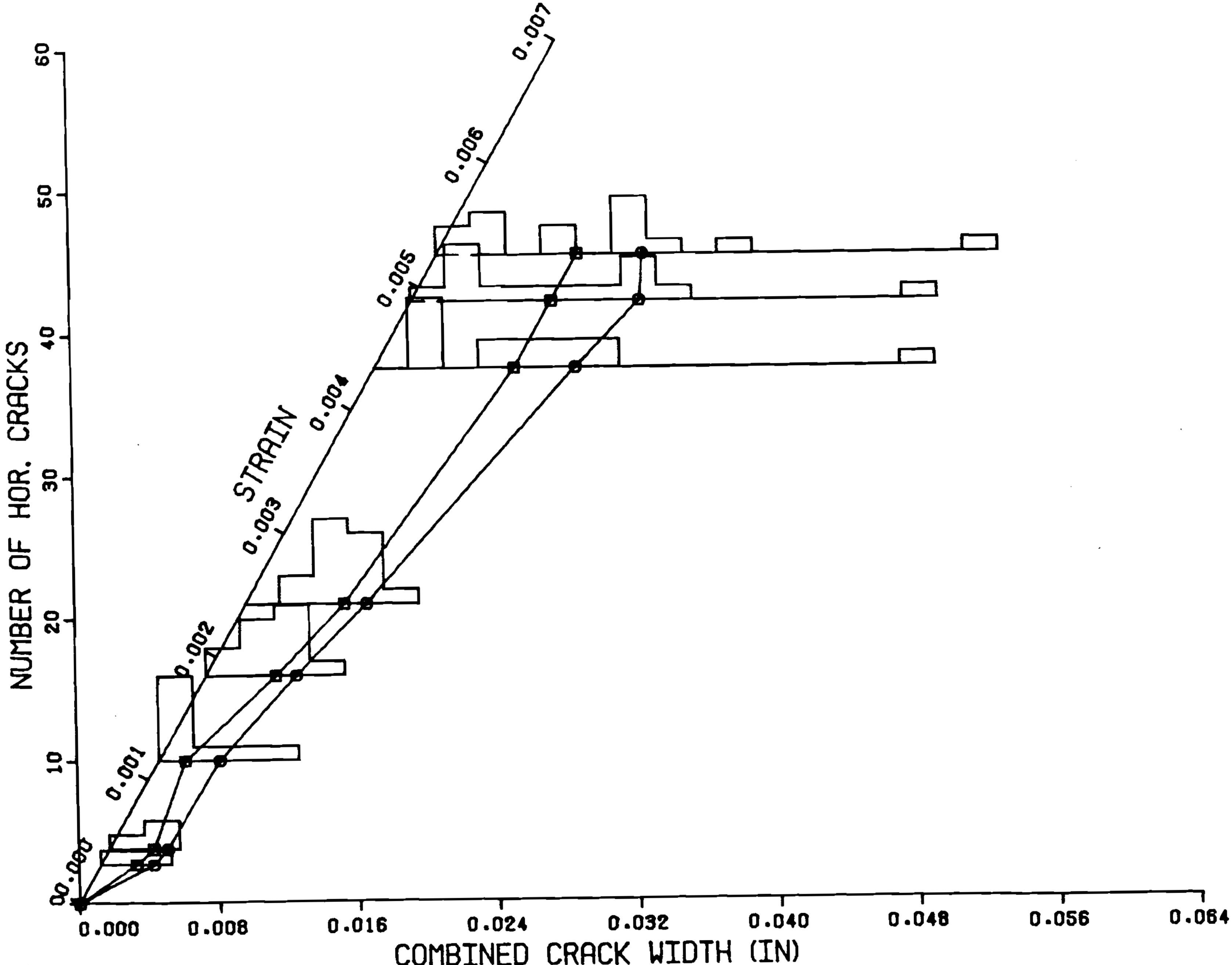

(a) Horizontal Cracks

Figure 4.11.12 Distribution of Crack Widths, Segment 12, Face A

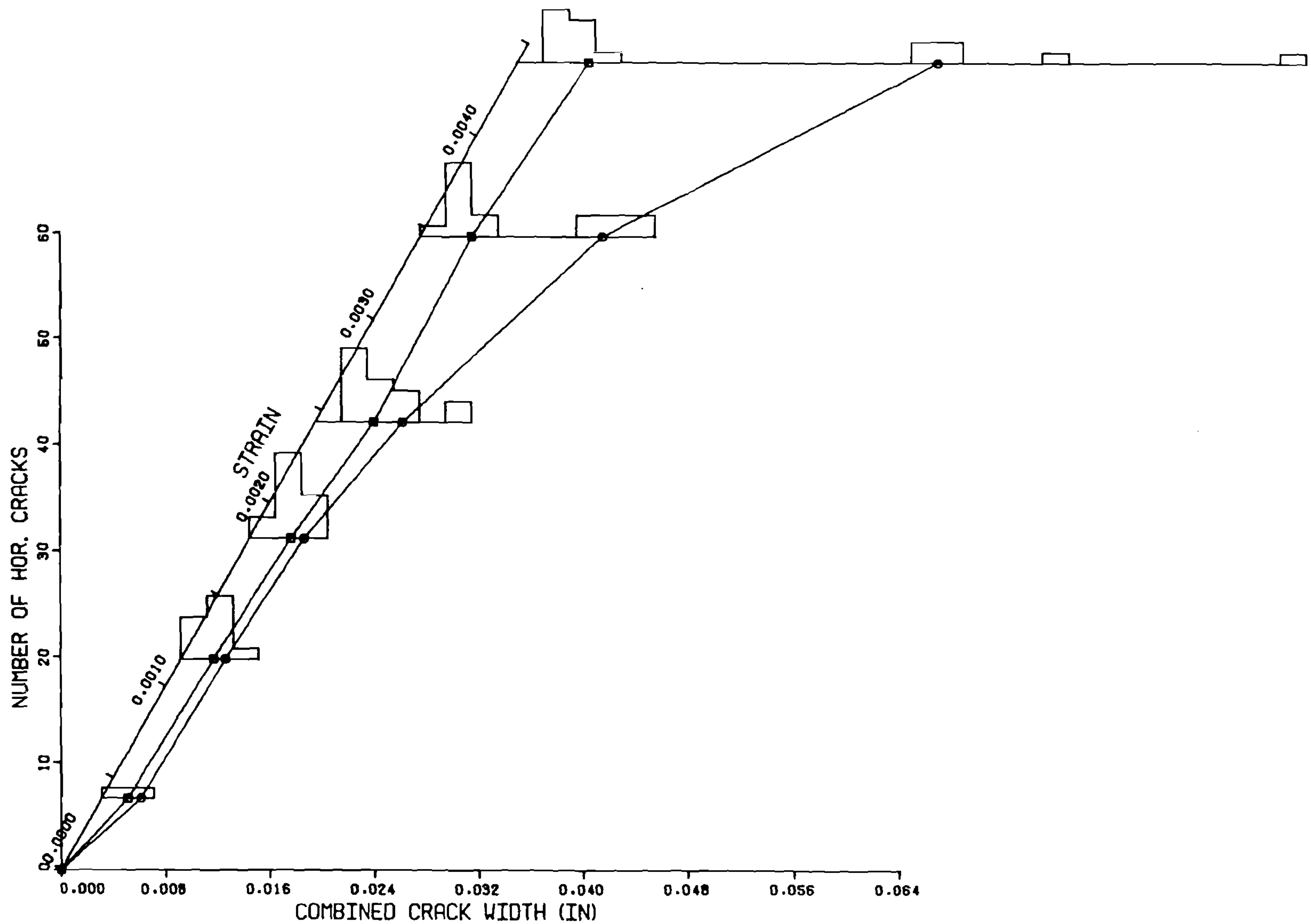

(a) Horizontal Cracks

Figure 4.11.12 Distribution of Crack Widths, Segment 12, Face B

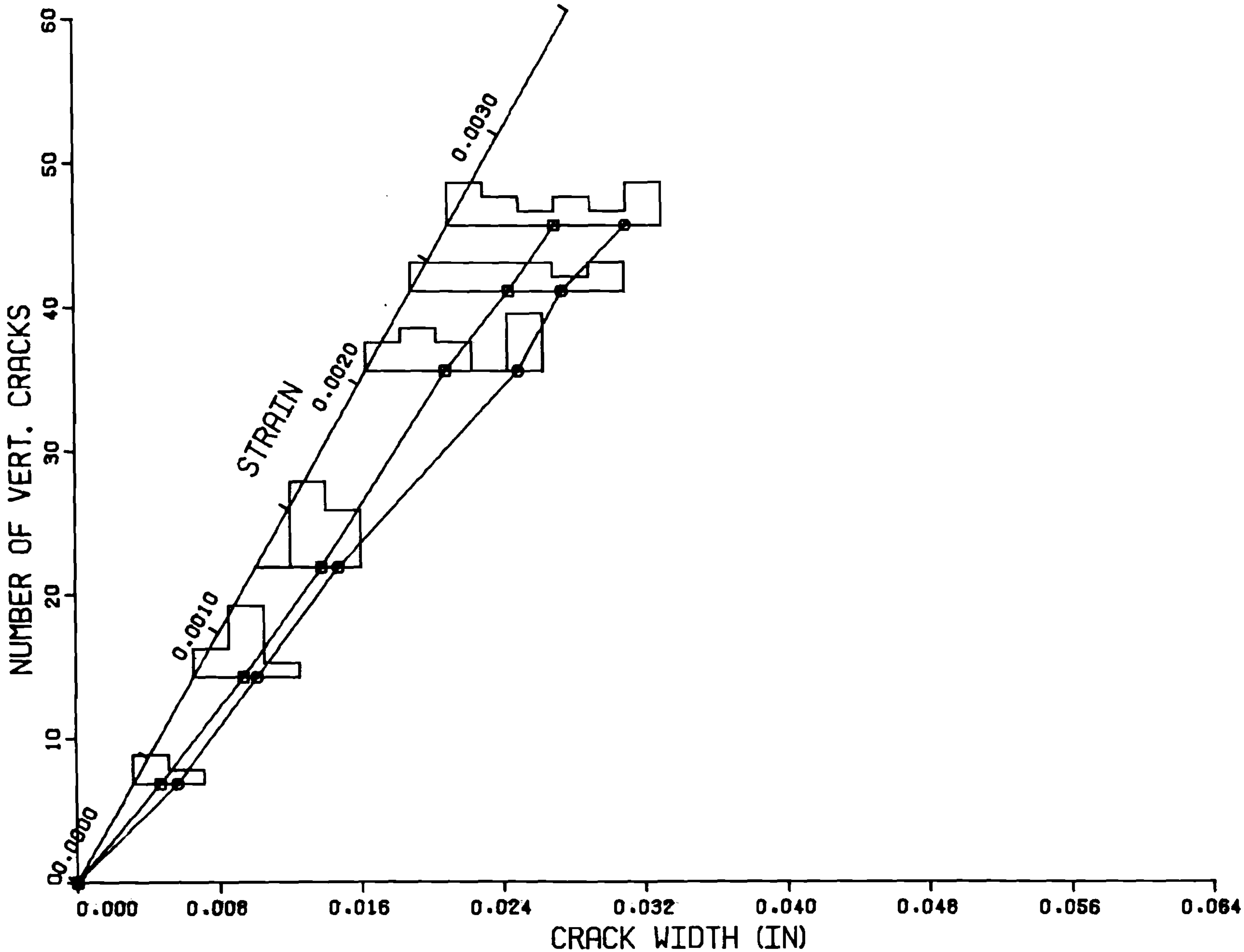

(c) Vertical Cracks

Figure 4.11.12 Distribution of Crack Widths, Segment 12, Face A

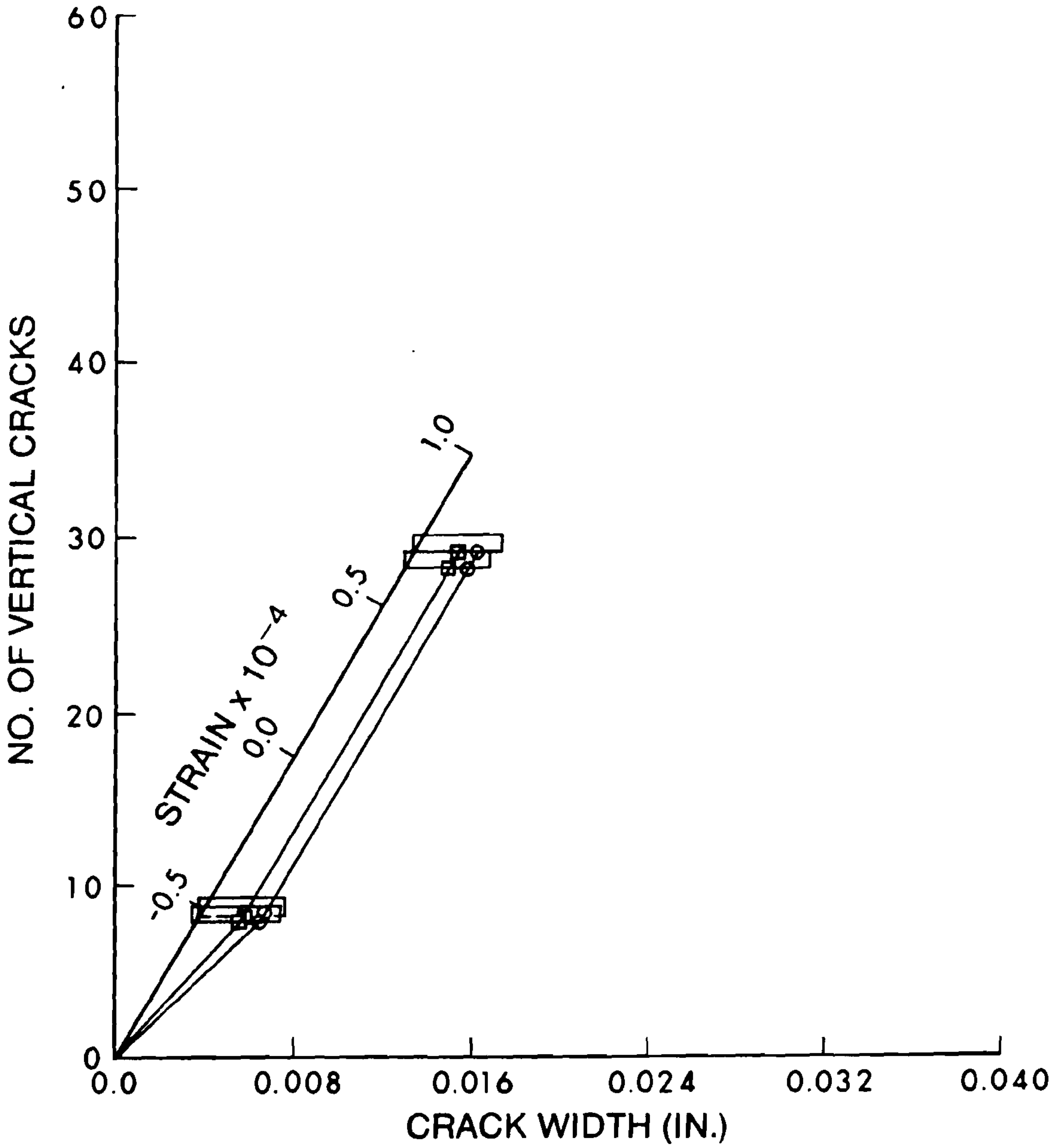

(d) Vertical Cracks

Figure 4.11.12 Distribution of Crack Widths, Segment 12, Face B

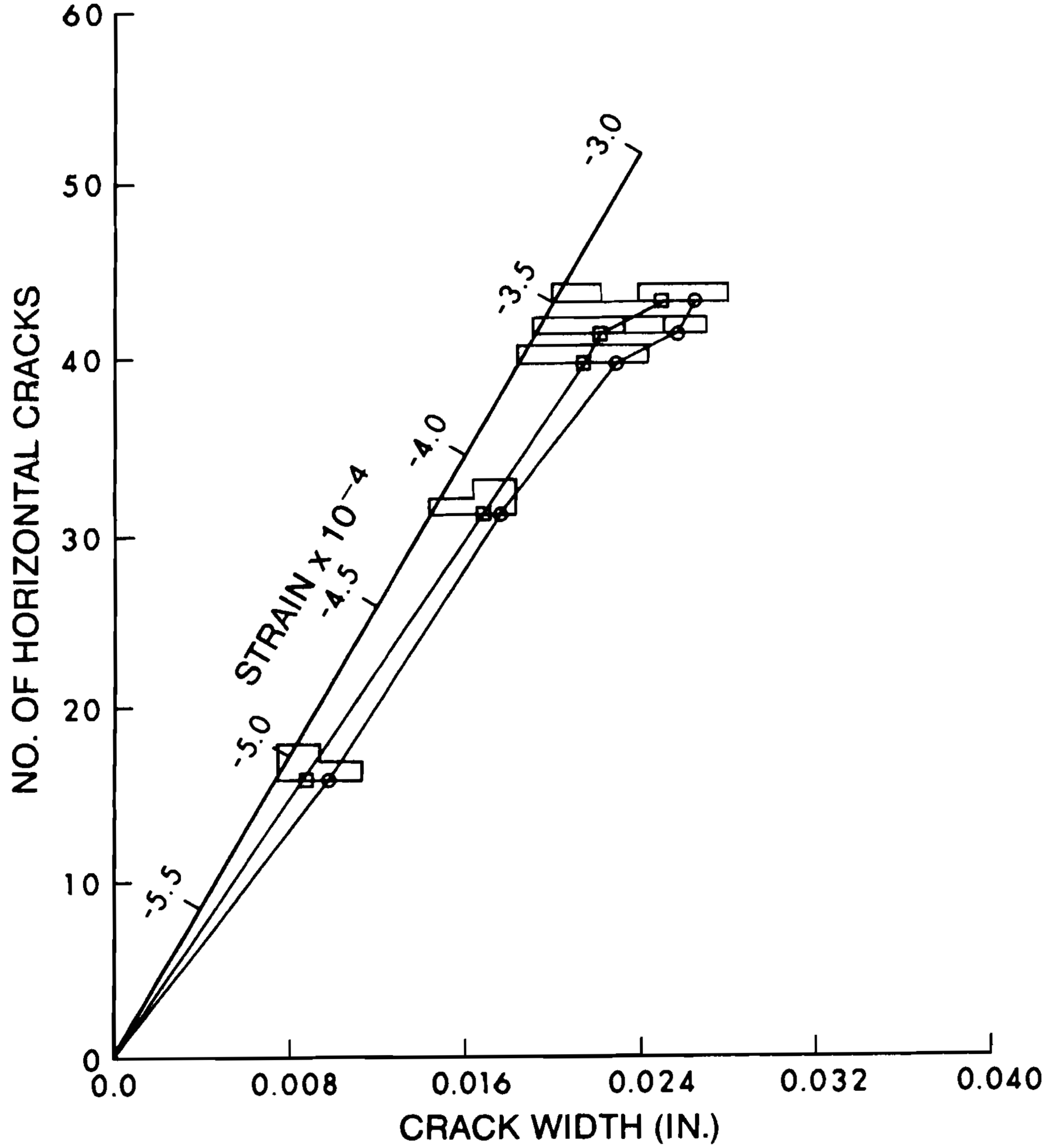

(a) Horizontal Cracks

Figure 4.11.13 Distribution of Crack Widths, Segment 13, Face A

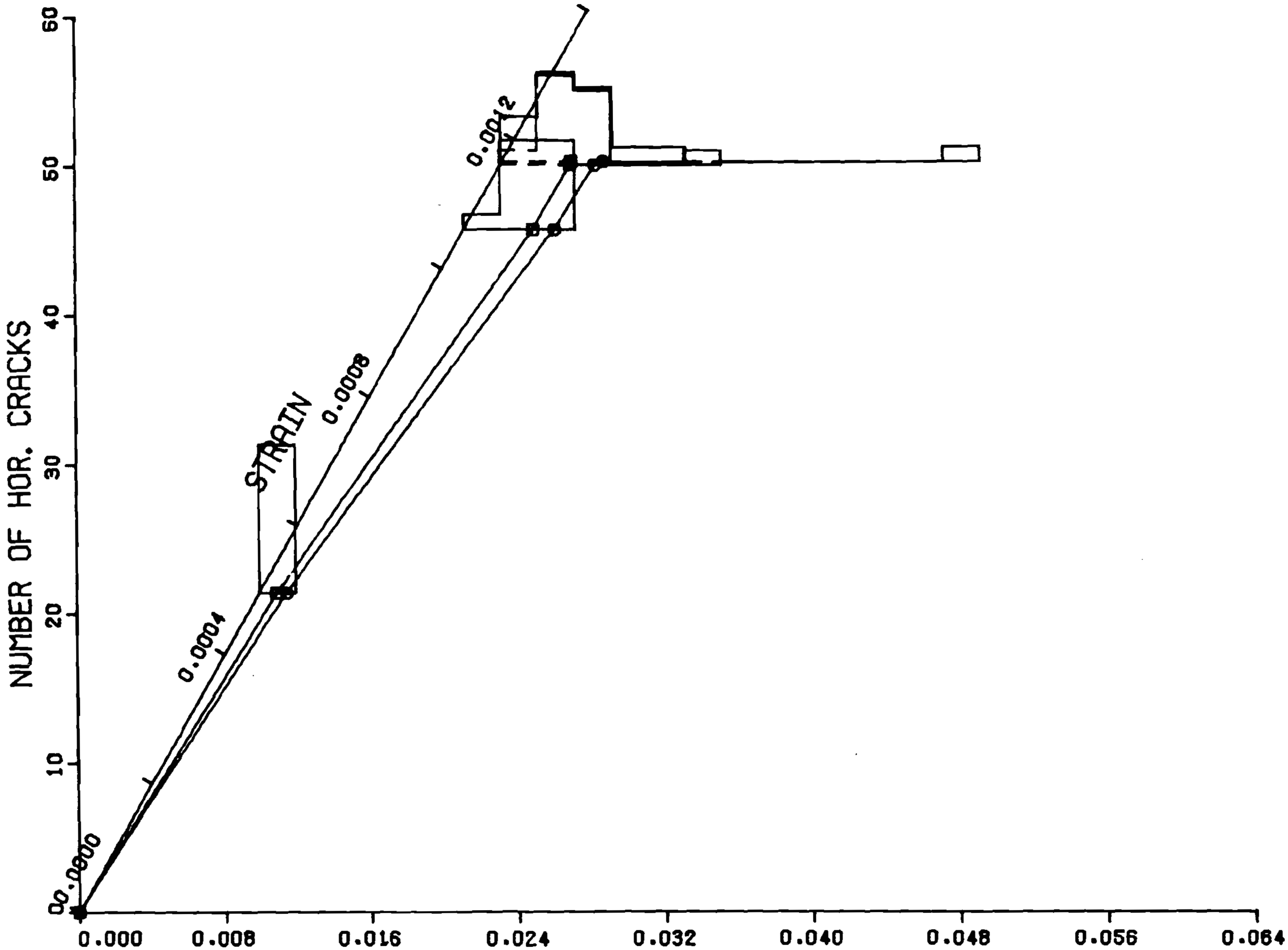

(b) Horizontal Cracks

Figure 4.11.13 Distribution of Crack Widths, Segment 13, Face B

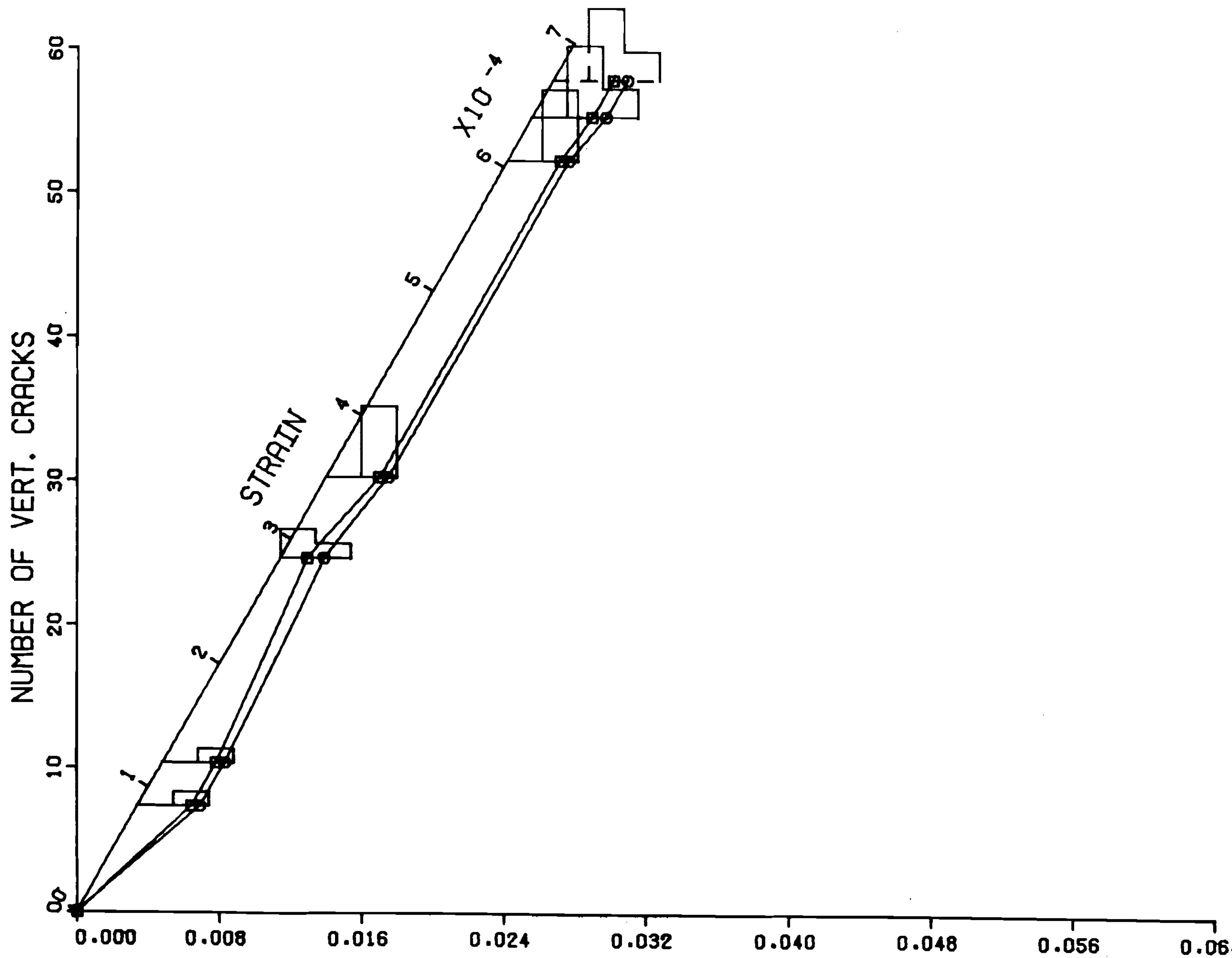

(c) Vertical Cracks

Figure 4.11.13 Distribution of Crack Widths, Segment 13, Face A

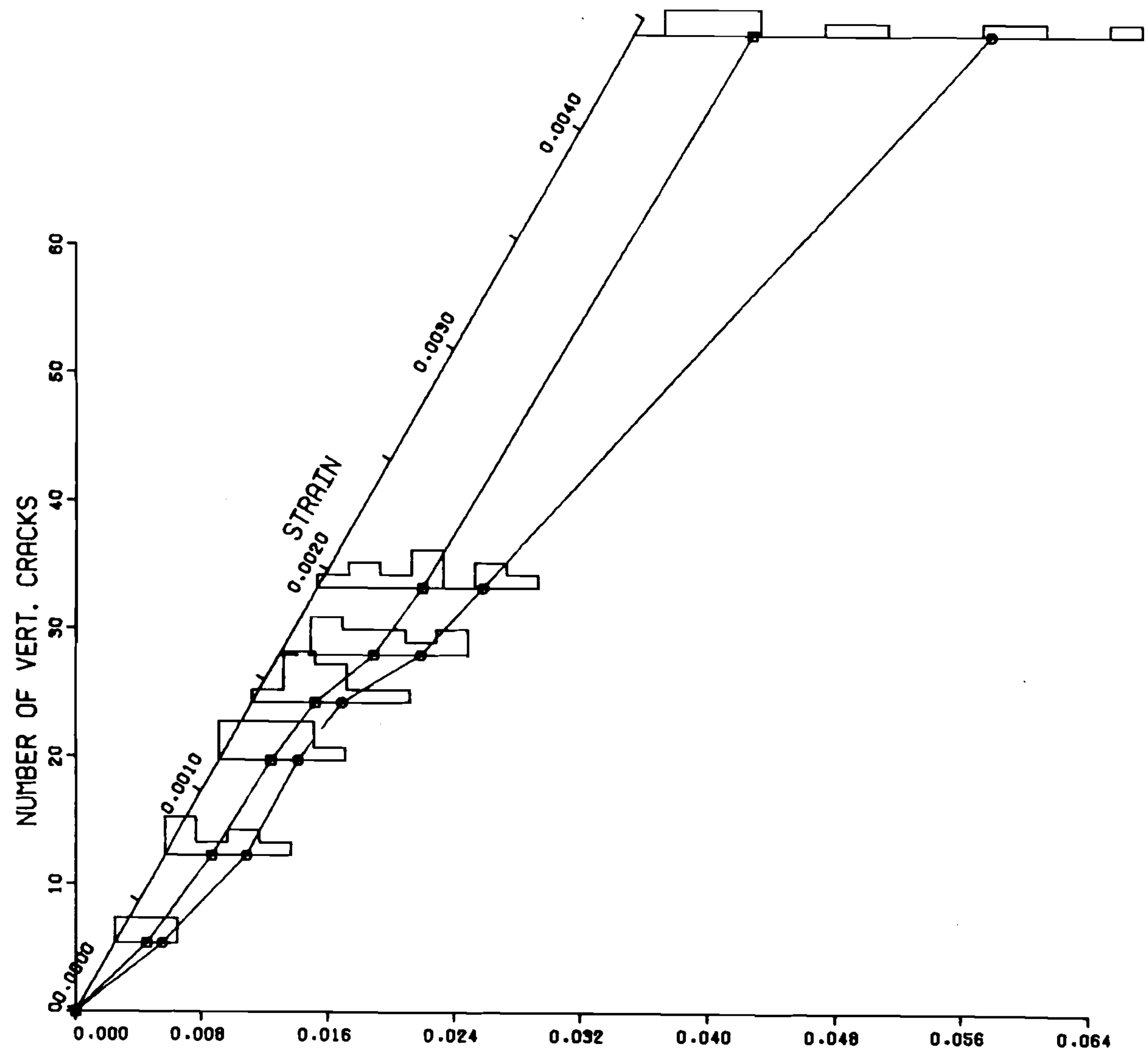

(d) Vertical Cracks

Figure 4.11.13 Distribution of Crack Widths, Segment 13, Face B

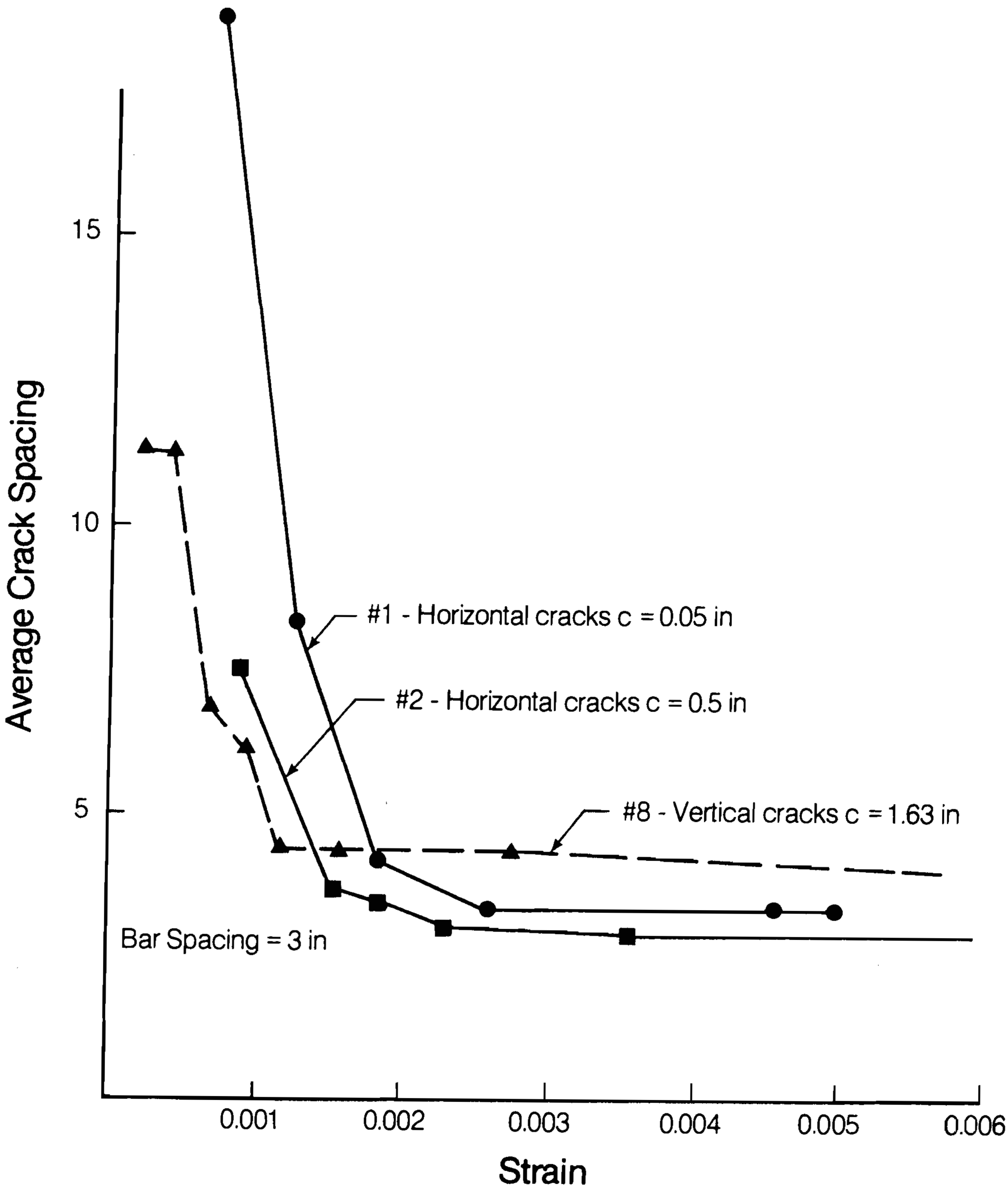

Figure 5.1 Effect of Cover, Bar Spacing and Strain on Crack Spacing

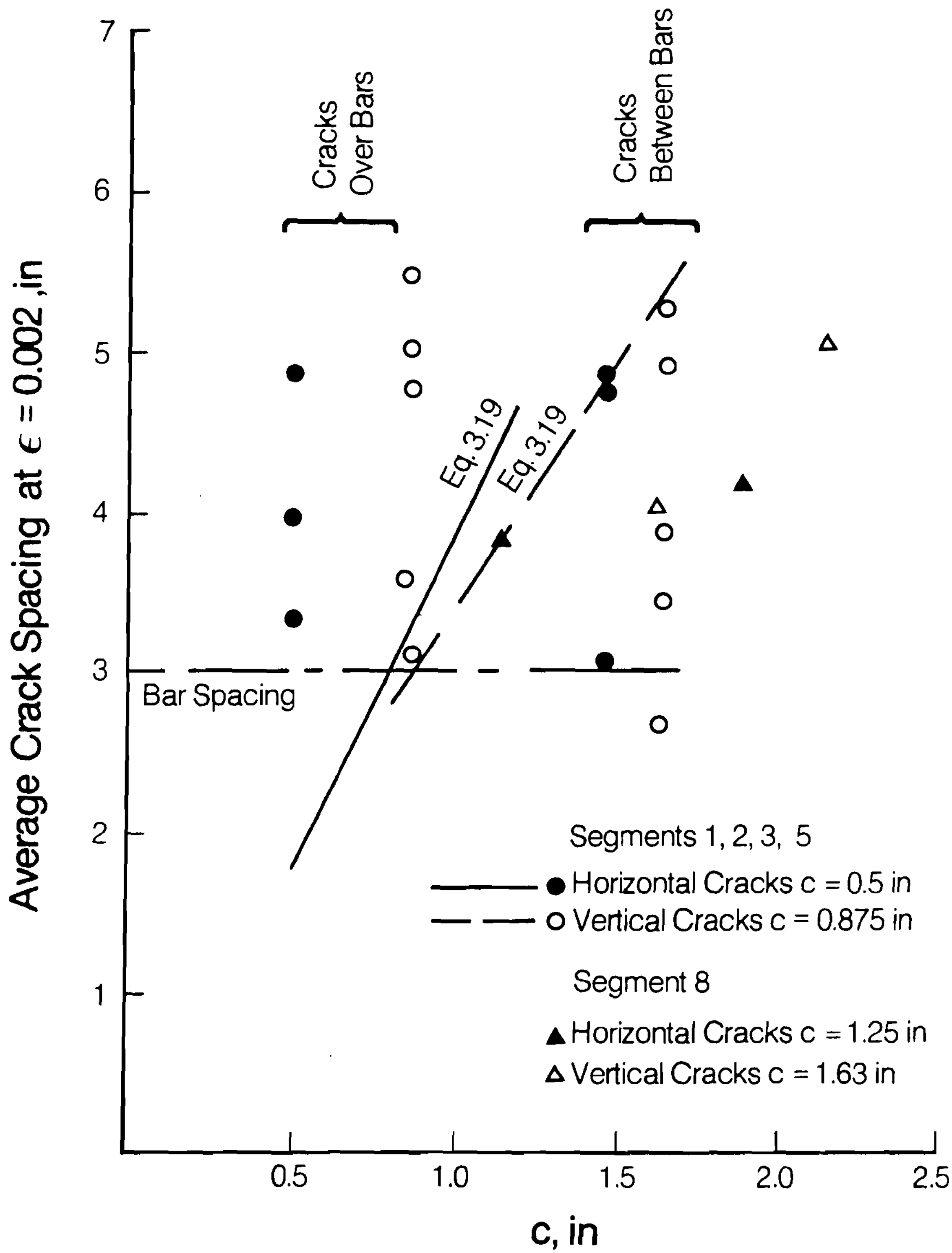

Figure 5.2 Effect of Radial Distance to Bar, c, on Crack Spacing

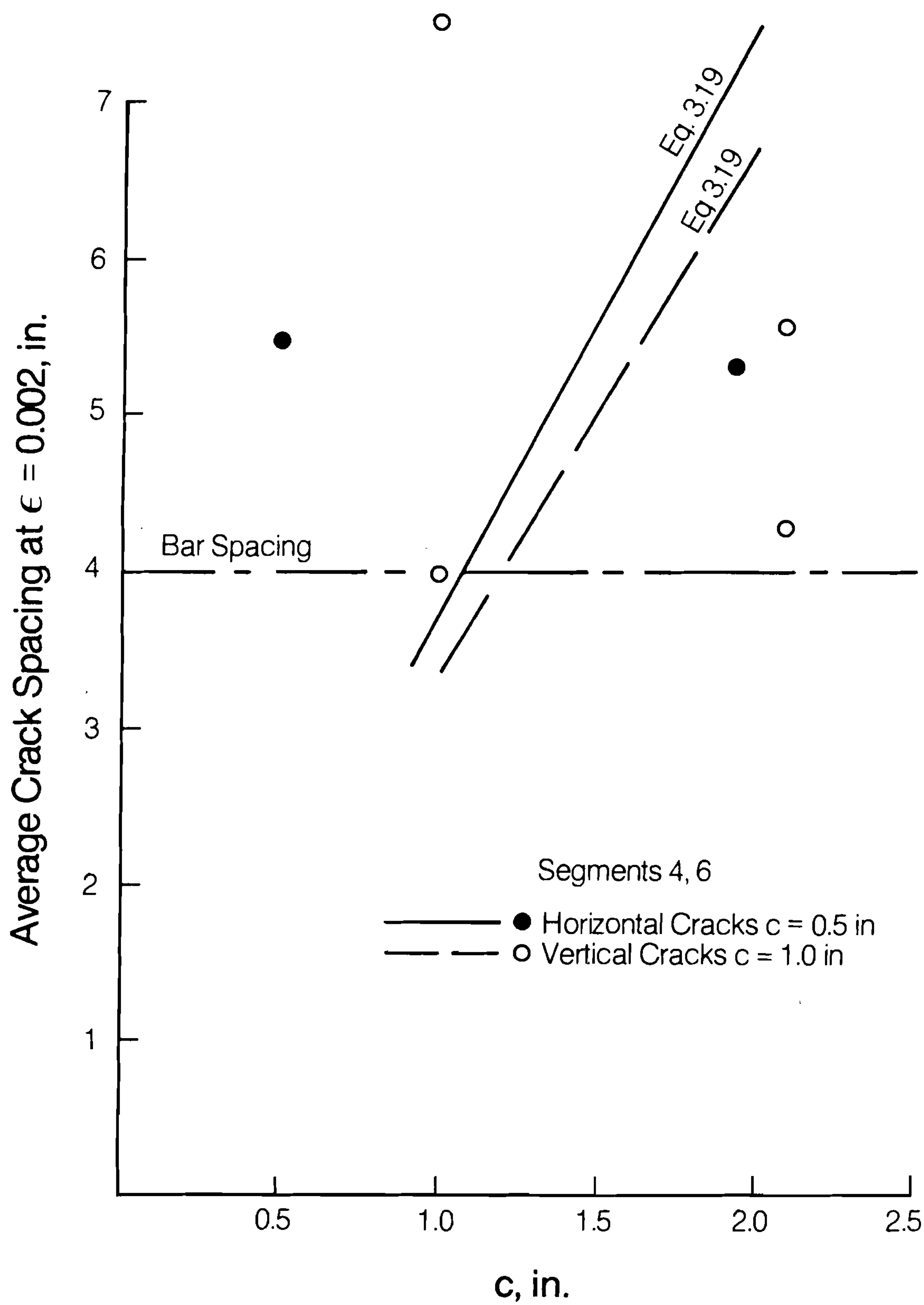

Figure 5.3 Effect of Radial Distance to Bar, c, on Crack Spacing

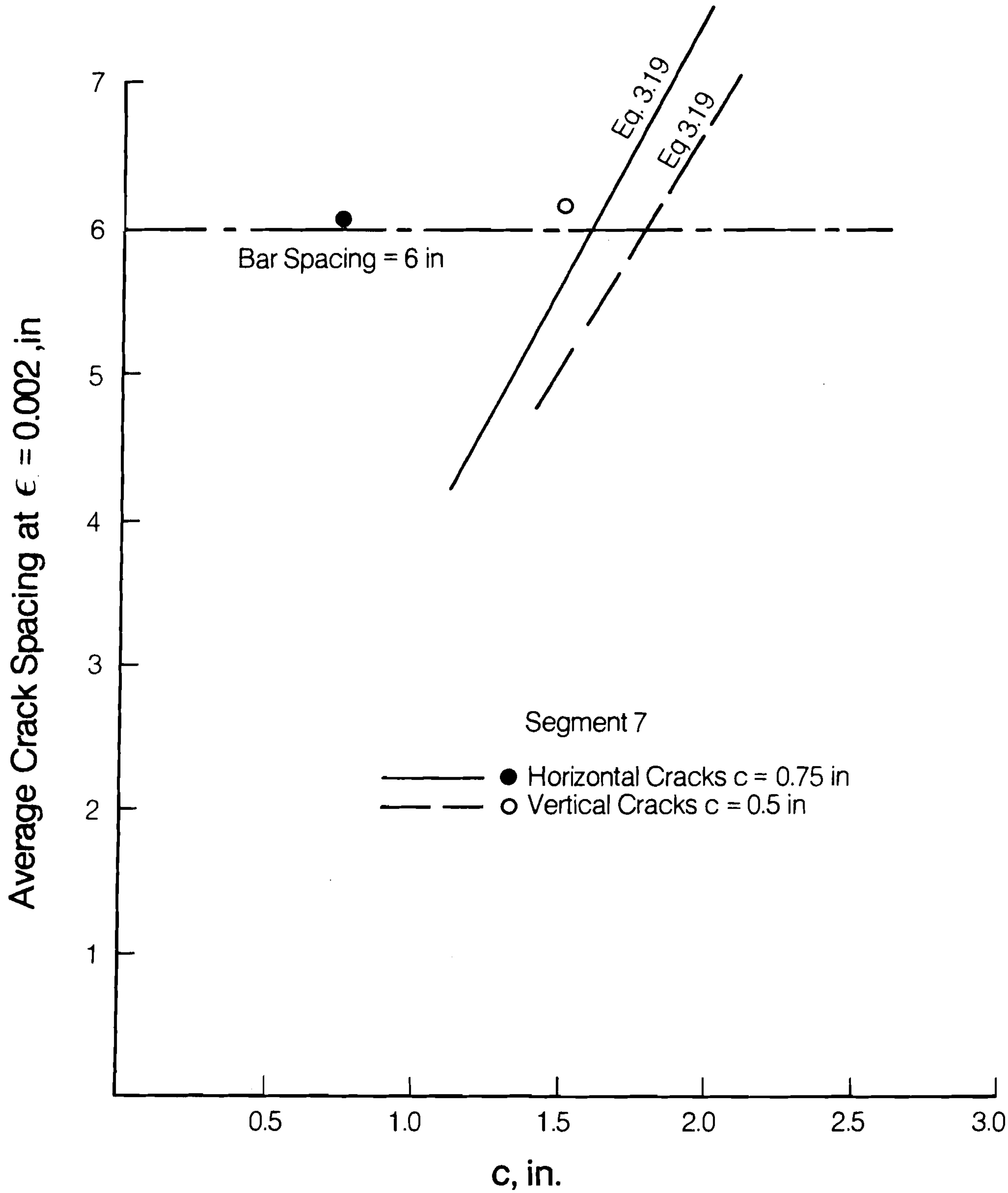

Figure 5.4 Effect of Radial Distance to Bar, c, on Crack Spacing

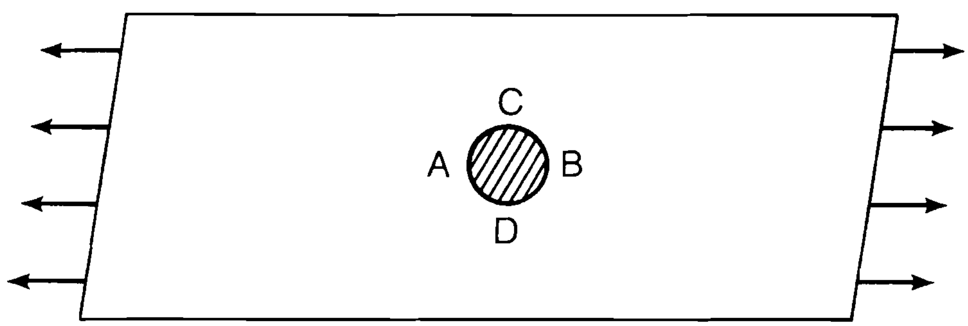

Figure 5.5 Bar Embedded in Concrete

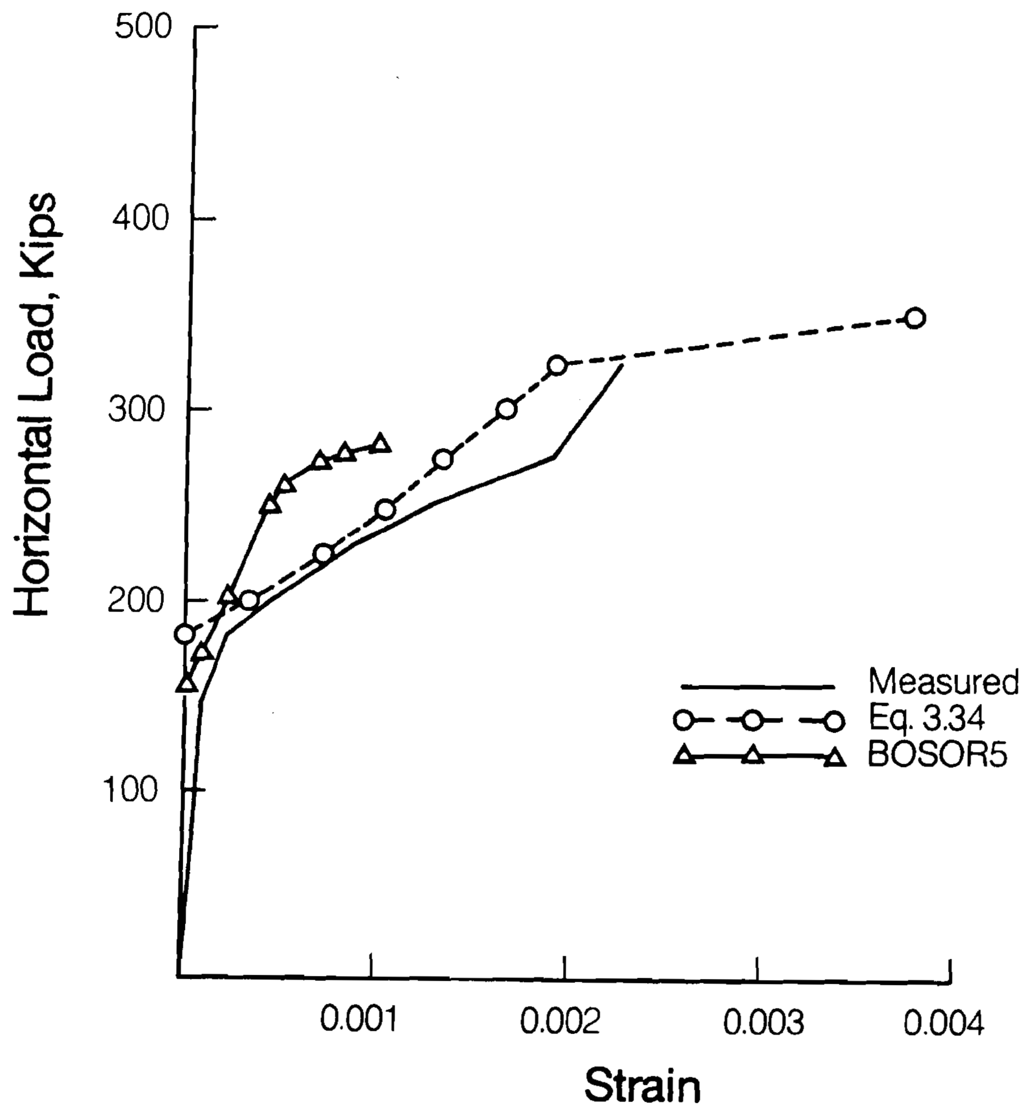

(a) Horizontal Strains

Figure 5.6.1 Measured and Computed Mean Strain, ε_m, Segment 1

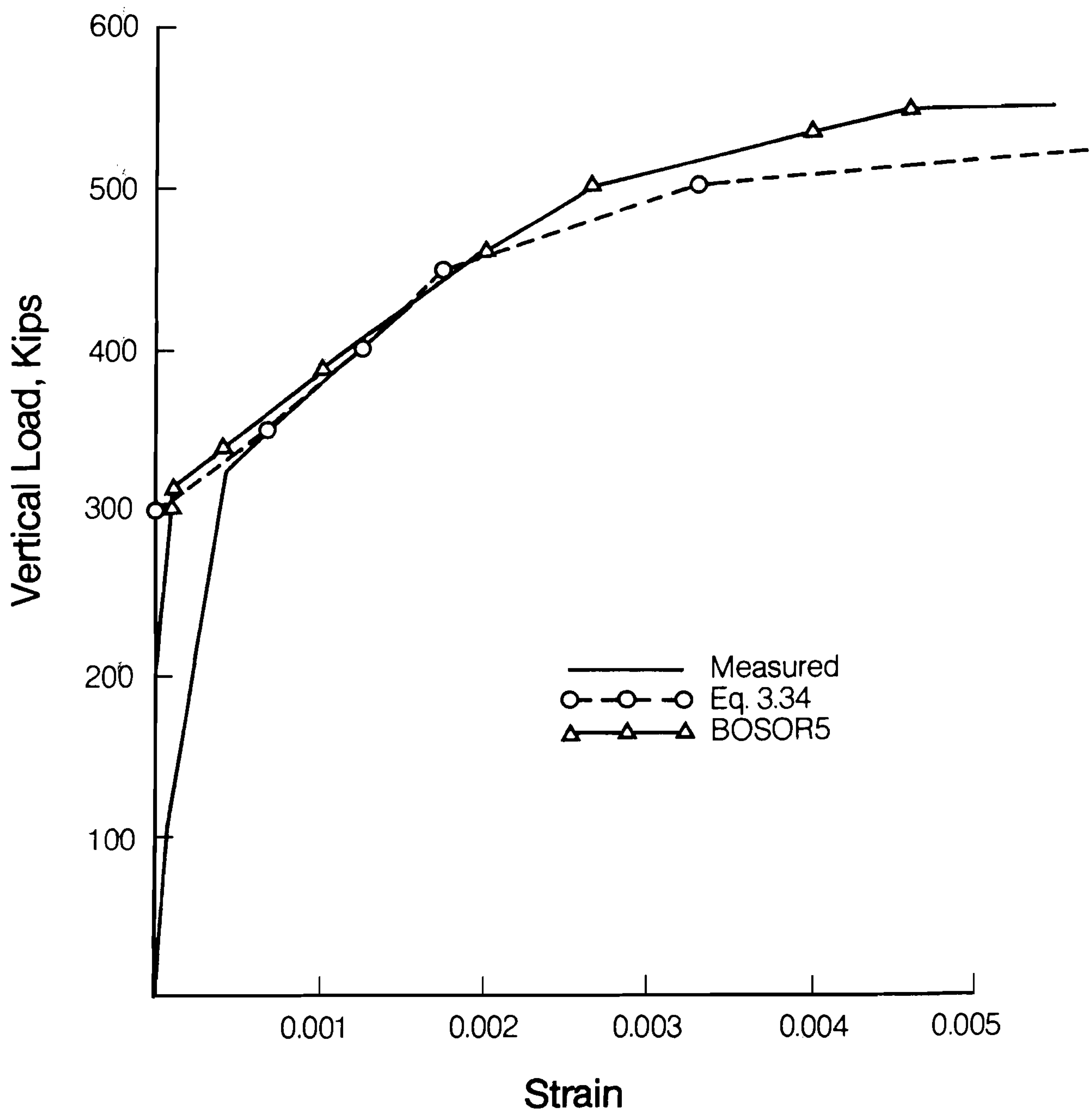

(b) Vertical Strains

Figure 5.6.1 Measured and Computed Mean Strain, ε_m, Segment 1

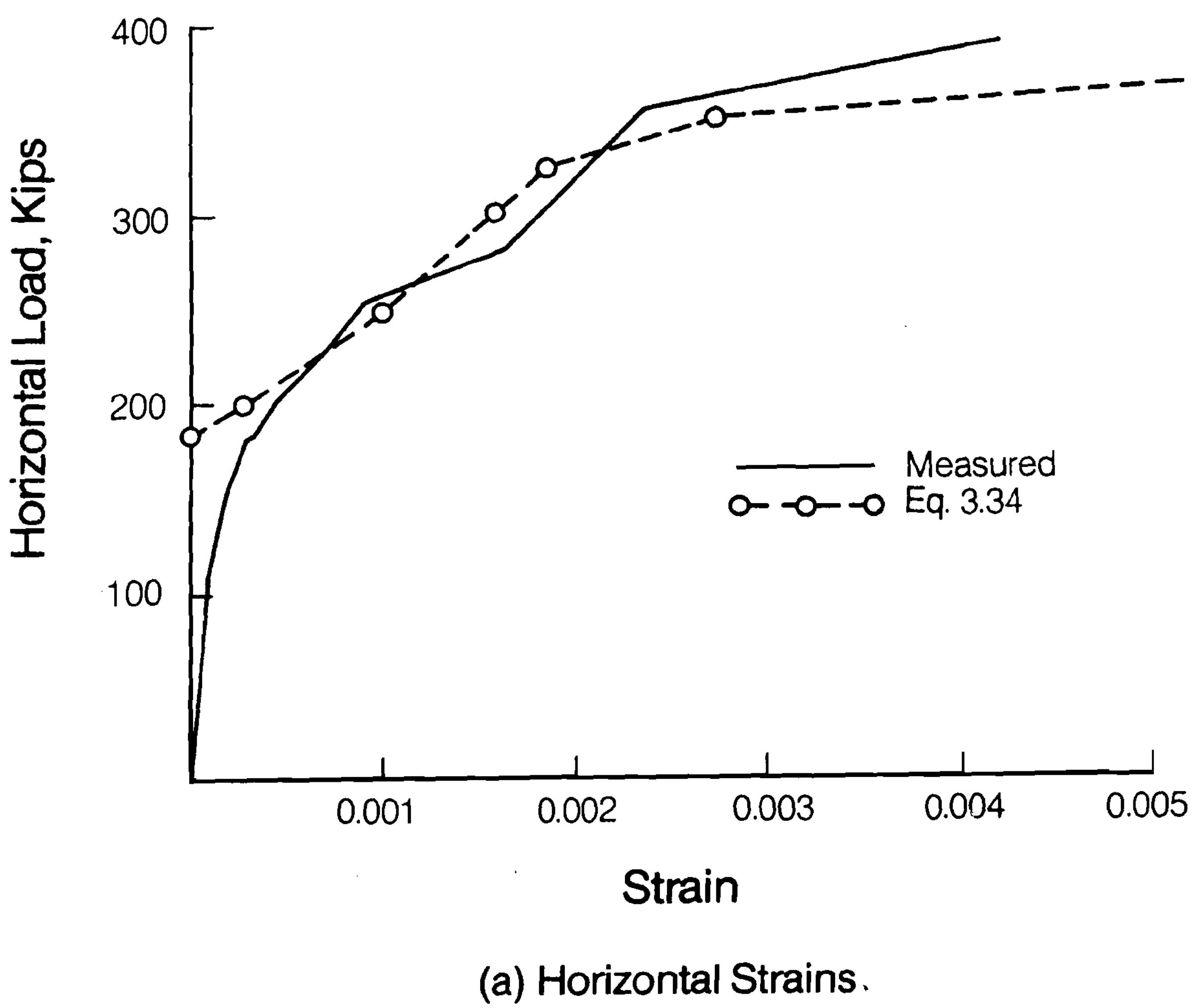

Figure 5.6.2 Measured and Computed Mean Strain, ε_m, Segment 2

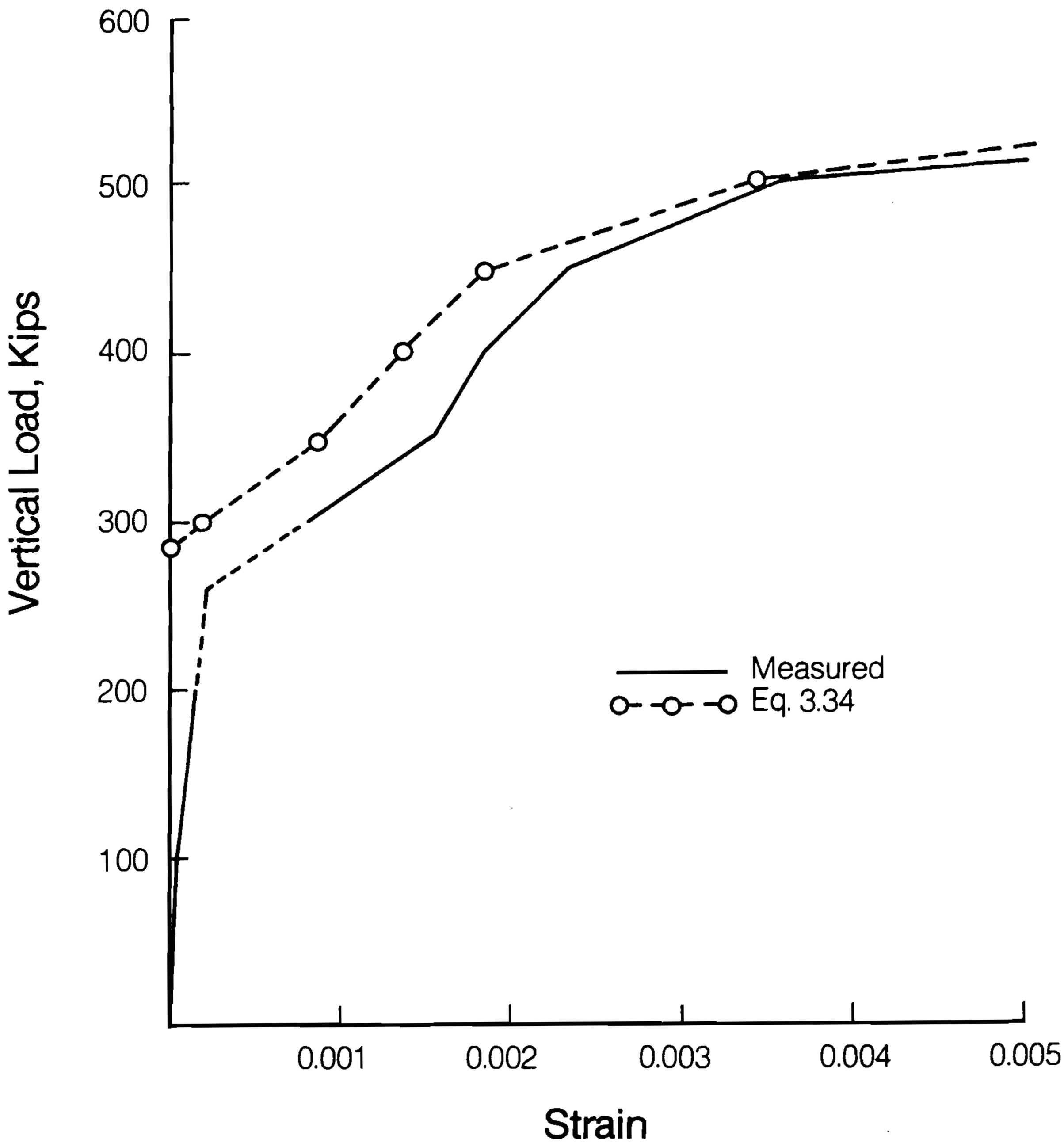

(b) Vertical Strains

Figure 5.6.2 Measured and Computed Mean Strain, ε_m, Segment 2

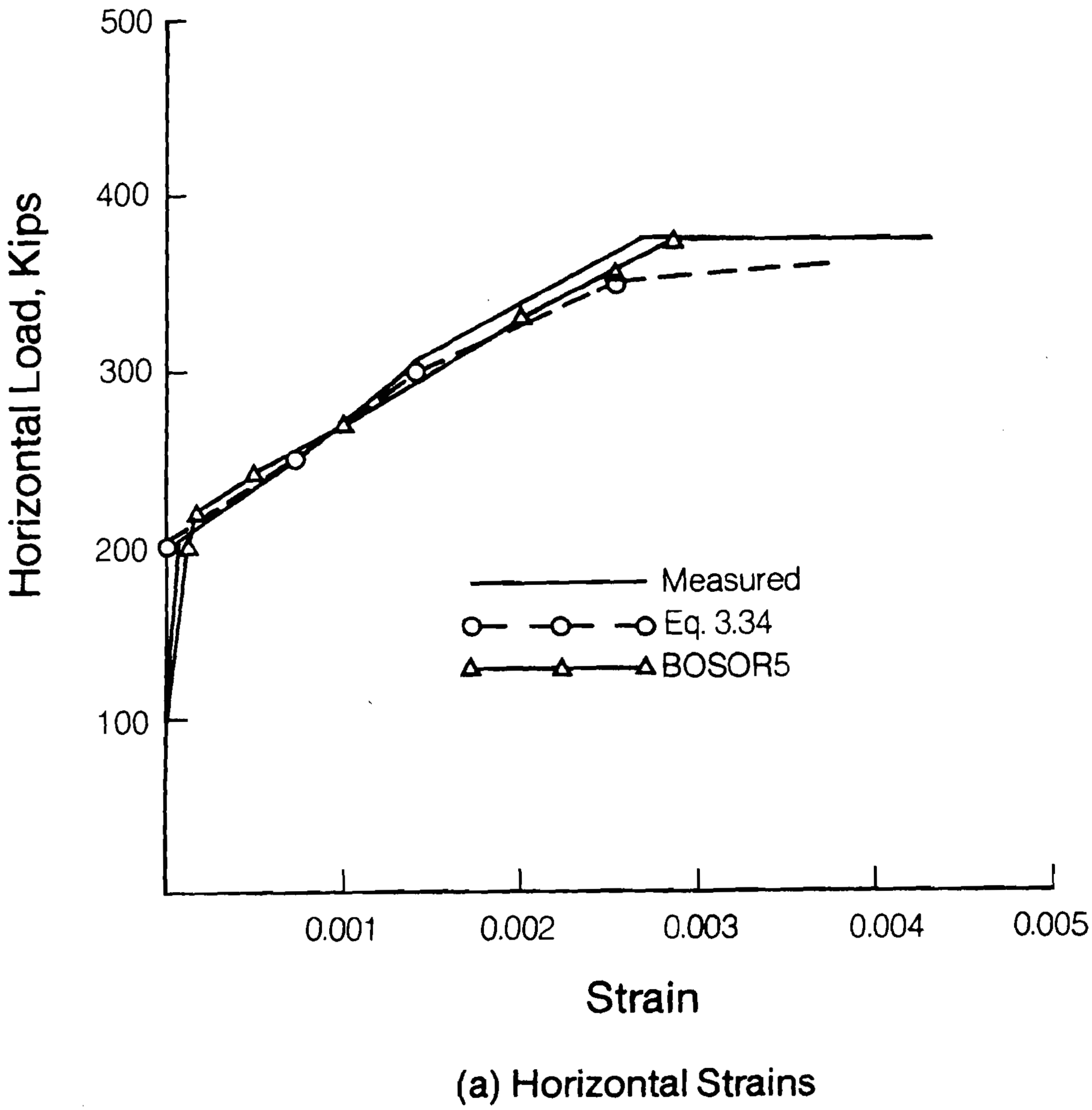

Figure 5.6.3 Measured and Computed Mean Strain, ε_m, Segment 3

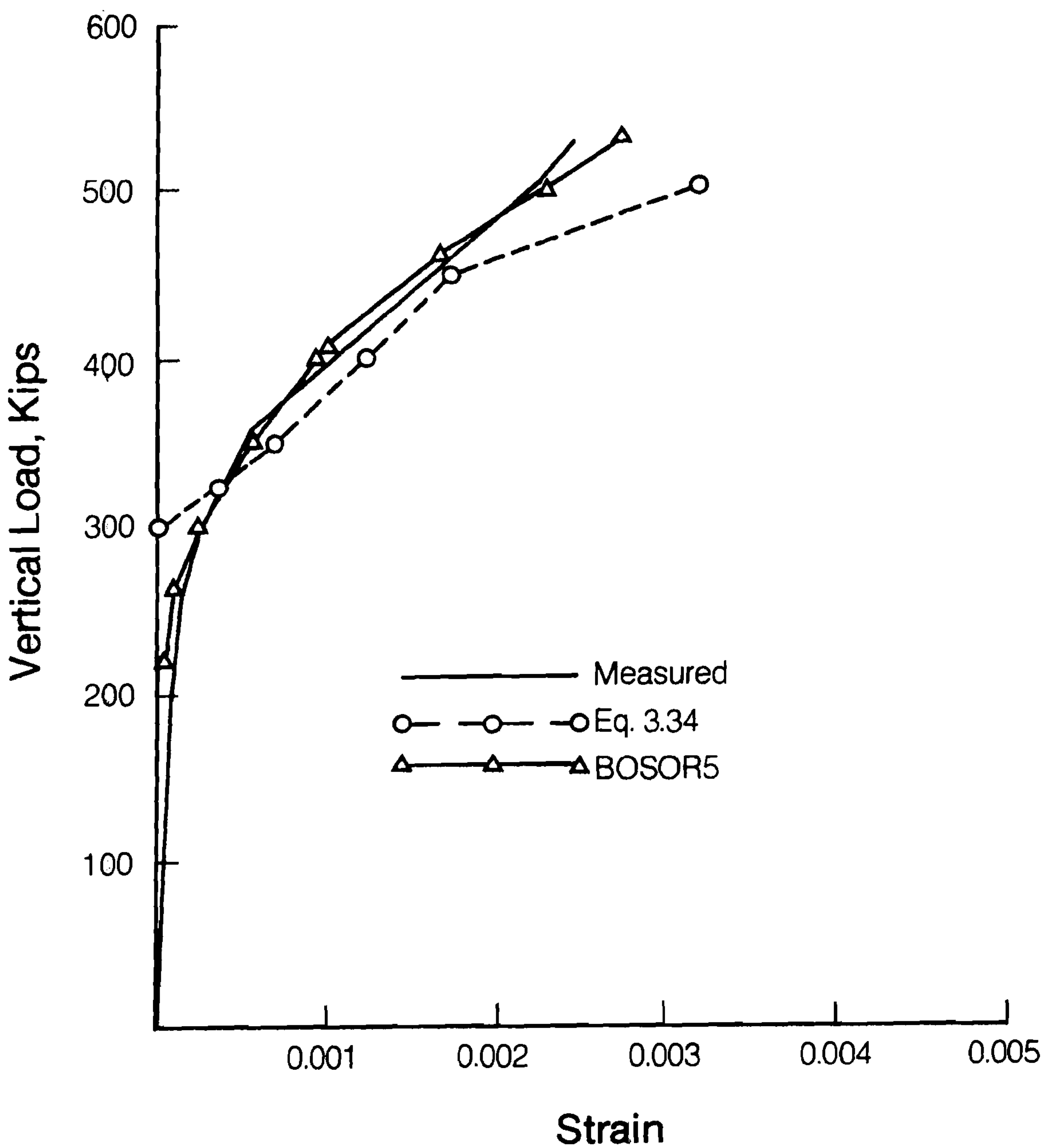

(b) Vertical Strains

Figure 5.6.3 Measured and Computed Mean Strain, ε_m, Segment 3

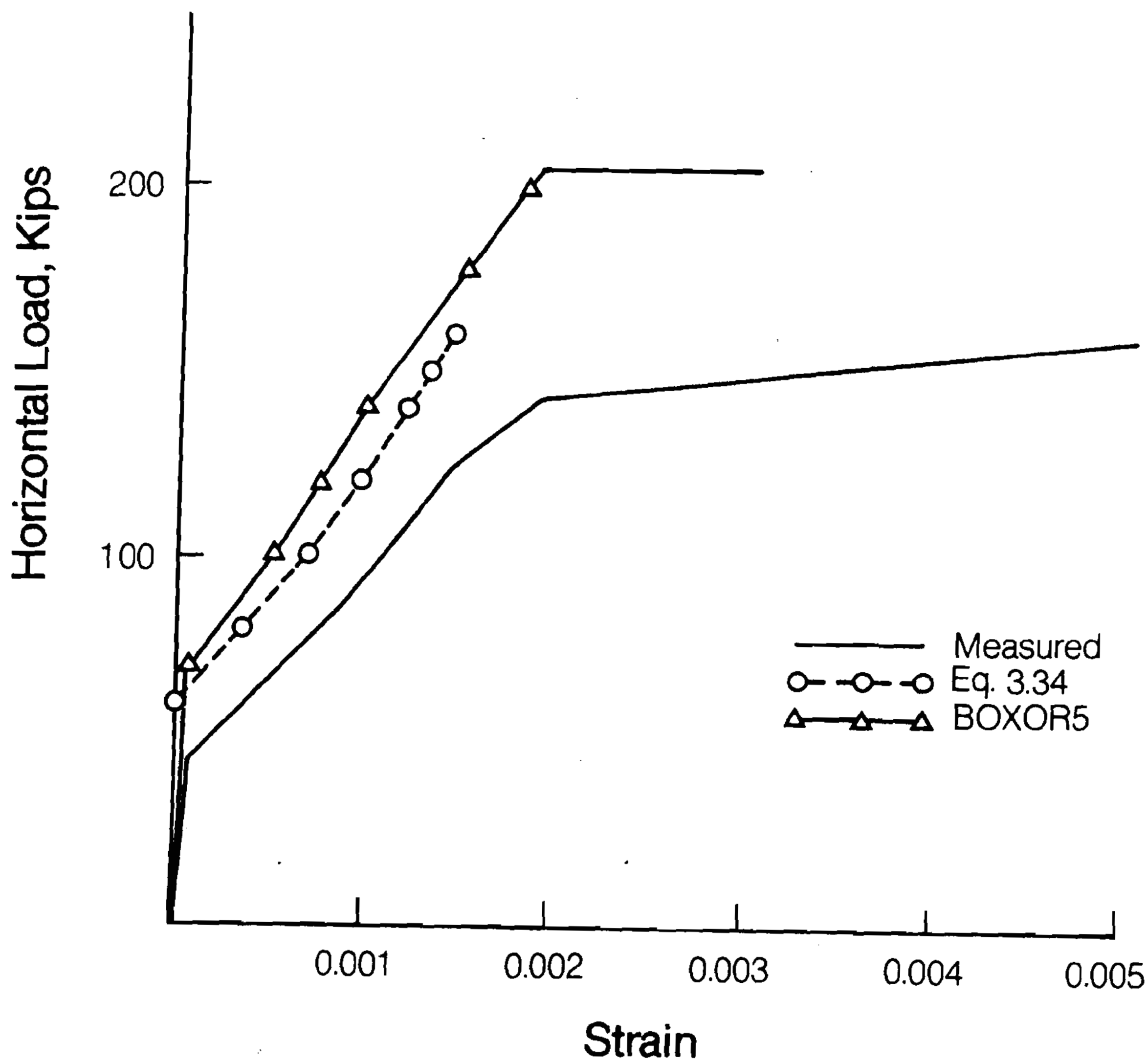

(a) Horizontal Strains

Figure 5.6.4 Measured and Computed Mean Strain, ε_m, Segment 4

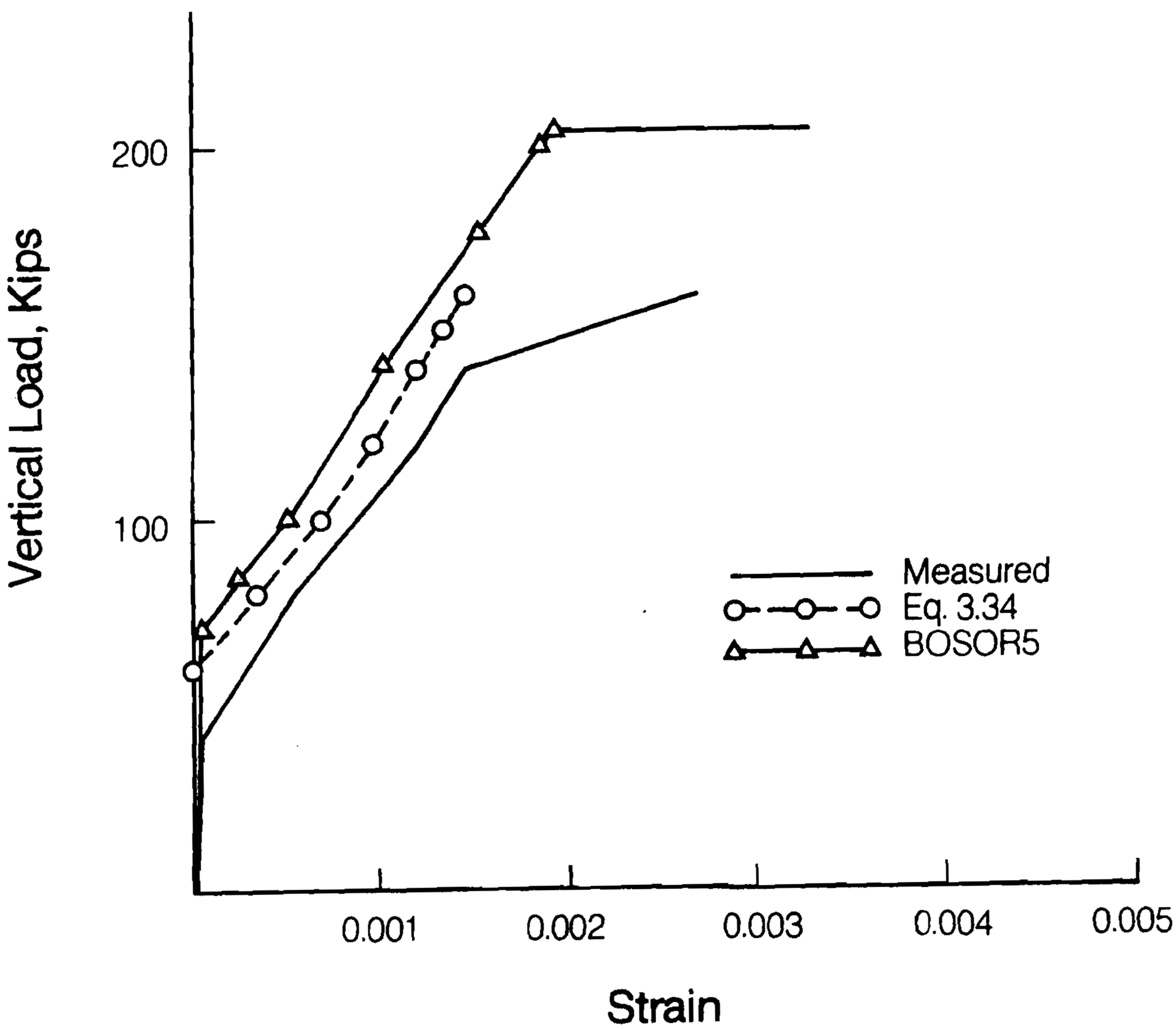

(b) Vertical Strains

Figure 5.6.4 Measured and Computed Mean Strain, ε_m, segment 4

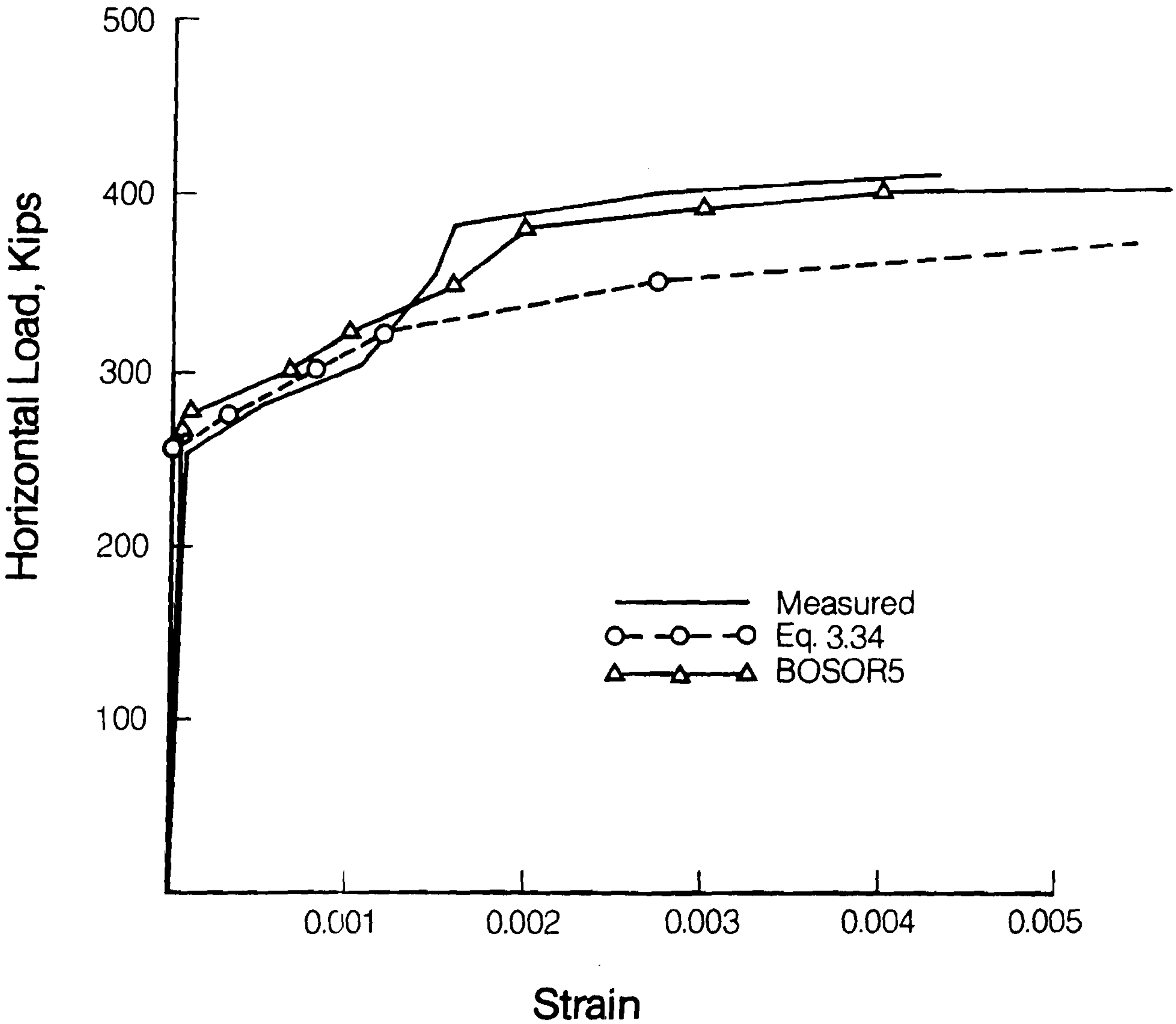

(a) Horizontal Strains

Figure 5.6.5 Measured and Computed Mean Strain, ε_m, Segment 5

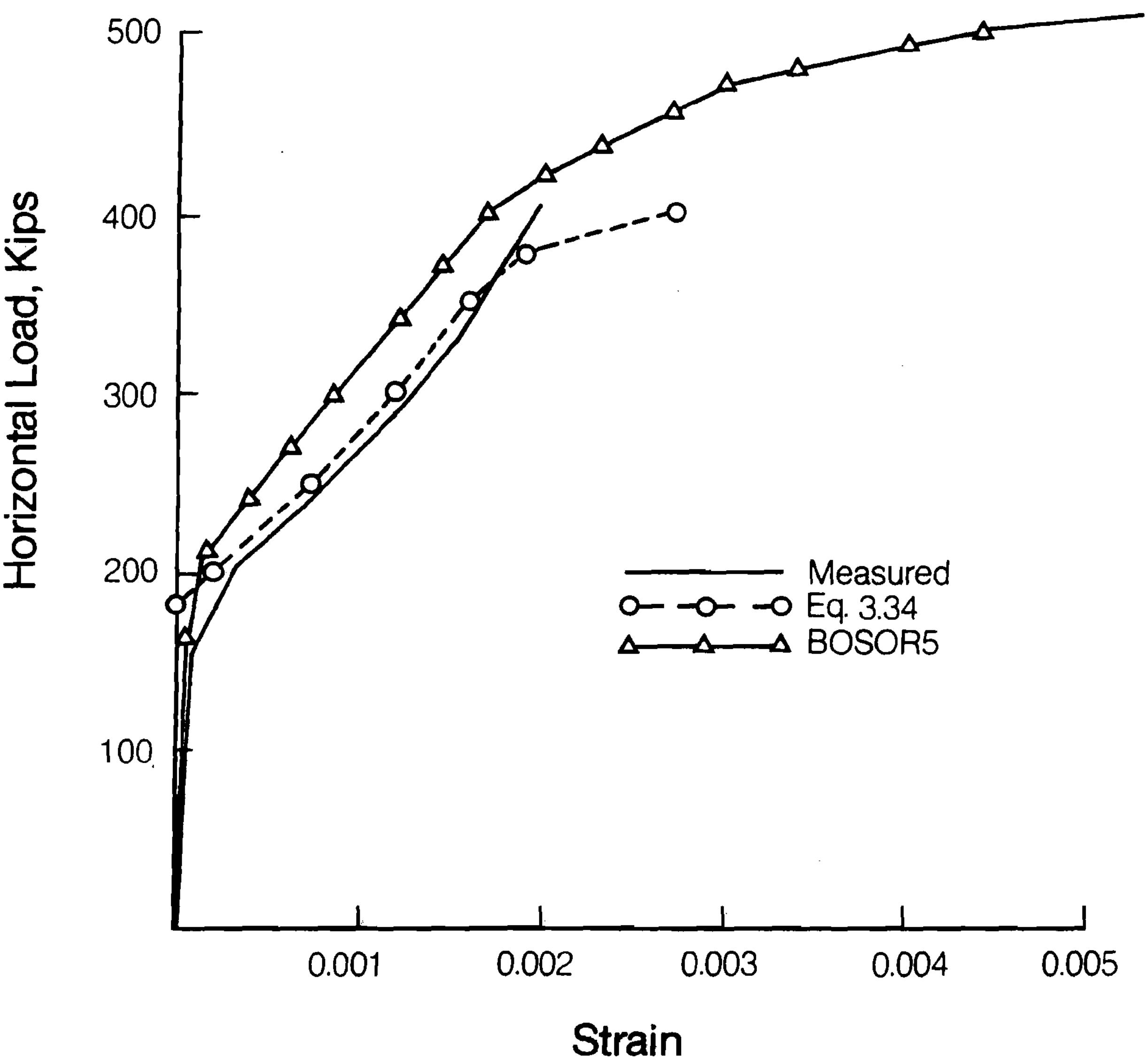

(a) Horizontal Strains

Figure 5.6.6 Measured and Computed Mean Strain, ε_m, Segment 6

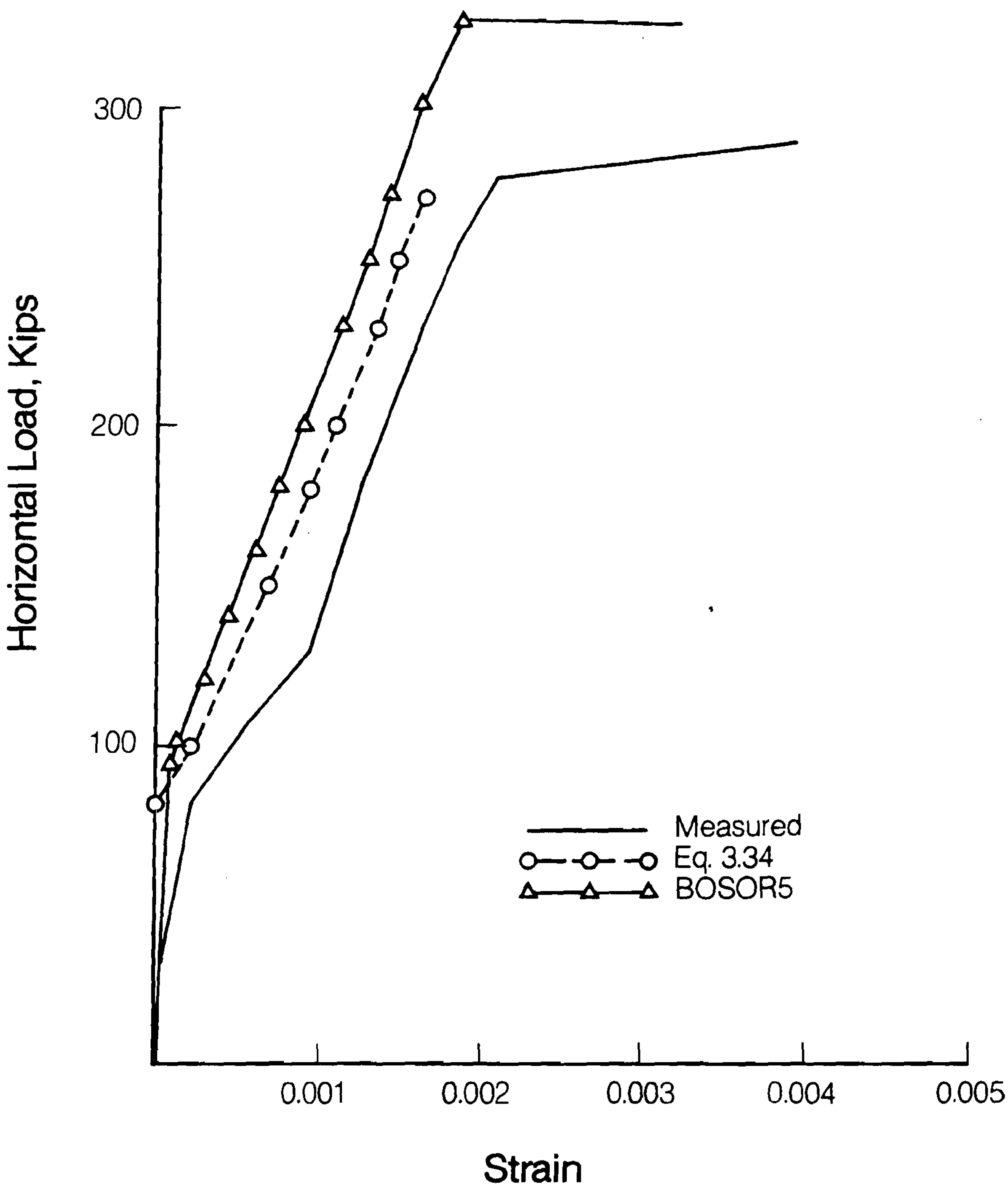

(a) Horizontal Strains

Figure 5.6.7 Measured and Computed Mean Strain, ε_m, Segment 7

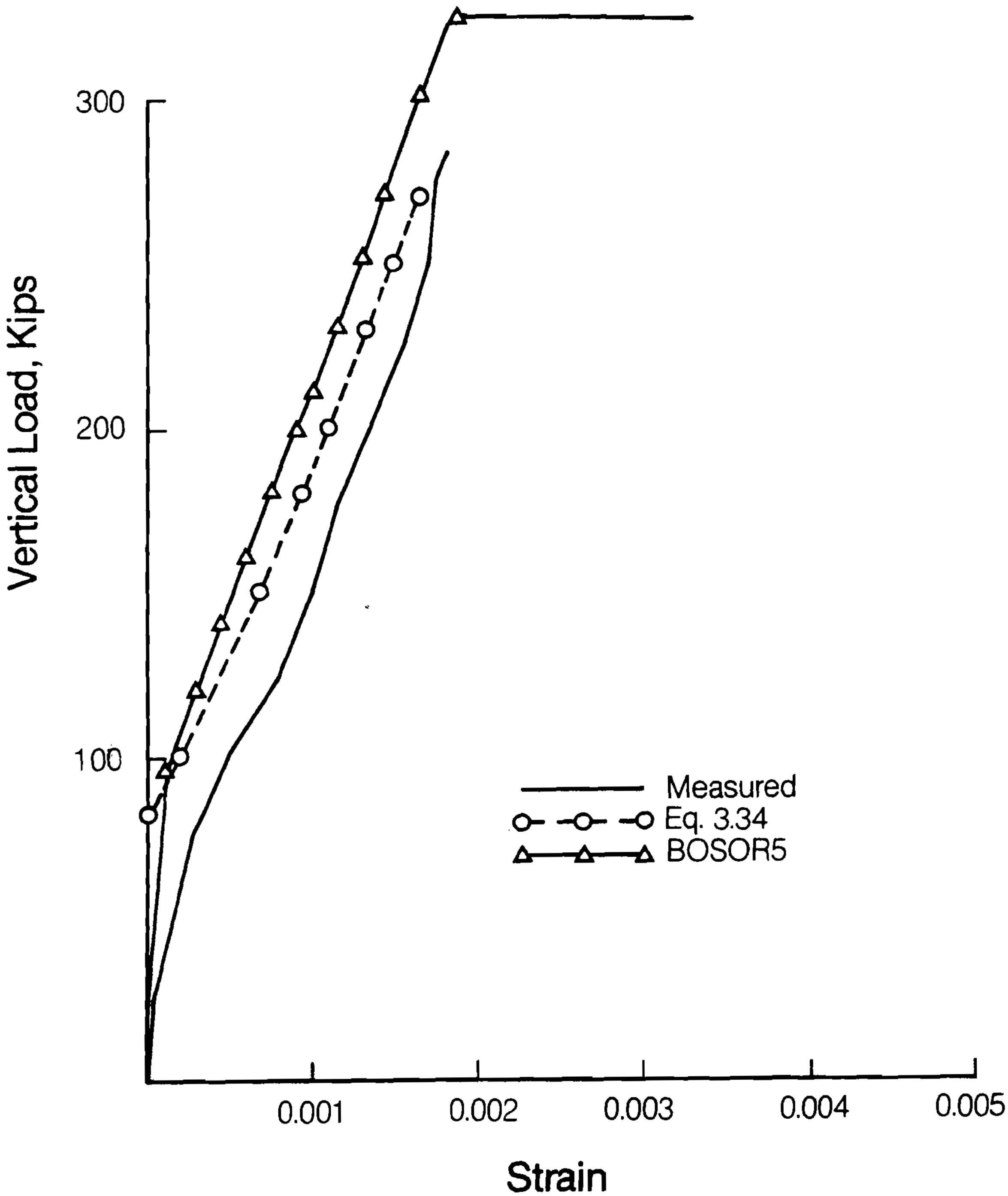

(b) Vertical Strains

Figure 5.6.7 Measured and Computed Mean Strain, ε_m, Segment 7

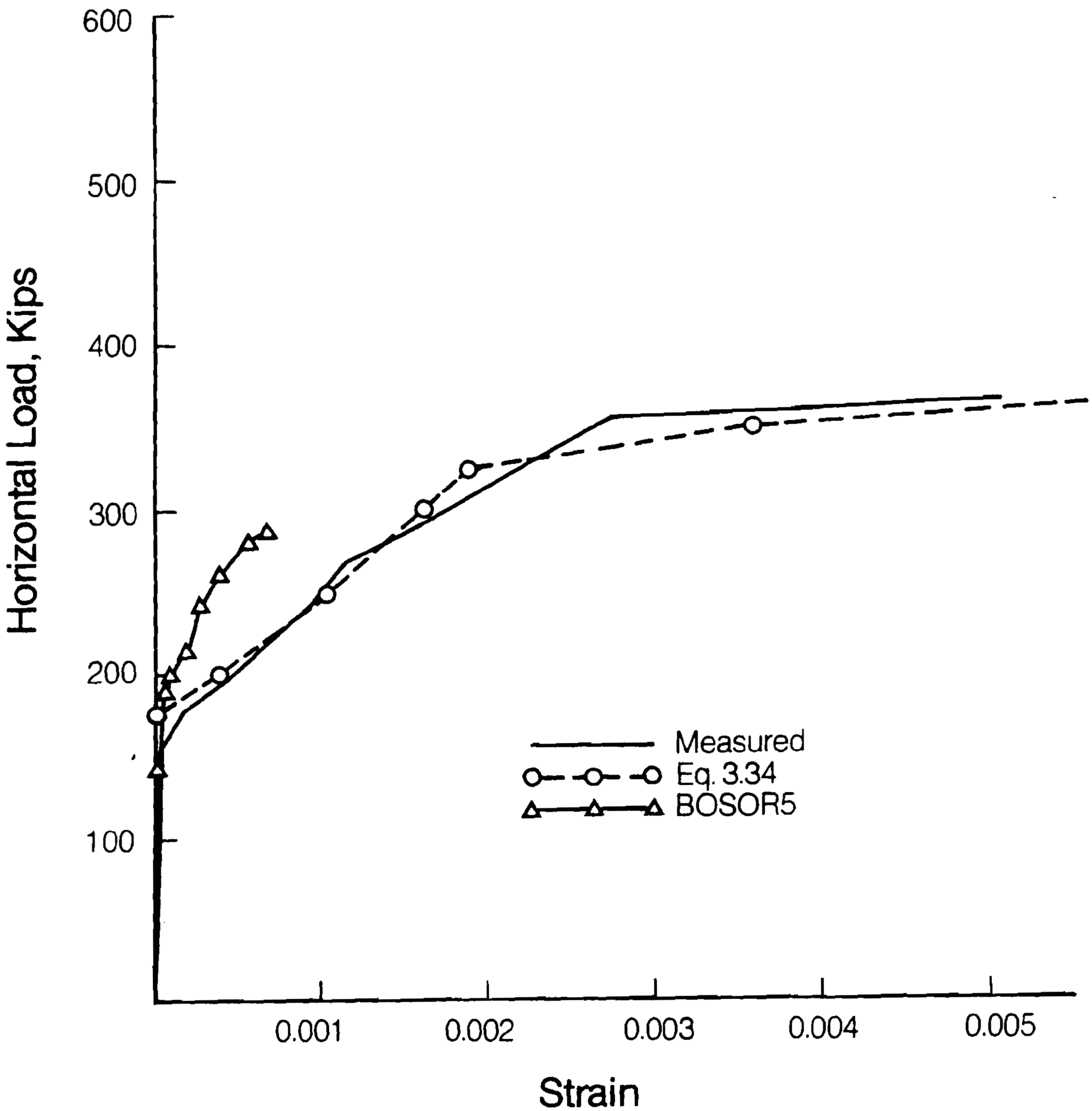

(a) Horizontal Strains

Figure 5.6.8 Measured and Computed Mean Strain, ε_m, Segment 8

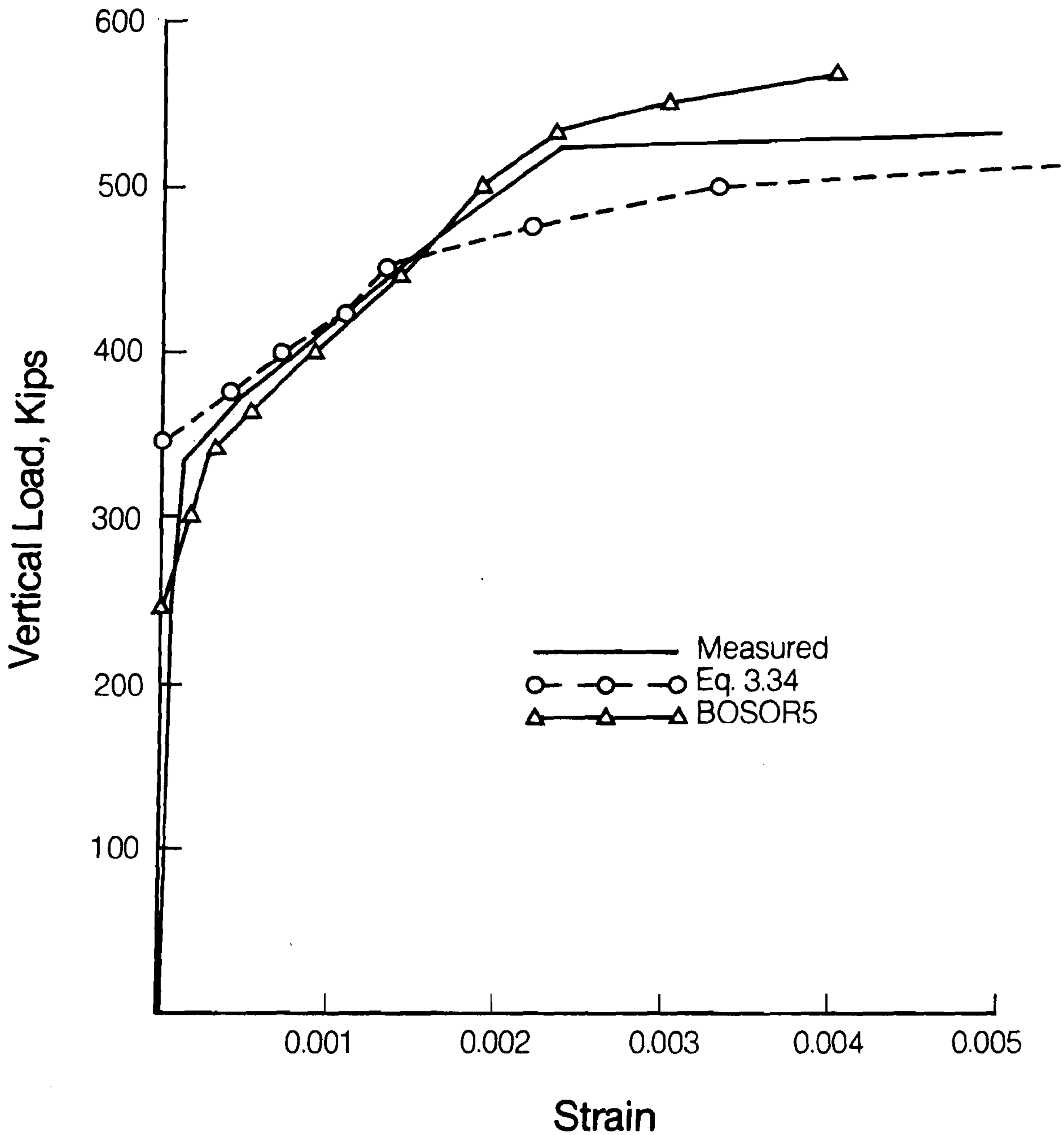

(b) Vertical Strains

Figure 5.6.8 Measured and Computed Mean Strain, ε_m, Segment 8

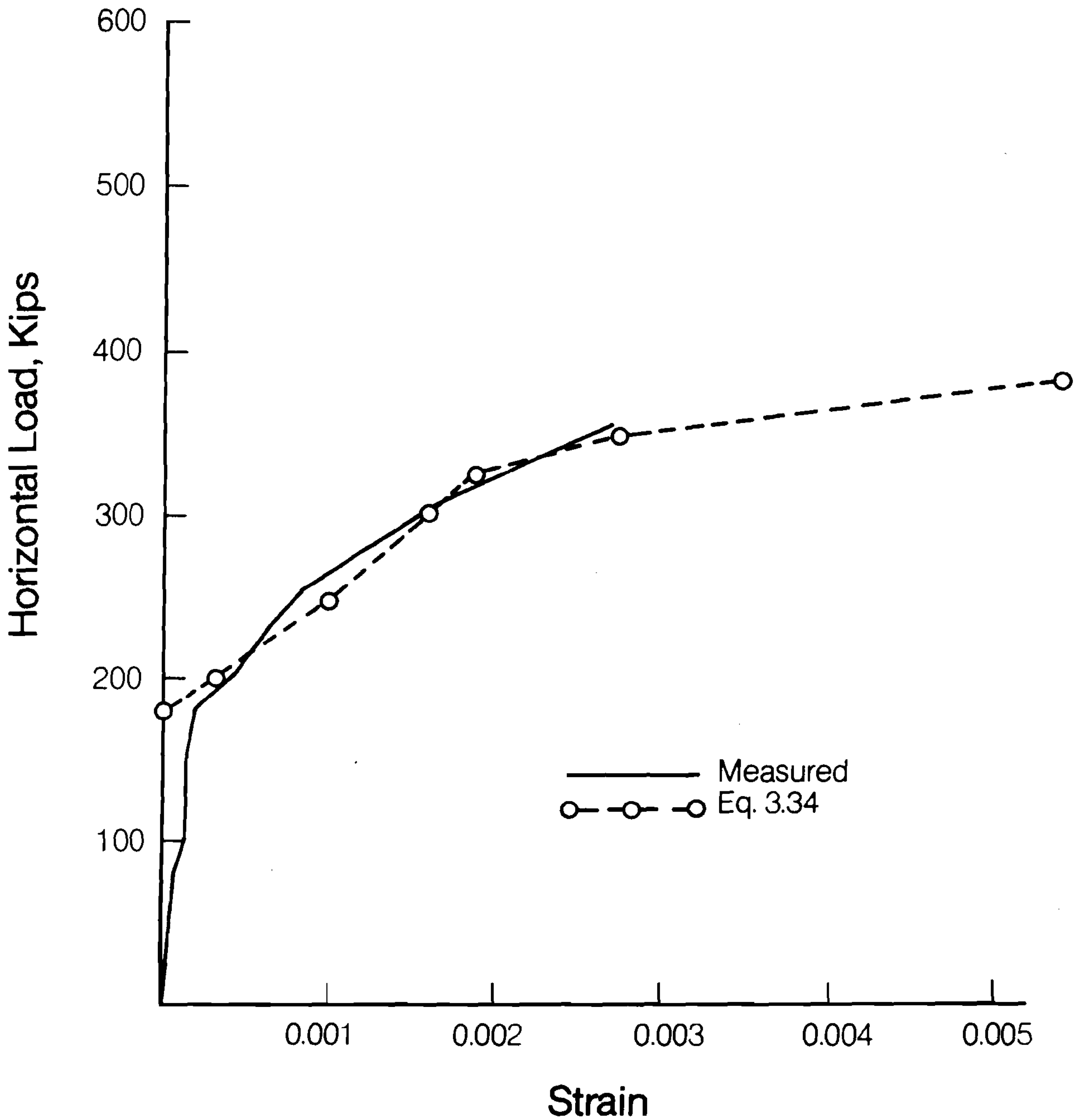

(a) Horizontal Strains

Figure 5.6.9 Measured and Computed Mean Strain, ε_m, Segment 9

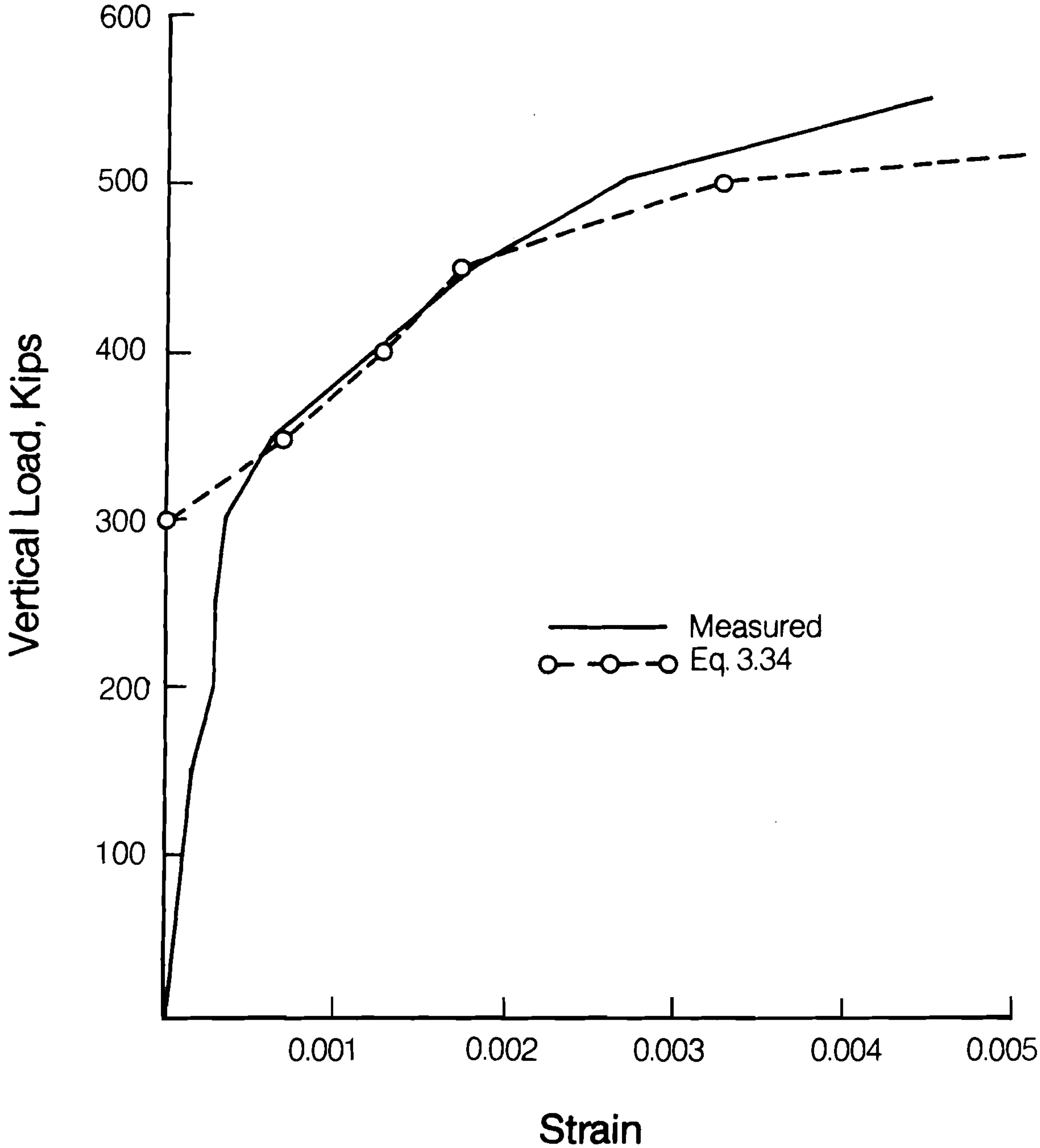

(b) Vertical Strains

Figure 5.6.9 Measured and Computed Mean Strain, ε_m, Segment 9

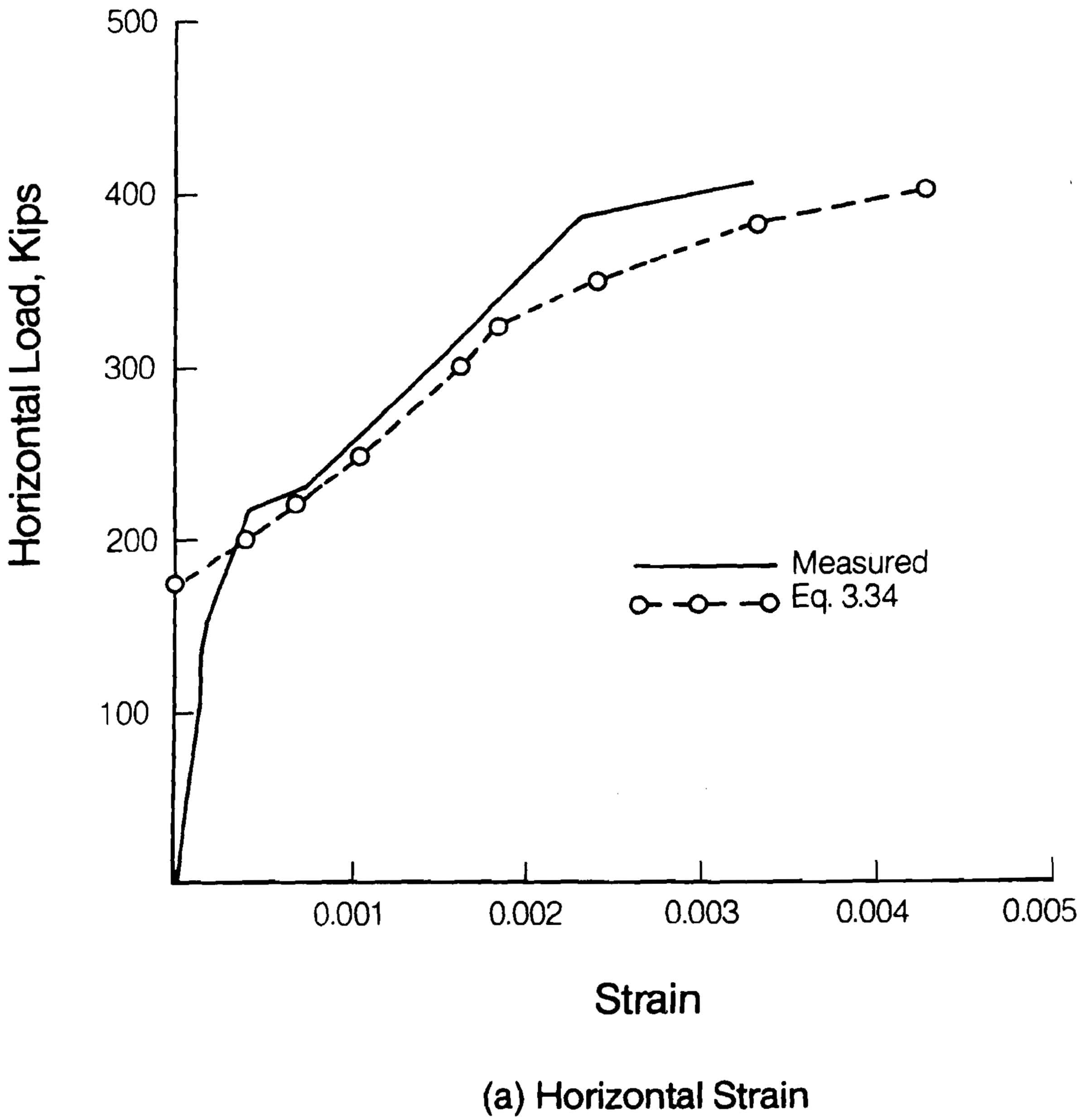

Figure 5.6.11 Measured and Computed Mean Strain, ε_m, Segment 11

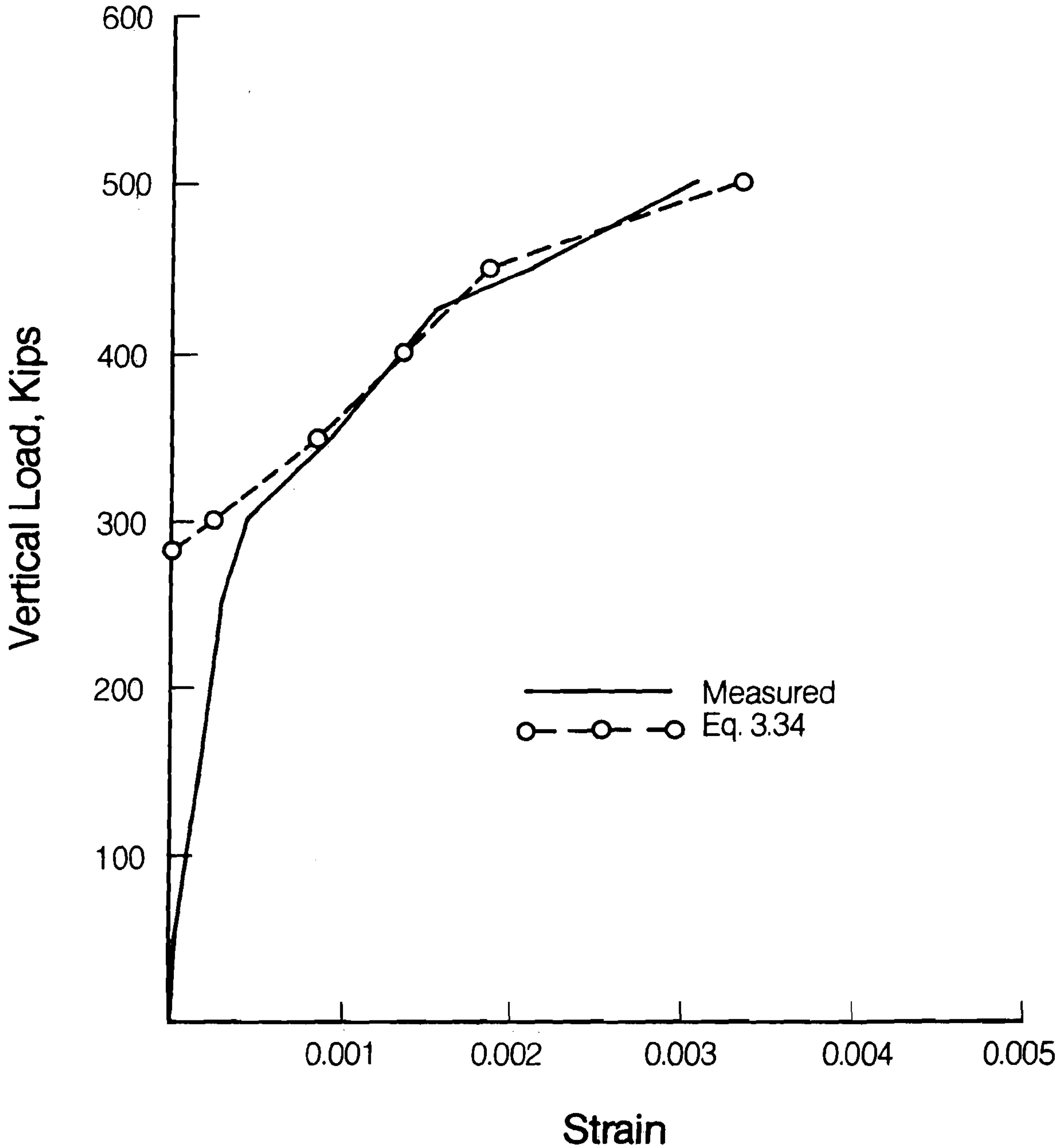

(b) Vertical Strains

Figure 5.6.11 Measured and Computed Mean Strain, ε_m, Segment 11

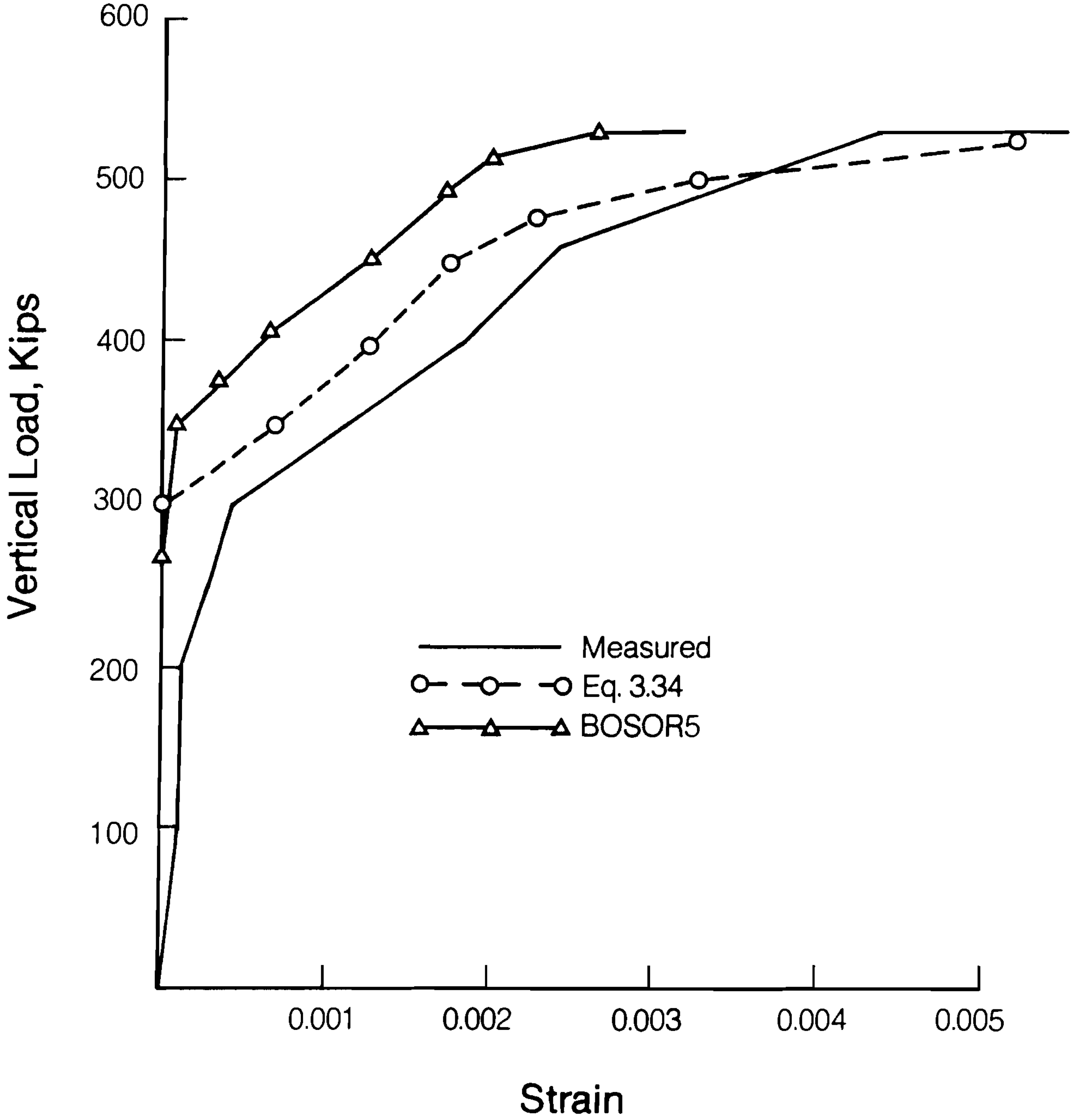

(a) Vertical Strains (Face A)

Figure 5.6.12 Measured and Computed Mean Strains, ε_m, Segment 12

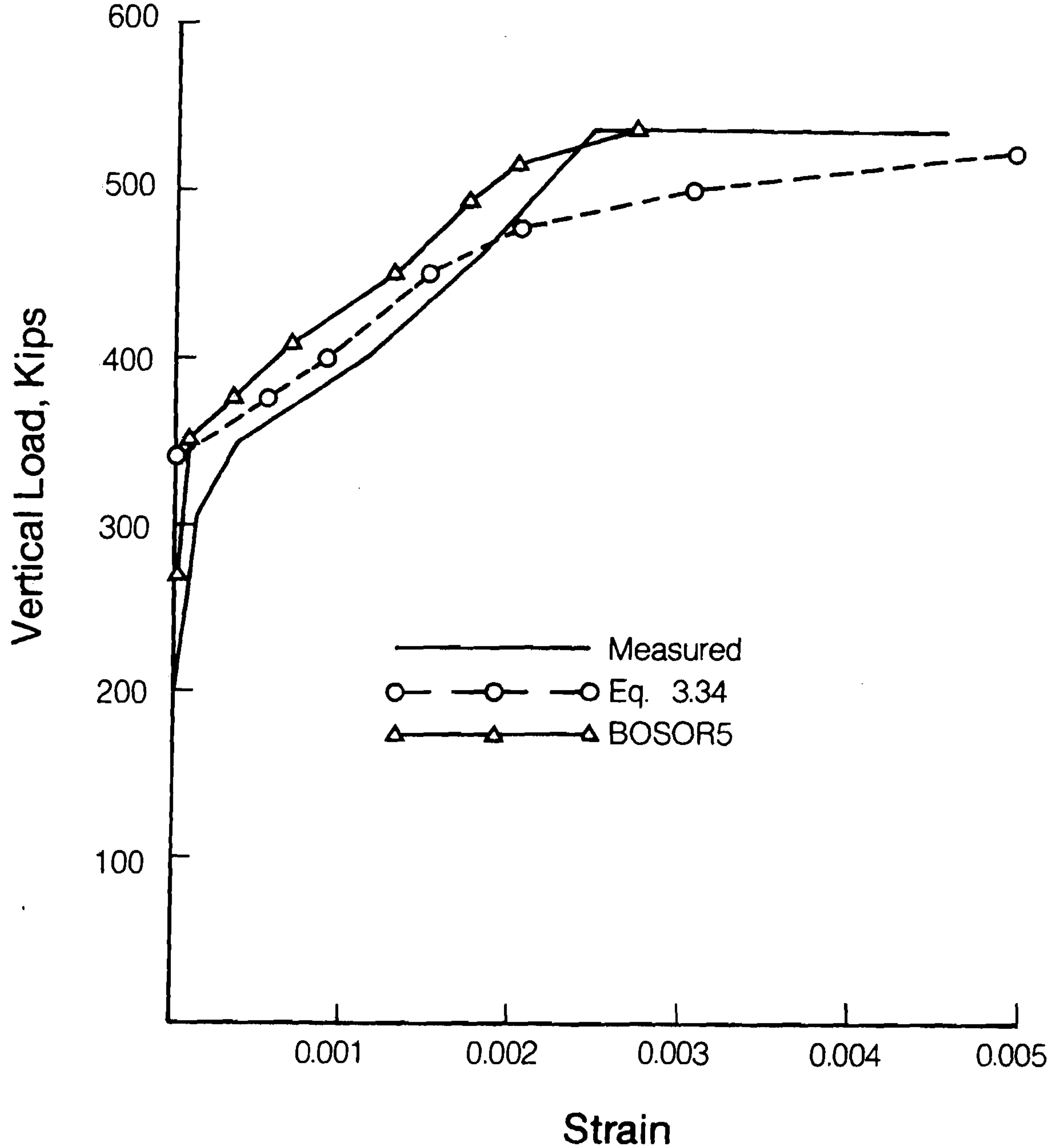

(b) Vertical Strains (Face B)

Figure 5.6.12 Measured and Computed Mean Strains, ε_m, Segment 12

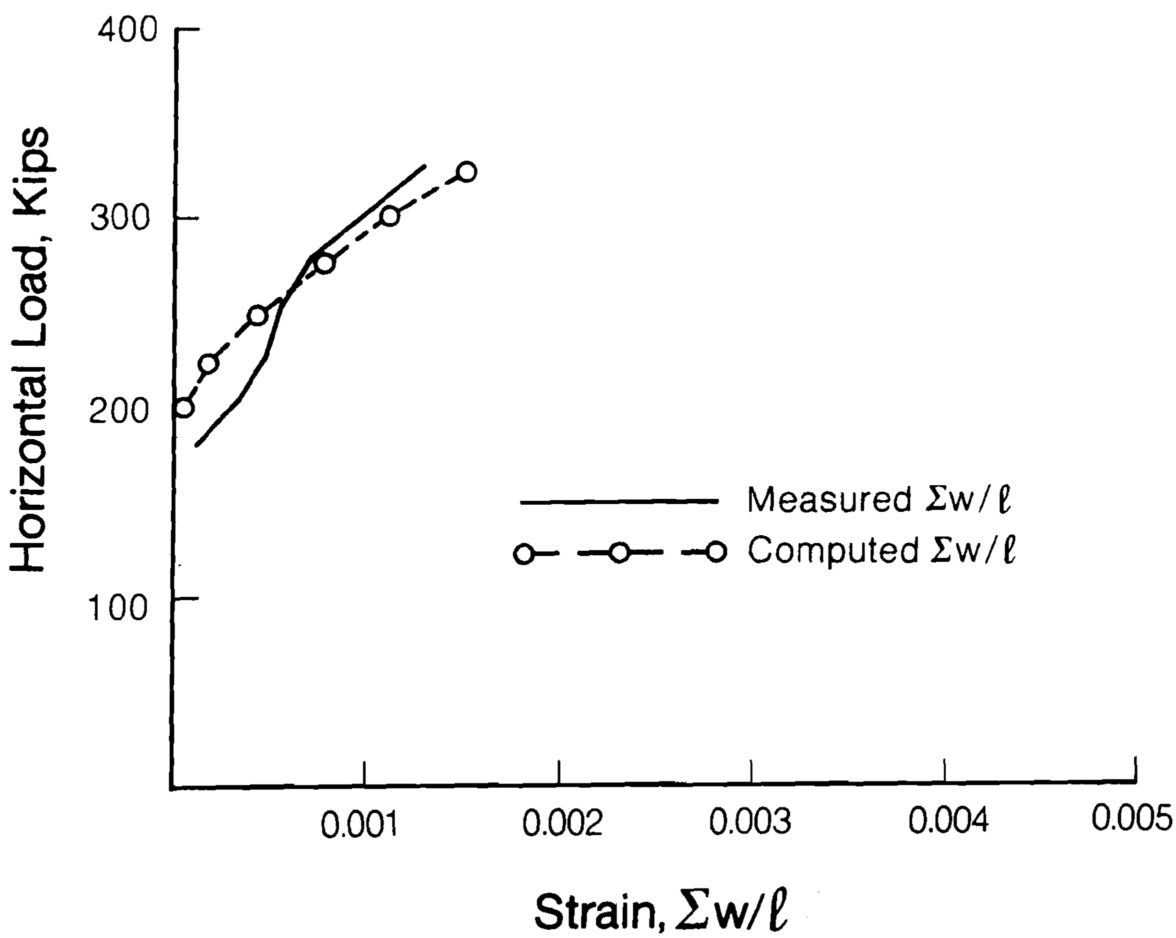

(a) Vertical Cracks

Figure 5.7.1 Measured and Computed Crack Strain, $\Sigma w/\ell$, Segment 1

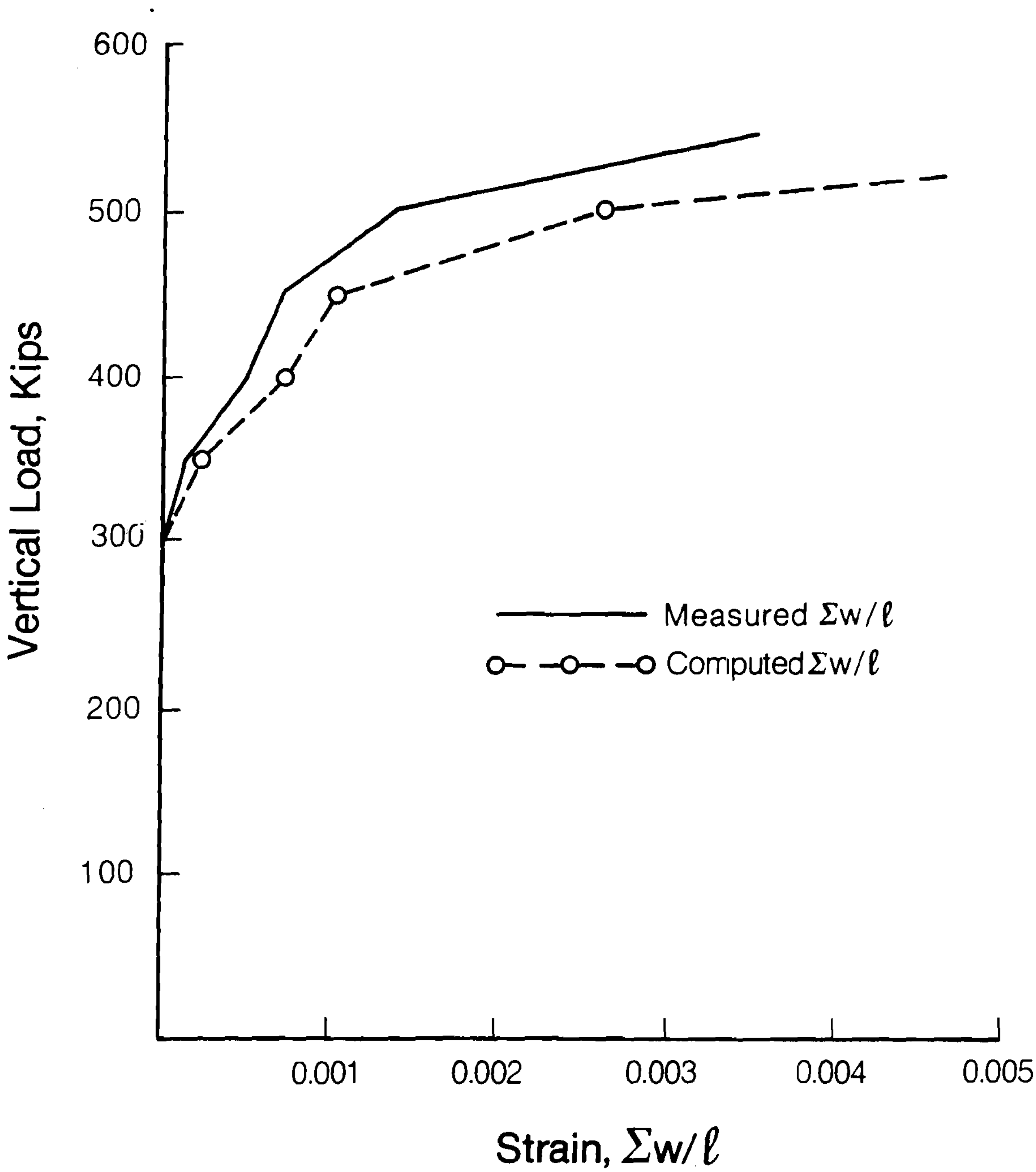

(b) Horizontal Crack

Figure 5.7.1 Measured and Computed Crack Strain, $\Sigma w/\ell$, Segment 1

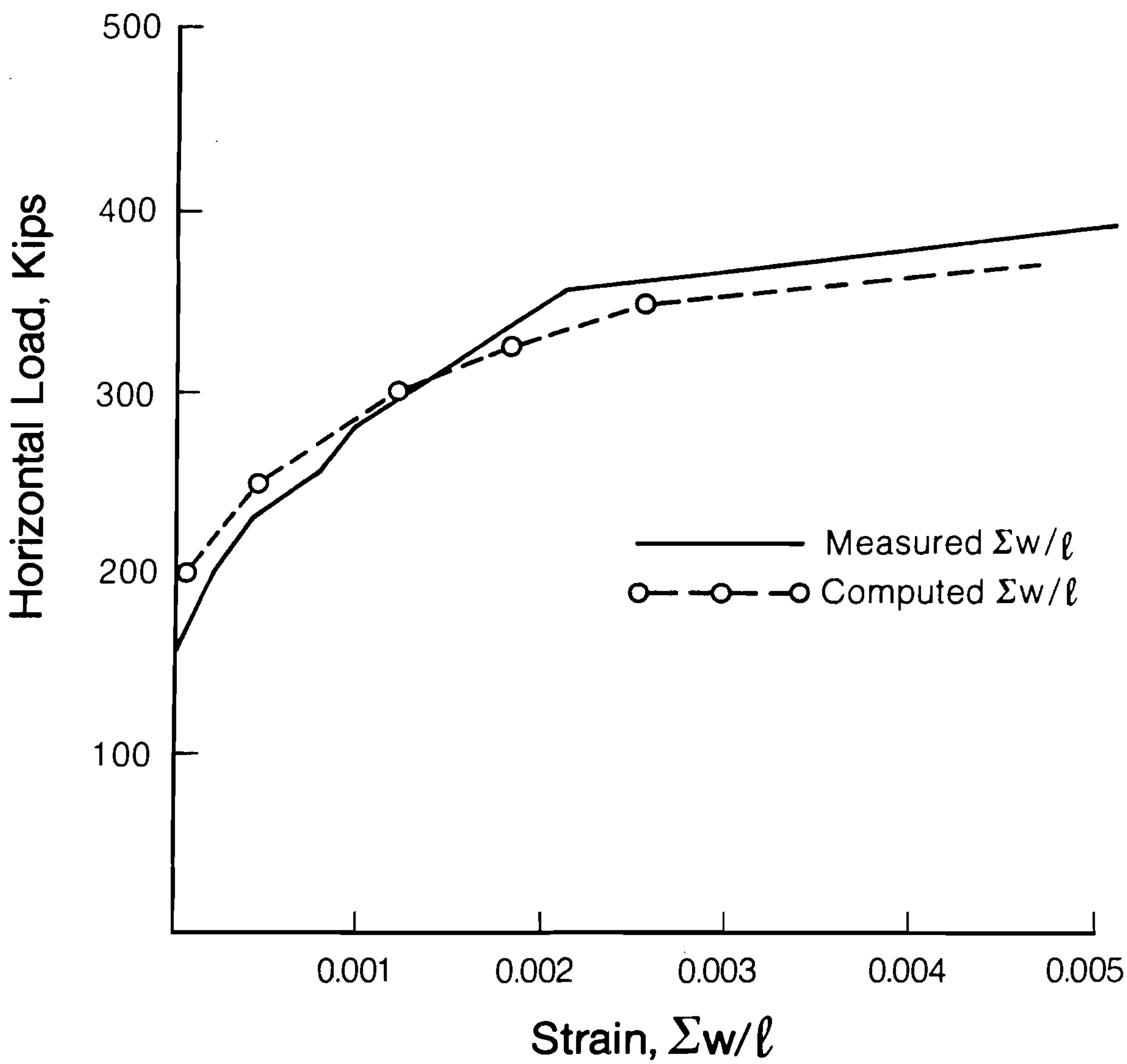

(a) Vertical Cracks

Figure 5.7.2 Measured and Computed Crack Strain, $\Sigma w/\ell$, Segment 2

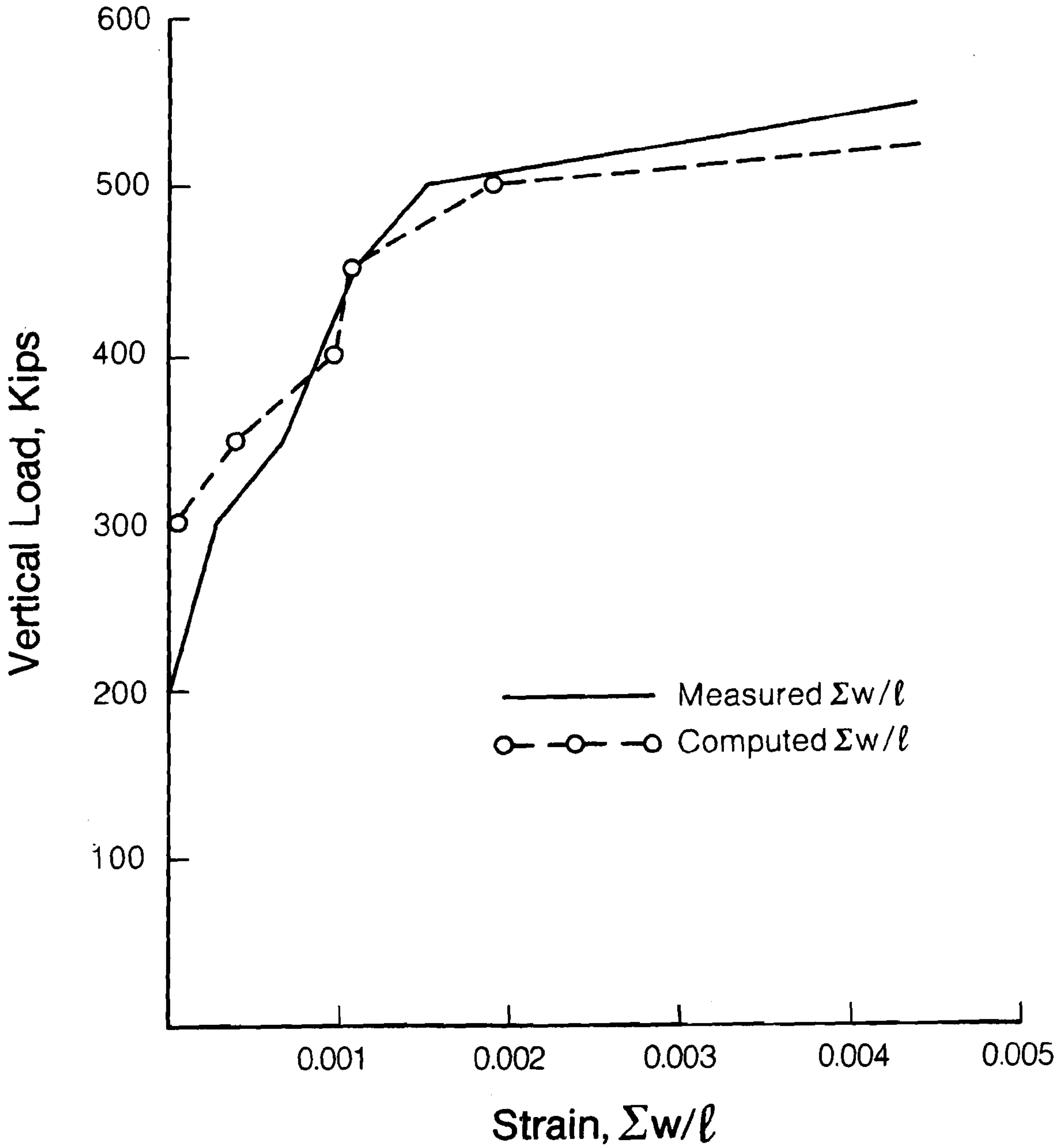

(b) Horizontal Cracks

Figure 5.7.2 Measured and Computed Crack Strain, $\Sigma w/\ell$, Segment 2

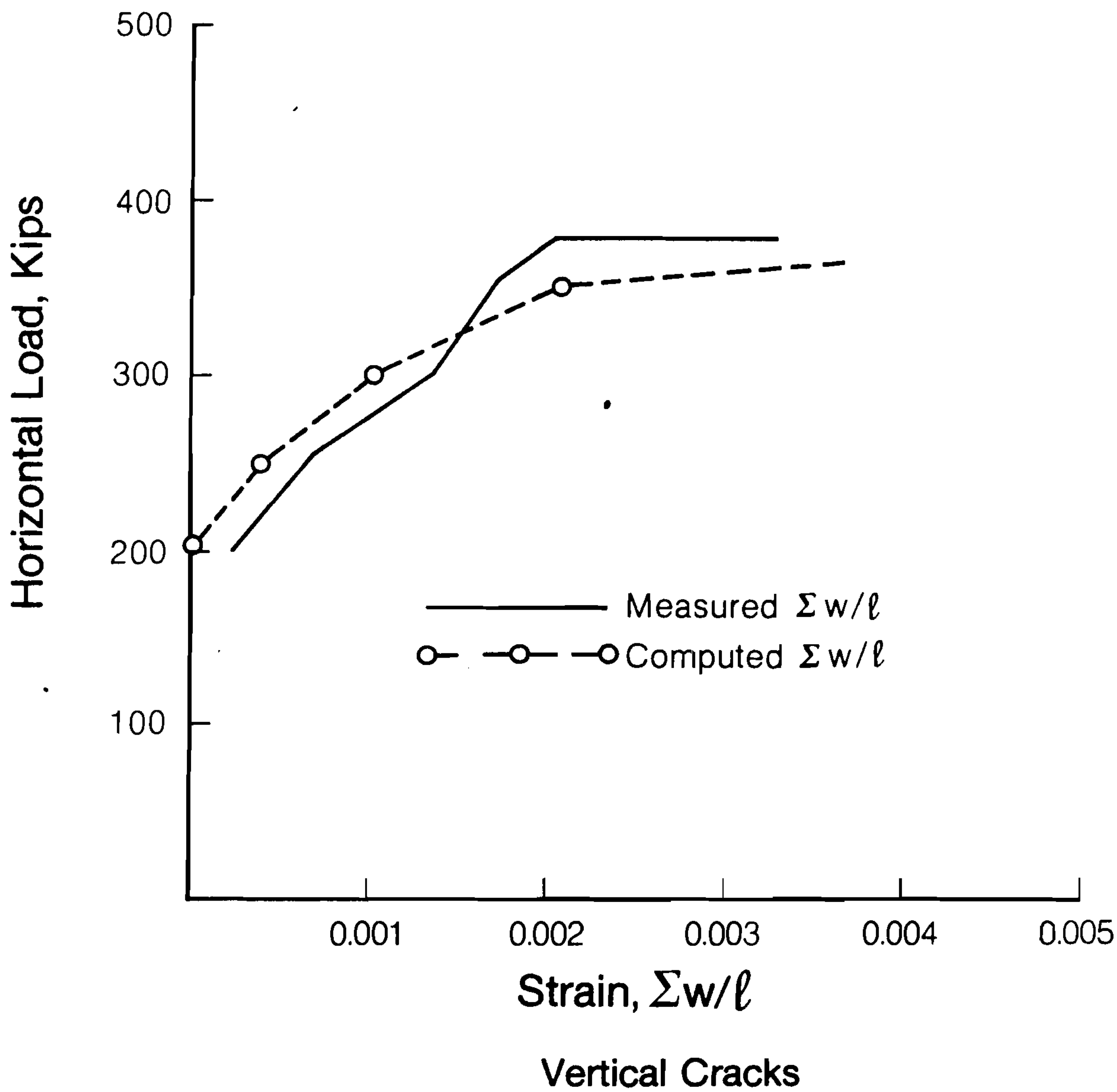

Figure 5.7.3 Measured and Computed Crack Strain, $\Sigma w/\ell$, Segment 3

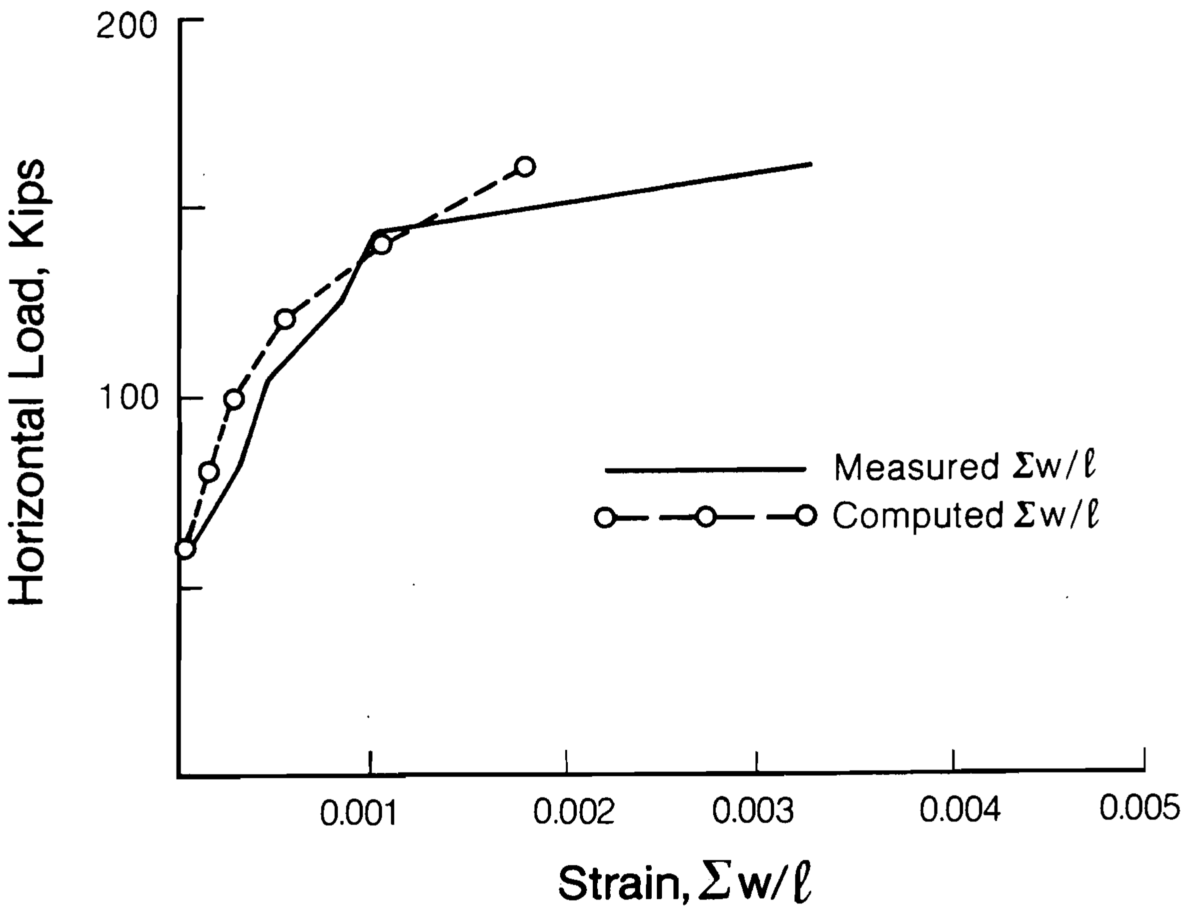

(a) Vertical Crack

Figure 5.7.4 Measured and Computed Crack Strain, $\Sigma w/\ell$, Segment 4

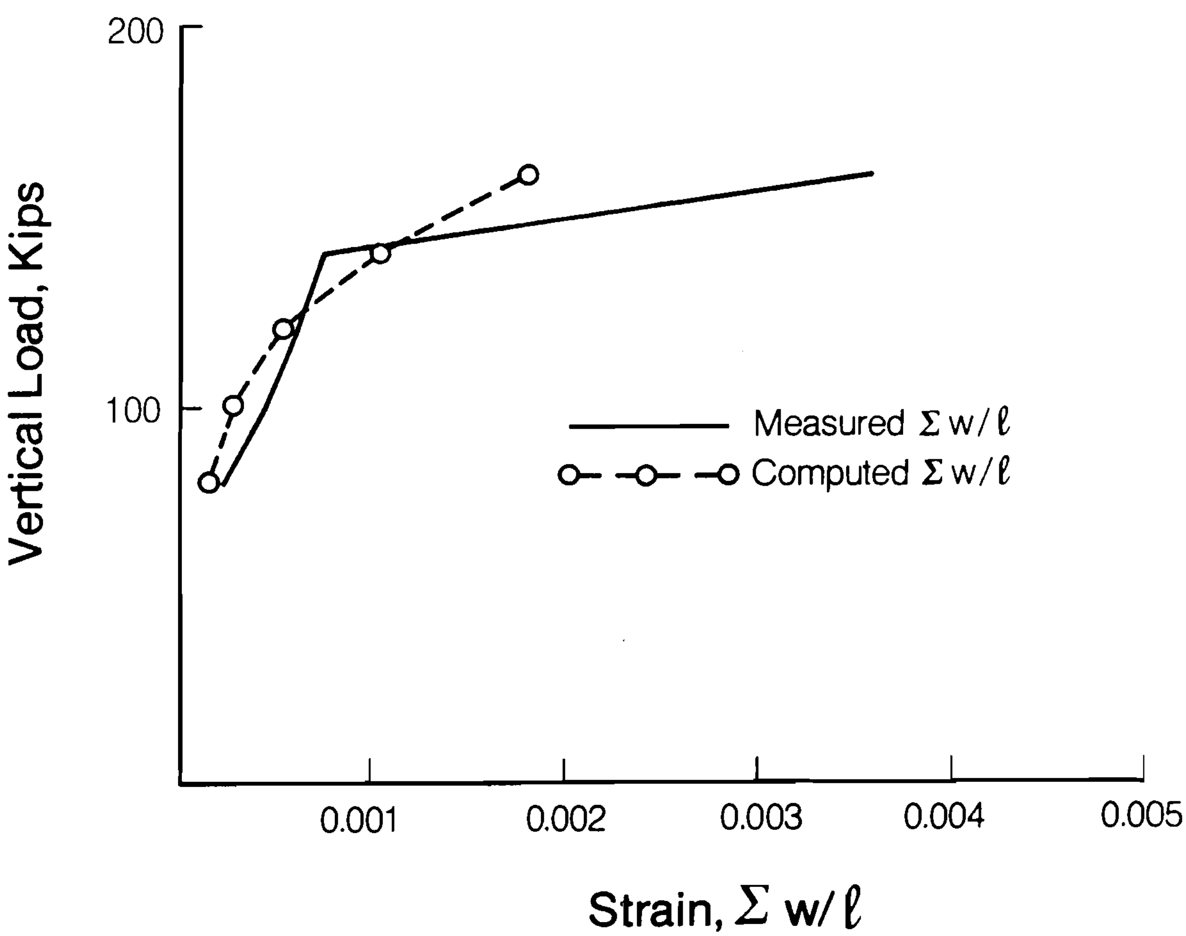

(b) Horizontal Cracks

Figure 5.7.4 Measured and Computed Crack Strain, $\Sigma w/\ell$, Segment 4

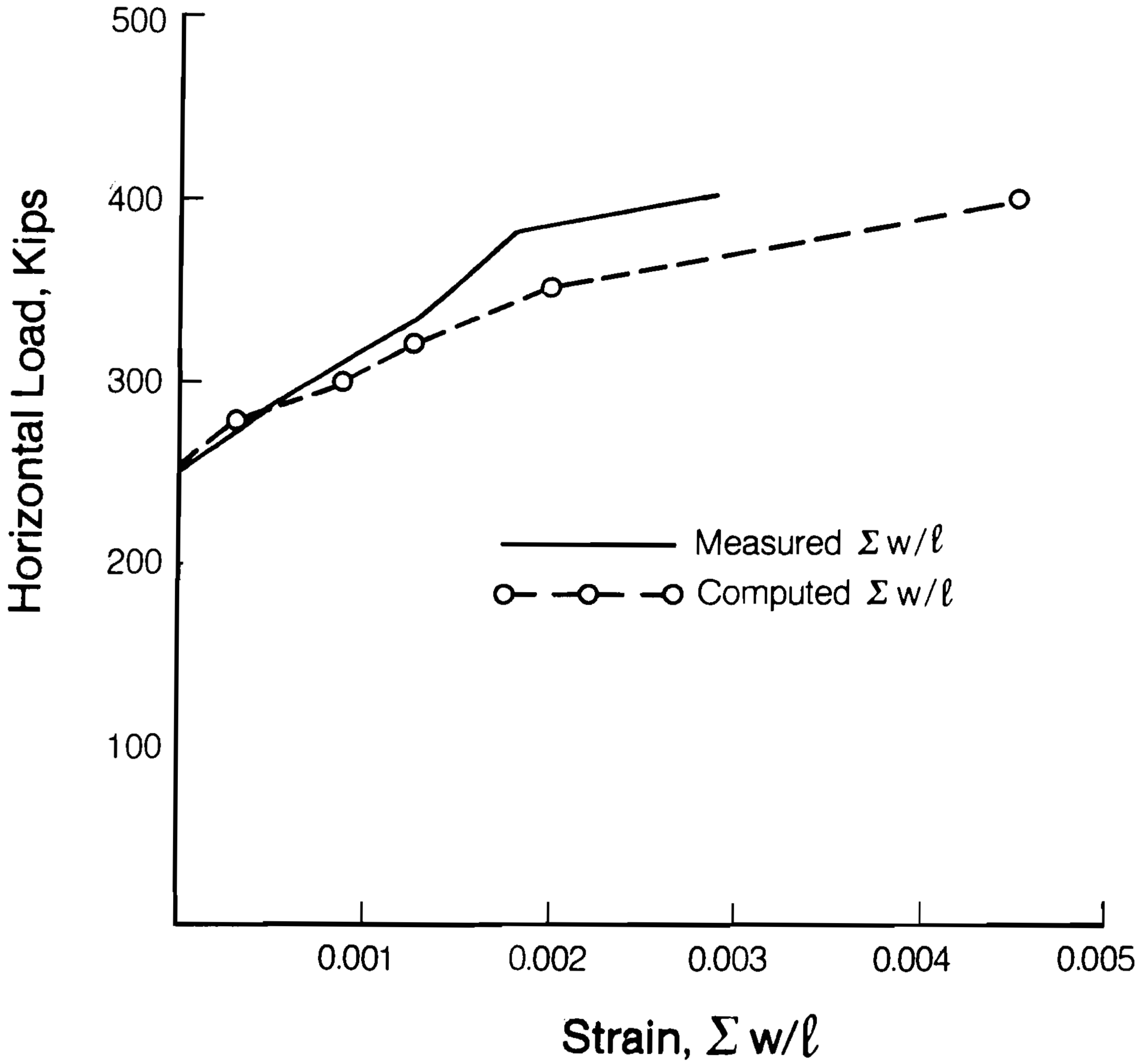

(a) Vertical Cracks

Figure 5.7.5 Measured and Computed Crack Strain, $\Sigma w/\ell$, Segment 5

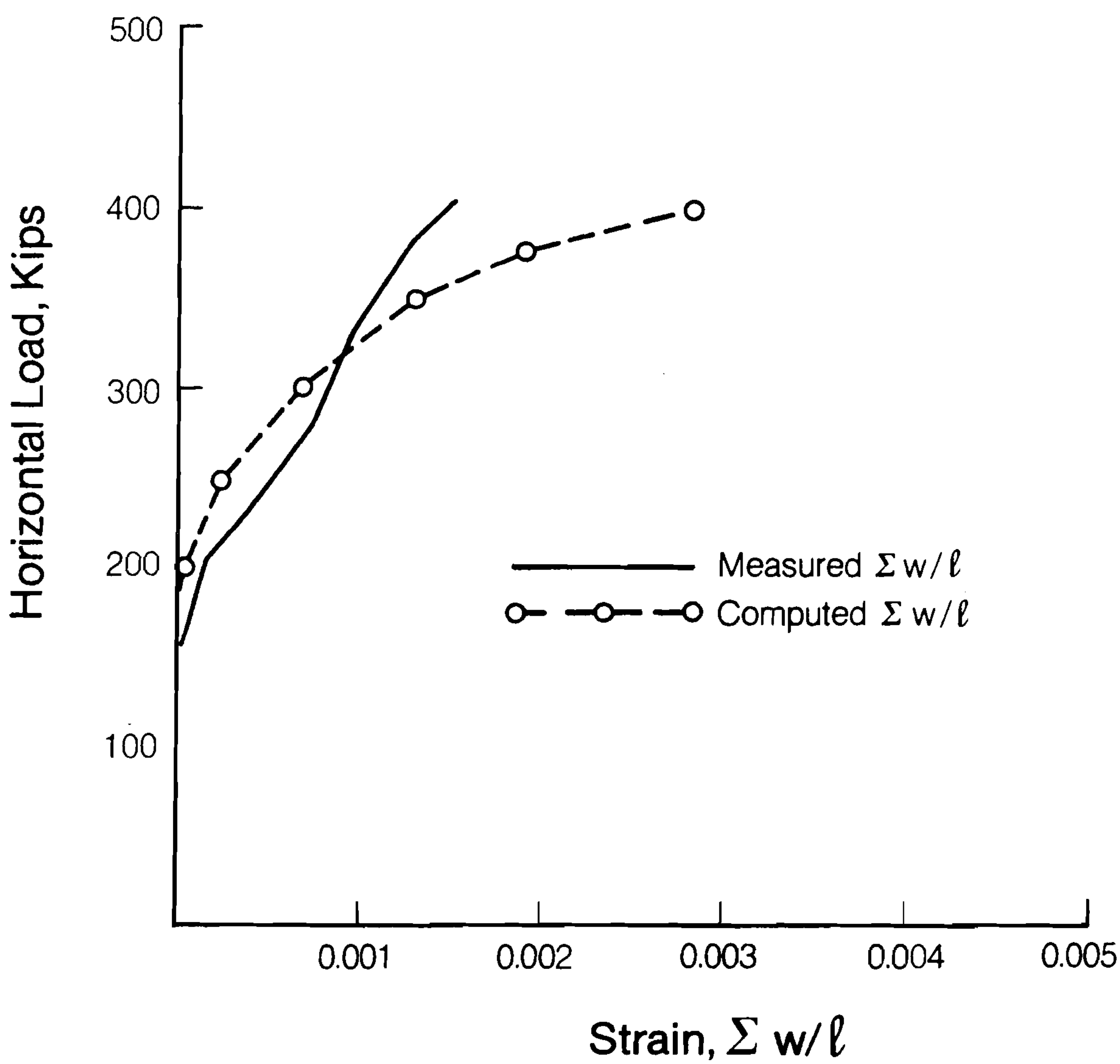

(a) Vertical Cracks

Figure 5.7.6 Measured and Computed Crack Strain, $\Sigma w/\ell$, Segment 6

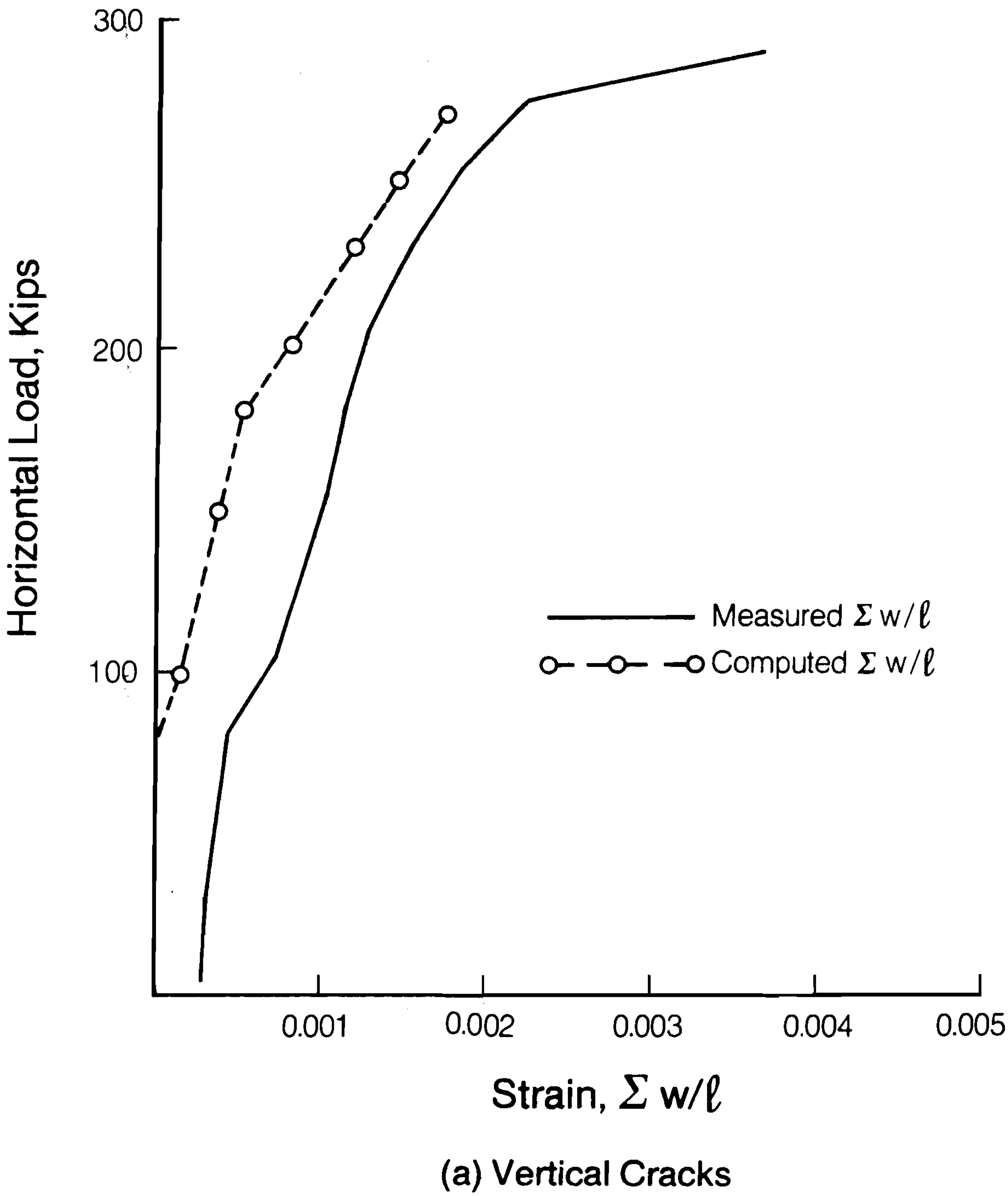

Figure 5.7.7 Measured and Computed Crack Strain, $\Sigma w/\ell$, Segment 7

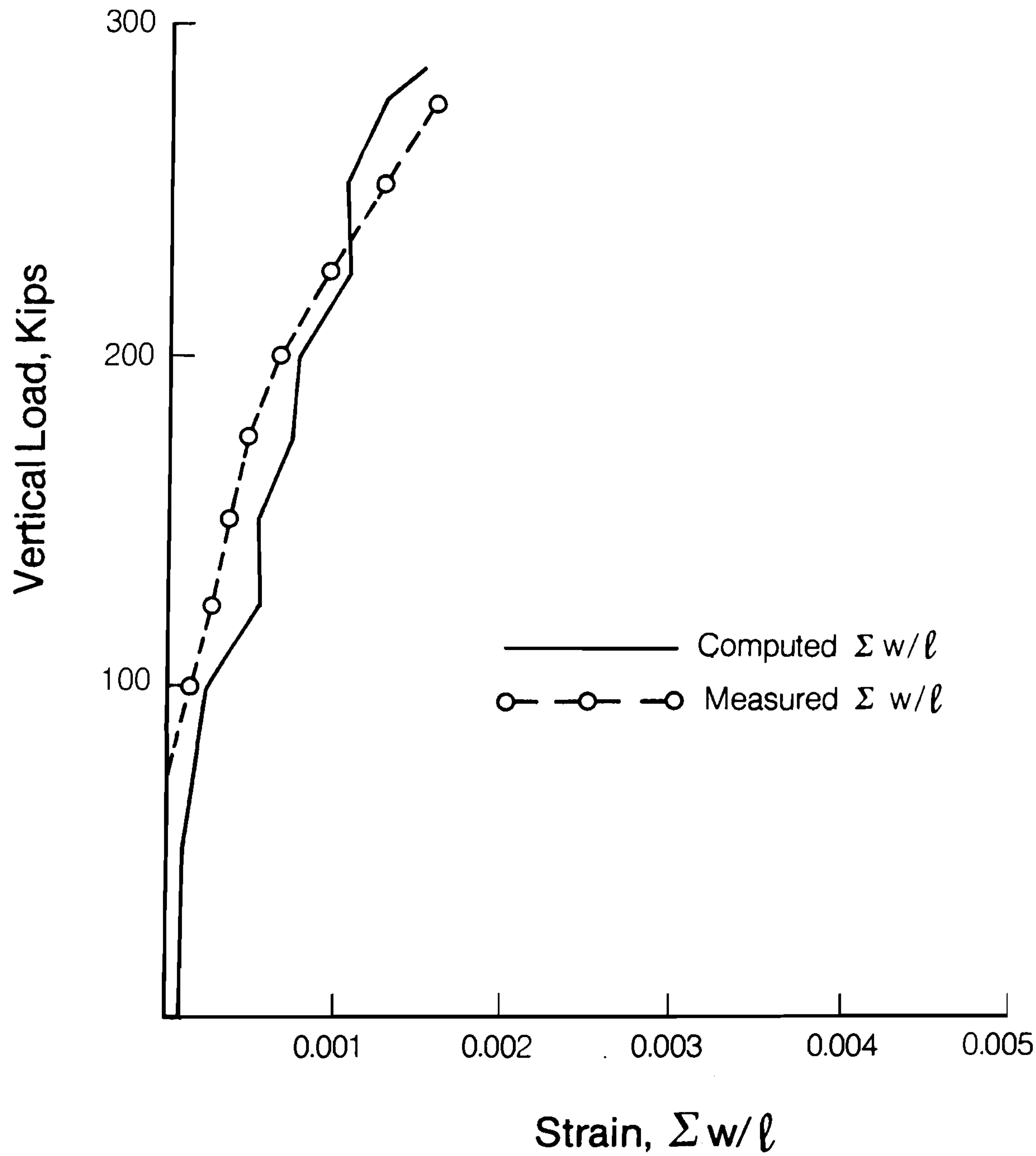

(b) Horizontal Cracks

Figure 5.7.7 Measured and Computed Crack Strain, $\Sigma w/\ell$, Segment 7

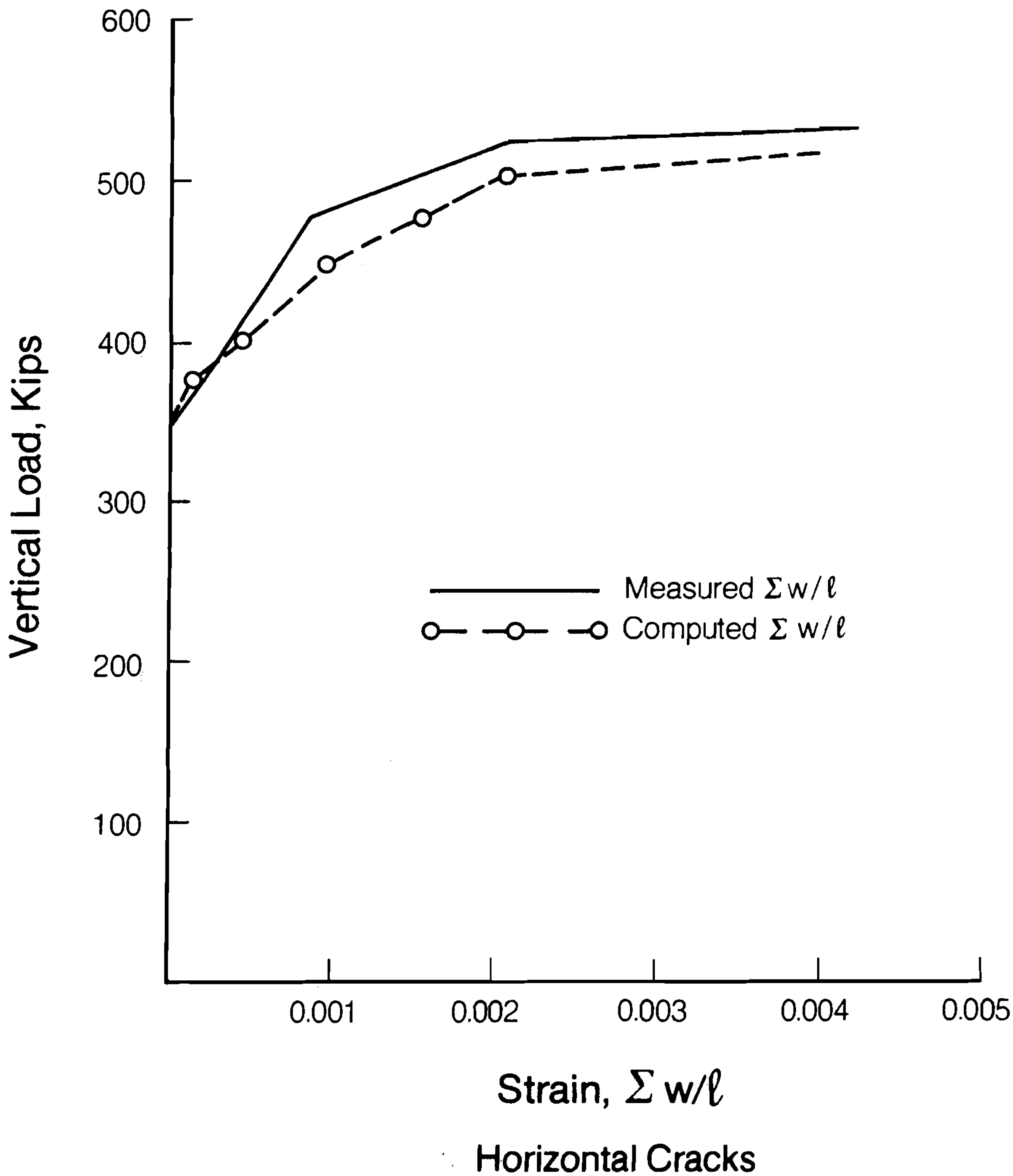

Figure 5.7.8 Measured and Computed Crack Strain, $\Sigma w/\ell$, Segment 8

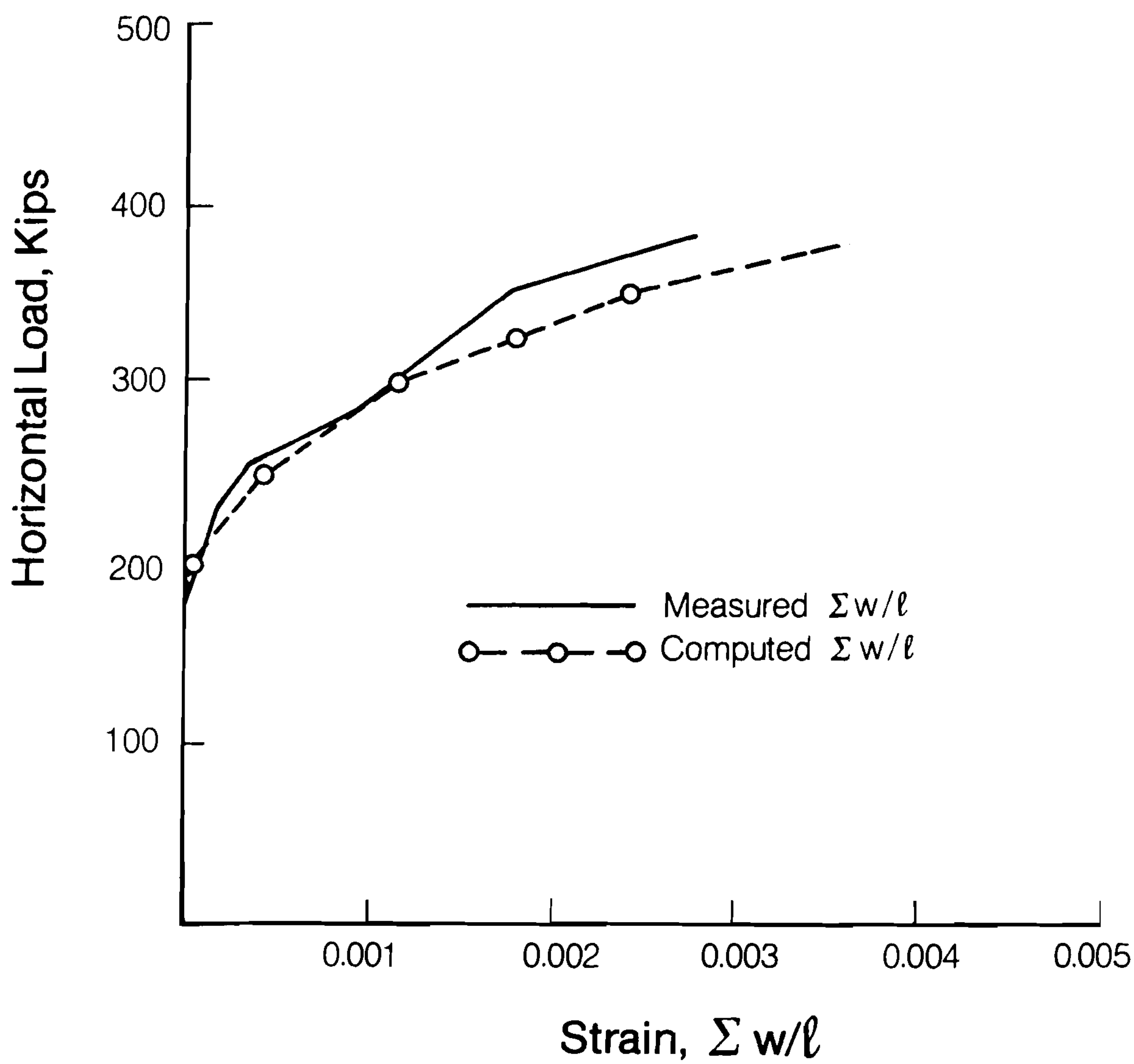

(a) Vertical Cracks

Figure 5.7.9 Measured and Computed Crack Strain, $\Sigma w/\ell$, Segment 9

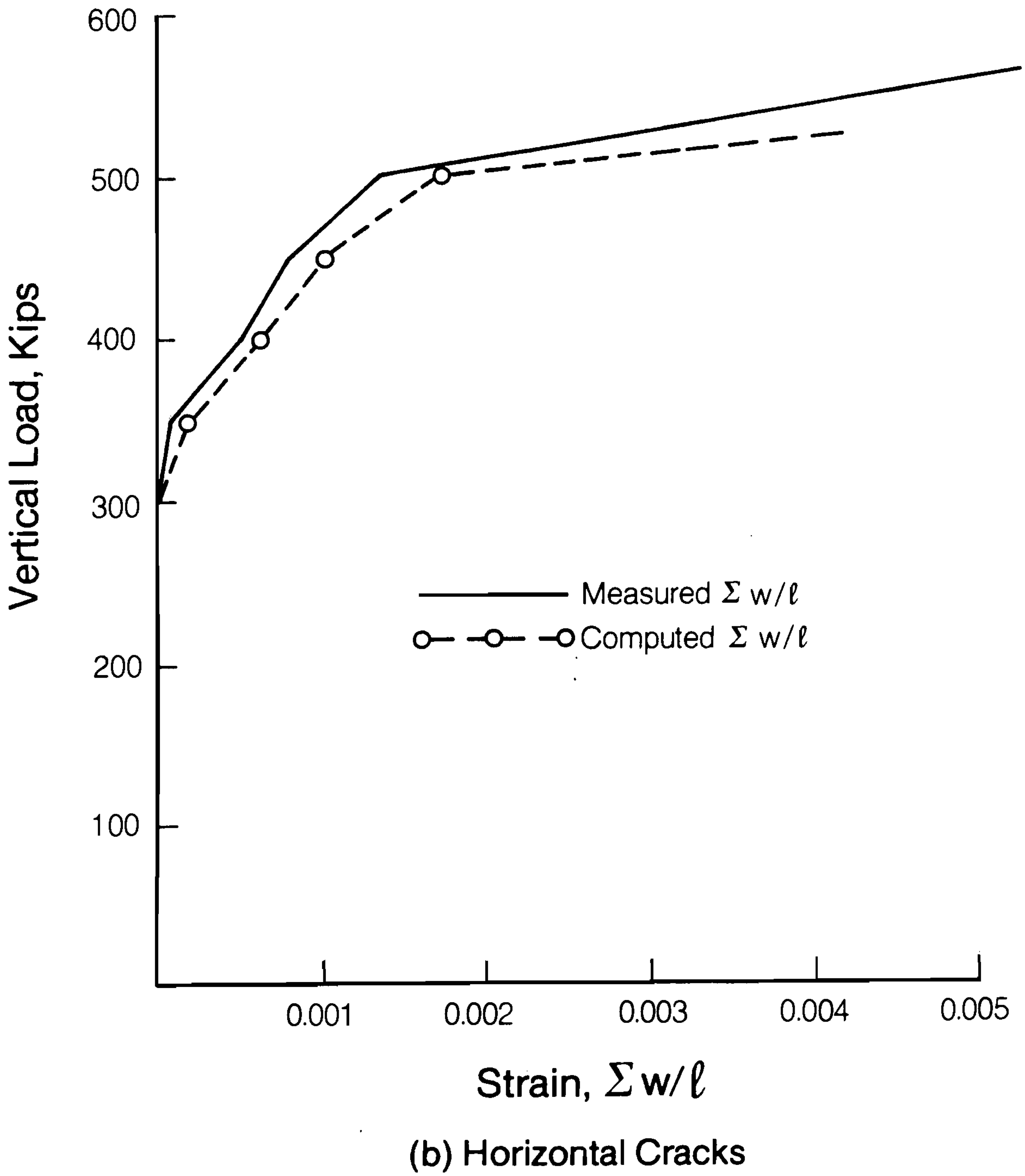

Figure 5.7.9 Measured and Computed Crack Strain, $\Sigma w/\ell$, Segment 9

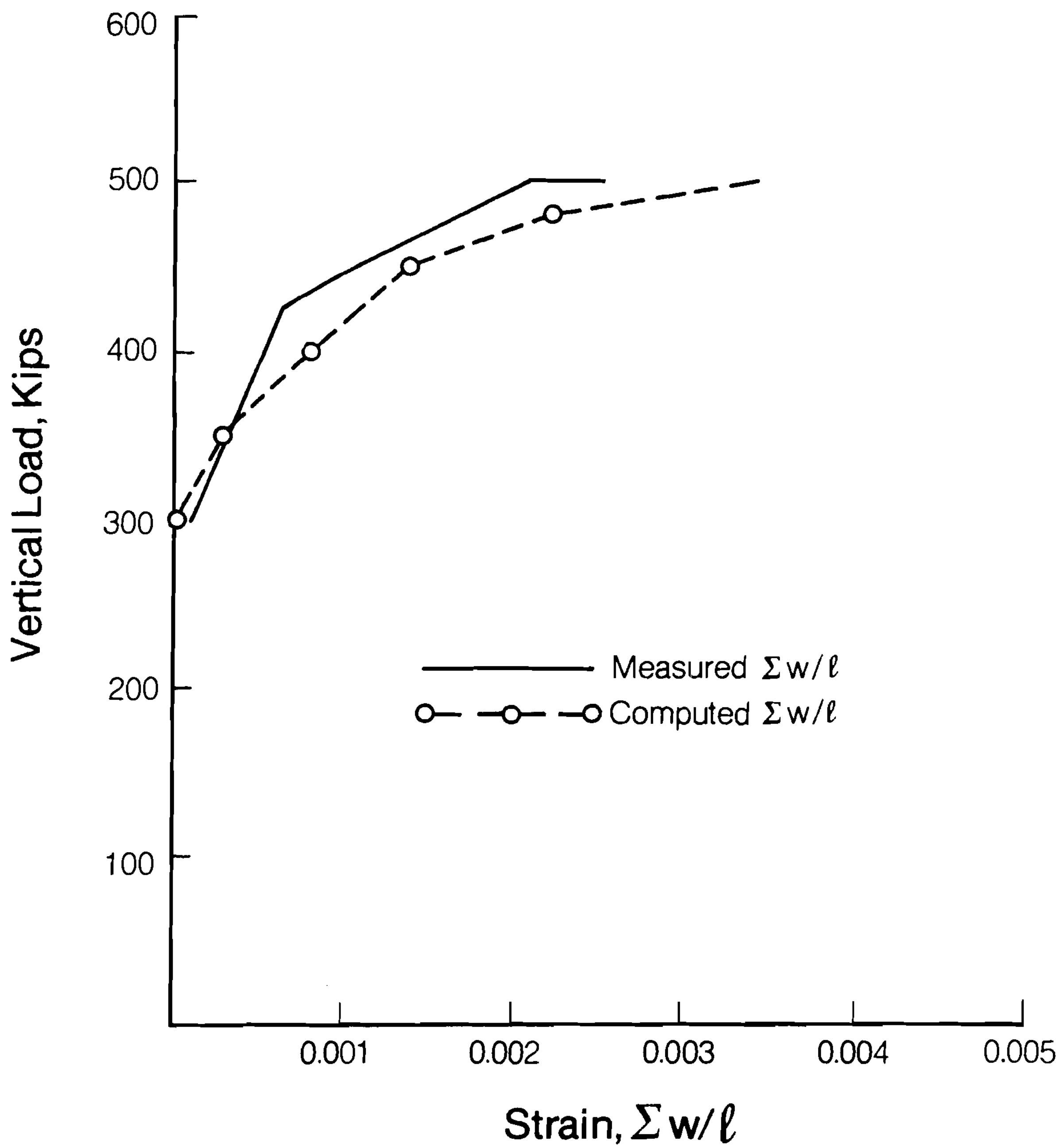

(b) Horizontal Cracks

Figure 5.7.11 Measured and Computed Crack Strain, $\Sigma w/\ell$, Segment 11

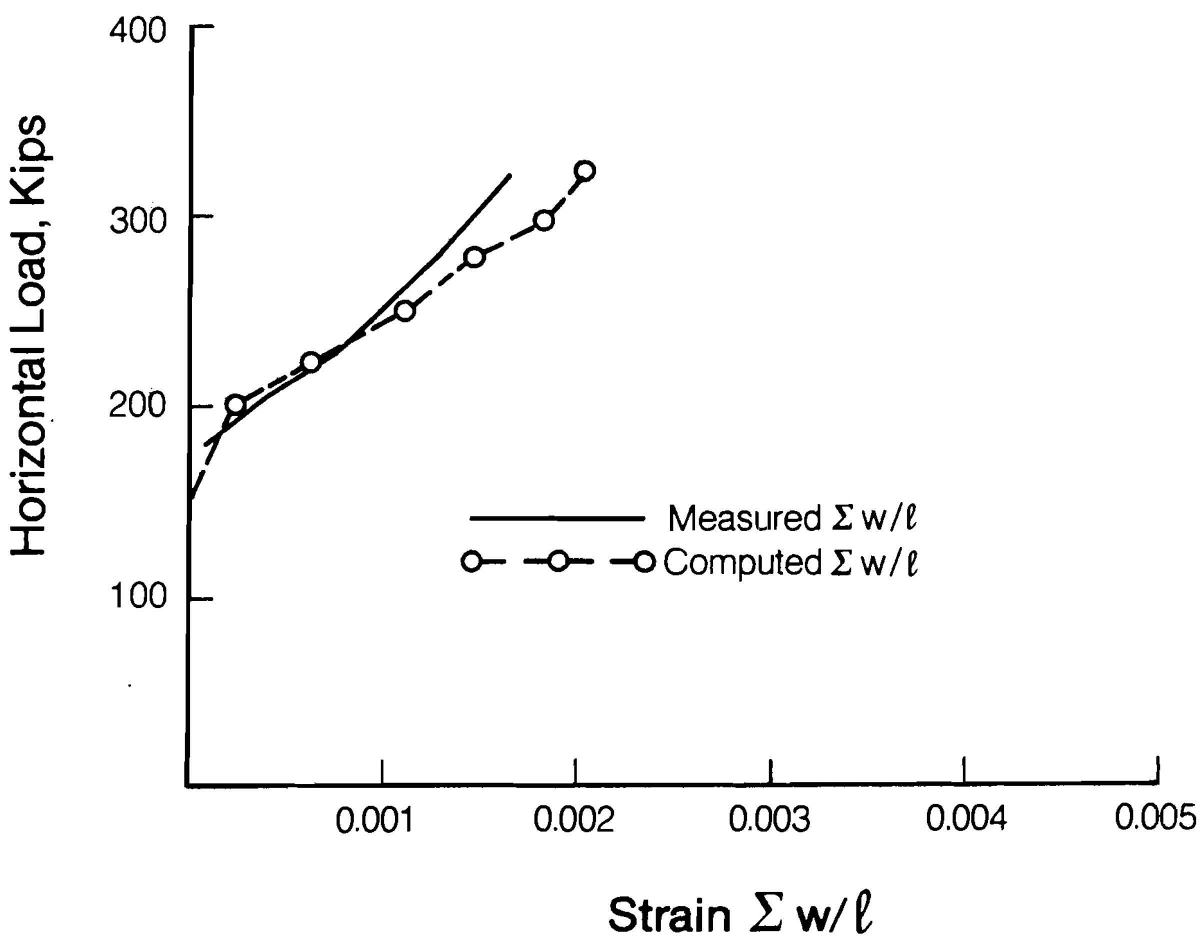

(a) Vertical Cracks (Face A)

Figure 5.7.12 Measured and Computed Crack Strains, $\Sigma w/\ell$, Segment 12

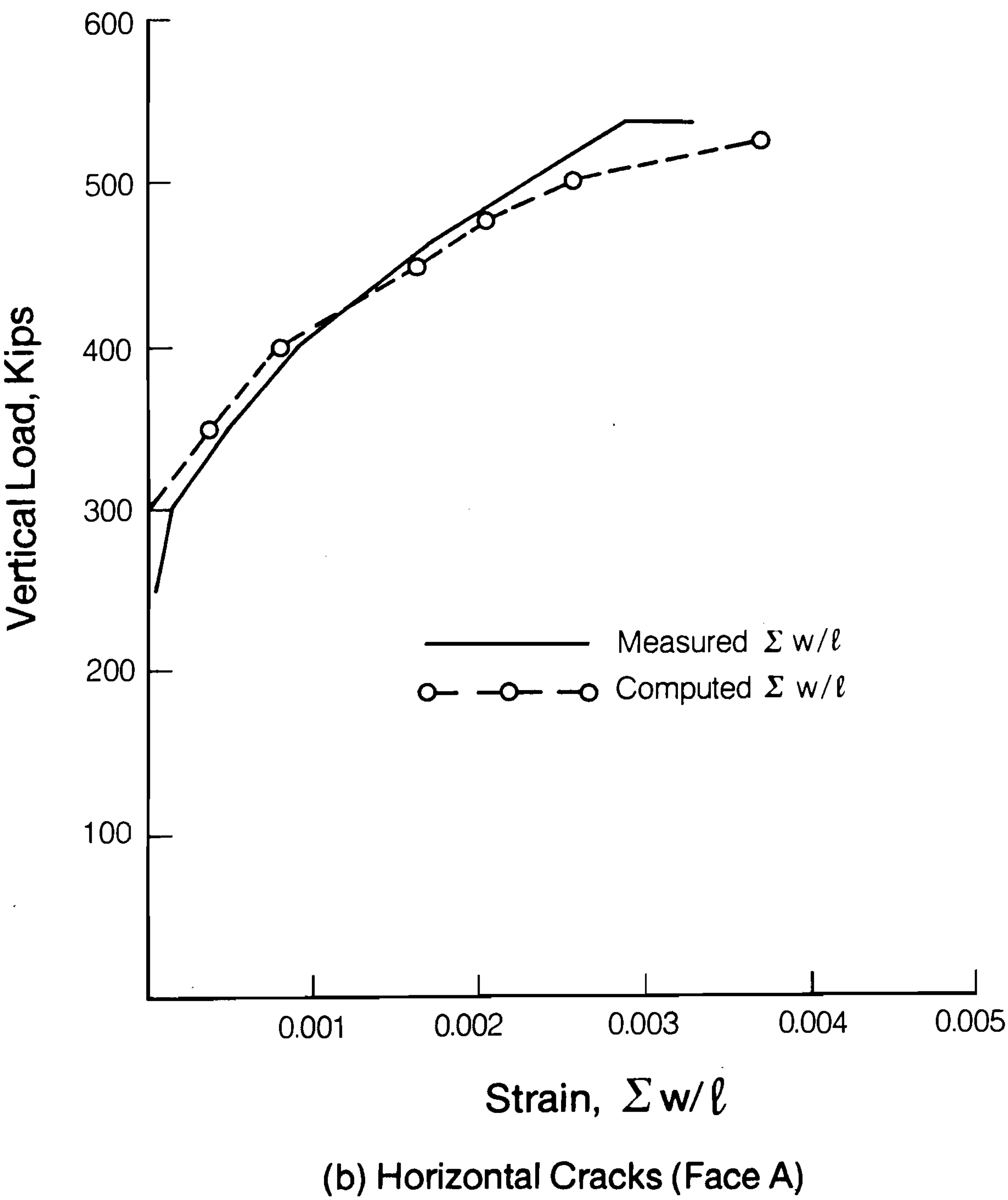

Figure 5.7.12 Measured and Computed Crack Strain, $\Sigma w/\ell$, Segment 12

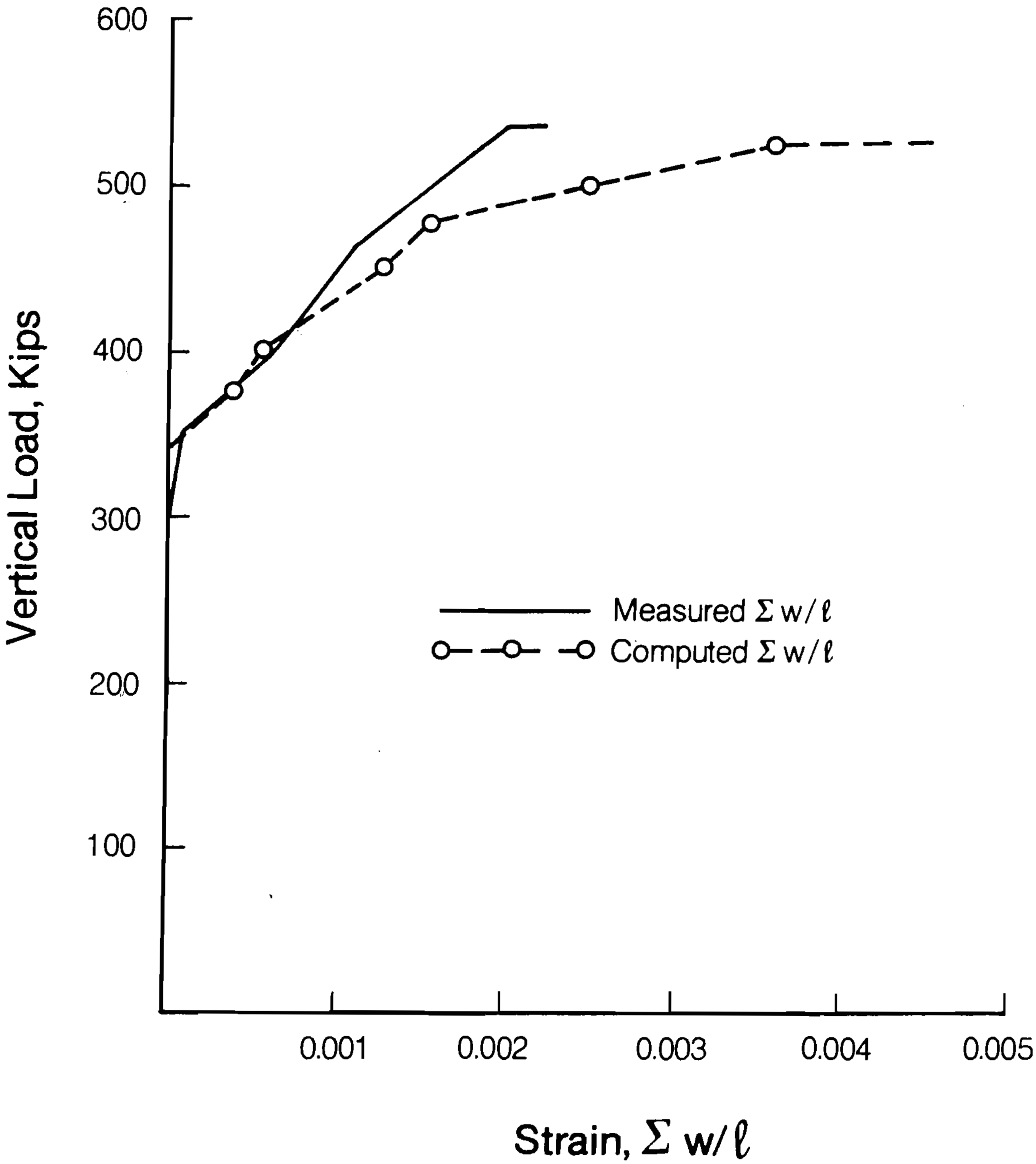

(c) Horizontal Cracks (Face B)

Figure 5.7.12 Measured and Computed Crack Strain, Σw/ℓ, Segment 12

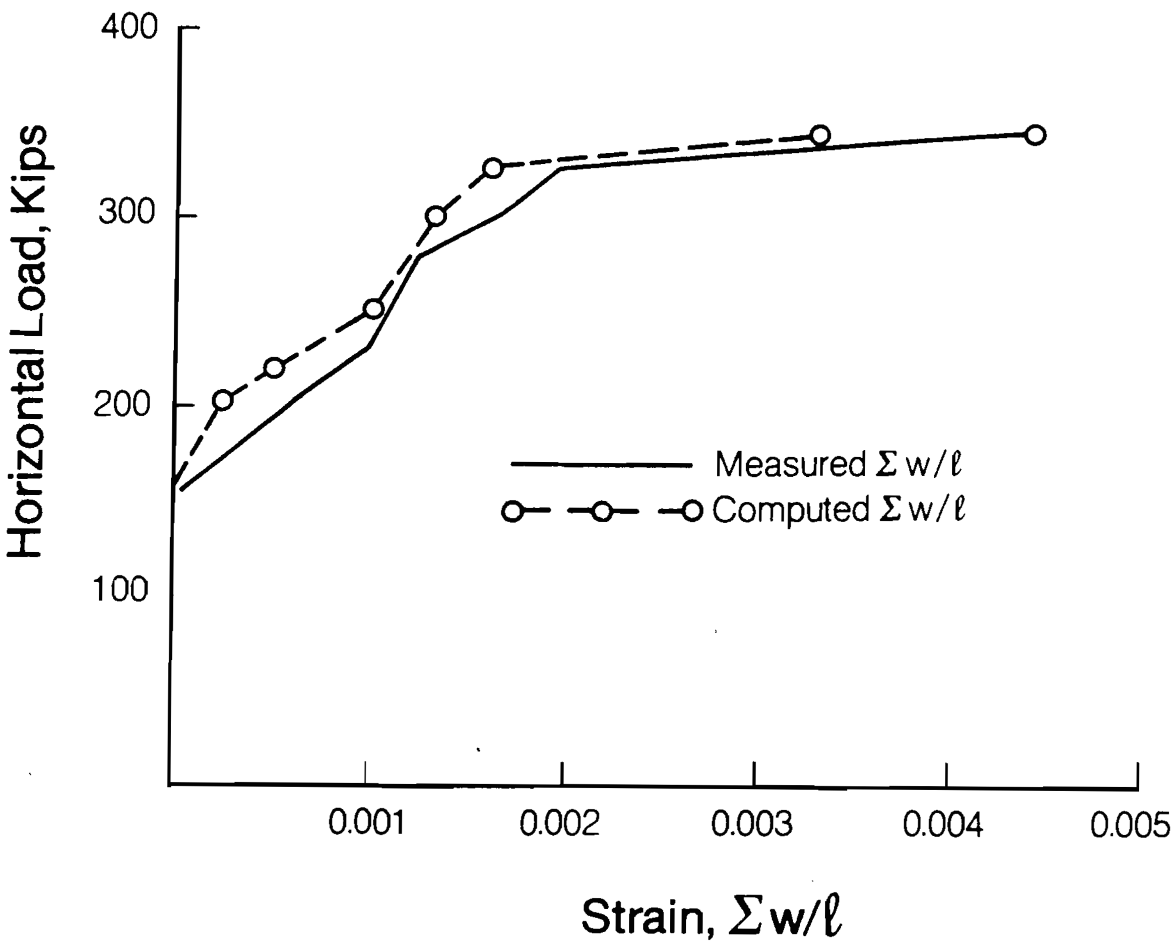

(a) Vertical Cracks (Face B)

Figure 5.7.13 Measured and Computed Crack Strains, $\Sigma w/\ell$, Segment 13

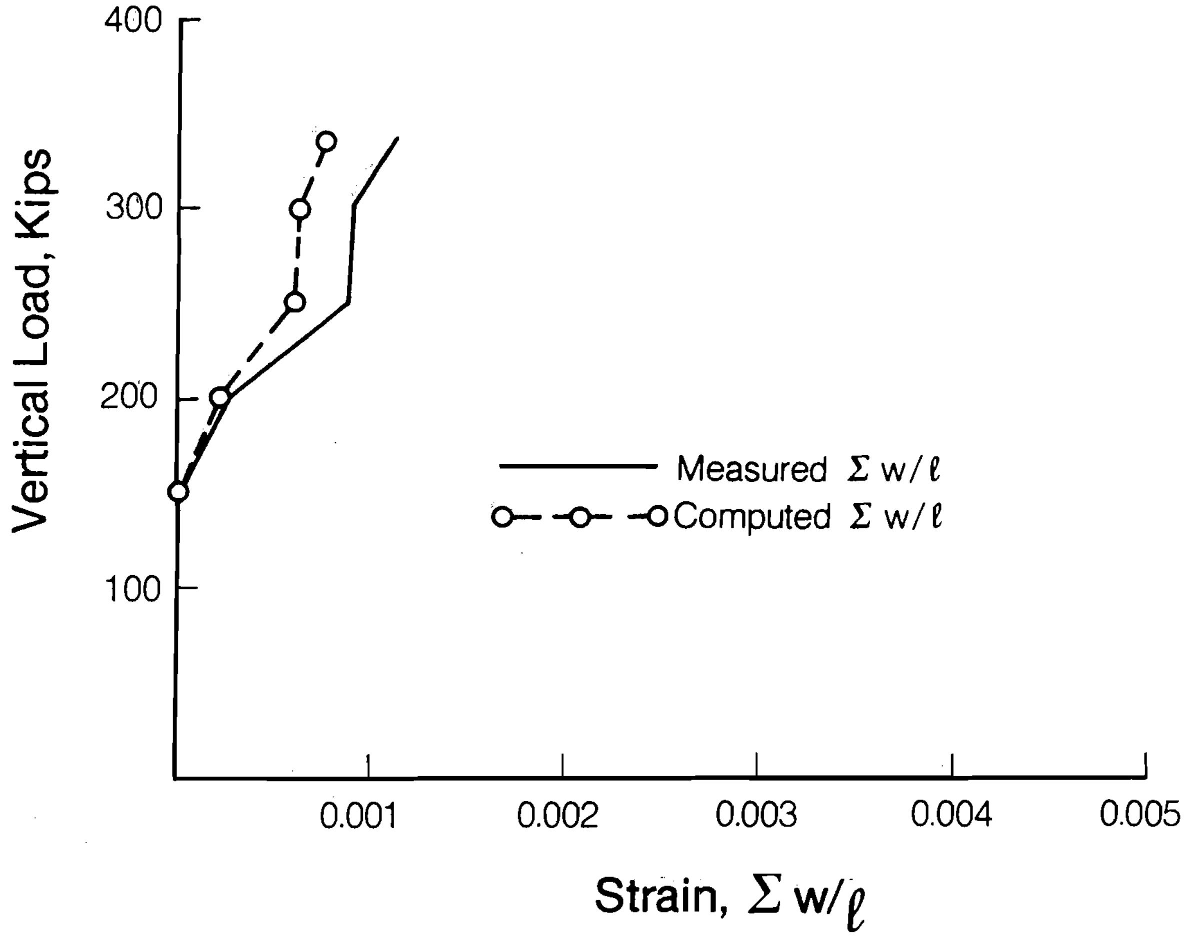

(b) Horizontal Cracks (Face B)

Figure 5.7.13 Measured and Computed Crack Strains, $\Sigma w/\ell$, Segment 13

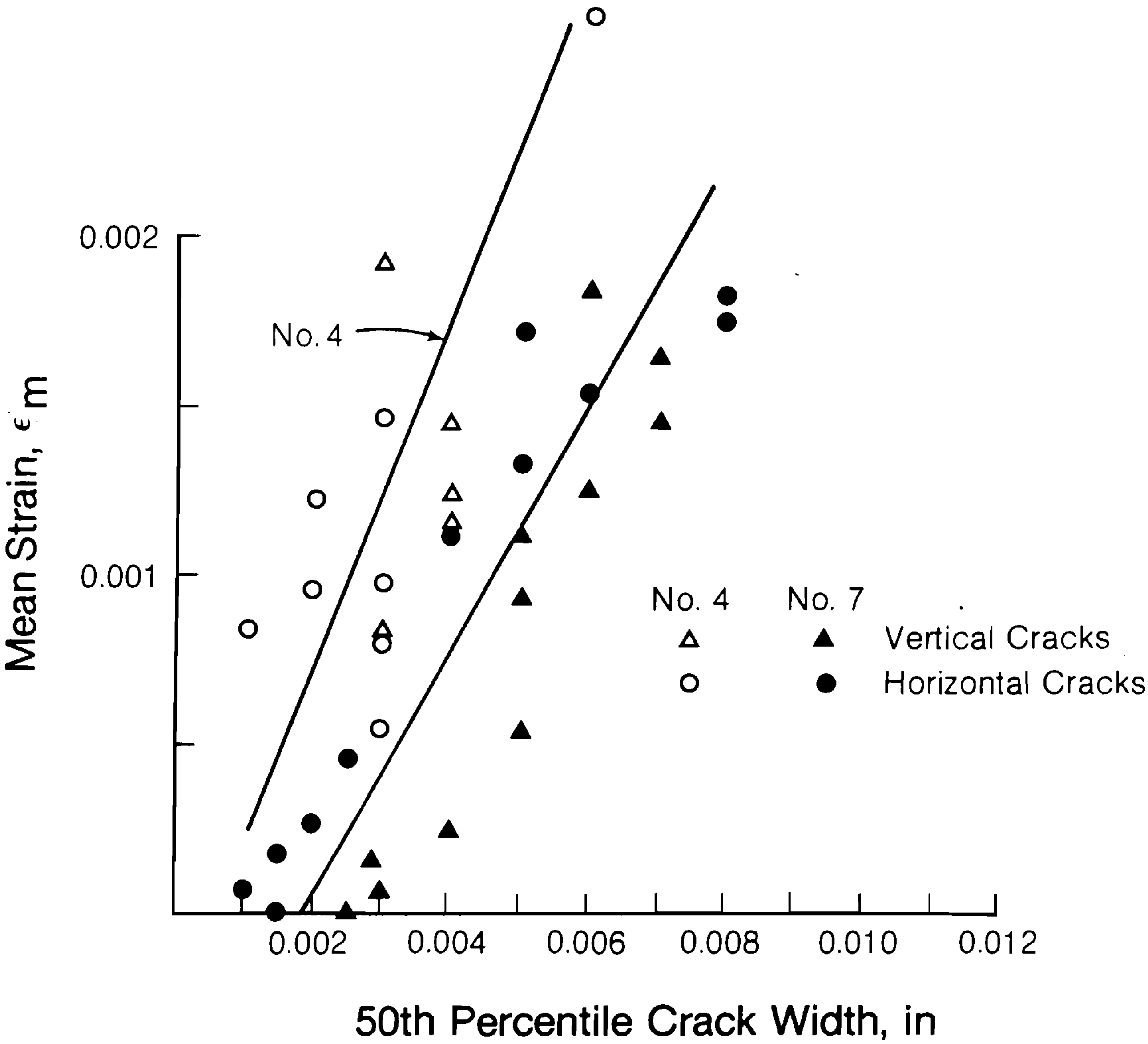

Figure 5.8 Median Crack Widths in Segments 4 and 7

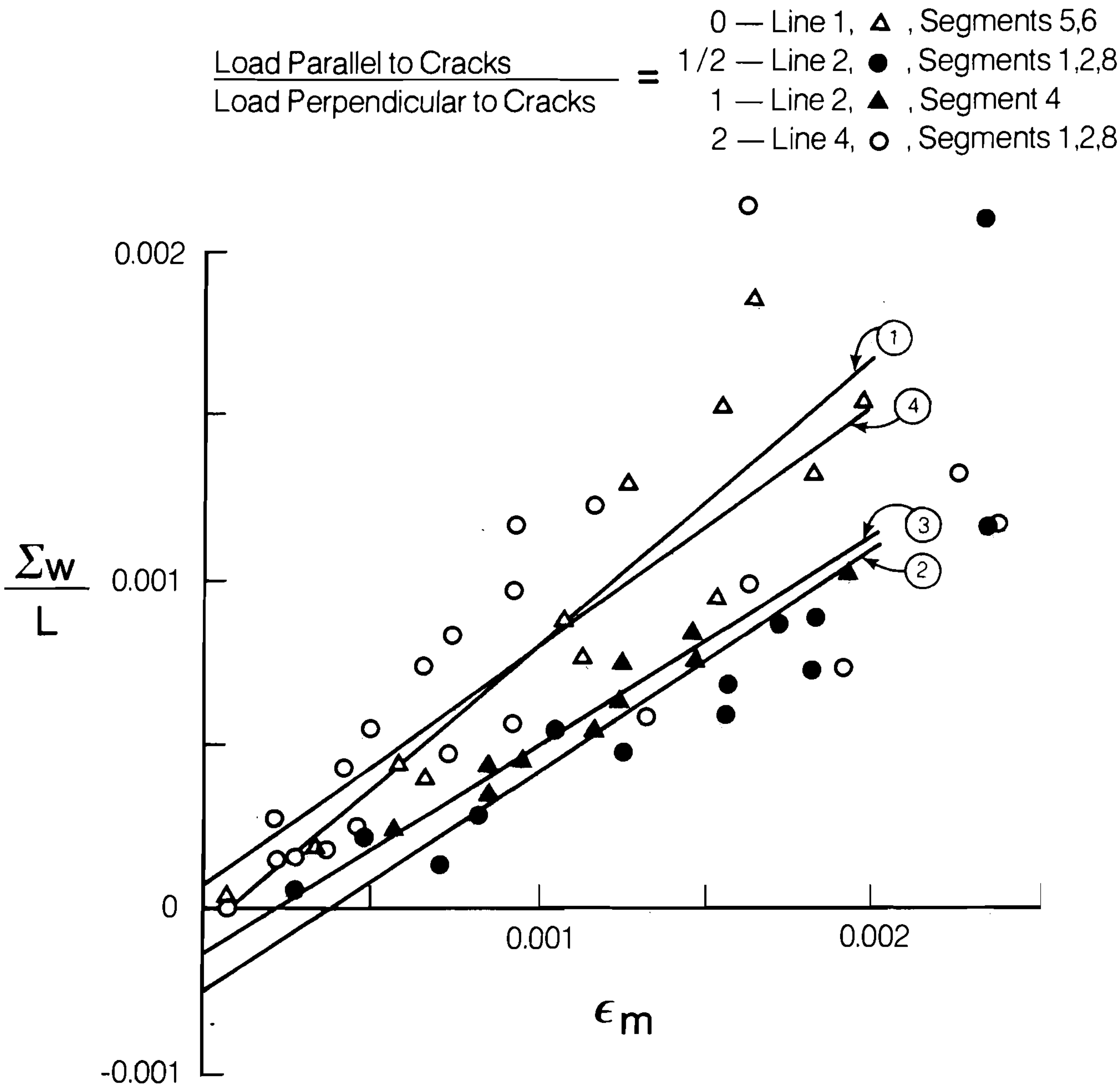

Figure 5.9 Effect of Transverse Stress on Crack Widths

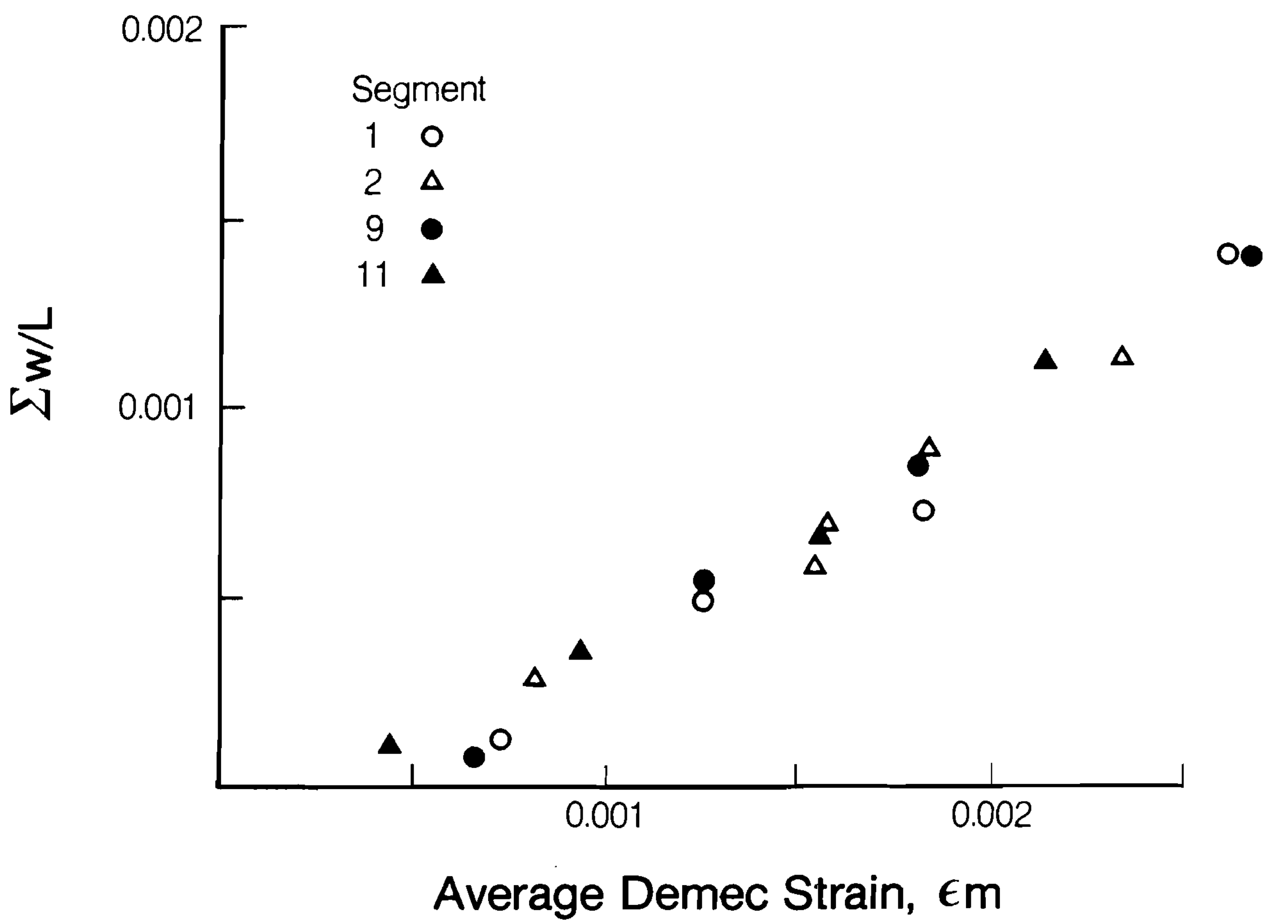

(a) Horizontal Cracks

Figure 5.10 Effect of Bar Splices on Crack Width

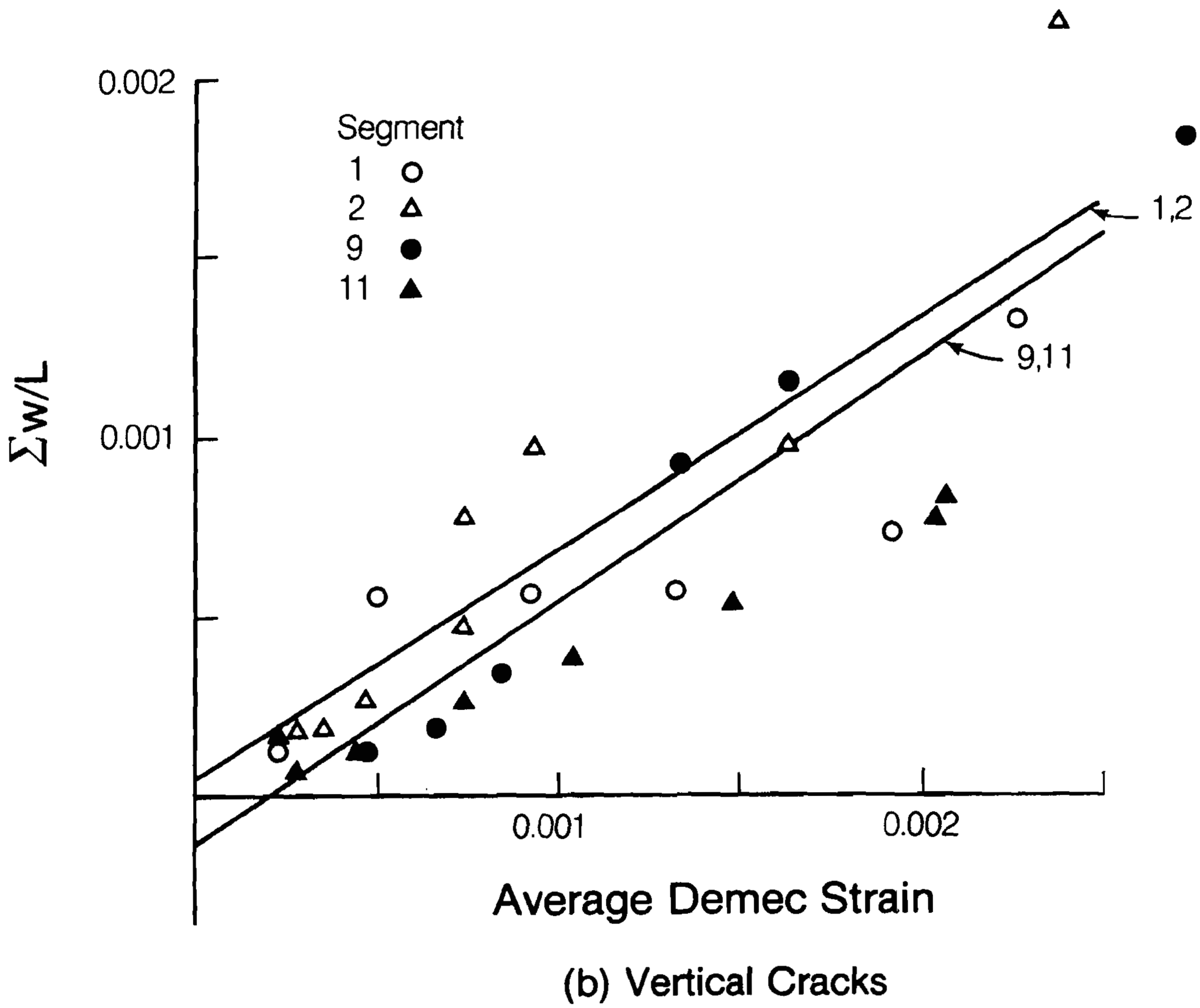

Figure 5.10 Effect of Bar Splices on Crack Width

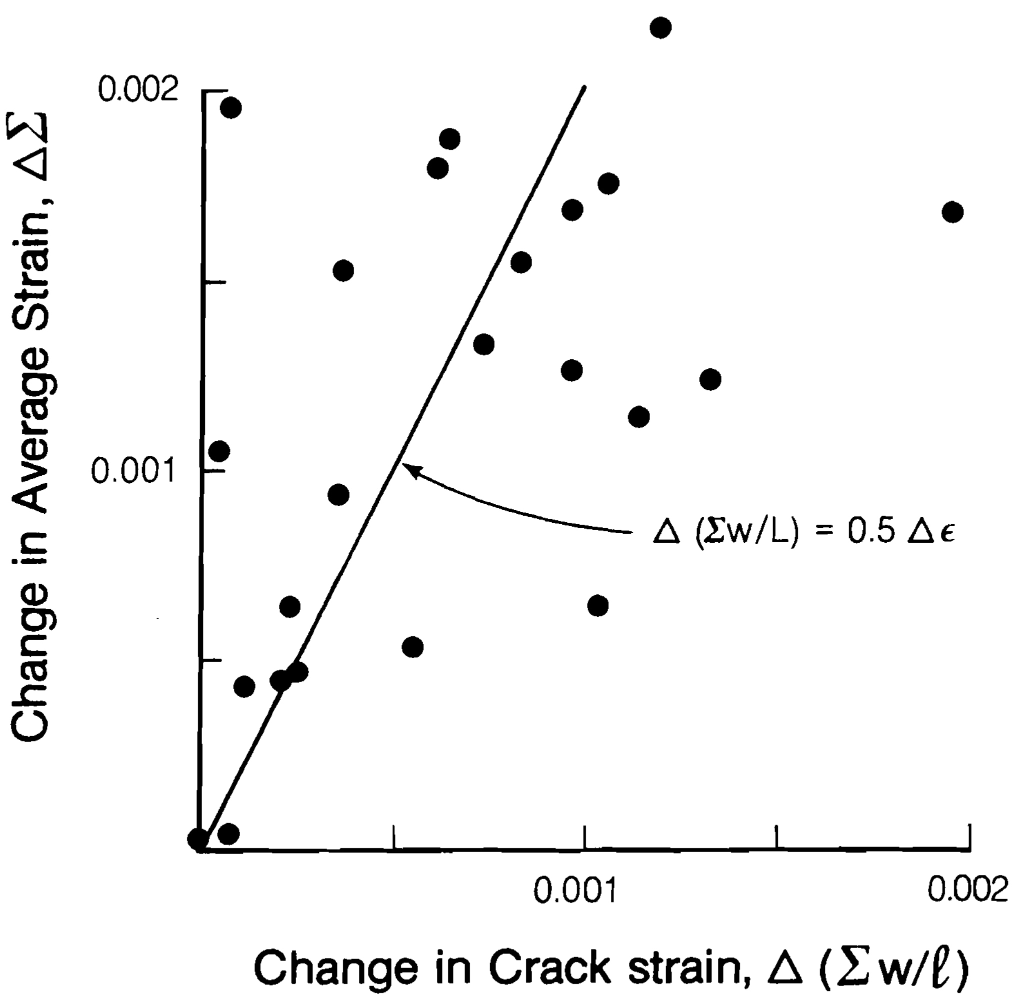

Figure 5.11 Relationship Between Changes in Average Strain and Crack Strain

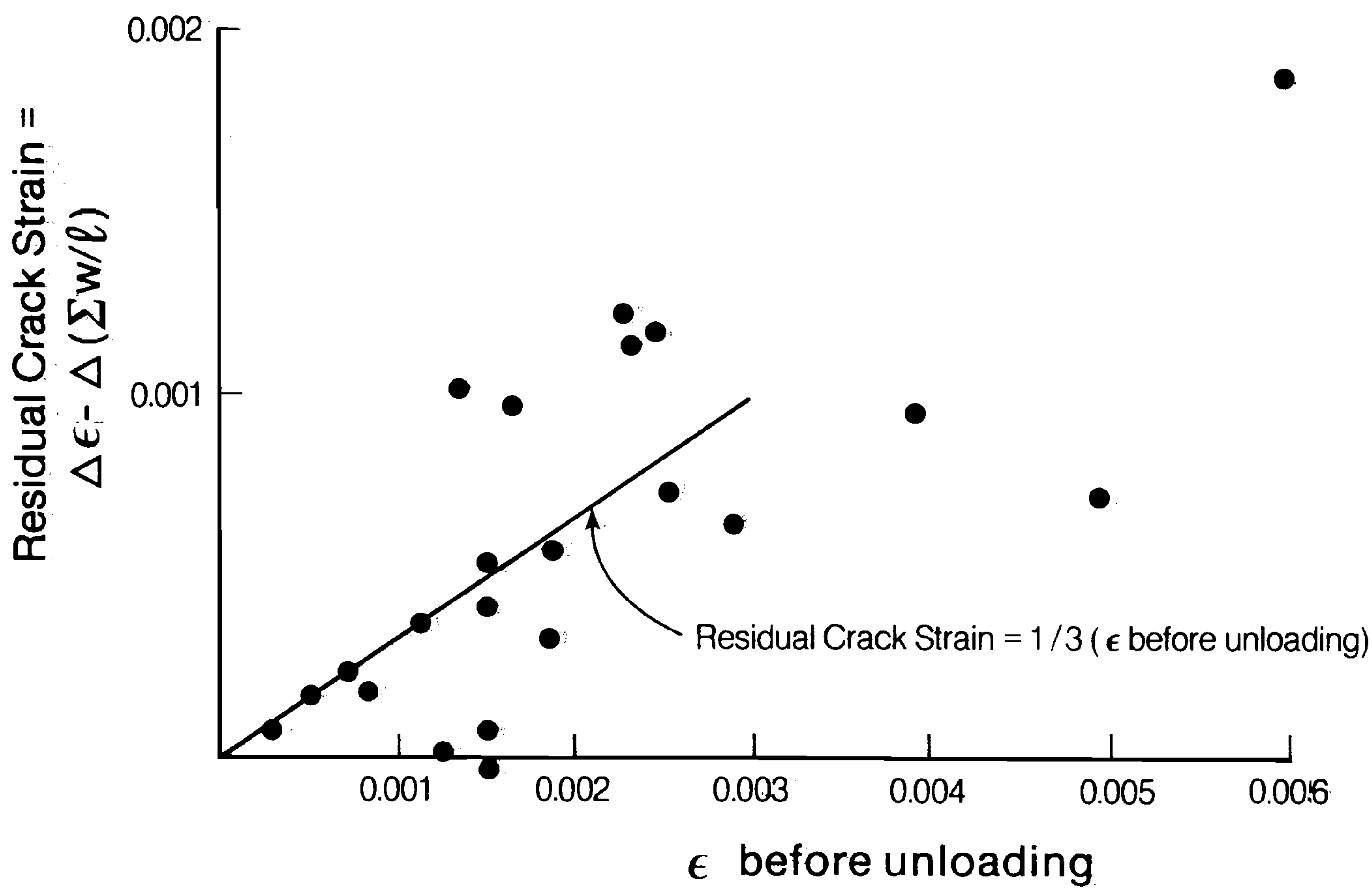

Figure 5.12 Residual Crack Strain as a Function of Strain Before Unloading